



Universiteit
Leiden
The Netherlands

Tuberculosis & type 2 diabetes

Vrieling, F.

Citation

Vrieling, F. (2020, September 3). *Tuberculosis & type 2 diabetes*. Retrieved from <https://hdl.handle.net/1887/136088>

Version: Publisher's Version

License: [Licence agreement concerning inclusion of doctoral thesis in the Institutional Repository of the University of Leiden](#)

Downloaded from: <https://hdl.handle.net/1887/136088>

Note: To cite this publication please use the final published version (if applicable).

Cover Page



Universiteit Leiden

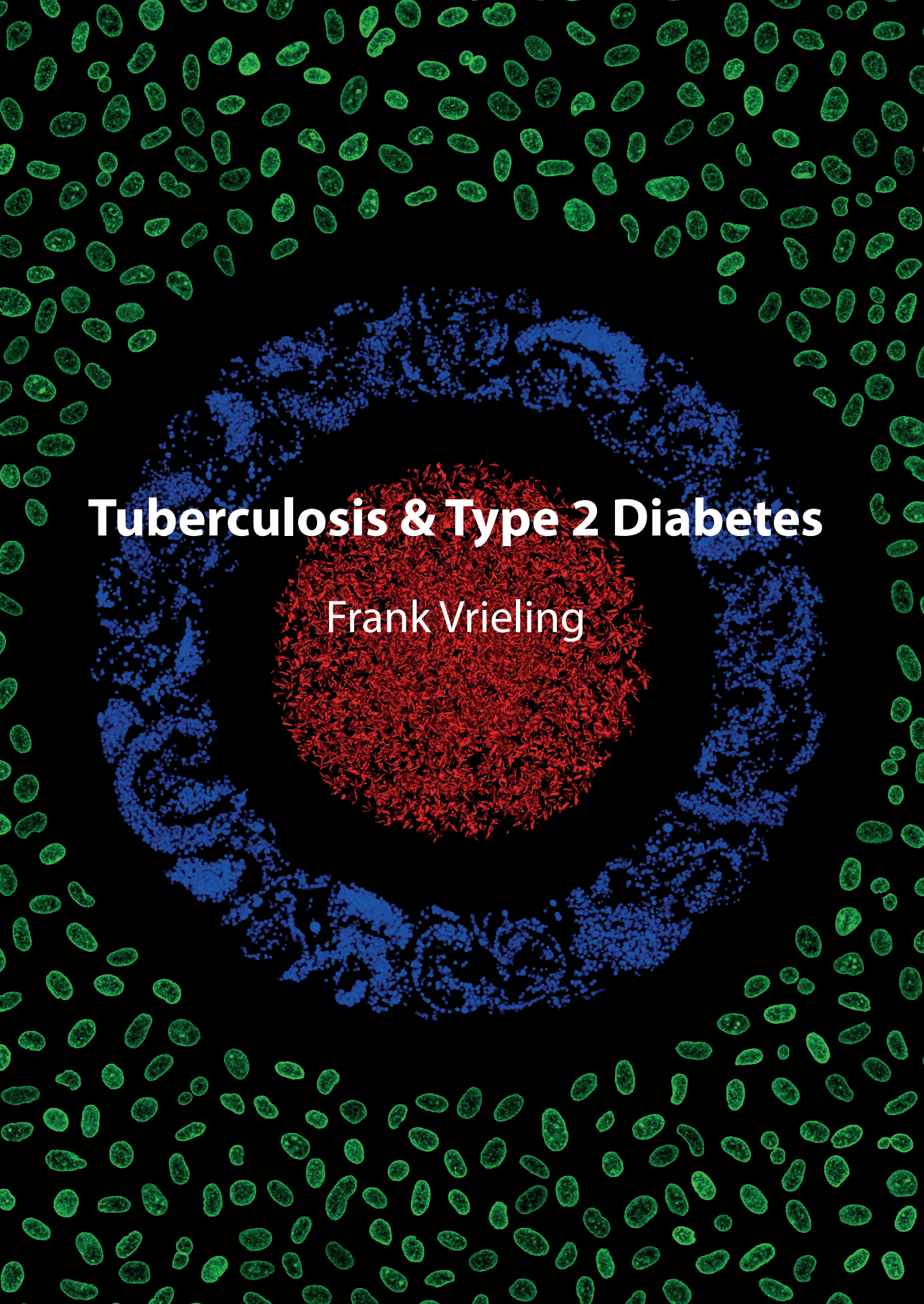


The handle <http://hdl.handle.net/1887/136088> holds various files of this Leiden University dissertation.

Author: Vrieling, F.

Title: Tuberculosis & type 2 diabetes

Issue date: 2020-09-03

The background of the cover is a dense field of small, green, rod-shaped structures, likely representing bacteria or cells. In the center, there is a large, circular, textured pattern. This pattern is composed of three concentric layers: an outermost layer of green, a middle layer of blue, and an innermost, dense core of red. The overall effect is a complex, multi-layered circular structure.

Tuberculosis & Type 2 Diabetes

Frank Vrieling

Tuberculosis & Type 2 Diabetes

Frank Vrieling

Tuberculosis & Type 2 Diabetes
PhD thesis, Leiden University, The Netherlands

Author: Frank Vrieling
Cover Artwork: Frank Vrieling
Printed & Layout: ProefschriftMaken.nl

ISBN: 978-94-6380-874-3

© Frank Vrieling, Wageningen, The Netherlands. All rights are reserved. No part of this thesis may be reproduced, stored in a retrieval system or transmitted in any form or by any means without prior permission of the author. The copyright of articles that have been published or accepted for publication has been transferred to the respective journals.

The conducted research was supported by the TANDEM (Tuberculosis and Diabetes Mellitus) Grant of the ECFP7 (European Union's Seventh Framework Programme) under Grant Agreement No. 305279; and by TBVAC2020 Grant of EC HOR2020 (Grant Agreement No. 643381).

Tuberculosis & Type 2 Diabetes

Proefschrift

ter verkrijging van
de graad van Doctor aan de Universiteit Leiden,
op gezag van Rector Magnificus prof.mr. C.J.J.M. Stolker,
volgens besluit van het College voor Promoties
te verdedigen op donderdag 3 september 2020
klokke 11.15 uur

door

Frank Vrieling

geboren te Alphen aan den Rijn

in 1989

Promotor:

Prof. dr. T.H.M. Ottenhoff

Co-promotor:

Dr. S.A. Joosten

Leden promotiecommissie:

Prof. dr. P.C.N. Rensen

Dr. B.G.A. Guigas

Prof. dr. H.P. Spaink

Prof. dr. R.C. Hoeben

Prof. dr. R. Shiri-Sverdlov (Department of Molecular Genetics,
School of Nutrition & Translational Research Maastricht, Universiteit van Maastricht)

Dr. J. van den Bossche (Amsterdam Universitair Medisch Centrum,
Department of Molecular Cell Biology and Immunology, Vrije Universiteit Amsterdam)

Table of Contents

Chapter 1:	General Introduction	9
Chapter 2:	Human M ϕ 2b macrophages exert intracellular bacterial control while M ϕ 2a/c/d support T cell responses	35
Chapter 3:	The effect of hyperglycaemia on in vitro cytokine production and macrophage infection with <i>Mycobacterium tuberculosis</i>	73
Chapter 4:	Oxidized low-density lipoprotein (oxLDL) supports <i>Mycobacterium tuberculosis</i> survival in macrophages by inducing lysosomal dysfunction	93
Chapter 5:	Patients with concurrent tuberculosis and diabetes have a pro-atherogenic plasma lipid profile	131
Chapter 6:	Plasma metabolomics in tuberculosis patients with and without concurrent type 2 diabetes at diagnosis and during antibiotic treatment	155
Chapter 7:	Analyzing the impact of <i>Mycobacterium tuberculosis</i> infection on primary human macrophages by combined exploratory and targeted metabolomics	185
Chapter 8:	Summarizing Discussion	217
	Nederlandse samenvatting	237
	Dankwoord	244
	Curriculum Vitae	246
	List of publications	247

CHAPTER

1

General Introduction

Frank Vrieling¹

¹ Department of Infectious Diseases, Leiden University Medical Center, Leiden, The Netherlands



***Mycobacterium tuberculosis*: an ancient but agile microbe**

Tuberculosis (TB) is an infectious disease of the lungs which is caused by infection with *Mycobacterium tuberculosis* (*Mtb*). Even though the first evidence of human TB infection can be traced back many millennia to the Neolithic era (~9,000 years ago)⁽¹⁾, it remains a major and important threat to global health to date. In 2017, an estimated 10 million people fell ill with TB and 1.6 million died as a result of the disease, making TB the leading cause of death by a single infectious agent worldwide⁽²⁾. TB ranks among the global top 10 causes of overall mortality. In total, 87% of the global TB burden is accounted for by 30 countries, of which India (27%), China (9%) and Indonesia (8%) encompass the top three of estimated new cases. The recommended TB treatment regimen consists of four first-line antibiotics (isoniazid, rifampicin, ethambutol and pyrazinamide) for a period of 6 months. However, multidrug-resistant TB (MDR-TB) and extensively drug-resistant TB (XDR-TB) comprise a major global health challenge due to a global rise in resistance to first-line drugs. Although treatment success rates of drug-susceptible TB are approximately 85% at an estimated cost of 40 US\$ per person, they drop to 55% for treatment of MDR-TB using second-line drugs with higher toxicity at significantly increased costs (>1000 US\$ per person). Furthermore, while vaccination with Bacille Calmette-Guérin (BCG), a live-attenuated *Mycobacterium bovis* vaccine which has been administered to humans since 1921, shows limited efficacy in preventing disease in children, a vaccine which induces adequate protection in adolescents and adults is still lacking⁽³⁾. Recently, the efficacy of two candidate subunit vaccines (M72/AS01_E and H4:IC31) for prevention of TB disease resp. infection in adults resp. adolescents was examined in phase 2 trials. Administration of M72/AS01_E to *Mtb*-infected adults resulted in 54.0% protection against TB⁽⁴⁾. Although H4:IC31 vaccination did not lead to prevention of primary QuantiFERON-TB Gold In-tube assay (QFT) conversion in adolescents from a high TB risk setting, it did show a trend towards reduced sustained QFT conversion for 3-6 months after initial measurement⁽⁵⁾. Importantly, a similar but significant effect was reported for revaccination with BCG in this trial, warranting further studies into the benefits of BCG revaccination for prevention of sustained QFT conversion⁽⁵⁾.

TB is spread through inhalation of mycobacteria-containing aerosols produced by sneezing or coughing, leading to *Mtb* infection of resident alveolar macrophages. The immune response to *Mtb* is characterized by formation of granulomas, complex immunological structures which shield the host from bacterial dissemination but simultaneously provide a niche for *Mtb* persistence⁽⁶⁾. First, additional mononuclear cells are recruited to the site of primary infection from neighboring blood vessels, which subsequently become infected by the expanding mycobacterial population and together form the early granuloma. After an initial delay (14-21 days) in the onset of adaptive immune responses, B and T lymphocytes are recruited to the granuloma, eventually leading to arrested *Mtb* growth but not to complete bacterial elimination. During this time of immunological deadlock the granuloma matures, which involves differentiation of

macrophages into lipid-loaded foamy, epithelioid and multinucleated giant cells and the formation of a fibrous cuff around the macrophage-rich layer. Whereas the early granuloma was adequately vascularized, *Mtb* now has to adapt to conditions of local hypoxia and nutrient-scarcity and consequently enters a state of dormancy, ensuing in a clinically asymptomatic period of latent TB infection (LTBI). It is estimated that approximately one quarter of the world's population is latently infected with *Mtb*⁽⁷⁾, 5-10% of which will reactivate and develop active disease during their life-time. The factors which determine granuloma outcome and TB reactivation are not clearly defined, but immune components appear key players. Induction of immune mediators on opposite sides of the inflammation spectrum result in a delicate immune balance. Pro-inflammatory cytokines such as tumor necrosis factor alpha (TNF- α) and interferon gamma (IFN- γ) are major contributors to TB immunity. Treatment with TNF- α neutralizing antibodies led to reactivation of TB in humans⁽⁸⁾ and cynomolgus macaques⁽⁹⁾. Mutations in the IFN- γ gene⁽¹⁰⁾, the IFN- γ receptor⁽¹¹⁾ or the interleukin (IL)-12/-23 axis⁽¹²⁾, which governs IFN- γ production⁽¹³⁾, impair anti-mycobacterial immunity. However, high levels of pro-inflammatory factors can also lead to extensive tissue damage, resulting in liquefying caseous necrosis, pulmonary cavitation and ultimately bacterial dissemination⁽¹⁴⁾.

As stated above, *Mtb* primarily infects macrophages, phagocytic cells of the myeloid lineage which play pivotal roles in immunity by direct microbe killing and presenting antigen to naïve T cells to induce adaptive responses. The primary route of killing or controlling intracellular bacteria is through the phagolysosomal pathway (**Figure 1**). After receptor-mediated uptake, bacteria are contained in compartments called phagosomes which rapidly mature by fusing with lysosomes, leading to vesicle acidification and the acquisition of antimicrobial peptides and hydrolases. To circumvent its eradication, *Mtb* inhibits phagosome maturation by manipulating the activity of GTP-binding Rab proteins which coordinate intracellular vesicle trafficking^(15,16), through targeting Vacuolar-type H⁺-ATPase for degradation to prevent phagosomal acidification⁽¹⁷⁾, and through blocking the function of the NADPH oxidase complex⁽¹⁸⁾, an important phagosomal component which produces antibacterial superoxide. Furthermore, *Mtb* induces perforation of the phagosome through expression of the ESX-1 secretion system^(19, 20), an important virulence factor which is absent in the non-virulent BCG strain. ESX-1 effector proteins ESAT6 and CFP10 have been shown to induce phagosomal membrane damage in macrophages⁽¹⁹⁻²²⁾, simultaneously halting vesicle maturation and providing access for *Mtb* to release important effectors in the cytosol. An unwanted consequence of phagosomal escape from the perspective of *Mtb* is the induction of autophagy which serves as an auxiliary host pathway for bacterial clearance, although its importance for TB outcome is still a topic of debate⁽²³⁾. Multiple autophagy pathways have been implicated in *Mtb* killing, including the detection of mycobacterial DNA by the STING-cGAS cytosolic surveillance pathway^(24,25), the recruitment of host galectins to damaged phagosomes^(26, 27) and ubiquitination of escaped mycobacteria by ubiquitin ligases such

as Parkin and Smurf1^(28, 29), among others⁽³⁰⁾. These pathways culminate in the recruitment of autophagy adaptors such as NDP52 and p62, which consecutively bind to membrane protein LC3 leading to the formation of degradative double membrane vesicles named autophagosomes. Again, *Mtb* has developed mechanisms to actively inhibit these clearance mechanisms, for instance by inducing expression of miR-33⁽³¹⁾, miR-155⁽³²⁾ and IL-10⁽³³⁾, all negative regulators of autophagy. Collectively, these strategies of *Mtb* to survive the hostile intracellular environment of the macrophage are major contributors to its pathogenic success.

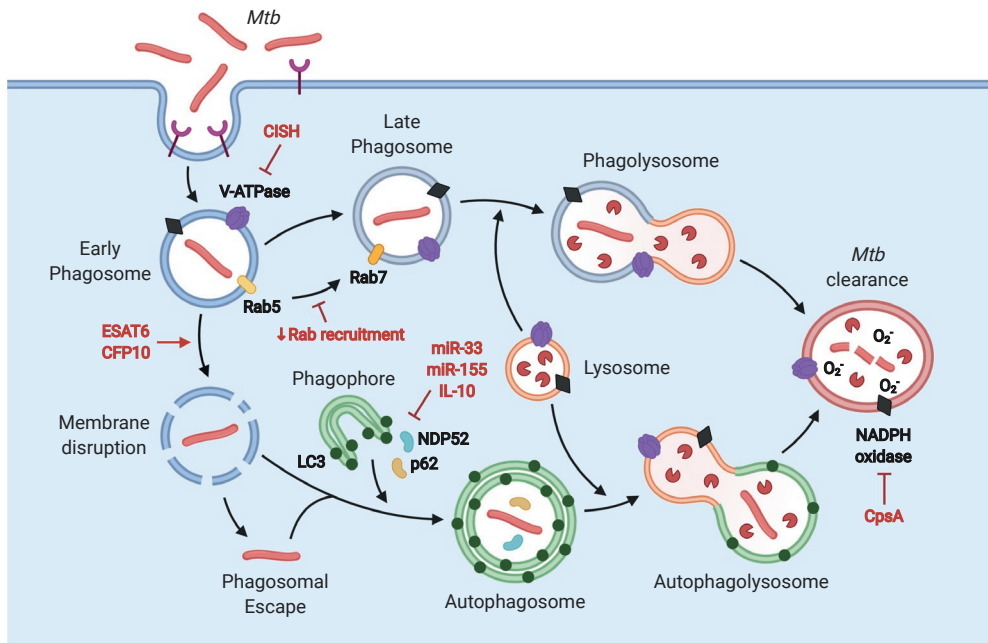


Figure 1: Overview of macrophage central energy metabolism.

After receptor-mediated uptake, *Mtb*-containing phagosomes mature by fusing with lysosomes, leading to vesicle acidification and ultimately mycobacterial eradication. *Mtb* can interfere phagosome maturation at multiple steps, including: 1) inhibition of Rab activity and recruitment, 2) induction of cytokine-inducible SH2-containing protein (CISH) to degrade Vacuolar-type H⁺-ATPase (V-ATPase), 3) inhibition of NADPH oxidase complex by Cold shock protein A (CspA), 4) phagosomal membrane disruption by ESX-1 effector proteins ESAT6 and CFP10 leading to *Mtb* escape. Autophagy can serve as an auxiliary pathway for *Mtb* killing, leading to autophagosome formation after binding of autophagy adaptors such as p62 and NDP52 to LC3. *Mtb* can negatively affect autophagy through induction of host microRNAs (miR-33 and miR-155) and IL-10.

Macrophage biology and immunometabolism during *Mtb* infection

While their importance in *Mtb* pathogenesis is undisputed, referring to macrophages as a single uniform cell type would be inaccurate. Macrophages exist in many different forms and functional states, and their significant plasticity has been the topic of many studies over the last decades. Initially, a dichotomic model of macrophage activation was proposed, spanning from pro-inflammatory ‘classically activated’⁽³⁴⁾ to anti-inflammatory ‘alternatively activated’⁽³⁵⁾ macrophages, which were later respectively labeled M1 and M2 macrophages, the myeloid equivalent of the classical Th1/Th2 paradigm⁽³⁶⁾. M1 polarization can be induced by Th1 cytokines (IFN- γ and TNF- α) and LPS, while M2 macrophages can be generated by Th2 cytokines IL-4 and IL-13. Alternatively, macrophage differentiation of monocytes using either M-CSF or GM-CSF also results in diametrically opposed functional phenotypes (termed M ϕ 1 and M ϕ 2)^(37,38). In analogy to the over simplistic Th1/Th2 paradigm (following the discovery of Th17, Th22, Tfh and other T cell subsets), the initial M1/M2 dichotomy soon became challenged, and variations in differentiating stimuli were shown to result in phenotypically distinct macrophage subsets not conforming to classical M1/M2⁽³⁹⁾. An extensive transcriptomics study on macrophage polarization under 29 differentiating conditions revealed a spectrum of macrophage activation which was far beyond what could be explained by the M1/M2 model, including distinct gene expression modules involved in granulomatous inflammation after stimulation with TNF- α , prostaglandin E2 and Pam3Cys⁽⁴⁰⁾. Moreover, it has become clear that many tissue-resident macrophage populations consist of self-renewing cells derived from embryonic precursors, such as Kupffer (liver) and Langerhans cells (skin), which do not rely on circulating blood monocytes during steady-state⁽⁴¹⁾, suggesting different lineages within the macrophage “compartment”. Combined, these findings have led to the rejection of the original binary view of macrophage polarization, and have given way to multidimensional models which take into account the effects of macrophage ontogeny and local tissue microenvironment^(42,43).

An important factor which is interconnected with the outcome of macrophage activation is their metabolic state. The interplay between immune cell function and metabolism has taken a prominent place in immunological studies over recent years, leading to the emergence of a new field of research: immunometabolism. Conceptually, functional immune cell activation demands recalibration of cellular metabolism to provide energy in the form of adenosine triphosphate (ATP) and other necessary biosynthetic intermediates. One of the pioneers of cellular physiology was Otto Warburg, who discovered that cancer cell metabolism is skewed towards energy production by glycolysis instead of mitochondrial respiration, even under aerobic conditions^(44,45), a process which is since referred to as the ‘Warburg effect’. During glycolysis, one molecule of glucose is sequentially converted to two molecules of pyruvate, leading to a net energy production of two ATP (**Figure 2**). Pyruvate is then either used to recycle oxidized nicotinamide adenine dinucleotide (NAD⁺) by conversion to lactate, or imported into mitochondria to

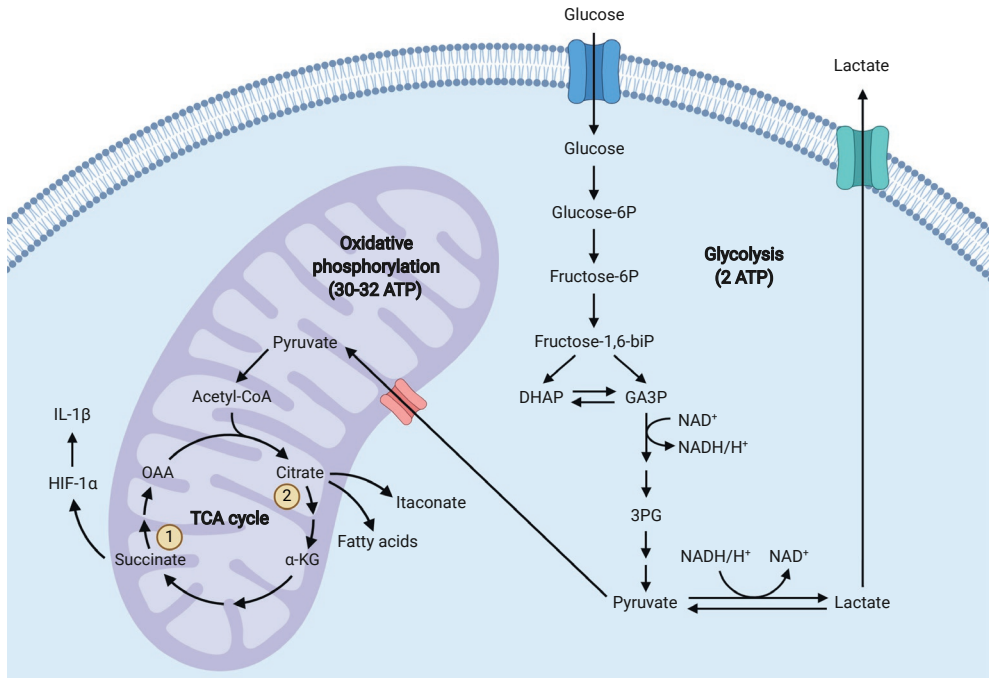


Figure 2: Interference of *Mycobacterium tuberculosis* with phagolysosomal clearance.

Glycolysis yields two molecules of ATP per molecule of glucose. Pyruvate formed after glycolysis is then either converted to lactate (regenerating NAD⁺) or shuttled to mitochondria to fuel the TCA cycle. Oxidative phosphorylation of pyruvate yields 30-32 ATP per molecule of glucose. Two breaks in the TCA cycle have been reported to occur in pro-inflammatory M1 macrophages: 1) accumulation of succinate was shown to stabilize HIF-1 α , leading to IL-1 β production; 2) citrate accumulation supports inflammatory action through synthesis of fatty acids and the anti-microbial metabolite itaconate.

form acetyl coenzyme A (acetyl-CoA). Acetyl-CoA subsequently enters the tricarboxylic acid (TCA) cycle, a series of biochemical reactions resulting in the formation of NADH and succinate which are used to produce ~30-32 ATP per glucose molecule during oxidative phosphorylation (OXPHOS). In macrophages and dendritic cells (DCs), a similar metabolic switch towards increased glycolysis was observed after stimulation with TLR ligands^(46,47), leading to the hypothesis that induction of the Warburg effect was important for pro-inflammatory activation. Indeed, stimulation with LPS was shown to induce expression of the glycolytic enzyme pyruvate kinase M2 (PKM2)⁽⁴⁸⁾, leading to the accumulation of the TCA intermediate succinate, stabilization of hypoxia-inducible factor 1 α (HIF-1 α) and production of IL-1 β , all of which could be abrogated by inhibiting glycolysis using 2-deoxyglucose (2DG)⁽⁴⁹⁾. Due to this redirection of mitochondrial metabolic flux, the TCA cycle has since referred to as being 'broken' in M1 macrophages. In addition to succinate, a second break in the TCA cycle occurs after citrate in these cells⁽⁵⁰⁾, which supports

pro-inflammatory M1 macrophage function through synthesis of fatty acids⁽⁵¹⁾ and the immunomodulatory metabolite itaconate⁽⁵²⁾. IL-4-induced M2 macrophage polarization, in contrast, is associated with increased OXPHOS and fatty acid oxidation⁽⁵³⁾ through activation of pathways downstream of signal transducer and activator of transcription 6 (STAT6) and peroxisome proliferator-activated receptor γ (PPAR- γ) coactivator 1 β (PGC-1 β)⁽⁵⁴⁾. However, metabolic rewiring during myeloid cell activation cannot simply be reduced to glycolysis versus oxidative phosphorylation as it strongly depends on the specific immunogenic stimuli which were used^(55,56).

A Warburg-like shift towards glycolysis with associated HIF-1 α stabilization and IL-1 β production was also observed after *in vitro* *Mtb* infection in both murine and human macrophages^(57,58). In mice, alveolar macrophages utilizing fatty acid oxidation (FAO) were shown to be more permissive to *Mtb* replication compared to glycolytic interstitial macrophages⁽⁵⁹⁾. Treatment with 2DG, an inhibitor of glycolysis, or etomoxir, an inhibitor of FAO, respectively increased and decreased bacterial growth, functionally linking glycolysis to improved *Mtb* control^(57,59). Interestingly, MDR W-Beijing *Mtb* strains were reported to overexpress phthiocerol dimycocerosate cell wall lipids (PDIMs) which dampen the glycolytic response and IL-1 β secretion through induction of IFN- β ⁽⁶⁰⁾, demonstrating direct mycobacterial modulation of macrophage immunometabolic pathways. In contrast, live *Mtb* infection was reported to result in an overall decreased bioenergetic phenotype in both THP-1 cells and primary human macrophages based on extensive metabolic flux analysis, including a diminished glycolytic rate, reduced lactate production and an increased mitochondrial dependency on fatty acids⁽⁶¹⁾. It has been proposed that these differences could be the result of a biphasic metabolic response of macrophages to *Mtb* infection, consisting of an early phase characterized by increased glycolysis and production of pro-inflammatory antimicrobial effector molecules, followed by a later phase of adaptation/resolution with intensified oxidative metabolism and decreased antimicrobial responses⁽⁶²⁾. However, more definitive evidence for this model will require additional longitudinal studies on the cellular metabolic dynamics during *Mtb* infection.

In addition to glycolysis, *Mtb* infection was found to be associated with other immunometabolic effects, including catabolism of amino acids. Arginine is an important metabolite involved in the antimicrobial response to *Mtb* as it fuels nitric oxide (NO) synthesis through inducible NO synthase (iNOS) in M1 macrophages⁽⁶³⁻⁶⁵⁾, a response which is limited by arginase 1 (Arg1) activity in murine M2 macrophages⁽⁶⁶⁾. In the absence of adequate levels of arginine, citrulline was shown to provide an alternative source of arginine for NO synthesis in response to *Mtb* infection⁽⁶⁷⁻⁶⁹⁾. Another key immunomodulatory amino acid is glutamine, the most abundant circulating free amino acid. Glutamine can be directly used as a substrate for the TCA cycle through glutaminolysis, which plays a major role in M2 macrophage polarization^(50,70). Both glutamine depletion and pharmacological inhibition of glutaminolysis decreased *in vitro* cytokine production of PBMCs in response

to *Mtb* lysate, and the transcriptional profile of TB patients and *Mtb*-infected macrophages showed marked changes in glutamine metabolism genes⁽⁷¹⁾, indicating a potential role for glutamine in the response to *Mtb*. Finally, tryptophan conversion to kynurenine by the immunoregulatory enzyme indoleamine 2,3-dioxygenase (IDO1/IDO2) was reported to support *Mtb* infection in a rhesus macaque infection model, as well as in isolated macrophages cocultured with CD4⁺ T cells⁽⁷²⁾, possibly by downregulating effector T cell functions⁽⁷³⁻⁷⁵⁾.

In conclusion, it has been unequivocally demonstrated that the functional outcome of macrophage activation is tightly interwoven with cellular metabolic state, and that the latter greatly impacts the outcome of *Mtb* infection. This raises the important question whether dysregulation of these processes as a consequences of metabolic diseases such as type 2 diabetes, a well-known risk factor for TB disease and TB severity, could be related to development TB.

Tuberculosis and diabetes: a reason for concern

The global burden of TB is heavily affected by several serious comorbidities which increase the risk of developing active disease, of which human immunodeficiency virus (HIV) co-infection has been the most prominent during the past decades. HIV infection leads to a 20-fold increased risk of disease reactivation (76). 920,000 people living with HIV developed TB in 2017, and 300,000 people died due to TB-HIV coinfection⁽²⁾. Other major TB-associated comorbidities include smoking, alcohol use, exposure to biomass fuel and malnourishment⁽⁷⁷⁾. However, an important TB risk factor which has only recently caught the public eye, despite having been previously described centuries ago⁽⁷⁸⁾, is diabetes mellitus (DM)⁽⁷⁹⁾. DM has been demonstrated to triple the risk of developing active TB disease (80), and approximately 15% of global TB cases can be attributed to concurrent TB-DM. While the number of TB deaths among HIV-infected patients has declined by 44% since 2000, the number of patients with concurrent TB-DM is predicted to rise dramatically as the number of people living with DM worldwide is estimated to increase by 48% during the coming 25 years, from 425 million people in 2017 to 629 million people in 2045⁽⁸¹⁾. The vast majority of this increase is expected to take place in TB-endemic low- and middle-income countries due to changes in lifestyle associated with economic development and urbanization. Furthermore, DM is associated with TB treatment failure and increased drug resistance, while active TB hampers management of glucose control⁽⁸²⁾. An international consortium, EC-FP7 supported TANDEM (www.tandem-fp7.eu), was initiated to unravel the relationships and potential mechanisms underlying concurrent TB-DM, and to optimize current treatment regimens and diagnosis⁽⁸³⁾.

DM is a metabolic disorder which is caused by either a lack of production of the glucose-regulating hormone insulin (type 1/T1DM) or the development of insulin resistance (type 2/T2DM), of which the latter comprises approximately 90% of global cases⁽⁸¹⁾. Both disease types are characterized by hyperglycemia due to the patient's inability

to control blood glucose levels. Clinical symptoms of DM include recurrent infections, weight gain, polyuria accompanied with excessive thirst, and impaired wound healing. Whereas T1DM is caused by an auto-immune reaction to pancreatic insulin-producing β -cells, the precise mechanisms underlying T2DM are not as clearly defined. Obesity and increasing weight are important risk factors for T2DM development, linking the disease with poor quality nutrition and physical inactivity, as well as family history⁽⁸⁴⁾. This clinical appearance is in stark contrast with the metabolic phenotype of TB patients, which is often accompanied by undernutrition and wasting syndrome⁽⁸⁵⁾. Through its association with obesity, many T2DM patients are also at high risk of cardiovascular complications such as atherosclerosis due to the presence of aberrations in blood lipid levels (dyslipidemia), including hypertriglyceridemia, hypertension and reduced levels high-density lipoprotein (HDL) cholesterol⁽⁸⁶⁾.

Insulin resistance does not only occur in the liver and skeletal muscle, the major organs involved in glucose metabolism, but also in the adipose tissue, kidneys, pancreas, gastrointestinal tract, vasculature and brain⁽⁸⁷⁾. Generally, the development of insulin resistance precedes T2DM by some time, placing increasing levels of stress on the pancreatic β -cells to produce more insulin which ultimately culminates in β -cell dysfunction⁽⁸⁸⁻⁹⁰⁾. Multiple molecular mechanisms of insulin resistance have been described, most of which are related to the phosphatidylinositol 3-kinase (PI3K) pathway⁽⁹¹⁾, a downstream signaling molecule of the insulin receptor. Binding of insulin to its receptor induces phosphorylation of insulin receptor substrates (IRS1 and IRS2), which bind to and activate PI3K⁽⁹²⁾, subsequently promoting translocation of glucose transporter 4 (GLUT4) protein to the cell surface. It has been demonstrated that increased serine phosphorylation of IRS proteins leads to insulin resistance by inhibiting tyrosine phosphorylation⁽⁹³⁾ and enhanced IRS protein degradation⁽⁹⁴⁾. Several factors contribute to this increased serine phosphorylation, including activation of protein kinase C (PKC) by accumulating diacylglycerol (DAG) due to ectopic lipid deposition in insulin-sensitive tissues⁽⁹⁵⁾, mitochondrial dysfunction⁽⁹⁶⁾ and systemic inflammation⁽⁹⁷⁾. Increased infiltration of immune cells and production of pro-inflammatory factors such as TNF- α have been linked to the development of insulin resistance in adipose tissue and in the liver, both in humans and in mice⁽⁹⁸⁾. Specifically, pro-inflammatory M1 macrophages and Th1 cells accumulate in adipose tissue during obesity, while numbers of anti-inflammatory M2 macrophages, Th2 and regulatory T cells (Treg) are reduced⁽⁹⁹⁻¹⁰¹⁾. Infiltrating macrophages induce adipocyte lipolysis, leading to high local levels of free saturated fatty acids (SFAs) which also contribute to local inflammation and insulin resistance⁽¹⁰²⁾, although the causal molecular mechanisms are still a topic of debate⁽¹⁰³⁾.

Potential mechanisms responsible for TB-DM disease interactions

While the association between TB and DM has been thoroughly established, the factors underlying this association remain largely unclear. From the above, it is evident that both diseases evoke distinct immunological and metabolic effects. Several studies have examined this interplay by exposing human immune cells to DM-associated conditions such as hyperglycemia, to analyze whether these conditions would disrupt immune responses to *Mtb* infection, while others compared the functional phenotypes of circulating leukocytes in diabetic TB patients or LTBI to normoglycemic controls.

Innate immunity: Monocytes from patients with poorly controlled DM displayed a reduced phagocytic capacity^(104, 105). A similar effect was observed in alveolar macrophages from mice with streptozotocin- or diet-induced diabetes, which showed reduced uptake of mycolic acid-coated beads as well as mycobacteria^(106, 107). This reduced phagocytic potential could negatively impact the capacity of antigen-presenting cells to control bacterial infection and to induce adaptive responses. Furthermore, TB-DM patients had decreased frequencies of circulating intermediate and classical monocytes as well as plasmacytoid and myeloid DCs compared to non-diabetic pulmonary TB patients, which normalized after anti-TB treatment^(108, 109). Other cells of the innate immune system with potentially compromised functions during DM are neutrophils and natural killer (NK) cells. The precise role of neutrophils during TB remains ambivalent, as they potentially contribute to disease protection through mycobacterial killing during early infection, but can also induce tissue damage through release of cytotoxic agents in later stages⁽¹¹⁰⁾. Increased neutrophil counts have been reported during TB-DM⁽¹¹¹⁾, however isolated neutrophils from DM patients displayed impaired mycobacterial phagocytosis⁽¹¹²⁾. Moreover, Prada-Medina *et al.* suggested a central role for neutrophilic inflammation in TB-DM based on Bayesian network analysis of cytokine and transcriptomics measurements from Indian patients⁽¹¹³⁾. NK cells regulate the anti-TB response in several ways, including supporting CD8⁺ effector T cell responses, enhancing phagocyte bactericidal function through secretion of IFN- γ and IL-22 and releasing antimicrobial effectors such as perforin and granulysin⁽¹¹⁴⁾. Importantly, peripheral NK cell numbers negatively correlated with lung inflammation at TB diagnosis, indicative of a relation between circulating NK levels and *Mtb* burden⁽¹¹⁵⁾. One study reported expansion of type 1 and type 17 cytokine-producing NK cell populations during TB-DM⁽¹¹⁶⁾, while others found reduced levels of circulating NK cells in these patients⁽¹¹⁷⁾. Interestingly, hyperactive NK cells contributed to inflammation and mortality in a mouse model of TB-DM by inducing IL-6 production in CD11c⁺ cells⁽¹¹⁸⁾.

Adaptive immunity: If innate immunity is indeed impaired as a result of TB-DM, this should also profoundly impact the induction of an ensuing adaptive immune response. Indeed, the adaptive response to *Mtb* was described to be further delayed in diabetic mice⁽¹¹⁹⁾, resulting in increased lung inflammation and bacterial burden⁽¹²⁰⁾. Th1, Th2 and Th17 cytokines were found to be decreased in LTBI with DM compared to normoglycemic controls with LTBI⁽¹²¹⁾. In contrast, several studies reported hyperinflammatory T cell

response in active TB patients with DM, including elevated TNF- α and IFN- γ production after whole blood stimulation ⁽¹²²⁾, increased circulating levels of pro-inflammatory Th1 and Th17 cytokines ⁽¹²³⁾ and elevated frequencies of central memory CD4⁺ and CD8⁺ T cells ⁽¹²⁴⁾. While circulating regulatory T cells were reportedly decreased during TB-DM ⁽¹²³⁾, Treg counts were found to be elevated in bronchoalveolar lavage fluid samples of TB-DM patients and associated with increased IL-10 but decreased IFN- γ concentrations ⁽¹²⁵⁾. Furthermore, T cells from hyperglycemic mice produced elevated levels of Th1, Th2 and Th17 cytokines due to hyperresponsiveness following T cell receptor ligation ⁽¹²⁶⁾. It has been suggested that these elevated inflammatory responses in TB-DM patients could be the result of an increased *Mtb* burden and be responsible for exacerbated lung pathology. Taken together, even though evidence in literature is somewhat conflicting, it can be clearly concluded that concurrent DM is associated with perturbations of both the innate and adaptive response during TB disease.

DM-induced metabolic changes: Mechanistically, several DM-associated factors have been suggested to contribute to dysfunctional immunity. High glucose levels were shown to reduce the phagocytic capacity of but to increase *Mtb* burden in macrophages ⁽¹²⁷⁾. In addition, hyperglycemia can lead to the formation of advanced glycation end-products (AGEs), which are pathologically glycosylated proteins or lipids that can modify cellular functions through binding to the AGE receptor (RAGE) ⁽¹²⁸⁾. Podell *et al.* *e.g.* reported that *Mtb* infection increased serum levels of AGEs in guinea pigs ⁽¹²⁹⁾. AGEs have been shown to induce oxidative stress and ROS production ^(130,131), inhibit NO synthesis ⁽¹³²⁾ and increase the expression of scavenger receptors such as CD36 by macrophages. CD36 is involved in the formation of lipid-loaded foam cells through uptake of oxidized low-density lipoprotein (oxLDL) ^(133, 134). In resemblance to AGEs, oxLDL is a pathologically modified lipoprotein which is elevated in patients with T2DM as a result of oxidative stress ^(135, 136). Interestingly, *Mtb* infection of guinea pigs was associated with oxLDL accumulation in granulomas and increased macrophage scavenger receptor expression, with enhanced mycobacterial replication in macrophages loaded with oxLDL *in vitro* ⁽¹³⁷⁾. A major contributor to oxidative stress in DM is reduced synthesis of glutathione (GSH), a tripeptide of glutamate, cysteine and glycine with strong antioxidative properties. GSH levels were found to be reduced in TB patients and infected guinea pigs ^(138, 139). As GSH has been demonstrated to have direct antimicrobial effects and to support macrophage control of *Mtb* ⁽¹⁴⁰⁻¹⁴²⁾, decreased levels of GSH could potentially contribute to TB-DM pathogenesis ^(143, 144). Finally, DM and obesity are associated with dysbiosis of the gut microbiome leading to alterations in species which produce short-chain fatty acids (SCFAs) ^(145, 146), bacterial metabolites with immunomodulatory capacities ⁽¹⁴⁷⁾. TB patients showed increased frequencies of butyrate- and propionate-producing bacteria in the gut ⁽¹⁴⁸⁾, and butyrate treatment decreased the production of pro-inflammatory cytokines while increasing IL-10 secretion in PBMCs stimulated with *Mtb* lysate ⁽¹⁴⁹⁾, warranting further research into possible dysregulation of gut microbiota during TB-DM.

Specific metabolites: An alternative method which could illuminate potential metabolic components of TB-DM pathophysiology is the use of metabolomics to identify specific alterations in patients associated with disease. Metabolomics is defined as the study of the metabolome, which constitutes the complete collection of small molecule intermediates of metabolism, commonly known as metabolites, within biological samples. The value of this approach is clearly demonstrated by a recent study from Weiner *et al.* that described a prognostic metabolite signature with good predictive power within 5 months of TB diagnosis⁽¹⁵⁰⁾. Remarkably, specific changes could already be detected at 12 months before onset of disease, which included elevated levels of cortisol. Several studies reported that TB is associated with elevated kynurenine and decreased tryptophan levels⁽¹⁵¹⁻¹⁵³⁾ indicative of increased IDO activity, illustrating how metabolomics measurements can reflect the involvement of relevant immunological mechanisms. However, studies which have analyzed the combined effect of TB and DM on patient metabolic profiles are currently lacking. It would especially be of interest to study measures of lipid metabolism in these patients, as DM and obesity are often associated increased circulating levels of lipids and cholesterol while hypercholesterolemia and dysregulated lipid metabolism are associated with hampered TB immunity and granuloma progression⁽¹⁵⁴⁻¹⁵⁷⁾.

Taken together, concurrent TB-DM and DM-associated metabolic changes are clearly related to alterations in both the innate and the adaptive immune response, although their respective contributions to increased risk of active disease is unclear at present. Extensive analysis of patient materials and *in vitro* infection experiments are required to elucidate the innerworkings of TB-DM comorbidity, which brings us to the outline of this thesis.

Thesis outline

The aim of this thesis was to unravel the pathophysiological mechanisms underlying TB-DM comorbidity, for which we employed several approaches. For the majority of our *in vitro* experiments, we utilized a primary human macrophage model of *Mtb* infection. In **Chapter 2**, we first performed a comparative phenotypic, innate and adaptive functional analysis of various forms/subsets of M ϕ 2 macrophage polarization. We identify M ϕ 2b macrophages (polarized in the presence of LPS and immune complexes) as a subset with potent antimycobacterial capabilities. M ϕ 2b differentiation could be a target for host-directed therapy in intracellular infections.

Secondly, we investigated whether metabolic conditions associated with DM could modulate macrophage activation and function in the context of *Mtb* infection. In **Chapter 3**, we investigated the effect of hyperglycemia on cytokine secretion and *Mtb* infection. We report that PBMCs and macrophages cultured under high glucose conditions showed increased production of several cytokines after stimulation (TNF- α , IL-1 β , IL-6 and IL-10). However, *Mtb* survival or outgrowth was not affected by high glucose levels *in vitro*. In **Chapter 4**, we studied the impact of oxLDL on macrophage function and

infection with *Mtb*. We show that oxLDL treatment induced foamy macrophage formation which supported mycobacterial survival through lysosomal cholesterol accumulation and subsequent dysfunction.

Thirdly, we used metabolomics to dissect the relative impact of TB and TB-DM on patients' *ex vivo* metabolic profiles. In **Chapter 5**, we utilized a NMR biomarker profiling platform to analyze circulating levels of amongst others lipids and amino acids in plasma samples of TB, TB-DM and DM patients from South Africa. We find that TB-DM patients possess metabolic characteristics of both diseases and that these are associated with an overall pro-atherogenic plasma lipid profile. We further expand upon the current knowledge of TB metabolomics in **Chapter 6** by measuring plasma concentrations of amines and acylcarnitines in TB and TB-DM patients from Indonesia.

Fourthly, we studied the direct effects of *Mtb* infection on macrophage metabolism to identify new and relevant host metabolic pathways modulated by infection. **Chapter 7** describes the combined results of Seahorse metabolic flux analyses, RNA-seq and (un)targeted cellular metabolomics of *Mtb*-stimulated/-infected macrophages. We find that *Mtb* greatly impacts macrophage metabolism, and highlight specific cellular pathways and metabolic intermediates which are altered as a result of infection.

Finally, the overall results and conclusions of this thesis are summarized and discussed in the concluding **Chapter 8**.

References

1. Hershkovitz I, Donoghue HD, Minnikin DE, Besra GS, Lee OY, Gernaey AM, et al. Detection and molecular characterization of 9,000-year-old *Mycobacterium tuberculosis* from a Neolithic settlement in the Eastern Mediterranean. *PloS one*. 2008;3(10):e3426.
2. World Health Organization. *Global Tuberculosis Report*. Geneva, Switzerland: 2018.
3. Coppola M, van den Eeden SJF, Robbins N, Wilson L, Franken K, Adams LB, et al. Vaccines for Leprosy and Tuberculosis: Opportunities for Shared Research, Development, and Application. *Frontiers in immunology*. 2018;9:308.
4. Van Der Meeren O, Hatherill M, Nduba V, Wilkinson RJ, Muyoyeta M, Van Brakel E, et al. Phase 2b Controlled Trial of M72/AS01E Vaccine to Prevent Tuberculosis. *N Engl J Med*. 2018;379(17):1621-34.
5. Nemes E, Geldenhuys H, Rozot V, Rutkowski KT, Ratangee F, Bilek N, et al. Prevention of *M. tuberculosis* Infection with H4:IC31 Vaccine or BCG Revaccination. *N Engl J Med*. 2018;379(2):138-49.
6. Russell DG, Cardona PJ, Kim MJ, Allain S, Altare F. Foamy macrophages and the progression of the human tuberculosis granuloma. *Nature immunology*. 2009;10(9):943-8.
7. Houben RM, Dodd PJ. The Global Burden of Latent Tuberculosis Infection: A Re-estimation Using Mathematical Modelling. *PLoS Med*. 2016;13(10):e1002152.
8. Keane J, Gershon S, Wise RP, Mirabile-Levens E, Kasznica J, Schwieterman WD, et al. Tuberculosis associated with infliximab, a tumor necrosis factor alpha-neutralizing agent. *N Engl J Med*. 2001;345(15):1098-104.
9. Lin PL, Myers A, Smith L, Bigbee C, Bigbee M, Fuhrman C, et al. Tumor necrosis factor neutralization results in disseminated disease in acute and latent *Mycobacterium tuberculosis* infection with normal granuloma structure in a cynomolgus macaque model. *Arthritis Rheum*. 2010;62(2):340-50.
10. Cooper AM, Dalton DK, Stewart TA, Griffin JP, Russell DG, Orme IM. Disseminated tuberculosis in interferon gamma gene-disrupted mice. *The Journal of experimental medicine*. 1993;178(6):2243-7.
11. Jouanguy E, Lamhamedi-Cherradi S, Altare F, Fondaneche MC, Tuerlinckx D, Blanche S, et al. Partial interferon-gamma receptor 1 deficiency in a child with tuberculoid bacillus Calmette-Guerin infection and a sibling with clinical tuberculosis. *The Journal of clinical investigation*. 1997;100(11):2658-64.
12. Bustamante J, Boisson-Dupuis S, Abel L, Casanova JL. Mendelian susceptibility to mycobacterial disease: genetic, immunological, and clinical features of inborn errors of IFN-gamma immunity. *Semin Immunol*. 2014;26(6):454-70.
13. Martinez-Barricarte R, Markle JG, Ma CS, Deenick EK, Ramirez-Alejo N, Mele F, et al. Human IFN-gamma immunity to mycobacteria is governed by both IL-12 and IL-23. *Sci Immunol*. 2018;3(30).

14. Basaraba RJ, Hunter RL. Pathology of Tuberculosis: How the Pathology of Human Tuberculosis Informs and Directs Animal Models. *Microbiol Spectr*. 2017;5(3).
15. Seto S, Tsujimura K, Koide Y. Rab GTPases regulating phagosome maturation are differentially recruited to mycobacterial phagosomes. *Traffic*. 2011;12(4):407-20.
16. Kuijl C, Savage ND, Marsman M, Tuin AW, Janssen L, Egan DA, et al. Intracellular bacterial growth is controlled by a kinase network around PKB/AKT1. *Nature*. 2007;450(7170):725-30.
17. Queval CJ, Song OR, Carralot JP, Saliou JM, Bongiovanni A, Deloison G, et al. Mycobacterium tuberculosis Controls Phagosomal Acidification by Targeting CISH-Mediated Signaling. *Cell reports*. 2017;20(13):3188-98.
18. Koster S, Upadhyay S, Chandra P, Papavinasasundaram K, Yang G, Hassan A, et al. Mycobacterium tuberculosis is protected from NADPH oxidase and LC3-associated phagocytosis by the LCP protein CpsA. *Proceedings of the National Academy of Sciences of the United States of America*. 2017;114(41):E8711-E20.
19. Simeone R, Bobard A, Lippmann J, Bitter W, Majlessi L, Brosch R, et al. Phagosomal rupture by Mycobacterium tuberculosis results in toxicity and host cell death. *PLoS pathogens*. 2012;8(2):e1002507.
20. Augenreich J, Arbues A, Simeone R, Haanappel E, Wegener A, Sayes F, et al. ESX-1 and phthiocerol dimycocerosates of Mycobacterium tuberculosis act in concert to cause phagosomal rupture and host cell apoptosis. *Cellular microbiology*. 2017;19(7).
21. van der Wel N, Hava D, Houben D, Fluitsma D, van Zon M, Pierson J, et al. M. tuberculosis and M. leprae translocate from the phagolysosome to the cytosol in myeloid cells. *Cell*. 2007;129(7):1287-98.
22. Houben D, Demangel C, van Ingen J, Perez J, Baldeon L, Abdallah AM, et al. ESX-1-mediated translocation to the cytosol controls virulence of mycobacteria. *Cellular microbiology*. 2012;14(8):1287-98.
23. Behar SM, Baehrecke EH. Tuberculosis: Autophagy is not the answer. *Nature*. 2015;528(7583):482-3.
24. Collins AC, Cai H, Li T, Franco LH, Li XD, Nair VR, et al. Cyclic GMP-AMP Synthase Is an Innate Immune DNA Sensor for Mycobacterium tuberculosis. *Cell host & microbe*. 2015;17(6):820-8.
25. Watson RO, Bell SL, MacDuff DA, Kimmey JM, Diner EJ, Olivas J, et al. The Cytosolic Sensor cGAS Detects Mycobacterium tuberculosis DNA to Induce Type I Interferons and Activate Autophagy. *Cell host & microbe*. 2015;17(6):811-9.
26. Jia J, Abudu YP, Claude-Taupin A, Gu Y, Kumar S, Choi SW, et al. Galectins Control mTOR in Response to Endomembrane Damage. *Mol Cell*. 2018;70(1):120-35 e8.
27. Mittal E, Skowyra ML, Uwase G, Tinaztepe E, Mehra A, Koster S, et al. Mycobacterium tuberculosis Type VII Secretion System Effectors Differentially Impact the ESCRT Endomembrane Damage Response. *MBio*. 2018;9(6).
28. Manzanillo PS, Ayres JS, Watson RO, Collins AC, Souza G, Rae CS, et al. The ubiquitin ligase parkin mediates resistance to intracellular pathogens. *Nature*. 2013;501(7468):512-6.

29. Franco LH, Nair VR, Scharn CR, Xavier RJ, Torrealba JR, Shiloh MU, et al. The Ubiquitin Ligase Smurf1 Functions in Selective Autophagy of Mycobacterium tuberculosis and Anti-tuberculous Host Defense. *Cell host & microbe*. 2017;21(1):59-72.
30. van der Vaart M, Korbee CJ, Lamers GE, Tengeler AC, Hosseini R, Haks MC, et al. The DNA damage-regulated autophagy modulator DRAM1 links mycobacterial recognition via TLR-MYD88 to autophagic defense (corrected]. *Cell host & microbe*. 2014;15(6):753-67.
31. Ouimet M, Koster S, Sakowski E, Ramkhelawon B, van Solingen C, Oldebeken S, et al. Mycobacterium tuberculosis induces the miR-33 locus to reprogram autophagy and host lipid metabolism. *Nature immunology*. 2016;17(6):677-86.
32. Etna MP, Sinigaglia A, Grassi A, Giacomini E, Romagnoli A, Pardini M, et al. Mycobacterium tuberculosis-induced miR-155 subverts autophagy by targeting ATG3 in human dendritic cells. *PLoS pathogens*. 2018;14(1):e1006790.
33. Harris J, De Haro SA, Master SS, Keane J, Roberts EA, Delgado M, et al. T helper 2 cytokines inhibit autophagic control of intracellular Mycobacterium tuberculosis. *Immunity*. 2007;27(3):505-17.
34. Mackaness GB. Cellular resistance to infection. *The Journal of experimental medicine*. 1962;116:381-406.
35. Doyle AG, Herbein G, Montaner LJ, Minty AJ, Caput D, Ferrara P, et al. Interleukin-13 alters the activation state of murine macrophages in vitro: comparison with interleukin-4 and interferon-gamma. *Eur J Immunol*. 1994;24(6):1441-5.
36. Mills CD, Kincaid K, Alt JM, Heilman MJ, Hill AM. M-1/M-2 macrophages and the Th1/Th2 paradigm. *Journal of immunology*. 2000;164(12):6166-73.
37. Verreck FA, de BT, Langenberg DM, Hoeve MA, Kramer M, Vaisberg E, et al. Human IL-23-producing type 1 macrophages promote but IL-10-producing type 2 macrophages subvert immunity to (myco)bacteria. *Proc Natl Acad Sci USA*. 2004;101(13):4560-5.
38. Verreck FA, de BT, Langenberg DM, van der Zanden L, Ottenhoff TH. Phenotypic and functional profiling of human proinflammatory type-1 and anti-inflammatory type-2 macrophages in response to microbial antigens and IFN-gamma- and CD40L-mediated costimulation. *J Leukoc Biol*. 2006;79(2):285-93.
39. Mantovani A, Sica A, Sozzani S, Allavena P, Vecchi A, Locati M. The chemokine system in diverse forms of macrophage activation and polarization. *Trends Immunol*. 2004;25(12):677-86.
40. Xue J, Schmidt SV, Sander J, Draffehn A, Krebs W, Quester I, et al. Transcriptome-based network analysis reveals a spectrum model of human macrophage activation. *Immunity*. 2014;40(2):274-88.
41. Ginhoux F, Jung S. Monocytes and macrophages: developmental pathways and tissue homeostasis. *Nature reviews Immunology*. 2014;14(6):392-404.
42. Murray PJ, Allen JE, Biswas SK, Fisher EA, Gilroy DW, Goerdt S, et al. Macrophage Activation and Polarization: Nomenclature and Experimental Guidelines. *Immunity*. 2014;41(1):14-20.
43. Ginhoux F, Schultze JL, Murray PJ, Ochando J, Biswas SK. New insights into the multidimensional concept of macrophage ontogeny, activation and function. *Nature immunology*. 2016;17(1):34-40.

44. Warburg O. On the origin of cancer cells. *Science*. 1956;123(3191):309-14.
45. Warburg O, Wind F, Negelein E. The Metabolism of Tumors in the Body. *J Gen Physiol*. 1927;8(6):519-30.
46. Rodriguez-Prados JC, Traves PG, Cuenca J, Rico D, Aragones J, Martin-Sanz P, et al. Substrate fate in activated macrophages: a comparison between innate, classic, and alternative activation. *Journal of immunology*. 2010;185(1):605-14.
47. Krawczyk CM, Holowka T, Sun J, Blagih J, Amiel E, DeBerardinis RJ, et al. Toll-like receptor-induced changes in glycolytic metabolism regulate dendritic cell activation. *Blood*. 2010;115(23):4742-9.
48. Palsson-McDermott EM, Curtis AM, Goel G, Lauterbach MA, Sheedy FJ, Gleeson LE, et al. Pyruvate kinase M2 regulates Hif-1alpha activity and IL-1beta induction and is a critical determinant of the warburg effect in LPS-activated macrophages. *Cell Metab*. 2015;21(1):65-80.
49. Tannahill GM, Curtis AM, Adamik J, Palsson-McDermott EM, McGettrick AF, Goel G, et al. Succinate is an inflammatory signal that induces IL-1beta through HIF-1alpha. *Nature*. 2013;496(7444):238-42.
50. Jha AK, Huang SC, Sergushichev A, Lampropoulou V, Ivanova Y, Loginicheva E, et al. Network integration of parallel metabolic and transcriptional data reveals metabolic modules that regulate macrophage polarization. *Immunity*. 2015;42(3):419-30.
51. Wei X, Song H, Yin L, Rizzo MG, Sidhu R, Covey DF, et al. Fatty acid synthesis configures the plasma membrane for inflammation in diabetes. *Nature*. 2016;539(7628):294-8.
52. Michelucci A, Cordes T, Ghelfi J, Pailot A, Reiling N, Goldmann O, et al. Immune-responsive gene 1 protein links metabolism to immunity by catalyzing itaconic acid production. *Proceedings of the National Academy of Sciences of the United States of America*. 2013;110(19):7820-5.
53. Huang SC, Everts B, Ivanova Y, O'Sullivan D, Nascimento M, Smith AM, et al. Cell-intrinsic lysosomal lipolysis is essential for alternative activation of macrophages. *Nature immunology*. 2014;15(9):846-55.
54. Vats D, Mukundan L, Odegaard JI, Zhang L, Smith KL, Morel CR, et al. Oxidative metabolism and PGC-1beta attenuate macrophage-mediated inflammation. *Cell Metab*. 2006;4(1):13-24.
55. Stienstra R, Netea-Maier RT, Riksen NP, Joosten LAB, Netea MG. Specific and Complex Reprogramming of Cellular Metabolism in Myeloid Cells during Innate Immune Responses. *Cell Metab*. 2017;26(1):142-56.
56. Lachmandas E, Boutens L, Ratter JM, Hijmans A, Hooiveld GJ, Joosten LA, et al. Microbial stimulation of different Toll-like receptor signalling pathways induces diverse metabolic programmes in human monocytes. *Nature microbiology*. 2016;2:16246.
57. Gleeson LE, Sheedy FJ, Palsson-McDermott EM, Triglia D, O'Leary SM, O'Sullivan MP, et al. Cutting Edge: Mycobacterium tuberculosis Induces Aerobic Glycolysis in Human Alveolar Macrophages That Is Required for Control of Intracellular Bacillary Replication. *Journal of immunology*. 2016;196(6):2444-9.

58. Braverman J, Sogi KM, Benjamin D, Nomura DK, Stanley SA. HIF-1alpha Is an Essential Mediator of IFN-gamma-Dependent Immunity to Mycobacterium tuberculosis. *Journal of immunology*. 2016;197(4):1287-97.
59. Huang L, Nazarova EV, Tan S, Liu Y, Russell DG. Growth of Mycobacterium tuberculosis in vivo segregates with host macrophage metabolism and ontogeny. *The Journal of experimental medicine*. 2018;215(4):1135-52.
60. Howard NC, Marin ND, Ahmed M, Rosa BA, Martin J, Bambouskova M, et al. Mycobacterium tuberculosis carrying a rifampicin drug resistance mutation reprograms macrophage metabolism through cell wall lipid changes. *Nature microbiology*. 2018;3(10):1099-108.
61. Cumming BM, Addicott KW, Adamson JH, Steyn AJ. Mycobacterium tuberculosis induces decelerated bioenergetic metabolism in human macrophages. *Elife*. 2018;7.
62. Shi L, Jiang Q, Bushkin Y, Subbian S, Tyagi S. Biphasic Dynamics of Macrophage Immunometabolism during Mycobacterium tuberculosis Infection. *MBio*. 2019;10(2).
63. Van den Bossche J, Baardman J, Otto NA, van der Velden S, Neele AE, van den Berg SM, et al. Mitochondrial Dysfunction Prevents Repolarization of Inflammatory Macrophages. *Cell reports*. 2016;17(3):684-96.
64. Munder M, Eichmann K, Modolell M. Alternative metabolic states in murine macrophages reflected by the nitric oxide synthase/arginase balance: competitive regulation by CD4+ T cells correlates with Th1/Th2 phenotype. *Journal of immunology*. 1998;160(11):5347-54.
65. MacMicking JD, North RJ, LaCourse R, Mudgett JS, Shah SK, Nathan CF. Identification of nitric oxide synthase as a protective locus against tuberculosis. *Proceedings of the National Academy of Sciences of the United States of America*. 1997;94(10):5243-8.
66. El Kasmi KC, Qualls JE, Pesce JT, Smith AM, Thompson RW, Henao-Tamayo M, et al. Toll-like receptor-induced arginase 1 in macrophages thwarts effective immunity against intracellular pathogens. *Nature immunology*. 2008;9(12):1399-406.
67. Rapovy SM, Zhao J, Bricker RL, Schmidt SM, Setchell KD, Qualls JE. Differential Requirements for L-Citrulline and L-Arginine during Antimycobacterial Macrophage Activity. *Journal of immunology*. 2015;195(7):3293-300.
68. Qualls JE, Subramanian C, Rafi W, Smith AM, Balouzian L, DeFreitas AA, et al. Sustained generation of nitric oxide and control of mycobacterial infection requires argininosuccinate synthase 1. *Cell host & microbe*. 2012;12(3):313-23.
69. Lange SM, McKell MC, Schmidt SM, Zhao J, Crowther RR, Green LC, et al. L-Arginine Synthesis from L-Citrulline in Myeloid Cells Drives Host Defense against Mycobacteria In Vivo. *Journal of immunology*. 2019.
70. Liu PS, Wang H, Li X, Chao T, Teav T, Christen S, et al. alpha-ketoglutarate orchestrates macrophage activation through metabolic and epigenetic reprogramming. *Nature immunology*. 2017;18(9):985-94.
71. Koeken V, Lachmandas E, Riza A, Matzaraki V, Li Y, Kumar V, et al. Role of Glutamine Metabolism in Host Defense Against Mycobacterium tuberculosis Infection. *J Infect Dis*. 2019;219(10):1662-70.

72. Gautam US, Foreman TW, Bucsan AN, Veatch AV, Alvarez X, Adekambi T, et al. In vivo inhibition of tryptophan catabolism reorganizes the tuberculoma and augments immune-mediated control of *Mycobacterium tuberculosis*. *Proceedings of the National Academy of Sciences of the United States of America*. 2018;115(1):E62-E71.
73. Munn DH, Sharma MD, Lee JR, Jhaver KG, Johnson TS, Keskin DB, et al. Potential regulatory function of human dendritic cells expressing indoleamine 2,3-dioxygenase. *Science*. 2002;297(5588):1867-70.
74. Terness P, Bauer TM, Rose L, Dufter C, Watzlik A, Simon H, et al. Inhibition of allogeneic T cell proliferation by indoleamine 2,3-dioxygenase-expressing dendritic cells: mediation of suppression by tryptophan metabolites. *The Journal of experimental medicine*. 2002;196(4):447-57.
75. Fallarino F, Grohmann U, You S, McGrath BC, Cavener DR, Vacca C, et al. Tryptophan catabolism generates autoimmune-preventive regulatory T cells. *Transpl Immunol*. 2006;17(1):58-60.
76. Pawlowski A, Jansson M, Skold M, Rottenberg ME, Kallenius G. Tuberculosis and HIV co-infection. *PLoS pathogens*. 2012;8(2):e1002464.
77. Dheda K, Barry CE, 3rd, Maartens G. Tuberculosis. *Lancet*. 2016;387(10024):1211-26.
78. Morton R. *Phthisiologia: or a treatise of consumptions*. London: Smith and Walford; 1694.
79. Ronacher K, Joosten SA, van CR, Dockrell HM, Walzl G, Ottenhoff TH. Acquired immunodeficiencies and tuberculosis: focus on HIV/AIDS and diabetes mellitus. *ImmunolRev*. 2015;264(1):121-37.
80. Jeon CY, Murray MB. Diabetes mellitus increases the risk of active tuberculosis: a systematic review of 13 observational studies. *PLoS Med*. 2008;5(7):e152.
81. IDF Diabetes Atlas. 6th ed., Brussels, Belgium. International Diabetes Federation, 2013 2013. Report No.
82. van Crevel R, Koesoemadinata R, Hill PC, Harries AD. Clinical management of combined tuberculosis and diabetes. *Int J Tuberc Lung Dis*. 2018;22(12):1404-10.
83. van CR, Dockrell HM. TANDEM: understanding diabetes and tuberculosis. *Lancet Diabetes Endocrinol*. 2014;2(4):270-2.
84. DeFronzo RA. Banting Lecture. From the triumvirate to the ominous octet: a new paradigm for the treatment of type 2 diabetes mellitus. *Diabetes*. 2009;58(4):773-95.
85. Schwenk A, Macallan DC. Tuberculosis, malnutrition and wasting. *Curr Opin Clin Nutr Metab Care*. 2000;3(4):285-91.
86. Taskinen MR, Boren J. New insights into the pathophysiology of dyslipidemia in type 2 diabetes. *Atherosclerosis*. 2015;239(2):483-95.
87. DeFronzo RA, Ferrannini E, Groop L, Henry RR, Herman WH, Holst JJ, et al. Type 2 diabetes mellitus. *Nat Rev Dis Primers*. 2015;1:15019.
88. Weyer C, Bogardus C, Mott DM, Pratley RE. The natural history of insulin secretory dysfunction and insulin resistance in the pathogenesis of type 2 diabetes mellitus. *The Journal of clinical investigation*. 1999;104(6):787-94.

89. Cnop M, Vidal J, Hull RL, Utzschneider KM, Carr DB, Schraw T, et al. Progressive loss of beta-cell function leads to worsening glucose tolerance in first-degree relatives of subjects with type 2 diabetes. *Diabetes Care*. 2007;30(3):677-82.
90. Stancakova A, Javorsky M, Kuulasmaa T, Haffner SM, Kuusisto J, Laakso M. Changes in insulin sensitivity and insulin release in relation to glycemia and glucose tolerance in 6,414 Finnish men. *Diabetes*. 2009;58(5):1212-21.
91. Cusi K, Maezono K, Osman A, Pendergrass M, Patti ME, Pratipanawat T, et al. Insulin resistance differentially affects the PI 3-kinase- and MAP kinase-mediated signaling in human muscle. *The Journal of clinical investigation*. 2000;105(3):311-20.
92. Virkamaki A, Ueki K, Kahn CR. Protein-protein interaction in insulin signaling and the molecular mechanisms of insulin resistance. *The Journal of clinical investigation*. 1999;103(7):931-43.
93. Copps KD, White MF. Regulation of insulin sensitivity by serine/threonine phosphorylation of insulin receptor substrate proteins IRS1 and IRS2. *Diabetologia*. 2012;55(10):2565-82.
94. Hiratani K, Haruta T, Tani A, Kawahara J, Usui I, Kobayashi M. Roles of mTOR and JNK in serine phosphorylation, translocation, and degradation of IRS-1. *Biochem Biophys Res Commun*. 2005;335(3):836-42.
95. Itani SI, Ruderman NB, Schmieder F, Boden G. Lipid-induced insulin resistance in human muscle is associated with changes in diacylglycerol, protein kinase C, and I κ B α . *Diabetes*. 2002;51(7):2005-11.
96. Morino K, Petersen KF, Dufour S, Befroy D, Frattini J, Shatzkes N, et al. Reduced mitochondrial density and increased IRS-1 serine phosphorylation in muscle of insulin-resistant offspring of type 2 diabetic parents. *The Journal of clinical investigation*. 2005;115(12):3587-93.
97. Olefsky JM, Glass CK. Macrophages, inflammation, and insulin resistance. *Annu Rev Physiol*. 2010;72:219-46.
98. de Alvaro C, Teruel T, Hernandez R, Lorenzo M. Tumor necrosis factor alpha produces insulin resistance in skeletal muscle by activation of inhibitor kappaB kinase in a p38 MAPK-dependent manner. *The Journal of biological chemistry*. 2004;279(17):17070-8.
99. Lumeng CN, Bodzin JL, Saltiel AR. Obesity induces a phenotypic switch in adipose tissue macrophage polarization. *JClinInvest*. 2007;117(1):175-84.
100. Nishimura S, Manabe I, Nagasaki M, Eto K, Yamashita H, Ohsugi M, et al. CD8⁺ effector T cells contribute to macrophage recruitment and adipose tissue inflammation in obesity. *Nature medicine*. 2009;15(8):914-20.
101. Feuerer M, Herrero L, Cipolletta D, Naaz A, Wong J, Nayer A, et al. Lean, but not obese, fat is enriched for a unique population of regulatory T cells that affect metabolic parameters. *Nature medicine*. 2009;15(8):930-9.
102. Shi H, Kokoeva MV, Inouye K, Tzamelis I, Yin H, Flier JS. TLR4 links innate immunity and fatty acid-induced insulin resistance. *JClinInvest*. 2006;116(11):3015-25.
103. Lancaster GI, Langley KG, Berglund NA, Kammoun HL, Reibe S, Estevez E, et al. Evidence that TLR4 Is Not a Receptor for Saturated Fatty Acids but Mediates Lipid-Induced Inflammation by Reprogramming Macrophage Metabolism. *Cell Metab*. 2018;27(5):1096-110 e5.

104. Restrepo BI, Twahirwa M, Rahbar MH, Schlesinger LS. Phagocytosis via complement or Fc-gamma receptors is compromised in monocytes from type 2 diabetes patients with chronic hyperglycemia. *PLoSOne*. 2014;9(3):e92977.
105. Gomez DI, Twahirwa M, Schlesinger LS, Restrepo BI. Reduced Mycobacterium tuberculosis association with monocytes from diabetes patients that have poor glucose control. *Tuberculosis(Edinb)*. 2013;93(2):192-7.
106. Alim MA, Sikder S, Bridson TL, Rush CM, Govan BL, Ketheesan N. Anti-mycobacterial function of macrophages is impaired in a diet induced model of type 2 diabetes. *Tuberculosis (Edinb)*. 2017;102:47-54.
107. Martinez N, Ketheesan N, West K, Vallerskog T, Kornfeld H. Impaired Recognition of Mycobacterium tuberculosis by Alveolar Macrophages From Diabetic Mice. *J Infect Dis*. 2016;214(11):1629-37.
108. Kumar NP, Moideen K, Dhakshinraj SD, Banurekha VV, Nair D, Dolla C, et al. Profiling leucocyte subsets in tuberculosis-diabetes co-morbidity. *Immunology*. 2015;146(2):243-50.
109. Kumar NP, Moideen K, Sivakumar S, Menon PA, Viswanathan V, Kornfeld H, et al. Modulation of dendritic cell and monocyte subsets in tuberculosis-diabetes co-morbidity upon standard tuberculosis treatment. *Tuberculosis (Edinb)*. 2016;101:191-200.
110. Lowe DM, Redford PS, Wilkinson RJ, O'Garra A, Martineau AR. Neutrophils in tuberculosis: friend or foe? *Trends Immunol*. 2012;33(1):14-25.
111. Andrade BB, Kumar NP, Sridhar R, Banurekha VV, Jawahar MS, Nutman TB, et al. Heightened plasma levels of heme oxygenase-1 and tissue inhibitor of metalloproteinase-4 as well as elevated peripheral neutrophil counts are associated with TB-diabetes comorbidity. *Chest*. 2014;145(6):1244-54.
112. Raposo-Garcia S, Guerra-Laso JM, Garcia-Garcia S, Juan-Garcia J, Lopez-Fidalgo E, Diez-Tascon C, et al. Immunological response to Mycobacterium tuberculosis infection in blood from type 2 diabetes patients. *Immunol Lett*. 2017;186:41-5.
113. Prada-Medina CA, Fukutani KF, Pavan Kumar N, Gil-Santana L, Babu S, Lichtenstein F, et al. Systems Immunology of Diabetes-Tuberculosis Comorbidity Reveals Signatures of Disease Complications. *Sci Rep*. 2017;7(1):1999.
114. Choreno Parra JA, Martinez Zuniga N, Jimenez Zamudio LA, Jimenez Alvarez LA, Salinas Lara C, Zuniga J. Memory of Natural Killer Cells: A New Chance against Mycobacterium tuberculosis? *Frontiers in immunology*. 2017;8:967.
115. Roy Chowdhury R, Vallania F, Yang Q, Lopez Angel CJ, Darboe F, Penn-Nicholson A, et al. A multi-cohort study of the immune factors associated with M. tuberculosis infection outcomes. *Nature*. 2018;560(7720):644-8.
116. Kumar NP, Sridhar R, Nair D, Banurekha VV, Nutman TB, Babu S. Type 2 diabetes mellitus is associated with altered CD8(+) T and natural killer cell function in pulmonary tuberculosis. *Immunology*. 2015;144(4):677-86.
117. Medellin-Garibay SE, Cortez-Espinosa N, Milan-Segovia RC, Magana-Aquino M, Vargas-Morales JM, Gonzalez-Amaro R, et al. Clinical Pharmacokinetics of Rifampin in Patients with Tuberculosis

- and Type 2 Diabetes Mellitus: Association with Biochemical and Immunological Parameters. *Antimicrob Agents Chemother.* 2015;59(12):7707-14.
118. Cheekatla SS, Tripathi D, Venkatasubramanian S, Nathella PK, Paidipally P, Ishibashi M, et al. NK-CD11c+ Cell Crosstalk in Diabetes Enhances IL-6-Mediated Inflammation during *Mycobacterium tuberculosis* Infection. *PLoS pathogens.* 2016;12(10):e1005972.
 119. Vallerskog T, Martens GW, Kornfeld H. Diabetic mice display a delayed adaptive immune response to *Mycobacterium tuberculosis*. *Journal of immunology.* 2010;184(11):6275-82.
 120. Martens GW, Arikian MC, Lee J, Ren F, Greiner D, Kornfeld H. Tuberculosis susceptibility of diabetic mice. *AmJRespirCell MolBiol.* 2007;37(5):518-24.
 121. Kumar NP, George PJ, Kumaran P, Dolla CK, Nutman TB, Babu S. Diminished systemic and antigen-specific type 1, type 17, and other proinflammatory cytokines in diabetic and prediabetic individuals with latent *Mycobacterium tuberculosis* infection. *J Infect Dis.* 2014;210(10):1670-8.
 122. Restrepo BI, Fisher-Hoch SP, Pino PA, Salinas A, Rahbar MH, Mora F, et al. Tuberculosis in poorly controlled type 2 diabetes: altered cytokine expression in peripheral white blood cells. *ClinInfectDis.* 2008;47(5):634-41.
 123. Kumar NP, Sridhar R, Banurekha VV, Jawahar MS, Nutman TB, Babu S. Expansion of pathogen-specific T-helper 1 and T-helper 17 cells in pulmonary tuberculosis with coincident type 2 diabetes mellitus. *J Infect Dis.* 2013;208(5):739-48.
 124. Kumar NP, Moideen K, Viswanathan V, Kornfeld H, Babu S. Effect of standard tuberculosis treatment on naive, memory and regulatory T-cell homeostasis in tuberculosis-diabetes comorbidity. *Immunology.* 2016;149(1):87-97.
 125. Sun Q, Zhang Q, Xiao H, Cui H, Su B. Significance of the frequency of CD4+CD25+CD127- T-cells in patients with pulmonary tuberculosis and diabetes mellitus. *Respirology.* 2012;17(5):876-82.
 126. Martinez N, Vallerskog T, West K, Nunes-Alves C, Lee J, Martens GW, et al. Chromatin decondensation and T cell hyperresponsiveness in diabetes-associated hyperglycemia. *Journal of immunology.* 2014;193(9):4457-68.
 127. Montoya-Rosales A, Castro-Garcia P, Torres-Juarez F, Enciso-Moreno JA, Rivas-Santiago B. Glucose levels affect LL-37 expression in monocyte-derived macrophages altering the *Mycobacterium tuberculosis* intracellular growth control. *Microbial pathogenesis.* 2016;97:148-53.
 128. Goldin A, Beckman JA, Schmidt AM, Creager MA. Advanced glycation end products: sparking the development of diabetic vascular injury. *Circulation.* 2006;114(6):597-605.
 129. Podell BK, Ackart DF, Kirk NM, Eck SP, Bell C, Basaraba RJ. Non-diabetic hyperglycemia exacerbates disease severity in *Mycobacterium tuberculosis* infected guinea pigs. *PloS one.* 2012;7(10):e46824.
 130. Wautier MP, Chappey O, Corda S, Stern DM, Schmidt AM, Wautier JL. Activation of NADPH oxidase by AGE links oxidant stress to altered gene expression via RAGE. *Am J Physiol Endocrinol Metab.* 2001;280(5):E685-94.

131. Ding Y, Kantarci A, Hasturk H, Trackman PC, Malabanan A, Van Dyke TE. Activation of RAGE induces elevated O₂⁻ generation by mononuclear phagocytes in diabetes. *J Leukoc Biol.* 2007;81(2):520-7.
132. Bucala R, Tracey KJ, Cerami A. Advanced glycosylation products quench nitric oxide and mediate defective endothelium-dependent vasodilatation in experimental diabetes. *The Journal of clinical investigation.* 1991;87(2):432-8.
133. Kishikawa H, Mine S, Kawahara C, Tabata T, Hirose A, Okada Y, et al. Glycated albumin and cross-linking of CD44 induce scavenger receptor expression and uptake of oxidized LDL in human monocytes. *Biochem Biophys Res Commun.* 2006;339(3):846-51.
134. Iwashima Y, Eto M, Hata A, Kaku K, Horiuchi S, Ushikubi F, et al. Advanced glycation end products-induced gene expression of scavenger receptors in cultured human monocyte-derived macrophages. *Biochem Biophys Res Commun.* 2000;277(2):368-80.
135. Toshima S, Hasegawa A, Kurabayashi M, Itabe H, Takano T, Sugano J, et al. Circulating oxidized low density lipoprotein levels. A biochemical risk marker for coronary heart disease. *Arteriosclerosis, thrombosis, and vascular biology.* 2000;20(10):2243-7.
136. Njajou OT, Kanaya AM, Holvoet P, Connelly S, Strotmeyer ES, Harris TB, et al. Association between oxidized LDL, obesity and type 2 diabetes in a population-based cohort, the Health, Aging and Body Composition Study. *Diabetes/metabolism research and reviews.* 2009;25(8):733-9.
137. Palanisamy GS, Kirk NM, Ackart DF, Obregon-Henao A, Shanley CA, Orme IM, et al. Uptake and accumulation of oxidized low-density lipoprotein during Mycobacterium tuberculosis infection in guinea pigs. *PLoSOne.* 2012;7(3):e34148.
138. Venketaraman V, Millman A, Salman M, Swaminathan S, Goetz M, Lardizabal A, et al. Glutathione levels and immune responses in tuberculosis patients. *Microbial pathogenesis.* 2008;44(3):255-61.
139. Palanisamy GS, Kirk NM, Ackart DF, Shanley CA, Orme IM, Basaraba RJ. Evidence for oxidative stress and defective antioxidant response in guinea pigs with tuberculosis. *PloS one.* 2011;6(10):e26254.
140. Venketaraman V, Dayaram YK, Amin AG, Ngo R, Green RM, Talaue MT, et al. Role of glutathione in macrophage control of mycobacteria. *Infection and immunity.* 2003;71(4):1864-71.
141. Venketaraman V, Dayaram YK, Talaue MT, Connell ND. Glutathione and nitrosoglutathione in macrophage defense against Mycobacterium tuberculosis. *Infection and immunity.* 2005;73(3):1886-9.
142. Morris D, Guerra C, Khurasany M, Guilford F, Saviola B, Huang Y, et al. Glutathione supplementation improves macrophage functions in HIV. *J Interferon Cytokine Res.* 2013;33(5):270-9.
143. Tan KS, Lee KO, Low KC, Gamage AM, Liu Y, Tan GY, et al. Glutathione deficiency in type 2 diabetes impairs cytokine responses and control of intracellular bacteria. *J Clin Invest.* 2012;122(6):2289-300.
144. Lagman M, Ly J, Saing T, Kaur Singh M, Vera Tudela E, Morris D, et al. Investigating the causes for decreased levels of glutathione in individuals with type II diabetes. *PloS one.* 2015;10(3):e0118436.

145. Qin J, Li Y, Cai Z, Li S, Zhu J, Zhang F, et al. A metagenome-wide association study of gut microbiota in type 2 diabetes. *Nature*. 2012;490(7418):55-60.
146. Karlsson FH, Tremaroli V, Nookaew I, Bergstrom G, Behre CJ, Fagerberg B, et al. Gut metagenome in European women with normal, impaired and diabetic glucose control. *Nature*. 2013;498(7452):99-103.
147. Tan J, McKenzie C, Potamitis M, Thorburn AN, Mackay CR, Macia L. The role of short-chain fatty acids in health and disease. *Adv Immunol*. 2014;121:91-119.
148. Maji A, Misra R, Dhakan DB, Gupta V, Mahato NK, Saxena R, et al. Gut microbiome contributes to impairment of immunity in pulmonary tuberculosis patients by alteration of butyrate and propionate producers. *Environ Microbiol*. 2018;20(1):402-19.
149. Lachmandas E, van den Heuvel CN, Damen MS, Cleophas MC, Netea MG, van Crevel R. Diabetes Mellitus and Increased Tuberculosis Susceptibility: The Role of Short-Chain Fatty Acids. *Journal of diabetes research*. 2016;2016:6014631.
150. Weiner J, Maertzdorf J, Sutherland JS, Duffy FJ, Thompson E, Suliman S, et al. Metabolite changes in blood predict the onset of tuberculosis. *Nature communications*. 2018;9(1):5208.
151. Suzuki Y, Suda T, Asada K, Miwa S, Suzuki M, Fujie M, et al. Serum indoleamine 2,3-dioxygenase activity predicts prognosis of pulmonary tuberculosis. *Clin Vaccine Immunol*. 2012;19(3):436-42.
152. Feng S, Du YQ, Zhang L, Zhang L, Feng RR, Liu SY. Analysis of serum metabolic profile by ultra-performance liquid chromatography-mass spectrometry for biomarkers discovery: application in a pilot study to discriminate patients with tuberculosis. *Chin Med J (Engl)*. 2015;128(2):159-68.
153. Weiner J, 3rd, Parida SK, Maertzdorf J, Black GF, Repsilber D, Telaar A, et al. Biomarkers of inflammation, immunosuppression and stress with active disease are revealed by metabolomic profiling of tuberculosis patients. *PloS one*. 2012;7(7):e40221.
154. Martens GW, Arikian MC, Lee J, Ren F, Vallerskog T, Kornfeld H. Hypercholesterolemia impairs immunity to tuberculosis. *Infection and immunity*. 2008;76(8):3464-72.
155. Soh AZ, Chee CB, Wang YT, Yuan JM, Koh WP. Dietary Cholesterol Increases the Risk whereas PUFAs Reduce the Risk of Active Tuberculosis in Singapore Chinese. *J Nutr*. 2016;146(5):1093-100.
156. Kim MJ, Wainwright HC, Locketz M, Bekker LG, Walther GB, Dittrich C, et al. Caseation of human tuberculosis granulomas correlates with elevated host lipid metabolism. *EMBO molecular medicine*. 2010;2(7):258-74.
157. Lee W, VanderVen BC, Fahey RJ, Russell DG. Intracellular Mycobacterium tuberculosis exploits host-derived fatty acids to limit metabolic stress. *The Journal of biological chemistry*. 2013;288(10):6788-800.

CHAPTER

2

Human M ϕ 2b macrophages exert intracellular bacterial control while M ϕ 2a/c/d support T cell responses

Frank Vrieling^{1*}, Kimberley V. Walburg^{1*}, Jeroen de Keijzer²,
Krista E. van Meijgaarden¹, George M. Janssen², Simone A. Joosten¹,
Peter A. van Veelen², Tom H. M. Ottenhoff¹, and Mariëlle C. Haks¹

* Contributed equally

¹ Department of Infectious Diseases, Leiden University Medical Center, Leiden, The Netherlands.

² Center for Proteomics and Metabolomics, Leiden University Medical Center, Leiden, The Netherlands.

Macrophages are highly plastic myeloid cells with important functions in innate immunity, bacterial control and tissue homeostasis. While originally classified as either classically-activated (M ϕ 1) or alternatively-activated (M ϕ 2) cells, there recently has been increasing appreciation of macrophage diversity and plasticity. Nevertheless, phenotypic, functional and comparative characterization of key primary macrophage subsets, particularly in humans, is lacking. Here, we compared and evaluated primary human monocyte-derived DCs, M ϕ 1, M ϕ 2, M ϕ 2a, M ϕ 2b, M ϕ 2c and M ϕ 2d to uncover relevant different functionalities regarding antigen presentation and bacterial infection control. We identified M ϕ 2b as a polarized macrophage subset with reduced capacity to stimulate CD4⁺ T cell responses but with superior antimicrobial activity against both *Mycobacterium tuberculosis* and *Salmonella* Typhimurium. M ϕ 2b were characterized by elevated secretion of vascular endothelial growth factor (VEGF) and a marked type I interferon signature at both the transcriptomic and protein level. Importantly, M ϕ 2 subsets could be repolarized towards M ϕ 2b after initial differentiation, highlighting their potential for macrophage-centred host-directed treatment of infectious diseases.

Introduction

Tuberculosis (TB) is still one of the leading causes of death worldwide, with 1.6 million deaths recorded in 2017 ⁽¹⁾. TB is caused by infection with *Mycobacterium tuberculosis* (*Mtb*) and is transmitted through inhalation of bacteria-containing aerial particles formed during sneezing or coughing. *Mtb* primarily infects alveolar macrophages in the lung, in which it is able to persist by actively interfering with antimicrobial mechanisms of the host. Chemotactic signals derived from infected macrophages result in the recruitment of additional immune cells and fibroblasts which together form the early TB granuloma, a complex immunological structure that sequesters bacteria, often without achieving their complete eradication. *Mtb* can remain dormant in the granuloma for years ⁽²⁾. While physically and nutritionally restraining, the granulomatous environment can prove beneficial for the bacteria as the influx of immune cells provides further niches for replication. Reactivation occurs in approximately 3-10% of latently infected individuals and is associated with central necrosis of infected macrophages, leading to disintegration of the granuloma and dissemination of *Mtb*. The local balance of immunoregulatory mediators is thought to be of crucial importance for granuloma outcome as these determine macrophage activation ⁽³⁾.

Salmonella is another intracellular pathogen capable of infecting human macrophages and actively interfering with antimicrobial mechanisms of the host. Salmonella infections pose a major health problem worldwide and account for 93.8 million people falling ill and 155,000 deaths per year. Salmonellosis, both typhoidal and nontyphoidal, results from foodborne infections and represent 1 of the 4 key global causes of diarrhoeal diseases (the acute and most common symptom of foodborne infections). The severity of Salmonella infections depends on the serotype involved and the immune status of the human host, with children below the age of 5 years and elderly people being most susceptible ⁽⁴⁻⁶⁾.

Macrophages are characterized by remarkable plasticity as they can rapidly change their function in response to local immunoregulatory stimuli. Their polarization has been reported to affect both granuloma formation and outcome during *Mtb* infection *in vitro* and *in vivo* ^(7, 8). However, it remains unclear which specific macrophage subsets are beneficial or detrimental for clearance of *Mtb* or other intracellular bacteria such as Salmonella. Initially, two diametrically opposed types of macrophages were described, namely classically activated macrophages (M ϕ 1) and alternatively activated macrophages (M ϕ 2) ⁽⁹⁾. Our laboratory demonstrated that these distinct macrophage phenotypes can be generated from the same monocytic precursor ^(10, 11) by *in vitro* differentiation of human monocytes in the presence of either granulocyte-macrophage colony-stimulating factor (GM-CSF; M ϕ 1) or macrophage colony-stimulating factor (M-CSF; M ϕ 2) ^(10, 12). M ϕ 1 are characterized by the production of pro-inflammatory cytokines upon stimulation, e.g. with lipopolysaccharide (LPS), produce interleukin (IL)-12p40, IL-23 and tumour necrosis factor- α (TNF- α) and efficiently present (myco)bacterial antigens to support Th1 responses ^(10, 11),

thus promoting effective host immune defence. In contrast, M ϕ 2 are known to secrete anti-inflammatory cytokines such as IL-10 upon activation and perform various tissue-maintenance functions *in vivo* ⁽¹³⁾. Furthermore, they are potent inducers of regulatory T cell (T_{reg}) responses ⁽¹⁴⁾ and possess relatively poor antigen-presenting capacities for Th1 cells (10). Macrophage polarization towards either end of the inflammatory spectrum can have detrimental effects during a spectrum of diseases ⁽¹⁵⁾. For instance, accumulation of M ϕ 1 in adipose tissue or atherosclerotic plaques promotes insulin resistance and atherosclerosis, respectively ^(16, 17) while immunosuppressive M ϕ 2-like macrophages can contribute to the development of leprosy lesions and different types of tumours ⁽¹⁸⁻²¹⁾.

Recent studies have demonstrated that the original dichotomous view of macrophage activation described above does not accurately reflect the *in vivo* situation, in which precursor monocytes are subjected to a much broader range of tissue-specific stimuli ⁽²²⁻²⁴⁾. Mantovani *et al.* proposed an alternative nomenclature which distinguishes four different M ϕ 2 polarized states termed M ϕ 2a to M ϕ 2d ⁽²⁵⁾. M ϕ 2a are induced by the T helper 2 (Th2) cell cytokines IL-4 and IL-13 and play a role in the integration and promotion of Th2 responses and angiogenesis ^(26, 27). M ϕ 2b are also known as regulatory macrophages because of their high production of IL-10 ^(28, 29) and can be induced by combined exposure to immune complexes and Toll-like receptor (TLR) or IL-1-receptor-agonists ⁽³⁰⁾. M ϕ 2c are induced by IL-10 and/or glucocorticoids ⁽³¹⁾ and were shown to have superior T_{reg}-inducing capacities compared to M ϕ 2a ⁽³²⁾. Furthermore, they can efficiently clear apoptotic cells because of their relatively high expression of the MER Receptor Tyrosine Kinase (MerTK) (33). Another variant of the alternatively activated macrophages are the M ϕ 2d or tumour-associated macrophages (TAMs), which exhibit pro-tumoral functions ^(34, 35). TAMs are recruited and polarized by several factors present in the tumour microenvironment, of which Prostaglandin E2 (PGE2) and IL-6 have been recognized to be of great importance ^(36, 37). However, many of these studies were performed using murine macrophages, and appropriate translation to human conditions is mostly lacking.

In addition, to the best of our knowledge, the different macrophage subsets have not yet been analysed in-depth side by side, and consequently subset specific phenotypic markers to accurately distinguish them *in vivo* are lacking. Here, we identify M ϕ 2b as a subset that outperforms other macrophage subsets in controlling intracellular bacteria, including *Mtb* and *Salmonella enterica* serovar Typhimurium (*Stm*), while showing minor T cell activating capacities, suggesting a strong innate immune profile capable of limiting bacterial outgrowth. Indeed, subsequent proteomic and transcriptional profiling revealed that M ϕ 2b express a marked type I interferon signature both at baseline and during infection. Importantly, we demonstrate that other M ϕ 2 subsets can be repolarized towards an M ϕ 2b phenotype after initial differentiation, reinforcing the potential of targeting macrophage differentiation as a therapeutic approach for human infectious diseases.

Materials & Methods

Ethics statement

The use of buffy coats for research purposes was approved by the Institutional Review Board of the Leiden University Medical Center, The Netherlands. Buffy coats were collected from healthy anonymous blood bank donors (Dutch, adults) that had signed written informed consent for scientific use of blood products.

Reagents

Hygromycin B was acquired from Life Technologies-Invitrogen, Bleiswijk, The Netherlands. Ampicillin was purchased from Calbiochem Merck-Millipore, Darmstadt, Germany. Gentamicin sulfate was obtained from Lonza BioWhittaker, Basel, Switzerland.

Cell culture

PBMCs and granulocytes were isolated by FICOLL separation from buffy coats of anonymous healthy blood bank donors (Sanquin Bloodbank, Amsterdam, The Netherlands). Subsequently, monocytes were isolated by CD14 MACS sorting (Miltenyi Biotec, Leiden, The Netherlands) and cultured in Gibco Roswell Park Memorial Institute (RPMI) 1640 medium (Life Technologies-Invitrogen) supplemented with 2mM GlutaMAX (Gibco/Life Technologies-Invitrogen), 10% Fetal Bovine Serum (FBS; Greiner Bio-One, Alphen a/d Rijn, The Netherlands), and 100 U/ml penicillin and 100 μ g/ml streptomycin (Life Technologies-Invitrogen). To generate M ϕ 1 and M ϕ 2, monocytes were cultured with 5 ng/ml granulocyte-macrophage colony-stimulating factor (GM-CSF; R&D Systems, Abingdon, UK) or 50 ng/ml macrophage colony-stimulating factor (M-CSF; R&D Systems), respectively, for 6 days as reported previously⁽¹⁰⁾. M ϕ 2a/b/c/d subsets⁽²⁵⁾ were obtained by culturing monocytes with 50 ng/ml M-CSF for 3 days followed by polarization for another 3 days in 10 ng/ml IL-4 and 10 ng/ml IL-13 (Peprotech, Rocky Hill, NJ, USA) for M ϕ 2a; 10 ng/ml LPS (Life Technologies-Invitrogen) and 1 μ g/ml IgG-Ovalbumin (OVA) immune complexes (ICs) (generated by mixing a 25-fold excess of anti-ovalbumin polyclonal antibody (Polysciences, Eppelheim, Germany) with OVA protein (Sigma-Aldrich, Zwijndrecht, The Netherlands) to acquire M ϕ 2b; 10 ng/ml IL-10 (R&D Systems) to acquire M ϕ 2c; and 10 ng/ml IL-6 (R&D Systems) and 50 ng/ml PGE2 (Sigma-Aldrich) to acquire M ϕ 2d. DCs were generated by culturing monocytes with 10 ng/ml GM-CSF and 10 ng/ml IL-4 for the first 3 days, followed by addition of 30 ng/ml GM-CSF and 30 ng/ml IL-4 for the last 3 days. Macrophage morphology was investigated by light microscopy on a Leica AF6000 microscope using a 63x objective (Leica, Amsterdam, The Netherlands).

Flow cytometry

Expression of cell surface and intracellular markers was evaluated by flow cytometry using a LSRFortessa (BD Biosciences, Vianen, The Netherlands) and FlowJo software for Windows

version 10.4.2 (TreeStar, Ashland, OR, USA). Prior to staining, Fc-receptors were blocked with 5% human serum for 15 minutes. To assess surface markers, cells were incubated with saturating concentrations of antibodies for 30 min at 4°C in the dark, washed twice with PBS/0.1% BSA and fixed in 1% paraformaldehyde. For intracellular markers, cells were stained using a FIX&PERM® Cell Fixation and Permeabilization Kit (Nordic MUBio, Susteren, The Netherlands) according to manufacturer's instructions. Resulting geometric mean fluorescent intensities were \log_{10} transformed, mean centred and scaled to standard deviation units. Hierarchical clustering of the markers was performed using one minus Pearson correlation as distance metric and complete linkage.

The following antibodies specific for human antigens were used: CD1a-AF700 (clone HI149), CD3-Pacific Blue (clone HIT3a), CD4-PE-Cy7 (clone A161A1), CD11b-AF488 (clone ICRF44), CD14-FITC (clone HCD14), CD16-APC-Cy7 (clone 3G8), CD27-PerC-Cy5.5 (clone O323), CD32-FITC (clone FUN-2), CD33-PerCP-Cy5.5 (clone WM53), CD68-PerCP-Cy5.5 (clone Y1/82A), CD80-PE-Cy7 (clone 2D10), CD85k (ILT3)-AF647 (clone ZM4.1), CD86-BV650 (clone IT2.2), CD123-PE-Cy7 (clone 6H6), CD127 (IL-7R)-BV650 (clone A019D5), CD134L (OX40L)-Biotin (clone 11C3.1), CD137 (4-1BB)-PE-Cy5 (clone 4B4-1), CD137 (4-1BB)-APC (clone 4B4-1), CD150 (SLAMF1)-FITC (clone A12 (7D4)), CD163-AF647 (clone RM3/1), CD169 (SIGLEC1)-APC (clone 7-239), CD192 (CCR2)-PerCP-Cy5.5 (clone K036C2), CD200R-PE (clone OX-108), CD206-APC-Cy7 (clone 15-2), CD206-PE-Cy5 (clone 15-2), CD209-PE (clone DSC-8C1), CD274 (B7-H1, PD-L1)-PE-Cy7 (clone 29E.2A3), CD301 (CLEC10A)-PE (clone H037G3), DLL1-PE (clone MHD1-314), EGFR-PE-Cy7 (clone AY13), LIGHT-PE (clone T5-39), HLA-A2-FITC (clone BB7.2) (BioLegend, Uithoorn, The Netherlands), CD14-Pacific Blue (clone HCD14), HVEM-Biotin (clone eBioHVEM-122), RANKL-Biotin (clone MIH24), TweakR-Biotin (clone ITEM-4) (Thermo Fisher Scientific, Bleiswijk, The Netherlands), CD137L (4-1BBL)-FITC (clone 5F4) (MBL International, Woburn, MA, USA), CD3-PE-CF594 (Clone UCHT1), CD8-Horizon V500 (clone RPA-T8), CD19-Pacific Blue (clone HIB19), CD28-FITC (clone CD28.2), CD70-FITC (clone Ki24), CD152 (CTLA4)-APC (clone BNI3), HLA-DR-FITC (clone L243 (G46-6)), total STAT1-PE (clone 1/Stat1) (BD Biosciences, Erembodegem, Belgium), CMKLR1-APC (clone 84939), DCSTAMP-APC (clone 788524), MERTK-APC (clone 125518), ISG15-APC (clone 851701) (R&D Systems), CD64-PE (clone 10.1), RANK-PE (clone 64C1385.1) (Santa Cruz, CA, USA), iNOS-Unconjugated (clone 4E5) (Novus Biologicals, Abingdon, UK), MARCO-PE-Cy5 (Bioss antibodies, Woburn, MA, USA), CD134 (OX40)-PerCP-Cy5.5 (clone ACT35) (Miltenyi Biotec), IFIT3-Unconjugated (clone OTI1G1), IFITM3-AF488 (Abcam, Cambridge, UK). Secondary staining was performed using Goat-anti-mouse IgG-PerCP (Jackson ImmunoResearch, Cambridgeshire, UK), Goat anti-mouse IgG AF647 (Abcam) or Streptavidin-PE-Cy7 (BioLegend). Live/dead gating was performed based on Vivid-Pacific Blue (Life Technologies-Invitrogen) staining.

Phagocytosis quantification assay

To quantify phagocytosis, fluorescent polystyrene particles (Fluoresbrite YG carboxylate microspheres; Polysciences) were used as described earlier ⁽³⁸⁾. Cells were incubated with

fluorescent beads in a ratio of 10 beads to 1 cell for 90 minutes at 37°C. Subsequently, cells were collected with a cell scraper, centrifuged at 1500 rpm for 10 minutes and resuspended in 100 μ l cell culture medium in the presence or absence of 0.4% Trypan blue (1:1) (Thermo Fisher Scientific). As a negative control, cells were pre-incubated with either 5 μ M cytochalasin D (Sigma-Aldrich) for 1h or 4% paraformaldehyde for 10 minutes. Internalization of the beads was quantified by flow cytometry on a LSRFortessa flow cytometer (BD Biosciences). Internalised beads were detected at 486 nm (green fluorescence) while non-internalised beads emitted a red fluorescent signal after Trypan blue quenching.

Analysis of secreted proteins

Multiplex analysis of human cytokines and chemokines in supernatants was performed using a customized Luminex multiplex suspension array system according to the manufacturer's instructions (Merck Millipore, Amsterdam, The Netherlands) The 19-plex magnetic bead panel encompassed cytokines/chemokines for: CXCL10, CCL2 (MCP-1), CCL3 (MIP-1 α), CCL4 (MIP-1 β), CCL5 (RANTES), CCL22 (MDC), EGF, Fractalkine, IFN α 2, IFN γ , IL-1 α , IL-1 β , IL-1Ra, IL-6, IL-8, IL-10, IL-12p70, TNF- α and VEGF. For each donor, cytokine concentrations were mean centred and scaled to standard deviation units. Hierarchical clustering of cytokines was performed with one minus Pearson correlation as distance metric and average linkage.

Concentrations of single analytes in supernatants were determined using enzyme-linked immunosorbent assay (ELISA) according to the manufacturer's instructions. The human IFN γ ELISA kit was purchased from U-CyTech, Utrecht, The Netherlands and the human VEGF DuoSet ELISA kit was obtained from R&D Systems.

Bacterial infections

Mycobacteria were cultured in Difco Middlebrook 7H9 broth (Becton Dickinson, Breda, The Netherlands) supplemented with 10% ADC (Sigma-Aldrich), 0.5% Tween-80 (Sigma-Aldrich), and 50 μ g/ml Hygromycin. *Salmonella enterica* serovar Typhimurium (*Stm*) was cultured in Difco LB broth (Becton Dickinson) supplemented with 100 μ g/ml Ampicillin⁽³⁹⁾.

Mycobacterial cultures (*Mtb* strain H37Rv-DsRed) were diluted to pre-log phase density one day prior to infection (optical density at 600 nm (OD600) of 0.4). *Stm* strain SL1344-pMW215-DsRed was grown overnight in LB broth containing appropriate antibiotics. Following overnight incubation, *Stm* liquid cultures were diluted 1:33 and cultured for an additional 3-4h. Bacterial density was determined by measuring the OD600 and the bacterial suspension was diluted in cell culture medium (RPMI 1640 medium supplemented with 2mM GlutaMAX and 10% FBS) without antibiotics to a concentration of 30 \times 10⁶ bacteria/ml to reach a multiplicity of infection (MOI) of 10. Accuracy of bacterial density measurements was verified by a standard colony forming unit (CFU) assay.

Cell cultures, seeded at a density of 300,000 cells/well in a 24-wells plate one day before infection, were inoculated with 100 μ l bacterial suspension, centrifuged for 3 min at 800 rpm and incubated at 37°C/5% CO₂. After 20 min if infected with *Stm* or 60 min if infected with *Mtb*, plates were washed with cell culture medium containing 30 μ g/ml gentamicin sulfate and subsequently incubated O/N at 37°C/5% CO₂ in cell culture medium containing 5 μ g/ml gentamicin sulfate. Bacterial load was determined by colony forming unit (CFU) assay using the track dilution method described previously⁽⁴⁰⁾.

Arginase activity assay

Arginase activity was assessed using a quantitative colorimetric Arginase Assay Kit (Abnova, Taipei, Taiwan) according to manufacturer's protocol. Briefly, 1×10^6 cells were lysed in 40 μ l lysis buffer containing 10 mM Tris-HCl (pH 7.4), 1 μ M pepstatin A, 1 μ M leupeptin, and 0.4% (w/v) Triton X-100. Lysates were centrifuged for 10 min at 15,000 rpm and mixed with 10 μ l 5x substrate buffer (containing L-arginine) in 96-well flat-bottom plates. Following 2h incubation at 37°C, reactions were terminated by adding 200 μ l urea reagent to the wells. Plates were subsequently incubated at room temperature for another 20 minutes and urea production was determined by measuring the OD at 450nm.

T cell activation assay

The antigen presenting capacity of cells was determined as described previously (10) by measuring proliferation and IFN γ secretion of the HLA-DR2-restricted CD4⁺ T cell clone R2F10 specific for *M.leprae* hsp65 (amino acids 418-427) and the HLA-DR1-restricted CD4⁺ T cell clone HA1.7 specific for hemagglutinin of influenza virus (amino acids 306-318). Antigen presenting cells from HLA-DR-matched donors were seeded in triplicate in Iscove's Modified Dulbecco's Medium (IMDM; Life Technologies-Invitrogen) supplemented with 2mM GlutaMAX, 10% human serum, 100 U/ml penicillin and 100 μ g/ml streptomycin at a density of 2.5×10^3 cells per well in 96-wells flat bottom plates in the presence or absence of LPS (100 ng/ml and 10 mg/ml) or mycobacterial sonicate (100 ng/ml and 10 mg/ml) for 16h. Subsequently, 1×10^4 T cells and 10 μ g/ml recombinant protein (hsp65) or 100 ng/ml synthetic peptide (hemagglutinin) were added to a final volume of 200 μ l and incubated for 72h. 50 μ l aliquots of supernatant were collected to measure IFN γ secretion. Proliferation was measured by [³H] TdR-incorporation (0.5 μ Ci/well, Perkin Elmer, Groningen, the Netherlands) for 16h. Cells were harvested with a 96-well Tomtec cell harvester (Synchron, Etten-Leur, The Netherlands) and counts per minute (cpm) were determined by liquid scintillation counting using a Wallac MicroBeta counter (Perkin Elmer).

T cell mediated suppression

T cell lines were generated in 24-wells plates by adding 1×10^6 PBMCs from an allogeneic donor to 2×10^5 differentiated M ϕ or DCs in IMDM medium supplemented with 2mM

GlutaMAX, 5% human serum, 100 U/ml penicillin and 100 μ g/ml streptomycin. At day 3, IL-15 (10 ng/ml; PeproTech, London, United Kingdom) was added to the co-cultures and cells were split. At day 6, M ϕ /DC-induced T cells were harvested and tested for their ability to inhibit proliferation of a Th1 indicator clone (Rp15 1-1) that recognizes *Mtb* hsp65 peptide 3-13 (41). Rp15 1-1 Th1 cells (1×10^4) were cultured in 96-well flat-bottom plates with irradiated (20 Gy), HLA-DR3 matched PBMCs as antigen presenting cells (5×10^4) and *Mtb* hsp65 p3-13 (5 ng/ml or 50 ng/ml) in the presence or absence of different amounts of M ϕ /DC-induced T cells (0.6×10^4 - 5×10^4). After 3 days of co-culture, proliferation was measured by [3 H] TdR-incorporation (0.5 μ Ci/well, Perkin Elmer) for 16h. Cells were harvested with a 96-well Tomtec cell harvester (Synchron) and counts per minute (cpm) were determined by liquid scintillation counting using a Wallac MicroBeta counter (Perkin Elmer).

T cell-mediated cytotoxicity

The Rp15 1-1 Th1 responder clone recognizing *Mtb* hsp65 peptide 3-13 was labelled with a low dose of CFSE (0.25 μ M) while R2F10, a HLA-DR2-restricted control CD4⁺ T cell clone specific for *M.leprae* hsp65 p418-427 was labelled with a high dose of CFSE (5 μ M). Both T cell clones (1×10^4 cells) were co-cultured in a 1:1 ratio in IMDM medium supplemented with 2mM GlutaMAX, 10% human serum, 100 U/ml penicillin and 100 μ g/ml streptomycin with *Mtb* hsp65 p3-13 (5 ng/ml and 50 ng/ml), *Mtb* Ag85b p56-65 (5 ng/ml and 50 ng/ml); irrelevant peptide not recognized by any of the 2 reporter T cell clones), irradiated HLA-DR3 positive HLA-DR2 negative PBMCs as antigen presenting cells (5×10^4), and M ϕ /DC-induced T cells (5×10^4) for 16h. Subsequently, cells were harvested, stained for CD3-PE-CF594, CD4-PE-Cy7 and CD8-Horizon V500 and analysed by flow cytometry on a LSRFortessa flow cytometer (BD Biosciences).

RT-qPCR analyses

Total RNA was isolated using Trizol Reagent (Thermo Fisher Scientific) and cDNA was synthesized using SuperScript IV Reverse Transcriptase (Life Technologies-Invitrogen) according to the manufacturer's protocols. RT-qPCR reactions were performed in MicroAmp[®] Fast Optical 96-Well Reaction Plates with Barcode in a final volume of 25 μ l containing 12.5 μ l TaqMan[®] Universal PCR Master Mix, No AmpErase[®] UNG, 1.25 μ l TaqMan[®] Gene Expression Assay, 6.25 μ l RNase-free water (all from Thermo Fisher Scientific) and 5 ng cDNA. PCR reactions were run on a Step One Plus Real Time PCR System (Thermo Fisher Scientific) and PCR cycling conditions consisted of 1 cycle at 50°C for 2 min, 1 cycle at 95°C for 10 min followed by 40 cycles of 95°C for 15 seconds and 60°C for 1 min. Gene expression levels were calculated relative to GAPDH using the $2^{-\Delta\Delta Ct}$ method. TaqMan[®] Gene Expression Assays used were Arg1-FAM (Hs00968979_m1) and GAPDH-FAM (Hs02758991_g1).

dcRT-MLPA assay and analysis

A dual-colour reverse transcription multiplex ligation-dependent probe amplification (dcRT-MLPA) assay was performed as described previously (42). Briefly, for each target-specific sequence, a specific RT primer was designed located immediately downstream of the left- and right-hand half-probe target sequence. Following reverse transcription, left- and right-hand half-probes were hybridized to the cDNA at 60°C overnight. Annealed half-probes were ligated and subsequently amplified by PCR (33 cycles of 30 seconds at 95°C, 30 seconds at 58°C and 60 seconds at 72°C, followed by 1 cycle of 20 min at 72°C). Primers and probes were from Sigma-Aldrich and MLPA reagents from MRC-Holland (Amsterdam, The Netherlands). PCR amplification products were diluted 1:10 in HiDi formamide containing 400HD ROX size standard and analysed on an Applied Biosystems 3730 capillary sequencer in GeneScan mode (BaseClear, Leiden, The Netherlands).

Trace data were analysed using GeneMapper software 5.0 (Applied Biosystems, Bleiswijk, The Netherlands). The areas of each assigned peak (in arbitrary units) were exported for further analysis in Microsoft Excel spreadsheet software. Data were normalized to the average signal of GAPDH and signals below the threshold value for noise cut-off in GeneMapper (\log_2 transformed peak area ≤ 7.64) were assigned the threshold value for noise cut-off. Finally, the normalized data were \log_2 transformed for statistical analysis and data visualization.

For data visualization, \log_2 -transformed peak areas were fit to a multilevel principal component analysis (PCA) using R version 3.5.0. and the mixOmics package, version 6.3.2 (43). Variable Importance for Projection (VIP) scores were extracted by fitting partial least squares discriminant analysis (PLS-DA) models for each individual cell type versus all other cell types combined. Hierarchical clustering of type I interferon genes was performed with one minus Pearson correlation as distance metric and complete linkage.

Quantitative proteomics by reductive dimethylation

Samples were prepared as described previously (44). In brief, *Mtb*-infected cells were washed twice in PBS, lysed in 4% SDS, 0.1 M DTT, 0.1 M Tris (pH 7.5-8.0) and mycobacteria were subsequently heated-killed for 10 min at 90°C. Cell lysates were mechanically disrupted by three cycles of bead-beating in a mini bead-beater 16 (BioSpec, Bartlesville, OK, USA) for 5 min using glass beads followed by cooling on ice for 5 min. Cell lysates were cleared from cell debris by centrifugation for 1 min at 14,000 g and supernatants were transferred to a fresh tube. Proteins were digested using the filter aided sample preparation (FASP) method (45). The resulting tryptic peptides were desalted on C18 SepPak columns (Waters, Milford, MA, USA) and on column labelled by dimethylation (46). Fractionation was performed using strong cation exchange (SCX) on an Agilent 1100 system equipped with an in-house packed SCX-column (320 μ m ID, 15 cm, polysulfoethyl A 3 μ m, Poly LC), run at 4 μ l/min. The SCX gradient started for 10 min at 100% solvent A (water/acetonitrile/formic acid; 70/30/0.1), after which a linear gradient reached 100% solvent B (250 mM KCl/

acetonitrile/formic acid 70/30/0.1) in 15 min, followed by 100% solvent C (500 mM KCl/ acetonitrile/formic acid 70/30/0.1) for 15 min. Eleven fractions were collected at 1 min intervals, lyophilized and reconstituted in 30 μ l (water/acetonitrile/formic acid 95/3/0.1) for nanoLC-MS/MS. All fractions were analysed by on-line nanoLC-MS system consisting of an Agilent 1100 gradient HPLC system (Agilent, Waldbronn, Germany) and an LTQ-FT Ultra mass spectrometer (Thermo Fisher Scientific). In addition, selected fractions were also analysed on a Q-Exactive mass spectrometer (Thermo Fisher Scientific). For both instruments the LC gradient was run from 0% to 30% solvent B (10/90/0.1 water/ acetonitrile/formic acid) in 10-155 min.

Proteomics data analysis

Peptides and proteins were identified and quantified using MaxQuant 1.4.0.3 (<https://maxquant.net/maxquant>)⁽⁴⁷⁾. The false discovery rate (FDR) was set to 0.01 for both proteins and peptides. Minimal peptide length was set to seven amino acids. For the data acquired on the LTQ-FT, the first search was conducted using 20 ppm, while the main search was performed with 10 ppm. For the data acquired on the Q-Exactive, the first search was performed using 10 ppm whereas the main search was performed using 4.5 ppm. Search of MS/MS spectra was performed with 0.5 Da using the Andromeda search engine for the LTQ-FT data files and 20 mmu for the Q-Exactive data⁽⁴⁸⁾. A total of 262 common contaminants were included in the searches by Andromeda. Trypsin specificity was set as C-terminal to arginine and lysine with proline restriction. A maximum of two missed cleavages was allowed. Variable modifications included N-terminal protein acetylation, methionine oxidation and corresponding dimethyl labels. Carbamidomethylation of cysteine was selected as a fixed modification. Proteins identified had a minimal peptide count of two peptides, including one unique peptide. All spectra were matched against a FASTA database of Homo sapiens (88665 entries). The MaxQuant output files and the raw data files, which provide access to all annotated spectra, have been deposited to the ProteomeXchange Consortium (<http://www.proteomexchange.org>)⁽⁴⁹⁾ via the PRIDE partner repository that can be accessed with the dataset identifier PXD003343.

Next, at each time point, log₂-transformed fold changes (FC) were calculated for individual proteins that were detectable in all cell subsets analysed. Proteins with a log₂-transformed FC of ≥ 1 or ≤ -1 were selected for Gene Ontology term enrichment analysis ('Biological Process') using clusterProfiler⁽⁵⁰⁾. Enrichment was tested versus a reference list of all detectable proteins per time point and complexity of the results was reduced by removing redundancy of enriched GO terms using the Relevance method⁽⁵¹⁾ incorporated in GOSemSim⁽⁵²⁾ with a similarity cut-off of 0.8. Additionally, GO term enrichment analysis was performed on all individual proteins detectable in all cell subsets analysed (irrespective of the log₂-transformed FC) versus the complete human genome followed by plotting of the top 100 most enriched pathways in an enrichment map. Enriched clusters

were coloured and annotated based on overarching biological pathways or subcellular localization.

Statistics

One-way ANOVA with Dunnett's multiple comparison test (multiple groups) was performed using GraphPad Prism version 8.0 (GraphPad Software, San Diego, California, USA; www.graphpad.com). Hierarchical clustering and heatmap generation were performed using Morpheus (<https://software.broadinstitute.org/morpheus>).

Results

M ϕ 2b display potent phagocytic and antibacterial capacities independent of arginase activity

We have previously demonstrated that outgrowth of intracellular *Mycobacterium tuberculosis* (*Mtb*) was more efficiently controlled by classically activated, pro-inflammatory M ϕ 1 than by alternatively activated, anti-inflammatory M ϕ 2⁽¹⁰⁾. However, increasing appreciation of macrophage diversity and plasticity *in vivo* recently underscored that macrophages comprise a broad spectrum of cells whose function depends on the stimuli they have been exposed to as well as their anatomical location⁽⁵³⁾. To map the functional heterogeneity of a diverse range of polarized macrophages, primary human monocyte-derived DCs, M ϕ 1, M ϕ 2, and M ϕ 2a/b/c/d were generated as displayed in **Figure 1**. To evaluate their capacity to control intracellular bacterial survival, polarized myeloid subsets were infected with either *Salmonella enterica* serovar Typhimurium (*Stm*) or *Mtb* and intracellular bacterial outgrowth determined by CFU assay (**Figure 2A**). The results confirmed that M ϕ 1 supported outgrowth of intracellular *Stm* and *Mtb* significantly less efficiently than M ϕ 2. Interestingly, DCs and M ϕ 2b infected with *Stm* or *Mtb* yielded even lower numbers of CFU, suggesting that these myeloid cell types may be exceptionally proficient in controlling intracellular bacteria. Of note, M ϕ 2b polarization in the presence of single triggers (either LPS or IgG-OVA immune complexes) resulted in similar phenotypes (**Supplementary Figure 1**). The marked differences observed in intracellular bacterial survival between myeloid cell types was not due to infection-induced cell death, as host cell survival after *Stm* and *Mtb* infections was similar across all cell subsets (**Figure 2B**).

To explore whether differences in phagocytic activity between myeloid subsets could account for the decreased intracellular bacterial survival found in DCs, M ϕ 1 and M ϕ 2b, cells were incubated with fluorescently labelled polystyrene beads and bead internalization was quantified by flow cytometry. Cytochalasin D, an inhibitor of actin polymerization, and the fixative paraformaldehyde (PFA) were included as negative controls (**Figure 2C**). Clearly, bead uptake was less efficient in DCs and M ϕ 1 compared to the various types of M ϕ 2, directly correlating the low CFU counts observed in DCs and M ϕ 1 in **Figure 2A** with diminished phagocytosis. In contrast, M ϕ 2b displayed potent phagocytic capacity, which was comparable to M ϕ 2, indicating that the lower post-

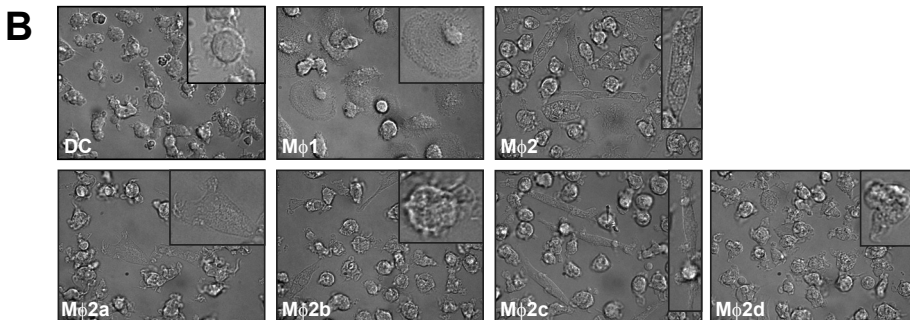
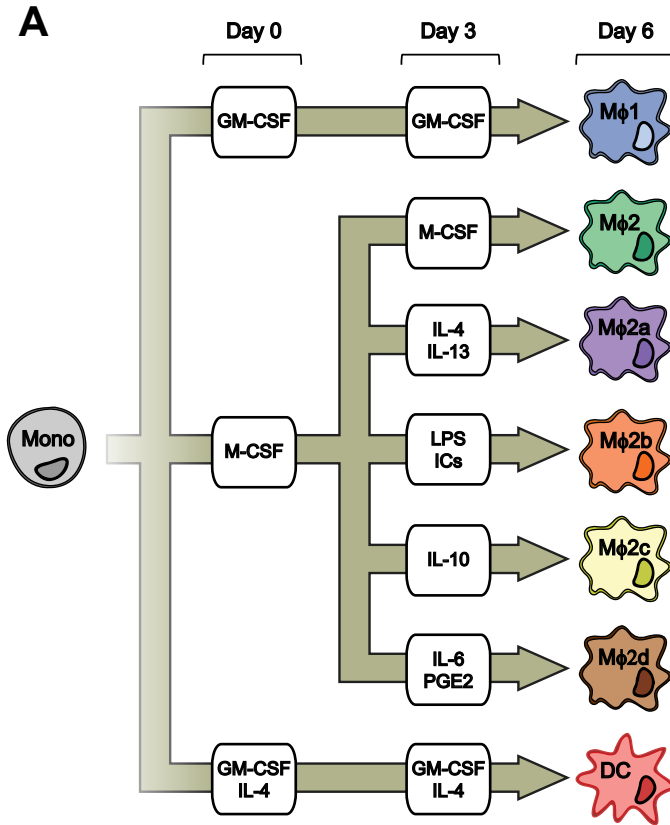


Figure 1: Macrophage polarization.

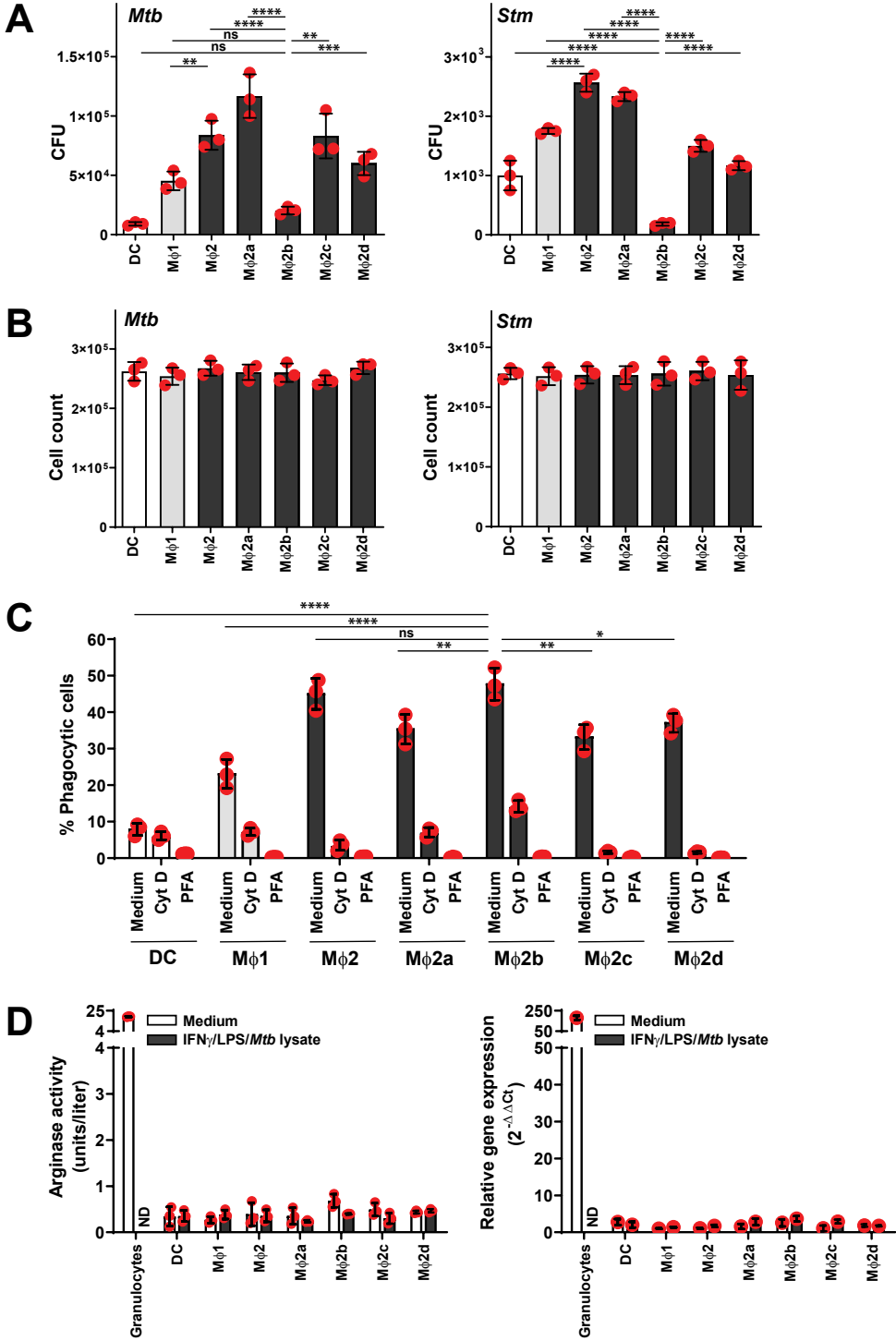
(A) CD14+ monocytes were isolated from buffy coats of healthy blood bank donors and differentiated according to the depicted outline into DCs and macrophage subsets in 6 days. ICs = immune complexes. (B) Morphology of differentiated myeloid subsets was assessed by light microscopy using a Leica AF6000 microscope (magnification 63x; scale bar 20 μ M). M ϕ 1, M ϕ 2b and M ϕ 2d subsets all displayed a round morphology, with M ϕ 1 completely lacking membrane protrusions, M ϕ 2d being characterized by a single large finger-like protrusion, and M ϕ 2b exhibiting many small surface protrusions. M ϕ 2 and M ϕ 2c subsets both displayed a spindle morphotype with M ϕ 2c being more elongated than M ϕ 2. M ϕ 2a were characterized by a mixture of different morphotypes.

infection bacterial yields in this macrophage subset were not due to reduced phagocytic capacity, but rather might be attributable to a strong intrinsic capacity to control the survival of intracellular bacteria.

Activated macrophages have been shown to mediate (myco)bacterial killing through production of reactive nitrogen intermediates (RNI) via inducible nitric oxide (NO) synthase (iNOS) ⁽⁵⁴⁾. In mice, RNI synthesis is regulated by the enzyme arginase I by competing for the iNOS substrate L-arginine ⁽⁵⁵⁾. To evaluate whether the marked decrease in intracellular bacterial outgrowth in human M ϕ 2b correlated with arginase activity, we assessed transcriptomic levels of *ARG1* and its enzymatic activity in polarized myeloid subsets. *ARG1* transcripts were near the lower detection threshold at baseline (C_t values >39.5) in all cell subsets analysed (**Figure 2D**). Also, activating myeloid subsets with a cocktail of IFN γ , LPS and *Mtb* lysate for 16h did neither enhance *ARG1* transcript levels nor arginase I activity, while both arginase I gene expression levels and activity were easily revealed in granulocytes that were included as a positive control. Taken together, these data demonstrate that M ϕ 2b have superior ability to control bacterial outgrowth, independent of their phagocytic or arginase I activity.

Figure 2: Control of intracellular bacterial infections by myeloid cell subsets.

(A) CFU assay data derived from human monocyte-derived DCs, M ϕ 1, M ϕ 2, and M ϕ 2a/b/c/d infected with either *Mtb* (left panel) or *Stm* (right panel) at a MOI of 10. Bars depict mean \pm standard deviation of 3 replicates from a representative donor out of 5 donors tested. Individual data points are represented by red dots and overlaid on the bar graph. Statistical significance between M ϕ 2b and all other myeloid subsets was tested using a one-way ANOVA with Dunnett's multiple comparisons test. **(B)** Host cell viability is depicted by calculating absolute cell numbers following infection with *Mtb* (left panel) or *Stm* (right panel). Staining of cells with Trypan blue indicated that >99% of all counted cells in each subset was viable. Bars depict mean \pm standard deviation of 3 replicates from a representative donor out of 5 donors tested (same donor as shown in **A**). Individual data points represented by red dots are overlaid on the bar graph. Statistical significance between myeloid subsets was tested using a one-way ANOVA with Dunnett's multiple comparisons test. **(C)** Phagocytic capacity of human monocyte-derived DCs, M ϕ 1, M ϕ 2, and M ϕ 2a/b/c/d incubated for 90 min with Fluoresbrite YG carboxylate microspheres in a ratio of 10 beads to 1 cell was quantified by flow cytometry. Cytochalasin D, an inhibitor of actin polymerization, and the fixative paraformaldehyde (PFA) were included as negative controls. Bars depict mean \pm standard deviation of 3 replicates from a representative donor out of 5 donors tested. Individual data points represented by red dots are overlaid on the bar graph. Statistical significance between M ϕ 2b and all other myeloid subsets was tested using a one-way ANOVA with Dunnett's multiple comparisons test. **(D)** Arginase I activity (left panel) and transcript levels (right panel) in resting and 16h activated (2.5 ng/ml IFN γ , 10 ng/ml LPS, and 10 mg/ml *Mtb* lysate) myeloid subsets. Bars depict mean \pm standard deviation of 3 replicates from a representative donor out of 3 donors tested. Individual data points represented by red dots are overlaid on the bar graph. ND = Not determined. (* = p-value <0.05, ** = p-value <0.01, *** = p-value <0.001, **** = p-value <0.0001, ns = not significant).

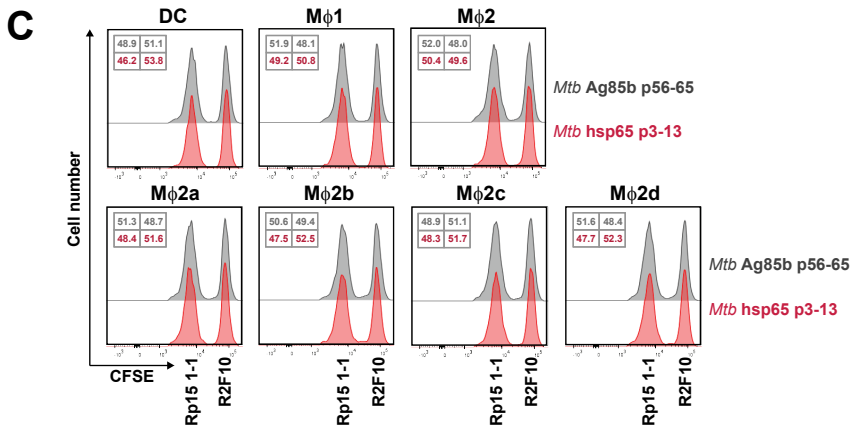
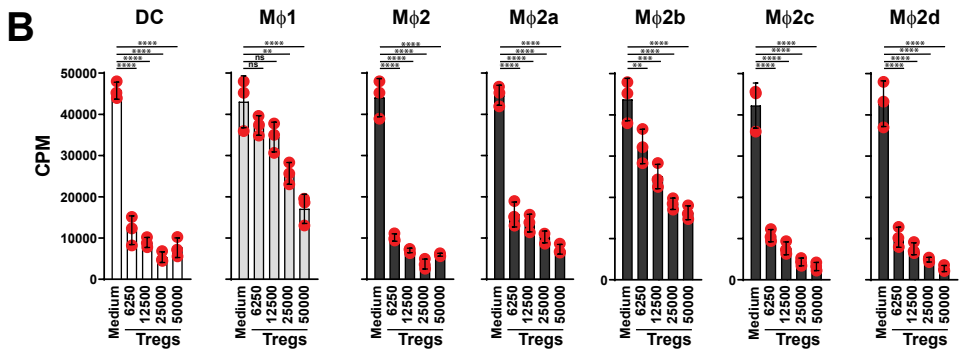
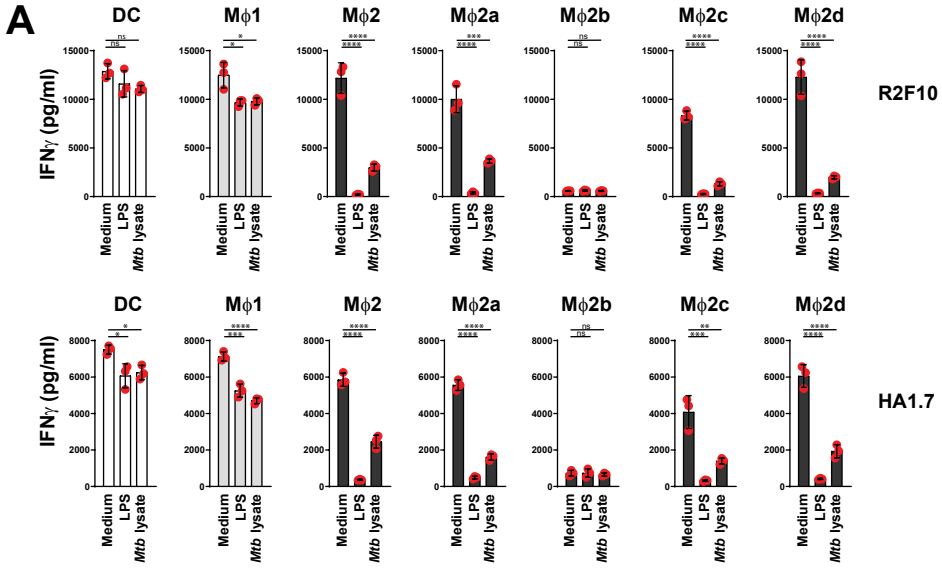


Mφ2b are poor inducers of T cell responses

Next, we addressed whether functional heterogeneity between myeloid subsets was also reflected in their capacity to elicit T cell responses. First, their ability to stimulate Th1 cell proliferation and IFN γ production was assessed by co-culturing HLA-DR-matched primary human monocyte-derived DCs, Mφ1, Mφ2, and Mφ2a/b/c/d (rested or activated with LPS or *Mtb* lysate) with either the HLA-DR2-restricted CD4⁺ T cell clone R2F10 or the HLA-DR1-restricted CD4⁺ T cell clone HA1.7 in the presence of their cognate antigen (*M.leprae* hsp65 p418-427 and influenza hemagglutinin p306-318, respectively) (**Figure 3A** and **Supplementary Figure 2**). With the noticeable exception of Mφ2b, resting myeloid subsets effectively induced a potent IFN γ response in both R2F10 (top panel) and HA1.7 (bottom panel) reporter T cell clones. Furthermore, the antigen-presenting capacity of Mφ2, Mφ2a, Mφ2c and Mφ2d was significantly inhibited by pre-activation with *Mtb* lysate and to an even greater extent by LPS stimulation, whereas the antigen-presenting capacity of Mφ1 and DCs was only marginally affected by these stimuli, in line with published data for Mφ2 and Mφ1⁽¹⁰⁾. Comparable results were obtained when using cell proliferation instead of IFN γ secretion as a read-out to determine the capacity to present antigen (**Supplementary Figure 2**).

Figure 3: Induction of T cell responses by polarized myeloid subsets.

(A) Antigen-presenting capacity of polarized myeloid subsets was determined following activation for 16h with LPS (100 ng/ml), *Mtb* lysate (100 ng/ml) or control medium before incubation with either the HLA-DR2-restricted CD4⁺ T cell clone R2F10 or the HLA-DR1-restricted CD4⁺ T cell clone HA1.7 in the presence of their cognate antigen (*M.leprae* p418-427; 10 μg/ml recombinant peptide) and influenza hemagglutinin (synthetic peptide HA p306-318; 100 ng/ml), respectively. After 3 days of co-culture IFN γ production by the responder T cell clones was determined in the supernatants by ELISA. No IFN γ production was detected in the absence of cognate antigen/peptide. Bars depict mean \pm standard deviation of 3 replicates from a representative donor out of 3 donors tested. Individual data points represented by red dots are overlaid on the bar graph. Statistical significance between rested and pre-activated cells was tested using a one-way ANOVA with Dunnett's multiple comparisons test. **(B)** T cells co-cultured with autologous polarized myeloid subsets for 6 days were added in different ratios to an HLA-DR3-restricted reporter Th1 clone (Rp15 1-1) together with irradiated HLA-DR3-expressing PBMCs as antigen presenting cells and the cognate peptide of Rp15 1-1 (*Mtb* hsp65 p3-13; 50 ng/ml). After 3 days of co-culture the proliferative response of the Rp15 1-1 indicator clone was determined by [³H] TdR-incorporation. No proliferation was detected in the absence of cognate peptide *Mtb* hsp65 p3-13. Data are expressed in counts per minute (CPM). Bars depict mean \pm standard deviation of 3 replicates from a representative donor out of 11 donors tested. Individual data points represented by red dots are overlaid on the bar graph. Statistical significance between medium and corresponding samples containing increasing numbers of DC/Mφ-induced T cells was tested using a one-way ANOVA with Dunnett's multiple comparisons test. **(C)** Rp15 1-1 Th1 responder clone specific for *Mtb* hsp65 p3-13 was labelled with a low dose of CFSE while HLA-DR2-restricted control CD4⁺ T cell clone R2F10 specific for *M.leprae* 60 kDa hsp p418-427 was labelled with a high concentration of CFSE. Both clones were co-cultured in a 1:1 ratio with *Mtb* hsp65 p3-13 (50 ng/ml), irrelevant peptide *Mtb* Ag85b p56-65 (50 ng/ml), irradiated HLA-DR3 matched PBMCs as antigen presenting cells and Mφ/DC-induced T cells for 16 hours followed by flow cytometric analysis. Histograms and quadrants display the relative percentages of CFSE^{lo} versus CFSE^{hi} cells when co-cultures were exposed to irrelevant peptide *Mtb* Ag85b p56-65 (grey) or *Mtb* hsp65 p3-13 (red). Data is shown from a representative donor out of 3 donors tested. (* = p-value <0.05, ** = p-value <0.01, *** = p-value <0.001, **** = p-value <0.0001, ns = not significant).



Since M ϕ 2 have been reported to induce strong regulatory T cell (T_{reg}) responses compared to M ϕ 1⁽¹⁴⁾, we also addressed the potential differences between different polarized myeloid subsets in inducing T cells with suppressive activity (**Figure 3B**). To this end, increasing numbers of Mf/DC-induced T cells were co-cultured with irradiated HLA-DR3 matched PBMCs as antigen presenting cells and the HLA-DR3 restricted Rp15 1-1 Th1 reporter clone in the presence of its cognate antigen (*Mtb* hsp65 p3-13). As expected, M ϕ 2-induced T cells markedly suppressed the proliferative response of indicator clone Rp15 1-1, while M ϕ 1-induced T cells were much less suppressive, confirming our previous results. Interestingly, M ϕ 2b were significantly less effective in generating T cells with regulatory capacities than M ϕ 2 and M ϕ 2a/c/d. To exclude the possibility that inhibition of proliferation was actually caused by lysis of the Rp15 1-1 responder T cell clone instead of the induction of regulatory T cells, an *in vitro* cytotoxicity assay was performed using indicator clone Rp15 1-1 recognizing *Mtb* hsp65 p3-13 and CD4⁺T cell clone R2F10 specific for *M.leprae* hsp65 p418-427 labelled with different doses of CFSE (**Figure 3C**). Indeed, no T cell cytotoxicity was observed, as similar numbers of responder Rp15 1-1 and control R2F10T cells were retrieved (ratio of 1) when exposed to *Mtb* hsp65 p3-13 or the irrelevant peptide *Mtb* Ag85b p56-65.

Collectively, these data demonstrate that M ϕ 2b are functionally distinct from the other M ϕ 2 subsets in that they possess relatively poor Th1- and T_{reg}-inducing abilities but are superior in controlling intracellular bacterial survival.

Identification of cellular and secreted markers that discriminate between macrophage subsets

Since⁽¹⁾ M ϕ 2 subsets, including M ϕ 2 and M ϕ 2a/b/c/d, comprise a functionally diverse group of anti-inflammatory macrophages and⁽²⁾ there is accumulating evidence that distinct macrophage subsets are associated with severity or progression of infectious and non-communicable diseases in humans, it is critical to develop tools to identify macrophage subsets *in vivo* based on subset-specific biomarkers⁽⁵⁶⁾. We first explored the possibility to accurately distinguish human polarized myeloid subsets based on the expression of a wide range of cell surface markers by flow cytometry. From the initial panel consisting of 43 markers (**Supplementary Table 1**), a selective panel was compiled consisting of eight cell surface markers (CD192, CD206, CD32, CD1a, EGFR, CD163, CD209 and CD14) that displayed the highest discriminatory power (**Figure 4A**). The classifying potential of this panel was subsequently examined by hierarchical clustering of myeloid subsets of two donors (**Figure 4B**). Monocytes could easily be separated based on their distinctively high expression of CD192 and CD14. DCs and M ϕ 1 could be separated from the other cell subsets by their exclusive CD206^{hi}/CD163^{lo} cell surface profile. Furthermore, M ϕ 1 could readily be distinguished from DCs based on the cell surface protein levels of CD209, CD1a and CD192. However, while M ϕ 2a could still be identified based on their

unique CD163^{hi}/CD209^{hi} expression profile, the remaining M ϕ 2 subsets did not display a combination of surface markers that could robustly separate them by cluster analysis.

We therefore further investigated whether rested and activated polarized myeloid subsets exhibited divergent protein secretory profiles that could be exploited for cell subset classification. In supernatants from resting cells, only limited amounts of secreted cytokines and chemokines could be detected using a customized Luminex 19-plex magnetic bead panel (**Figure 4C** and **Supplementary Table 2**). However, following stimulation for 16h with a mixture of IFN γ /LPS/*Mtb* lysate, DCs, M ϕ 1, M ϕ 2b, and to a lesser extent M ϕ 2 and M ϕ 2a could be discriminated by hierarchical clustering analysis. M ϕ 1 and DCs were characterized by the production of pro-inflammatory cytokine IL-12p70, but could be differentiated by their respective IL-1Ra^{hi}/IL-1 β ^{hi} and IL-Ra^{lo}/IL-1 β ^{lo} cytokine profiles. All M ϕ 2 subsets, with the exception of M ϕ 2b, produced IL-10 (albeit at variable levels) and none produced IL-12p70. Of note, M ϕ 2b exhibited a distinctive VEGF^{hi} protein secretion profile that was not shared by any of the other polarized myeloid subsets. This unique feature of M ϕ 2b was subsequently validated in 4 independent donors by ELISA (**Figure 4D**) and at the transcriptomic level by targeted gene expression profiling (**Figure 5D**). Although the cytokine/chemokine profiles of M ϕ 2 and M ϕ 2a were less typical, both could be separated to some extent by profound secretion of IL-10, while M ϕ 2 and M ϕ 2a could potentially be distinguished based on elevated CCL22 production by M ϕ 2a.

Taken together, polarized myeloid subsets could be classified based on either cell surface marker expression levels and/or cytokine secretion profiles in response to activation. The only exception was M ϕ 2c and M ϕ 2d which appeared remarkably similar for the tested parameters.

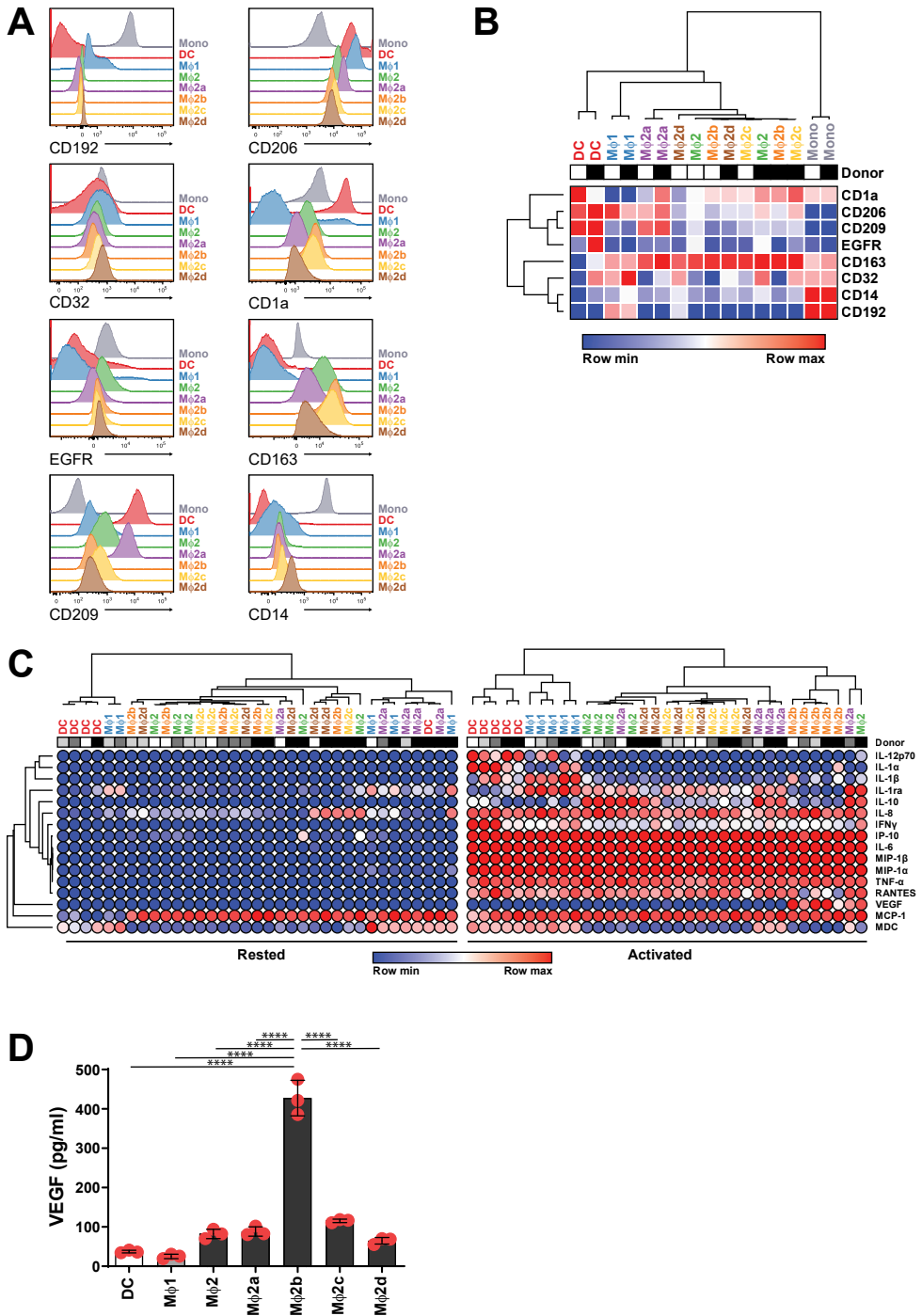


Figure 4: Identification of cellular and secretory markers that discriminate myeloid cell subsets.

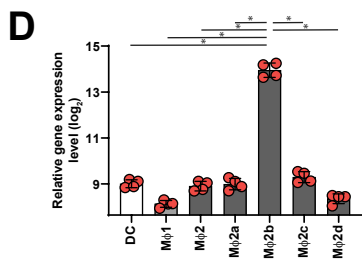
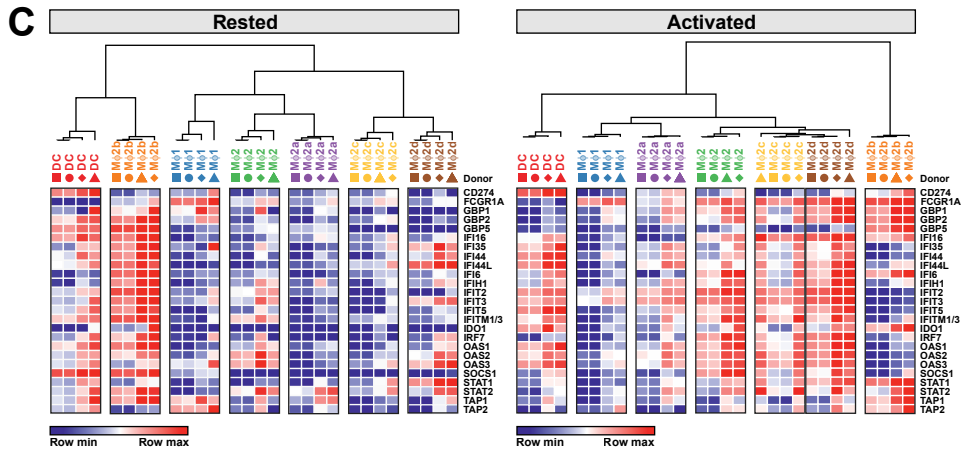
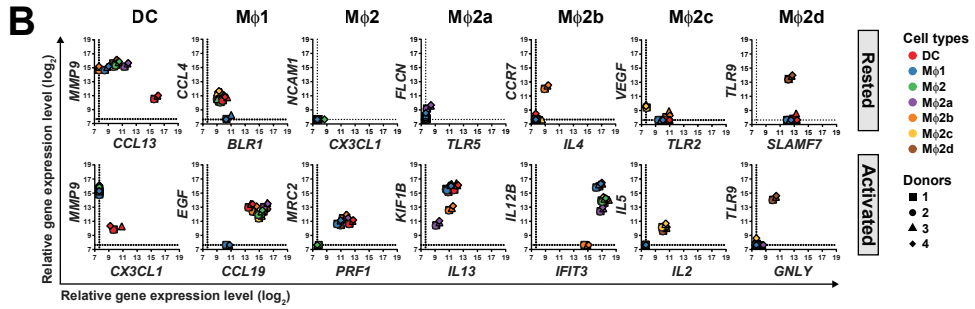
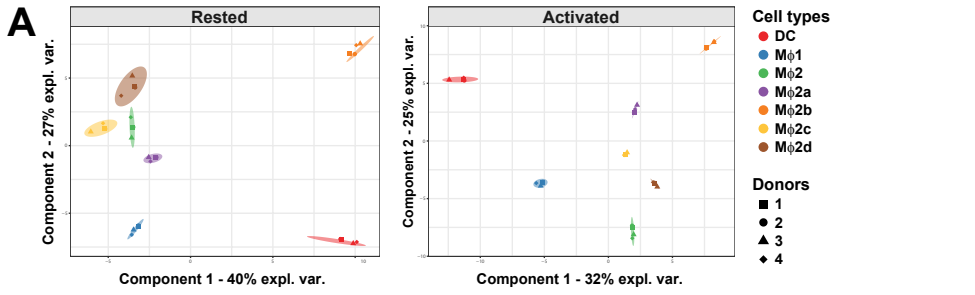
(A) Expression of cell surface markers on primary human monocyte-derived DCs, M ϕ 1, M ϕ 2, and M ϕ 2a/b/c/d was analysed by flow cytometry. Representative histograms display expression profiles of CD192, CD206, CD32, CD1a, EGFR, CD163, CD209 and CD14. **(B)** Hierarchical clustering of polarized myeloid subsets from 2 independent donors based on differentially expressed cell surface markers (\log_{10} -transformed geometric mean fluorescent intensities) using Pearson correlation complete-linkage clustering. Rows and columns correspond to the cell surface proteins and profiled myeloid subsets, respectively. Each row represents the relative expression of the indicated cell surface marker using a blue to white to red colour scale. Individual donors are presented in greyscale squares above each cell subset. **(C)** Cytokine/chemokine secretion by 16h activated (2.5 ng/ml IFN γ , 10 ng/ml LPS, and 10 mg/ml *Mtb* lysate) myeloid subsets was analysed by Luminex multiplex bead array. Hierarchical clustering of myeloid subsets from 5 independent donors based on differentially secreted cytokines/chemokines (average centred divided by the standard deviation) using Pearson correlation average-linkage clustering. Rows and columns correspond to the secreted proteins and profiled myeloid subsets, respectively. Each row represents the relative production of the indicated cytokine/chemokine using a blue to white to red colour scale. Individual donors are presented in greyscale squares above each cell subset. **(D)** ELISA analysis of VEGF levels in supernatants of 16h activated (2.5 ng/ml IFN γ , 10 ng/ml LPS, and 10 mg/ml *Mtb* lysate) polarized myeloid subsets. Bars depict mean \pm standard deviation of 3 replicates from a representative donor out of 4 donors tested. Individual data points represented by red dots are overlaid on the bar graph. Statistical significance between M ϕ 2b and all other myeloid subsets was tested using a one-way ANOVA with Dunnett's multiple comparisons test. (**** = p-value <0.0001).

Identification of molecular transcriptomic markers that can classify macrophage subsets

Since human monocyte-derived DCs, M ϕ 1, M ϕ 2, and M ϕ 2a/b/c/d could be distinguished by their cytokine and chemokine expression profiles, particularly upon activation, we next investigated the possible rewiring of transcriptomic networks following DC/M ϕ polarization in order to identify additional molecular markers to promote refined classification of myeloid subsets. Cell subsets were either rested or activated for 16h with a mixture of IFN γ /LPS/*Mtb* lysate, and transcriptomic levels were determined using focussed gene expression profiling^(42, 57). Selected probe sets covered 148 genes associated with innate and adaptive immunity and inflammatory responses (**Supplementary Tables 3 and 4**). First, multilevel PCA was applied to visualize global transcriptomic variances between rested or activated polarized myeloid subsets derived from 4 different donors (**Figure 5A**). Under resting conditions, DCs and M ϕ 2b displayed profound class separation based on the first component (explaining 40% of the variance), while the second component (explaining 27% of the variance) clearly distinguished DCs from M ϕ 2b. The first two components combined also clearly described M ϕ 1 whereas only the second component partially described the between-group variation amongst resting M ϕ 2 and M ϕ 2a/c/d cell subsets. Interestingly, cell type separation was particularly effective after activation for 16h with IFN γ /LPS/*Mtb* lysate, with the first two components explaining 32% and 25% of the variance, respectively (**Figure 5A**), signifying quite distinct transcriptional rewiring of polarized myeloid cells, which linked cell subset activation to alternate signalling networks.

Figure 5: Identification of molecular markers that can classify myeloid cell subsets.

(A) Multilevel Principle Component Analyses (PCA) PC1/PC2 score plots of rested (left panel) and 16h activated (2.5 ng/ml IFN γ , 10 ng/ml LPS, and 10 mg/ml *Mtb* lysate) (right panel) human monocyte-derived DCs, M ϕ 1, M ϕ 2, and M ϕ 2a/b/c/d derived from 4 independent donors. The ellipses represent the 95% confidence interval level. **(B)** Partial least squares-discriminant analyses (PLS-DA) models were fitted for each subset individually versus all other cell types combined, and the Variable Importance for Projection (VIP) scores were extracted to determine which variables (transcripts) explained the highest variance in each respective model. Shown are the log₂-transformed transcript levels of the top two genes with the highest VIP scores derived from either the rested or activated models as scatter plots for each cell type **(C)**. Hierarchical clustering of rested and activated polarized myeloid subsets from 4 different donors based on transcriptomic profiles of type I interferon signalling genes generated by dcRT-MLPA (average centred divided by the standard deviation) using Pearson correlation complete-linkage clustering. Rows and columns correspond to the transcripts and profiled myeloid subsets, respectively. Each row represents the relative expression of the indicated gene using a blue to white to red colour scale. In each panel, myeloid cell types are represented by distinctive colours and individual donors by unique symbols. **(D)** Log₂-transformed transcript levels of VEGF in 16h activated (2.5 ng/ml IFN γ , 10 ng/ml LPS, and 10 μ g/ml *Mtb* lysate) polarized myeloid subsets. Bars depict median of 4 independent donors tested while the whiskers represent the 95% confidence interval level. Red dots represent individual donors and are overlaid on the bar graph. Statistical significance between M ϕ 2b and all other myeloid subsets was tested using a Mann-Whitney U test. (* = p-value <0.05).



2

To identify important genes driving the separation between polarized myeloid subsets, PLS-DA models were fitted for each cell subset individually versus all other cell types combined, and the Variable Importance for Projection (VIP) scores were extracted to determine which variables (transcripts) explained the highest variance in each respective model (**Supplementary Table 5**). **Figure 5B** displays the relative expression levels of the two genes with the highest VIP scores derived from either the rested or activated model from individual cell types. DCs were characterized by significantly lower expression levels of *MMP9*, while M ϕ 2d could clearly be discriminated by higher transcript levels of *TLR9* in both resting and activated conditions. M ϕ 1 could be separated by relatively low *CCL4* and slightly elevated *BLR1* transcript levels in resting conditions and by *EGF^{lo}/CCL19^{lo}* expression values upon activation, while M ϕ 2b could readily be identified by their *CCR7^{hi}/IL4^{hi}* and *IL12B^{lo}/IFIT3^{lo}* transcriptomic profiles in resting and activated conditions, respectively. In contrast, resting M ϕ 2 and M ϕ 2a showed only weak separation from the other cell types but could easily be discriminated following activation based on lack of expression of *MRC2* and *PRF1* (M ϕ 2) or low expression of *KIF1B* and *IL13* (M ϕ 2a). Finally, resting M ϕ 2c could be distinguished by their *TLR2^{lo}/VEGF^{hi}* expression profile, while activated M ϕ 2c shared a distinctive *IL5^{hi}/IL2^{hi}* signature with activated M ϕ 2d. Nevertheless, activated M ϕ 2c and M ϕ 2d could still be separated based on enhanced transcriptomic levels of *TLR9*, as this is a unique feature of M ϕ 2d.

In summary, both cellular, immunological, and molecular markers enable accurate classification of myeloid polarizations states, corroborating the view that DC/M ϕ polarization is accompanied by re-wiring of cellular and molecular networks.

M ϕ 2b display a distinctive type I interferon signature

Since human monocyte-derived M ϕ 2 and M ϕ 2a/c/d were excellent supporters of T cell responses while M ϕ 2b were superior in controlling intracellular bacterial infections (**Figures 2 and 3**), we next performed quantitative proteomics on M ϕ 2 and M ϕ 2b at baseline (uninfected) and 4 or 24 hours after infection with *Mtb* to unravel the molecular mechanisms underlying this functional dichotomy. In total, 2724 proteins could be detected in both M ϕ 2 and M ϕ 2b. Gene ontology (GO) term enrichment analysis indicated these proteins were involved in general processes such as translation and cellular metabolism (**Supplementary Figure 3A**), but also in myeloid-specific pathways such as antigen presentation, and pathways known to be important for controlling intracellular bacterial infections including autophagy and Golgi/vesicle targeting (**Supplementary Figure 3B**). Using a log₂-transformed fold change (FC) cut-off of ≥ 1 or ≤ -1 , 459 proteins were identified to be differentially expressed between M ϕ 2 and M ϕ 2b, either at baseline (uninfected), following *Mtb* infection, or both conditions (**Figure 6A**). Processes found to be significantly overrepresented at baseline and 4 hours post-infection by GO term enrichment analysis included 'defense response (to virus)' and 'type I interferon signalling pathway' (**Figure 6B**). The latter pathway is of particular interest, as type I interferon

responses have been associated with detrimental effects on *Mtb* infection both *in vitro* and *in vivo* ⁽⁵⁸⁾. A heatmap of the proteins associated with this particular GO term indicated that type I interferon signalling proteins were more highly expressed in M ϕ 2b compared to M ϕ 2 at baseline and during *Mtb* infection (**Figure 6C**), identifying a strong type I interferon signature in M ϕ 2b. To validate these proteomic data in an independent approach, intracellular expression levels of five members of the type I interferon signalling pathway (STAT1, HLA-A2, IFIT3, IFITM3 and ISG15) were evaluated in M ϕ 2 and M ϕ 2b using flow cytometry. Indeed, all selected proteins were more highly expressed in M ϕ 2b than M ϕ 2, corroborating the findings obtained with quantitative proteomics (**Figure 6D**).

Next, we assessed whether the type I interferon signature identified in M ϕ 2b by quantitative proteomics could be validated at the transcriptional level. Hierarchical clustering analysis based on the transcriptomic profiles of 25 genes involved in type I interferon signalling convincingly separated both resting and activated polarized myeloid subsets (**Figure 5C**). As expected, resting M ϕ 2b expressed significantly higher levels of most type I interferon-inducible genes compared to the other myeloid subsets, including markers that were also found to be increased at the protein level (*GBP2*, *IFIT2*, *IFIT3*, *IFITM1/3*, *OAS2*, and *STAT2*) (**Figure 6C**). Upon activation, type I interferon signalling genes were noticeably induced in all M ϕ 2 subsets, occasionally even surpassing the levels observed in M ϕ 2b (e.g. in M ϕ 2 and M ϕ 2d) (**Figure 5C, right panel**). Nevertheless, activated M ϕ 2b retained a distinctive type I interferon transcriptional profile, including high expression levels of guanyl-binding proteins (*GBP1*, 2 and 5), transcription factors *STAT1* and *STAT2*, peptide transporters *TAP1* and *TAP2* and tryptophan-catabolizing enzyme *IDO1*. In conclusion, these results demonstrate that resting and activated M ϕ 2b are characterized by unique type I interferon signalling signatures.

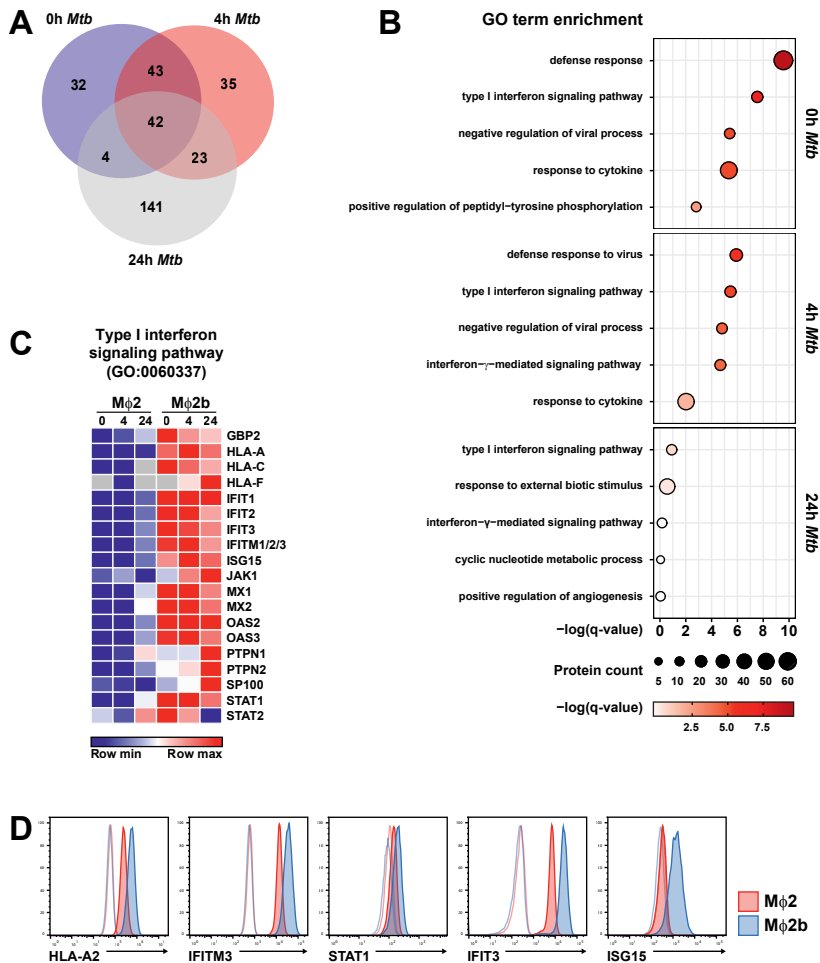


Figure 6: Quantitative proteomics reveals a type I interferon signature in Mφ2b.

Mφ2 and Mφ2b were infected with Mtb at a MOI of 10. Cells were lysed at 0, 4, and 24 hours post-infection and lysates were subjected to reductive dimethylation for semi-quantitative proteomics. Raw expression data of single proteins were used to calculate fold change (FC) differences between Mφ2b and Mφ2. **(A)** Venn-diagram depicting the distribution of differentially expressed proteins (Mφ2b/Mφ2 $\log_2(\text{FC}) \geq 1$ or ≤ -1) at 0, 4, and 24h post-infection. **(B)** Gene ontology (GO) term enrichment analysis of differentially expressed proteins (Mφ2b/Mφ2 $\log_2(\text{FC}) \geq 1$ or ≤ -1) at 0, 4, and 24h post-infection. Displayed are circle plots of the five most significantly enriched pathways at each time point. Enrichment significance levels are indicated by the brightness of the circles and their size indicates the number of proteins associated with the GO term or pathway. **(C)** Heatmap of proteins that are differentially expressed between Mφ2b and Mφ2 and belong to the GO term 'Type I interferon signalling pathway'. Rows and columns correspond to the cellular proteins and profiled myeloid subsets, respectively. Each row represents the relative amount of cellular protein using a blue to white to red colour scale. **(D)** Flow cytometric analysis of Mφ2 and Mφ2b stained for proteins of the type I interferon signalling pathway. Representative histograms for HLA-A2, IFITM3, STAT1, IFIT3, and ISG15 are shown. Stained (solid histogram) and unstained (open histogram) Mφ2 are shown in red, while Mφ2b are depicted in blue.

Repolarization of established M ϕ 2 subsets towards M ϕ 2b is accompanied by efficient control of intracellular *Mtb* outgrowth

Plasticity and flexibility are key features of human monocyte-derived myeloid subsets. It has recently been demonstrated *in vitro* that macrophages are capable of complete repolarization from M ϕ 2 to M ϕ 1, as macrophage polarization status dynamically adapts to changes in the cytokine microenvironment⁽⁵⁹⁾. Since it could be clinically relevant to repolarize macrophages in infectious disease towards M ϕ 2b, in view of their superior antibacterial activity, we investigated whether established M ϕ 2 and M ϕ 2a/c/d cultures could be repolarized towards M ϕ 2b with accompanying high antimicrobial activity, and whether M ϕ 2b could be repolarized towards M ϕ 2 accompanied by loss of control of intracellular infection. To this end, monocytes were first differentiated into M ϕ 2 and M ϕ 2a/b/c/d cell types according to the scheme outlined in **Figure 7**. A proportion of each cell subset was infected with *Mtb* and the intracellular bacterial survival was assessed by CFU assay. The remaining M ϕ 2 and M ϕ 2a/c/d cells were subsequently cultured under M ϕ 2b-polarizing conditions, while M ϕ 2b were exposed to M ϕ 2-polarizing conditions for another 7 days before infection with *Mtb* and examination of bacterial outgrowth (**Figure 7**). The results clearly demonstrated that while M ϕ 2b had significantly lower bacterial burden compared to the other M ϕ 2 subsets at day 7, this could be completely reversed by repolarization to M ϕ 2. Conversely, repolarization of M ϕ 2 and M ϕ 2a/c/d towards a M ϕ 2b phenotype resulted in radically improved control of intracellular *Mtb* compared to their original polarization state. These results provide proof of concept that M ϕ 2 reprogramming towards M ϕ 2b could provide a novel therapeutic strategy for host-directed therapy to treat and improve outcome of human infectious disease, including tuberculosis. The presence of macrophages within TB granulomas that display functional properties associated with a less favourable clinical outcome could potentially be converted into a cell subtype better equipped to control intracellular bacterial infection.

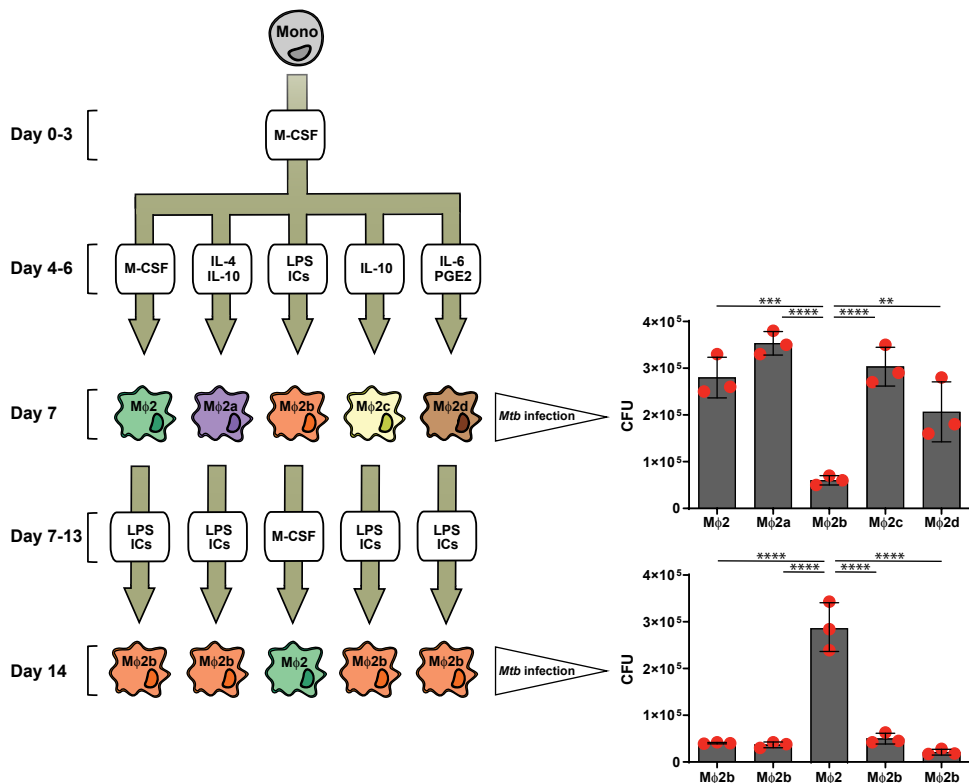


Figure 7: Repolarization of established Mφ2 subsets to Mφ2b is accompanied by efficient control of intracellular *Mtb* outgrowth.

Depicted on the left is a flowchart of the experimental setup. Human monocyte-derived Mφ2, and Mφ2a/b/c/d were harvested at day 6 and re-seeded into 24-well plates. Half of the wells of each cell subset was infected with *Mtb* (MOI = 10) at day 7 and bacterial load was determined by CFU assay. Cells in the remaining wells were re-polarized for 6 days followed by infection with *Mtb* (MOI = 10) at day 14 and bacterial load was again evaluated by CFU assay. Bars depict mean ± standard deviation of 3 replicates from a representative donor out of 10 donors tested. Individual data points are represented by red dots and overlaid on the bar graph. Statistical significance between Mφ2b and all other cell subsets (d7) or Mφ2 and all other cell subsets (d14) was tested using a one-way ANOVA with Dunnett's multiple comparisons test. (** = p-value < 0.01, *** = p-value < 0.001, **** = p-value < 0.0001). ICs = immune complexes.

Discussion

Phenotypic plasticity is a key feature of macrophages as they can rapidly and reversibly change their function and activation state in response to alterations in local microenvironmental signals provided by growth factors, cytokines, microbial products and glucocorticoids^(15, 60). The classical Mφ1-Mφ2 dichotomy initially proposed⁽¹⁰⁾ merely describes the extreme ends of the macrophage polarization spectrum and likely represents an oversimplified *in vitro* model of the continuous range of polarized myeloid states that occur *in vivo*^(9, 25). Moreover, most studies have been directed at dissecting the

role of macrophage polarization in mice. Therefore, we investigated the functional and phenotypic hallmarks of an extensive array of human monocyte-derived myeloid subsets and identified transcriptomic, proteomic and cell surface markers for subset identification. These results should help in developing tools to identify these subsets in human samples.

Notably, we show that M ϕ 2b are polarized macrophages with limited antigen presenting and T cell-activating functions but with potent phagocytic and antibacterial capabilities, highlighting their exceptional aptitude to control survival of intracellular bacteria. These characteristics are in sharp contrast with the functional traits observed for M ϕ 2 and M ϕ 2a/c/d which efficiently presented antigen to induce Th1 responses and were also capable of inducing potent regulatory T cell responses (**Figure 3** and **Supplementary Figure 2**), while none of these macrophage subsets were able to adequately control outgrowth of *Mtb* or *Stm* (**Figure 2**).

The precise mechanism underlying the functional differences observed between M ϕ 2b and the other M ϕ 2 cell types are not yet fully understood. Transcriptomic, proteomic and cell surface marker analysis unambiguously demonstrated that resting M ϕ 2b display a prominent type I interferon signature (**Figures 5 and 6**). *Mtb* infection is known to induce a type I interferon response both *in vitro* and *in vivo*, and while most studies have implicated enhanced expression of type I interferons with detrimental effects on *Mtb* infection^(58, 61, 62), others have demonstrated that the induction of type I interferons through the cytoplasmic surveillance pathway can result in improved mycobacterial control via autophagy⁽⁶³⁻⁶⁵⁾. Of note, signalling through TLR4 or Fc γ receptors alone was sufficient to polarize human monocytes into a phenotype that is superior in controlling intracellular *Mtb* survival (**Supplementary Figure 1**), implying that common signalling pathways downstream of these receptors are responsible for equipping M ϕ 2b with strong anti-microbial activity. Moreover, despite our observation that M ϕ 2b are poor activators of CD4⁺ T cell responses, the relatively increased abundance of proteins involved in MHC class I antigen presentation (e.g. HLA-A, HLA-C, TAP1, TAP2), as observed by quantitative proteomics (**Figure 6C**), suggests that M ϕ 2b could be potent activators of CD8⁺ T cell-responses. However, this remains to be investigated further.

Because human myeloid subsets exhibited profound heterogeneity in their functional profiles (**Figures 2 and 3**), it is crucial to identify markers to (1) classify macrophages present in peripheral blood and patient tissue samples; (2) monitor myeloid subset composition during treatment; and (3) associate alterations with disease severity, progression or resolution. Given the complexity of macrophage populations between rodents and humans in the normal and diseased host, it is key to identify and validate such markers in humans. Hierarchical clustering of eight cell surface markers successfully differentiated between monocytes (CD192^{hi}/CD14^{hi}), DCs (CD206^{hi}/CD209^{hi}/CD163^{lo}), M ϕ 1 (CD206^{hi}/CD209^{lo}/CD163^{lo}) and M ϕ 2a (CD209^{hi}/CD163^{hi}), but was unable to faithfully separate other polarized myeloid subsets analysed. However, subsequent cytokine secretion profiling in response to a mixture of IFN γ /LPS/*Mtb* lysate differentiated (next

to DCs and M ϕ 1) M ϕ 2b by a unique VEGF^{hi}/IL-Ra^{lo} signature (**Figure 4A-C**). Interestingly, targeted transcriptomics was able to discriminate between all myeloid subsets using a unique combination of only 2 transcripts per cell type (**Figure 5B**). Of note, we were unable to verify several markers previously associated with M ϕ 2b/c/d polarization, such as superior IL-10 production by M ϕ 2b⁽⁶⁶⁾, elevated cell surface expression levels of CD163 and MerTK by M ϕ 2c^(33, 67), and reduced cell surface expression levels of co-stimulatory molecules in M ϕ 2d⁽³⁷⁾. These discrepancies may be explained by a lack of standardization between differentiation protocols for polarized human macrophages and the evident translational difficulties between murine and human macrophages.

Since it has recently become clear that polarized myeloid subpopulations are not end-stages of selective differentiation paths of a common monocyte precursor, but rather adaptable intermediates of the monocyte-macrophage lineage characterized by diversity and plasticity, macrophage-centred therapeutic approaches are becoming viable options for host-directed treatment strategies. For example, functional skewing of macrophage subsets from a M ϕ 2 to a M ϕ 1 phenotype has previously been associated with the induction of anti-tumour responses⁽⁶⁸⁻⁷⁰⁾. In addition, several studies have shown that infection with *Mtb* induces macrophage reprogramming towards a M ϕ 2 phenotype by stimulating the secretion of IL-10 and type-2 cytokines while simultaneously interfering with IFN γ activation⁽⁷¹⁾, emphasizing the potential of targeting macrophage differentiation dynamics as adjunct host-directed therapy for treatment of tuberculosis. As proof-of-principle, we report here that M ϕ 2 and M ϕ 2a/c/d can all be redirected towards a M ϕ 2b phenotype concomitant with exceptional control of *Mtb* outgrowth (**Figure 7**). Further research should explore *in vivo* in animal models whether canonical TB therapy in conjunction with host-directed skewing of macrophages towards a M ϕ 2b phenotype by engaging TLRs and/or Fc γ receptors will markedly improve TB treatment outcome or significantly shorten the duration of current TB treatment regimens.

Author contributions

FV, KVW, KvM, JdK and GMJ designed and performed the experiments and processed the experimental data. FV, KVM, JdK, PvV, THMO and MCH contributed to the interpretation of the results. FV, KVW, and MCH wrote the manuscript and designed the figures with input from JdK, GMJ, PvV, SAJ, KvM and THMO. MCH supervised the project and all authors approved the final version of the manuscript.

Acknowledgements

This project was funded by the Netherlands Organization for Health Research and Development (ZonMw-TOP grant 91214038). We also gratefully acknowledge the support of EC TANDEM grant N° 305279. The funders had no role in study design, data collection and analysis, decision to publish, or preparation of the manuscript. The authors declare that they have no conflicting interests.

References

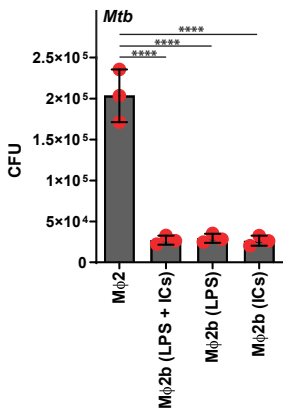
1. World Health Organization. Global Tuberculosis Report. Geneva, Switzerland: 2018.
2. Ramakrishnan L. Revisiting the role of the granuloma in tuberculosis. *Nature reviews Immunology*. 2012;12(5):352-66.
3. McClean CM, Tobin DM. Macrophage form, function, and phenotype in mycobacterial infection: lessons from tuberculosis and other diseases. *Pathogens and disease*. 2016;74(7).
4. G. B. D. Mortality Causes of Death Collaborators. Global, regional, and national life expectancy, all-cause mortality, and cause-specific mortality for 249 causes of death, 1980-2015: a systematic analysis for the Global Burden of Disease Study 2015. *Lancet*. 2016;388(10053):1459-544.
5. Eng S-K, Pusparajah P, Ab Mutalib N-S, Ser H-L, Chan K-G, Lee L-H. Salmonella: A review on pathogenesis, epidemiology and antibiotic resistance. *Frontiers in Life Science*. 2015;8(3):284-93.
6. World Health Organization. https://www.who.int/foodsafety/areas_work/foodborne-diseases/salmonella/en/. 2019.
7. Huang Z, Luo Q, Guo Y, Chen J, Xiong G, Peng Y, et al. Mycobacterium tuberculosis-Induced Polarization of Human Macrophage Orchestrates the Formation and Development of Tuberculous Granulomas In Vitro. *PLoS one*. 2015;10(6):e0129744.
8. Marino S, Cilfone NA, Mattila JT, Linderman JJ, Flynn JL, Kirschner DE. Macrophage polarization drives granuloma outcome during Mycobacterium tuberculosis infection. *Infection and immunity*. 2015;83(1):324-38.
9. Mosser DM. The many faces of macrophage activation. *JLeukocBiol*. 2003;73(2):209-12.
10. Verreck FA, de BT, Langenberg DM, Hoeve MA, Kramer M, Vaisberg E, et al. Human IL-23-producing type 1 macrophages promote but IL-10-producing type 2 macrophages subvert immunity to (myco)bacteria. *ProcNatlAcadSciUSA*. 2004;101(13):4560-5.
11. Verreck FA, de BT, Langenberg DM, van der Zanden L, Ottenhoff TH. Phenotypic and functional profiling of human proinflammatory type-1 and anti-inflammatory type-2 macrophages in response to microbial antigens and IFN-gamma- and CD40L-mediated costimulation. *JLeukocBiol*. 2006;79(2):285-93.
12. Fleetwood AJ, Lawrence T, Hamilton JA, Cook AD. Granulocyte-macrophage colony-stimulating factor (CSF) and macrophage CSF-dependent macrophage phenotypes display differences in cytokine profiles and transcription factor activities: implications for CSF blockade in inflammation. *JImmunol*. 2007;178(8):5245-52.
13. Mantovani A, Biswas SK, Galdiero MR, Sica A, Locati M. Macrophage plasticity and polarization in tissue repair and remodelling. *JPathol*. 2013;229(2):176-85.
14. Savage ND, de BT, Walburg KV, Joosten SA, van MK, Geluk A, et al. Human anti-inflammatory macrophages induce Foxp3+ GITR+ CD25+ regulatory T cells, which suppress via membrane-bound TGFbeta-1. *JImmunol*. 2008;181(3):2220-6.
15. Sica A, Mantovani A. Macrophage plasticity and polarization: in vivo veritas. *JClinInvest*. 2012;122(3):787-95.

16. Lumeng CN, Bodzin JL, Saltiel AR. Obesity induces a phenotypic switch in adipose tissue macrophage polarization. *JClinInvest*. 2007;117(1):175-84.
17. Mantovani A, Garlanda C, Locati M. Macrophage diversity and polarization in atherosclerosis: a question of balance. *ArteriosclerThrombVascBiol*. 2009;29(10):1419-23.
18. Kraaij MD, Savage ND, van der Kooij SW, Koekkoek K, Wang J, van den Berg JM, et al. Induction of regulatory T cells by macrophages is dependent on production of reactive oxygen species. *ProcNatlAcadSciUSA*. 2010;107(41):17686-91.
19. Montoya D, Cruz D, Teles RM, Lee DJ, Ochoa MT, Krutzik SR, et al. Divergence of macrophage phagocytic and antimicrobial programs in leprosy. *Cell HostMicrobe*. 2009;6(4):343-53.
20. van DM, Savage ND, Jordanova ES, Briaire-de Bruijn IH, Walburg KV, Ottenhoff TH, et al. Anti-inflammatory M2 type macrophages characterize metastasized and tyrosine kinase inhibitor-treated gastrointestinal stromal tumors. *IntJCancer*. 2010;127(4):899-909.
21. Sica A, Schioppa T, Mantovani A, Allavena P. Tumour-associated macrophages are a distinct M2 polarised population promoting tumour progression: potential targets of anti-cancer therapy. *EurJCancer*. 2006;42(6):717-27.
22. Wynn TA, Chawla A, Pollard JW. Macrophage biology in development, homeostasis and disease. *Nature*. 2013;496(7446):445-55.
23. Lavin Y, Mortha A, Rahman A, Merad M. Regulation of macrophage development and function in peripheral tissues. *NatRevImmunol*. 2015;15(12):731-44.
24. Amit I, Winter DR, Jung S. The role of the local environment and epigenetics in shaping macrophage identity and their effect on tissue homeostasis. *NatImmunol*. 2015;17(1):18-25.
25. Mantovani A, Sica A, Sozzani S, Allavena P, Vecchi A, Locati M. The chemokine system in diverse forms of macrophage activation and polarization. *Trends Immunol*. 2004;25(12):677-86.
26. Jetten N, Verbruggen S, Gijbels MJ, Post MJ, De Winther MP, Donners MM. Anti-inflammatory M2, but not pro-inflammatory M1 macrophages promote angiogenesis in vivo. *Angiogenesis*. 2014;17(1):109-18.
27. Gordon S, Martinez FO. Alternative activation of macrophages: mechanism and functions. *Immunity*. 2010;32(5):593-604.
28. Filardy AA, Pires DR, Nunes MP, Takiya CM, Freire-de-Lima CG, Ribeiro-Gomes FL, et al. Proinflammatory clearance of apoptotic neutrophils induces an IL-12(low)IL-10(high) regulatory phenotype in macrophages. *JImmunol*. 2010;185(4):2044-50.
29. Fleming BD, Mosser DM. Regulatory macrophages: setting the threshold for therapy. *EurJImmunol*. 2011;41(9):2498-502.
30. Anderson CF, Mosser DM. A novel phenotype for an activated macrophage: the type 2 activated macrophage. *JLeukocBiol*. 2002;72(1):101-6.
31. Goerdts S, Orfanos CE. Other functions, other genes: alternative activation of antigen-presenting cells. *Immunity*. 1999;10(2):137-42.
32. Lu J, Cao Q, Zheng D, Sun Y, Wang C, Yu X, et al. Discrete functions of M2a and M2c macrophage subsets determine their relative efficacy in treating chronic kidney disease. *Kidney Int*. 2013;84(4):745-55.

33. Zizzo G, Hilliard BA, Monestier M, Cohen PL. Efficient clearance of early apoptotic cells by human macrophages requires M2c polarization and MerTK induction. *J Immunol.* 2012;189(7):3508-20.
34. Galdiero MR, Garlanda C, Jaillon S, Marone G, Mantovani A. Tumor associated macrophages and neutrophils in tumor progression. *J Cell Physiol.* 2013;228(7):1404-12.
35. Qian BZ, Pollard JW. Macrophage diversity enhances tumor progression and metastasis. *Cell.* 2010;141(1):39-51.
36. Heusinkveld M, PJ dVvS, Goedemans R, Ramwadhoebe TH, Gorter A, Welters MJ, et al. M2 macrophages induced by prostaglandin E2 and IL-6 from cervical carcinoma are switched to activated M1 macrophages by CD4+ Th1 cells. *J Immunol.* 2011;187(3):1157-65.
37. Duluc D, Delneste Y, Tan F, Moles MP, Grimaud L, Lenoir J, et al. Tumor-associated leukemia inhibitory factor and IL-6 skew monocyte differentiation into tumor-associated macrophage-like cells. *Blood.* 2007;110(13):4319-30.
38. Leclerc L, Boudard D, Pourchez J, Forest V, Sabido O, Bin V, et al. Quantification of micro-sized fluorescent particles phagocytosis to a better knowledge of toxicity mechanisms. *Inhal Toxicol.* 2010;22(13):1091-100.
39. Korbee CJ, Heemskerk MT, Kocev D, van Strijen E, Rabiee O, Franken K, et al. Combined chemical genetics and data-driven bioinformatics approach identifies receptor tyrosine kinase inhibitors as host-directed antimicrobials. *Nature communications.* 2018;9(1):358.
40. Jett BD, Hatter KL, Huycke MM, Gilmore MS. Simplified agar plate method for quantifying viable bacteria. *Biotechniques.* 1997;23(4):648-50.
41. Joosten SA, van Meijgaarden KE, van Weeren PC, Kazi F, Geluk A, Savage ND, et al. Mycobacterium tuberculosis peptides presented by HLA-E molecules are targets for human CD8 T-cells with cytotoxic as well as regulatory activity. *PLoS pathogens.* 2010;6(2):e1000782.
42. Joosten SA, Goeman JJ, Sutherland JS, Opmeer L, de Boer KG, Jacobsen M, et al. Identification of biomarkers for tuberculosis disease using a novel dual-color RT-MLPA assay. *Genes Immun.* 2012;13(1):71-82.
43. Rohart F, Gautier B, Singh A, Le Cao KA. mixOmics: An R package for 'omics feature selection and multiple data integration. *PLoS Comput Biol.* 2017;13(11):e1005752.
44. de Keijzer J, de Haas PE, de Ru AH, van Veelen PA, van Soolingen D. Disclosure of selective advantages in the "modern" sublineage of the Mycobacterium tuberculosis Beijing genotype family by quantitative proteomics. *Mol Cell Proteomics.* 2014;13(10):2632-45.
45. Wisniewski JR, Zougman A, Nagaraj N, Mann M. Universal sample preparation method for proteome analysis. *Nat Methods.* 2009;6(5):359-62.
46. Boersema PJ, Raijmakers R, Lemeer S, Mohammed S, Heck AJ. Multiplex peptide stable isotope dimethyl labeling for quantitative proteomics. *Nat Protoc.* 2009;4(4):484-94.
47. Cox J, Mann M. MaxQuant enables high peptide identification rates, individualized p.p.b.-range mass accuracies and proteome-wide protein quantification. *Nat Biotechnol.* 2008;26(12):1367-72.

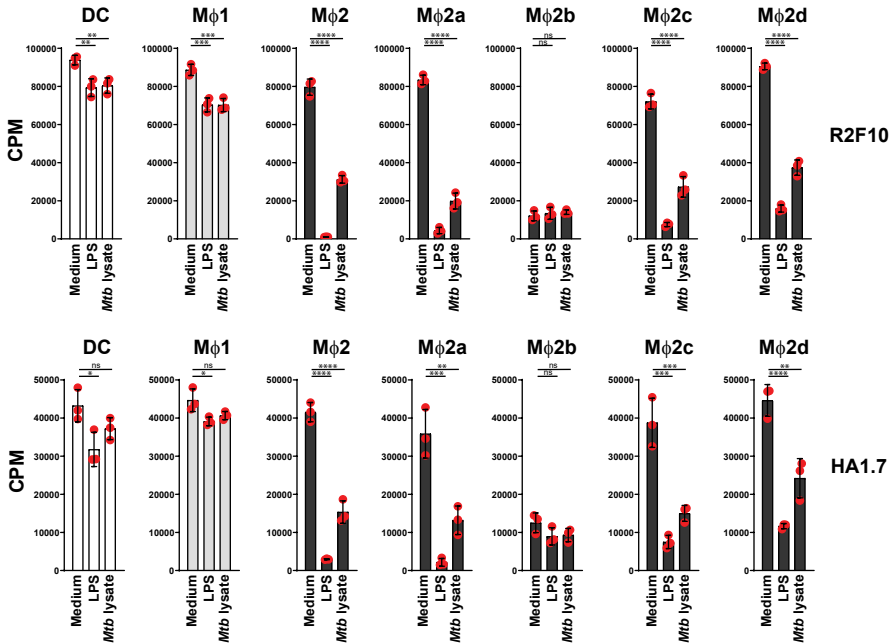
48. Cox J, Neuhauser N, Michalski A, Scheltema RA, Olsen JV, Mann M. Andromeda: a peptide search engine integrated into the MaxQuant environment. *JProteomeRes*. 2011;10(4):1794-805.
49. Vizcaino JA, Deutsch EW, Wang R, Csordas A, Reisinger F, Rios D, et al. ProteomeXchange provides globally coordinated proteomics data submission and dissemination. *NatBiotechnol*. 2014;32(3):223-6.
50. Yu G, Wang LG, Han Y, He QY. clusterProfiler: an R package for comparing biological themes among gene clusters. *OMICS*. 2012;16(5):284-7.
51. Schlicker A, Domingues FS, Rahnenfuhrer J, Lengauer T. A new measure for functional similarity of gene products based on Gene Ontology. *BMC Bioinformatics*. 2006;7:302.
52. Yu G, Li F, Qin Y, Bo X, Wu Y, Wang S. GOSemSim: an R package for measuring semantic similarity among GO terms and gene products. *Bioinformatics*. 2010;26(7):976-8.
53. Murray PJ. Macrophage Polarization. *Annu Rev Physiol*. 2017;79:541-66.
54. Bekker LG, Freeman S, Murray PJ, Ryffel B, Kaplan G. TNF-alpha controls intracellular mycobacterial growth by both inducible nitric oxide synthase-dependent and inducible nitric oxide synthase-independent pathways. *JImmunol*. 2001;166(11):6728-34.
55. Munder M, Eichmann K, Moran JM, Centeno F, Soler G, Modolell M. Th1/Th2-regulated expression of arginase isoforms in murine macrophages and dendritic cells. *JImmunol*. 1999;163(7):3771-7.
56. Williams KC, Kim WK. Editorial: Identification of in vivo markers for human polarized macrophages: a need that's finally met. *J Leukoc Biol*. 2015;98(4):449-50.
57. Haks MC, Goeman JJ, Magis-Escurra C, Ottenhoff TH. Focused human gene expression profiling using dual-color reverse transcriptase multiplex ligation-dependent probe amplification. *Vaccine*. 2015;33(40):5282-8.
58. McNab F, Mayer-Barber K, Sher A, Wack A, O'Garra A. Type I interferons in infectious disease. *Nature reviews Immunology*. 2015;15(2):87-103.
59. Davis MJ, Tsang TM, Qiu Y, Dayrit JK, Freij JB, Huffnagle GB, et al. Macrophage M1/M2 polarization dynamically adapts to changes in cytokine microenvironments in *Cryptococcus neoformans* infection. *MBio*. 2013;4(3):e00264-13.
60. Mosser DM, Edwards JP. Exploring the full spectrum of macrophage activation. *NatRevImmunol*. 2008;8(12):958-69.
61. Berry MP, Graham CM, McNab FW, Xu Z, Bloch SA, Oni T, et al. An interferon-inducible neutrophil-driven blood transcriptional signature in human tuberculosis. *Nature*. 2010;466(7309):973-7.
62. Novikov A, Cardone M, Thompson R, Shenderov K, Kirschman KD, Mayer-Barber KD, et al. Mycobacterium tuberculosis triggers host type I IFN signaling to regulate IL-1beta production in human macrophages. *Journal of immunology*. 2011;187(5):2540-7.
63. Collins AC, Cai H, Li T, Franco LH, Li XD, Nair VR, et al. Cyclic GMP-AMP Synthase Is an Innate Immune DNA Sensor for Mycobacterium tuberculosis. *Cell host & microbe*. 2015;17(6):820-8.

64. Watson RO, Bell SL, MacDuff DA, Kimmey JM, Diner EJ, Olivas J, et al. The Cytosolic Sensor cGAS Detects Mycobacterium tuberculosis DNA to Induce Type I Interferons and Activate Autophagy. *Cell host & microbe*. 2015;17(6):811-9.
65. Dey B, Dey RJ, Cheung LS, Pokkali S, Guo H, Lee JH, et al. A bacterial cyclic dinucleotide activates the cytosolic surveillance pathway and mediates innate resistance to tuberculosis. *Nature medicine*. 2015;21(4):401-6.
66. Gerber JS, Mosser DM. Reversing lipopolysaccharide toxicity by ligating the macrophage Fc gamma receptors. *Journal of immunology*. 2001;166(11):6861-8.
67. Ohlsson SM, Linge CP, Gullstrand B, Lood C, Johansson A, Ohlsson S, et al. Serum from patients with systemic vasculitis induces alternatively activated macrophage M2c polarization. *ClinImmunol*. 2014.
68. Guiducci C, Vicari AP, Sangaletti S, Trinchieri G, Colombo MP. Redirecting in vivo elicited tumor infiltrating macrophages and dendritic cells towards tumor rejection. *Cancer research*. 2005;65(8):3437-46.
69. Dominguez-Soto A, de las Casas-Engel M, Bragado R, Medina-Echeverz J, Aragoneses-Fenoll L, Martin-Gayo E, et al. Intravenous immunoglobulin promotes antitumor responses by modulating macrophage polarization. *Journal of immunology*. 2014;193(10):5181-9.
70. Pyonteck SM, Akkari L, Schuhmacher AJ, Bowman RL, Sevenich L, Quail DF, et al. CSF-1R inhibition alters macrophage polarization and blocks glioma progression. *Nature medicine*. 2013;19(10):1264-72.
71. Lugo-Villarino G, Verollet C, Maridonneau-Parini I, Neyrolles O. Macrophage polarization: convergence point targeted by mycobacterium tuberculosis and HIV. *Frontiers in immunology*. 2011;2:43.



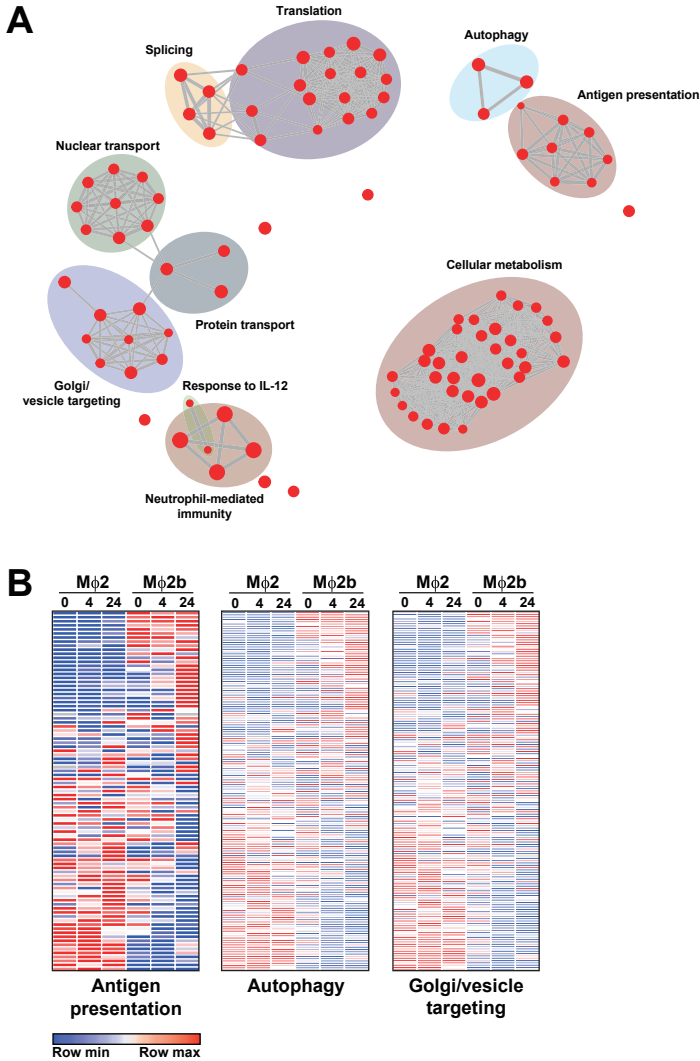
Supplementary Figure 1: Control of intracellular bacterial infections by Mφ2b.

CFU assay of human monocyte-derived Mφ2 and Mφ2b infected with *Mtb* at a MOI of 10. Mφ2b were generated by combined exposure to 10 ng/ml LPS and 1 μg/ml IgG-Ovalbumin (OVA) immune complexes (ICs) or the single stimuli. Bars depict mean ± standard deviation of 3 replicates from a representative donor out of 3 donors tested. Individual data points are represented by red dots and overlaid on the bar graph. Statistical significance between Mφ2 and all other myeloid subsets was tested using a one-way ANOVA with Dunnett's multiple comparisons test. (**** = p-value <0.0001).



Supplementary Figure 2: Induction of T cell responses by polarized myeloid subsets.

Antigen-presenting capacity of polarized myeloid subsets was determined following activation for 16h with LPS (100 ng/ml), *Mtb* lysate (100 ng/ml) or medium as a negative control before incubation with either the HLA-DR2-restricted CD4⁺ T cell clone R2F10 or the HLA-DR1-restricted CD4⁺ T cell clone HA1.7 in the presence of their cognate antigen (*M.leprae* hsp65 p418-427 (10 μg/ml recombinant peptide) and influenza hemagglutinin (synthetic peptide p306-318; 100 ng/ml), respectively. After 3 days of co-culture the proliferative response of the responder T cell clones was determined by [³H] TdR incorporation. No proliferation was detectable in the absence of cognate peptide. Data are expressed in counts per minute (CPM). Bars depict mean ± standard deviation of 3 replicates from a representative donor out of 3 donors tested. Individual data points represented by red dots are overlaid on the bar graph. Statistical significance between rested and pre-activated cells was tested using a one-way ANOVA with Dunnett's multiple comparisons test. (* = p-value <0.05, ** = p-value <0.01, *** = p-value <0.001, **** = p-value <0.0001, ns = not significant).



Supplementary Figure 3: Gene ontology (GO) term enrichment analysis of proteins expressed in both M ϕ 2 and M ϕ 2b independent of infection status.

(A) Gene ontology (GO) term enrichment analysis of a total of 2724 proteins detected in both M ϕ 2 and M ϕ 2b either at baseline (uninfected), following *Mtb* infection, or both. The top 100 most significantly enriched 'Biological Processes' are displayed as an enrichment map, and pathway clusters were further classified by their shared overarching cellular processes. (B) Heatmaps of individual proteins expressed by both M ϕ 2 and M ϕ 2b and involved in antigen presentation, autophagy or Golgi/vesicle targeting. Rows and columns correspond to the cellular proteins and profiled myeloid subsets, respectively. Each row represents the relative amount of cellular protein using a blue to white to red colour scale.

CHAPTER

3

The effect of hyperglycaemia on in vitro cytokine production and macrophage infection with *Mycobacterium tuberculosis*

Ekta Lachmandas^{1,2*}, Frank Vrieling^{3*}, Louis G. Wilson³, Simone A. Joosten³, Mihai G. Netea^{1,2}, Tom H. Ottenhoff³ and Reinout van Crevel^{1,2,#}

¹ Department of Internal Medicine, Radboud University Medical Center, Nijmegen, The Netherlands

² Radboud Center for Infectious Diseases, Radboud University Medical Center, Nijmegen, The Netherlands.

³ Department of Infectious Diseases, Leiden University Medical Center, Leiden, The Netherlands

* these authors contributed equally to this work

Type 2 diabetes mellitus is an established risk factor for tuberculosis but the underlying mechanisms are largely unknown. We examined the effects of hyperglycaemia, a hallmark of diabetes, on the cytokine response to and macrophage infection with *Mycobacterium tuberculosis*. Increasing in vitro glucose concentrations from 5 to 25 mmol/L had marginal effects on cytokine production following stimulation of peripheral blood mononuclear cells (PBMCs) with *M. tuberculosis* lysate, LPS or *Candida albicans*, while 40 mmol/L glucose increased production of TNF- α , IL-1 β , IL-6 and IL-10, but not of IFN- γ , IL-17A and IL-22. Macrophage differentiation under hyperglycaemic conditions of 25 mmol/L glucose was also associated with increased cytokine production upon stimulation with *M. tuberculosis* lysate and LPS but in infection experiments no differences in *M. tuberculosis* killing or outgrowth was observed. The phagocytic capacity of these hyperglycaemic macrophages also remained unaltered. The fact that only very high glucose concentrations were able to significantly influence cytokine production by macrophages suggests that hyperglycaemia alone cannot fully explain the increased susceptibility of diabetes mellitus patients to tuberculosis.

Introduction

Type 2 diabetes mellitus (DM) has been increasingly recognized as an important risk factor for tuberculosis (TB). Epidemiological studies have demonstrated that adults with diabetes have a significantly increased risk of developing active TB⁽¹⁾ and it is estimated that globally 15% of TB cases are attributable to DM⁽²⁾. The global prevalence of DM will rise by an estimated 55% over the next 20 years, with the largest increases in TB endemic regions of Africa and Asia⁽³⁾. As a result, DM will become an increasingly important factor contributing to the sustained TB epidemic^(4,5).

The causative pathogen of TB, *Mycobacterium tuberculosis* (MTB), primarily infects phagocytic cells of the lung, such as alveolar macrophages. The early stage of infection is characterised by the recruitment and accumulation of various innate immune cells at the site of infection including neutrophils, dendritic cells and interstitial macrophages, the latter of which subsequently become infected by the growing population of mycobacteria and ultimately develop into bacteria-sequestering granulomas^(6,7). Effective immunity against MTB is dependent on the production of pro-inflammatory cytokines like interferon- γ (IFN- γ) and tumour necrosis factor- α (TNF- α)⁽⁸⁻¹¹⁾, whilst anti-inflammatory cytokines such as interleukin-(IL)-10 can attenuate the anti-bacterial immune response^(10,12).

It has been hypothesised that alterations in the immune response of patients with diabetes give rise to either an enhanced susceptibility to infection or accelerated progression towards active TB disease⁽⁵⁾. A possible explanation for these immunological changes is chronic hyperglycaemia, a hallmark of DM. Various studies have demonstrated that diabetes and hyperglycaemia in particular is associated with a compromised innate immune response which includes impairments in phagocytosis, cytokine secretion and macrophage activation⁽¹³⁻¹⁸⁾. Other studies that have investigated the adaptive arm of the immune response have yielded conflicting results when comparing differences in cytokine production between diabetes patients with or without TB⁽¹⁹⁻²¹⁾. These inconsistent data illustrate both the complexity of the interaction between TB and DM and reveal limitations in the comparability of studies that use divergent methods, such as differences in cellular origins and patient populations.

To better understand the effects of hyperglycaemia on the innate immune response during concurrent diabetes and tuberculosis, we investigated whether elevated concentrations of glucose could directly regulate the functional capacities of human macrophages *in vitro*. We initially determined the effects of hyperglycaemia on the cytokine response of PBMCs and macrophages after stimulation with bacterial lipopolysaccharide (LPS) or whole pathogen lysates, and later in alternatively activated (M2) macrophages upon infection with the MTB strain H37Rv. Finally, we assessed the phagocytic ability of hyperglycaemic M2 macrophages and studied their capacity to support mycobacterial outgrowth.

Materials and Methods

Ethics Statement

PBMCs were isolated from buffy coats donated after written informed consent by healthy volunteers to the Sanquin Bloodbank (<http://www.sanquin.nl/en/>) in Nijmegen and Leiden. Blood was collected anonymously which, according to institutional ethical policy, does not require a separate review by the Ethical Committee. Experiments were conducted according to the principles expressed in the Declaration of Helsinki.

Healthy Volunteers

Since blood donations were anonymous no tuberculosis skin test or IFN- γ release assay could be performed but the incidence of TB in the indigenous Dutch population is extremely low (4/100,000) and Bacillus Calmette-Guérin (BCG) vaccination is not part of the routine vaccination program. The incidence of diabetes mellitus in the Dutch population for persons under 25 years of age is less than 1% and under 45 years of age is about 1.5%. Since the average age of blood donors in these experiments is approximately 45 years⁽²²⁾ we expect that almost none of them would have diabetes mellitus which would otherwise act as a confounding factor⁽²³⁾.

Cytokine Stimulation Experiments

Isolation of peripheral blood mononuclear cells (PBMCs) was performed by differential centrifugation over Ficoll-Paque (GE Healthcare) within 0-2 hours of collection. After counting (Casy Counter) cells were adjusted to 5×10^6 cells/mL were suspended in glucose free RPMI 1640 (Gibco) supplemented with 50 mg/mL gentamicin (Lonza) and 2 mM L-glutamine (Life Technologies). 100 μ L of PBMCs was incubated in flat bottom 96-well plates (Greiner) with varying final glucose concentrations from 5 mmol/L to 40 mmol/L D-glucose (Sigma-Aldrich) in glucose-free RPMI, and stimulated with 1 μ g/mL of H37Rv lysate, 1×10^6 microorganisms/mL of heat-killed *Candida albicans* (ATCC MYA-3573 (UC 820)) or 10 ng/mL LPS (Sigma-Aldrich, E. coli serotype 055:B5). The plates were incubated for 24 h, 48 h or 7 days at 37°C in a 5% CO₂ environment. Alternatively, 100 μ L of PBMCs (5×10^6 /mL) was incubated for 1 h at 37°C in 5% CO₂ and adherent monocytes were selected by washing out non-adherent cells with warm PBS. Adherent monocytes were differentiated into M2 macrophages (n=18) in 10% human pooled serum and 50 ng/mL M-CSF (R&D Systems) or M0 macrophages (n=23) in 10% human pooled serum for 6 days. Monocytes were differentiated in the presence of 5 mmol/L or 25 mmol/L glucose. In some cases monocytes were differentiated in 5 mmol/L glucose with 20 mmol/L mannitol (Sigma-Aldrich) to control for effects of osmolarity on cytokine production. Media containing M-CSF and/or serum and glucose were refreshed on day 3 of differentiation. Differentiated macrophages were stimulated on day 6 with RPMI (negative control), 1 μ g/mL H37Rv lysate or 10 ng/mL LPS (positive control). Cell culture supernatants were collected after 24 h.

Cytokine Measurements

Cell culture supernatants were collected and stored at -20°C for cytokine measurements, which were performed by ELISA: IL-1 β , TNF- α , IL-17A, IL-22 (R&D Systems); IL-6, IFN- γ and IL-10 (Sanquin).

H37Rv Lysates and Culture

Cultures of H37Rv MTB were grown to mid-log phase in Middlebrook 7H9 liquid medium (Difco, Becton-Dickinson) supplemented with oleic acid/albumin/dextrose/catalase (OADC) (BBL, Becton-Dickinson), washed three times in sterile saline, heat killed and then disrupted using a bead beater, after which the concentration was measured using a bicinchoninic acid (BCA) assay (Pierce, Thermo Scientific).

H37Rv Infection of M2 macrophages

CD14⁺ monocytes were isolated from PBMCs by magnetic cell sorting with anti-CD14⁺ coated beads (Miltenyi Biotec) and seeded in tissue culture-treated flasks (Corning). After 6 days of differentiation in the presence of 50 ng/mL M-CSF, M2 macrophages were harvested using trypsin and transferred to tissue culture-treated 24-well plates (Corning) with 300,000 macrophages per well. Macrophages were incubated O/N at 37°C in 5% CO₂ and subsequently infected with the H37Rv strain of MTB. Mycobacterial cultures were diluted to pre-log phase density one day before infection to ensure that the bacteria were in the log phase of the growth curve. Bacterial density was determined by measuring optical density at 600 nm (OD-600) and the bacterial suspension was diluted to a concentration of 30 x 10⁶ bacteria/mL (MOI 10:1). 100 μ L of the bacterial suspension was added to the cell cultures, after which the plates were centrifuged for 3 minutes at 800 rpm and incubated at 37°C in 5% CO₂. After 60 minutes the plates were washed with culture medium containing 30 μ g/mL gentamicin and subsequently incubated O/N at 37°C in 5% CO₂ in medium containing 5 μ g/mL gentamicin. Supernatants were collected and filtered before cytokine measurements. M2 macrophages were lysed in water for 5 minutes and plated on Middlebrook 7H10 agar (Difco, Becton-Dickinson) supplemented with OADC. CFUs were determined after 2-3 weeks.

Cell viability assay

Macrophage viability during prolonged H37Rv infection was assessed by using a LDH cytotoxicity kit according to the manufacturer's instructions (Pierce, Thermo Scientific). For each experimental condition 50 μ L of freshly harvested supernatant was incubated with 50 μ L LDH reaction mixture for 30 minutes at room temperature in a 96-well plate. The reaction was stopped by adding 50 μ L of stop solution and the plate was subsequently measured on a Mithras LB 940 microplate reader (Berthold Technologies) at 485 nm. Spontaneous and maximum LDH release controls were included in order to calculate

the percentage of cytotoxicity. Macrophages were additionally stained with Trypan Blue (Sigma-Aldrich) as a second measure of cell viability.

Phagocytosis Quantification Assay

To quantify phagocytic capacity, fluorescent polystyrene particles (Fluoresbrite YG carboxylate microspheres) were used as described by Leclerc *et al* ⁽²⁴⁾. In short, M2 macrophages were incubated with P-beads in a ratio of 10 beads to 1 cell for 90 minutes at 37°C. Subsequently cells were collected with a cell scraper and centrifuged at 1500 rpm for 10 minutes. Following centrifugation supernatant was discarded and cells were re-suspended in 100 µL culture medium or 100 µL culture medium and Trypan Blue (1:1) (Sigma-Aldrich). Internalisation of the beads was quantified by flow cytometry. Non-internalised beads emitted a red fluorescent signal after Trypan Blue quenching which was detected in the FL-3 channel whereas internalised beads were detected in the FL-1 channel.

Statistical Analysis

Differences were analysed using a Wilcoxon signed rank test (paired, non-parametric analysis) unless otherwise stated. Data was considered statistically significant at a p-value <0.05. Data are shown as cumulative results of levels obtained in all volunteers (means ± SEM).

Results

Hyperglycaemic culture conditions variably affect cytokine production from PBMCs.

Little or no difference was seen in cytokine production following stimulation and culture of PBMCs in glucose concentrations ranging from 5 to 25 mmol/L, while culture in 40 mmol/L glucose mostly led to higher cytokine production (Figure 1). Production of pro-inflammatory cytokines IL-6 and IL-1β significantly increased in a dose dependent manner upon H37Rv stimulation whereas TNF-α production only increased at the highest glucose concentrations of 40 mmol/L. Production of the anti-inflammatory cytokine IL-10 also increased upon H37Rv lysate and *Candida* stimulations in the presence of 25 mmol/L or 40 mmol/L glucose. In comparison, induction of T-cell cytokines showed a high degree of variability in response to varying glucose concentrations. Overall, compared to normal glucose concentrations of 5 mmol/L, 40 mmol/L glucose showed the most significant changes in cytokine production (all p-values <0.05).

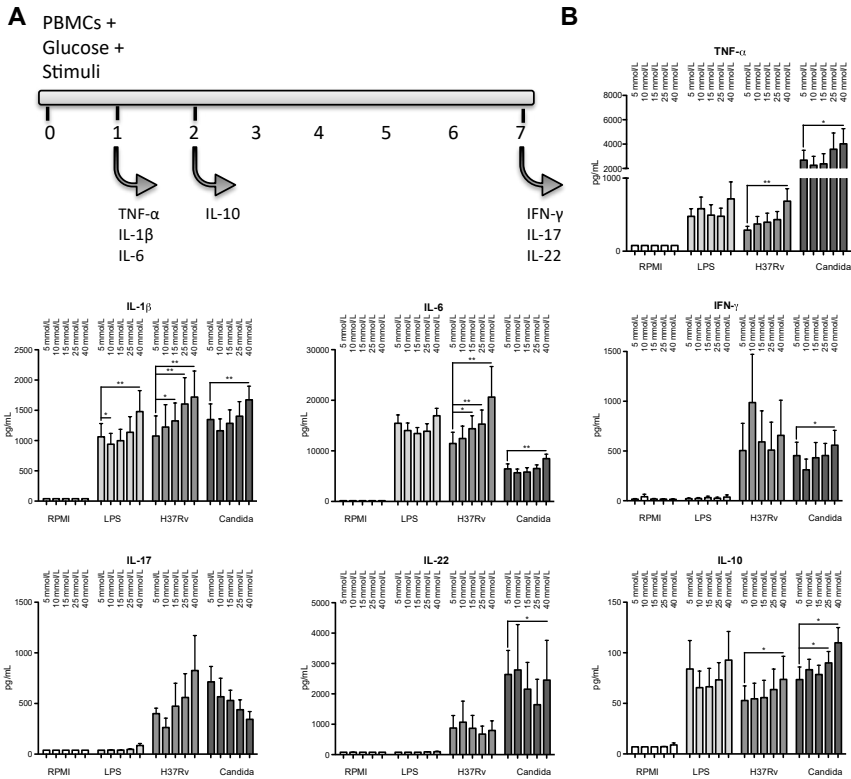


Figure 1: Cytokine production by PBMCs in response to antigenic stimuli in varying concentrations of glucose.

(A) PBMCs were stimulated in the presence of 5 mmol/L to 40 mmol/L glucose with RPMI, H37Rv lysate (1 μ g/mL), LPS (10 ng/mL) or heat-killed *Candida Albicans* (1 $\times 10^6$ microorganisms/mL). Cell culture supernatants were collected after 24 h, 48 h or 7 days. (B) Data are shown as mean \pm SEM of supernatant TNF- α , IL-1 β , IL-6, IFN- γ , IL-17, IL-22 and IL-10 levels obtained in ≥ 6 volunteers, * $p < 0.05$, ** $p < 0.01$.

Macrophage differentiation in hyperglycaemic conditions leads to hyper-responsive cytokine production.

The effect of hyperglycaemia on PBMC cytokine production was mild and mainly observed at the highest glucose concentrations (40 mmol/L). Both 25 mmol/L and 40 mmol/L of glucose can be observed in diabetes patients although the latter is rarely seen and is thus unlikely to account for the increase in TB susceptibility. We therefore proceeded by differentiating monocytes into M0 (serum derived) and M2 (M-CSF and serum derived) macrophages in the presence of 5 mmol/L glucose or the more clinically relevant hyperglycaemic condition of 25 mmol/L glucose. M2 macrophage differentiation was verified by assessing cell surface marker expression (CD14⁺/CD163⁺; Figure S1). Differentiated macrophages were stimulated with LPS or H37Rv lysate (Figure 2A). Cytokine production was generally higher in macrophages differentiated under high

glucose concentrations, although not all differences were statistically significant. Pro-inflammatory cytokines (TNF- α and IL-6) and anti-inflammatory cytokines (IL-10 and IL-1RA) from hyperglycaemic M2 macrophages were significantly increased after stimulation with H37Rv lysate and LPS. M0 macrophages displayed a similar pattern, except for TNF- α production. Sub-maximal concentrations of LPS and H37Rv were used to provide room for the potential boosting effects of hyperglycaemia on cytokine production.

Given the nature of these experiments the observed increase in cytokine production may have simply been a consequence of increased osmolarity during cell culture. To control for this, mannitol was used to achieve similar osmolarity in the 5 mmol/L and 25 mmol/L culture conditions (Figure S2). In most cases the elevated cytokine production from M0 and M2 hyperglycaemic macrophages, as seen in Figure 2B, was reproducible under osmolarity controlled conditions. Thus the effects of hyperglycaemia on cytokine production cannot simply be explained by a difference in osmolarity.

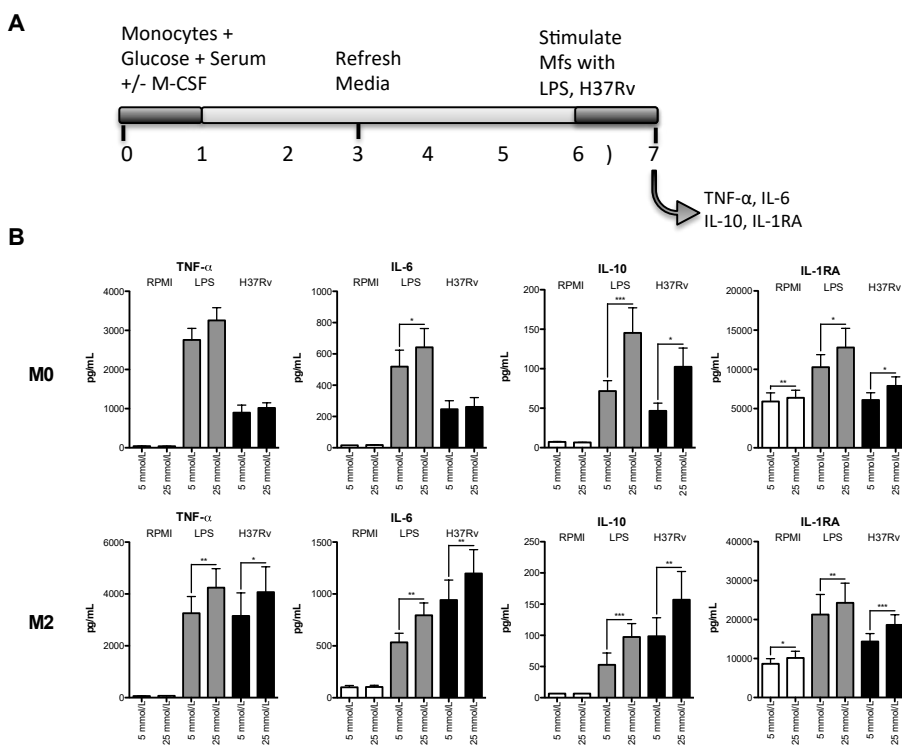


Figure 2: Cytokine production by M0 and M2 macrophages stimulated in varying concentrations of glucose.

(A) Adherent monocytes were differentiated in either 5 or 25 mmol/L glucose into M0 macrophages (serum only) or M2 macrophages (M-CSF and serum) for 6 days and stimulated with RPMI, H37Rv lysate (1 μ g/mL) or LPS (10 ng/mL). (B) Cell culture supernatants were collected and the pro-inflammatory cytokines TNF- α and IL-6 were measured along with the anti-inflammatory cytokines IL-10 and IL-1RA ($n = 23$). Data are shown as mean \pm SEM, * $p < 0.05$, ** $p < 0.01$ & , *** $p < 0.001$.

Hyperglycaemia does not affect the cytokine response to and the survival of *M. tuberculosis* in human macrophages.

After investigating the cytokine profiles of macrophages stimulated with either LPS or H37Rv lysate in the presence of varying glucose concentrations the effect of hyperglycaemia on the *in vitro* infection of M2 macrophages with the H37Rv strain of MTB was determined. M2 macrophages were used for the infection experiments as we have previously shown that this macrophage subtype is more adept in supporting mycobacterial survival and could therefore serve as the primary bacterial reservoir in the lungs during MTB infection⁽²⁵⁾. After 24 h of infection no differences in CFU counts (Figure 3B) or cytokine production (Figure 3C) were observed between euglycaemic (5 mmol/L) and hyperglycaemic (25 mmol/L) macrophages. We also examined the effect of hyperglycaemia on the phagocytic capacity of macrophages and outgrowth of H37Rv after prolonged infection. M2 macrophages were able to control MTB growth as was demonstrated by a 1 log reduction in CFU over time (Figure 4B). However, differentiation and stimulation of M2 macrophages in the presence of 5 or 25 mmol/L of glucose were not associated with differences in the phagocytosis of fluorescent P-beads (Figure 4A), mycobacterial uptake (D0 Sups) and H37Rv survival throughout the course of infection (Figure 4B). We assessed macrophage viability during infection by measuring LDH release and staining the cells with Trypan Blue and found no differences in viability between glucose conditions (Figure S3). Together these data demonstrate that hyperglycaemia influences neither *in vitro* H37Rv infection and survival nor the infection-induced cytokine response in human M2 macrophages.

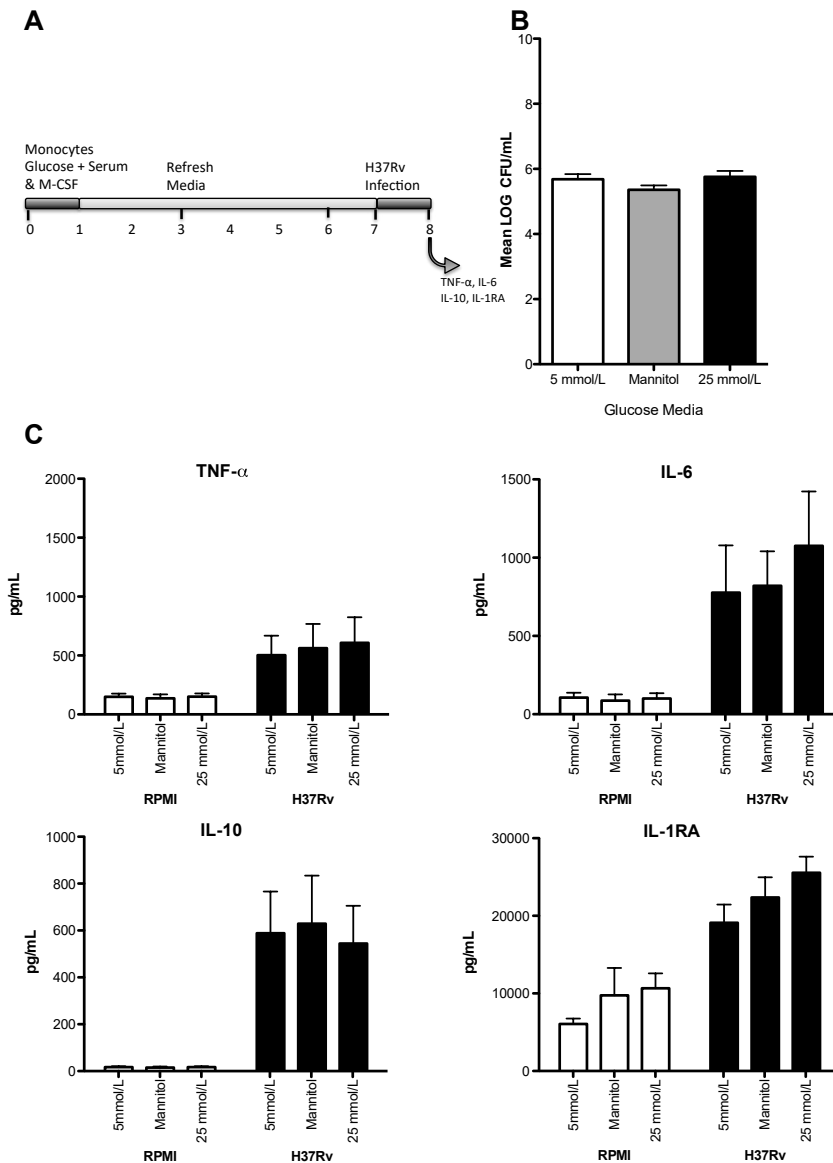


Figure 3: Effects of euglycaemic and hyperglycaemic culture conditions on H37RV infection and cytokine production *in vitro*.

(A) CD14⁺ selected monocytes were differentiated into M2 macrophages in the presence of 5 mmol/L glucose, 5 mmol/L glucose and 20 mmol/L mannitol or 25 mmol/L glucose. The macrophages were infected for 1 hour with H37Rv at an MOI of 10. After infection the macrophages were washed and fresh media containing the different glucose media was added. After 24 hours supernatants were collected and the cells were lysed by osmotic pressure. (B) Cell lysates were serially diluted and plated on Middlebrook 7H10 agar. CFUs were counted after 2-3 weeks of growth at 37°C. Data are shown as mean \pm SEM of two independent experiments (n=4). (C) Pro-inflammatory cytokines TNF- α and IL-6 were measured along with the anti-inflammatory cytokines IL-10 and IL-1RA. Data are shown as mean \pm SEM.

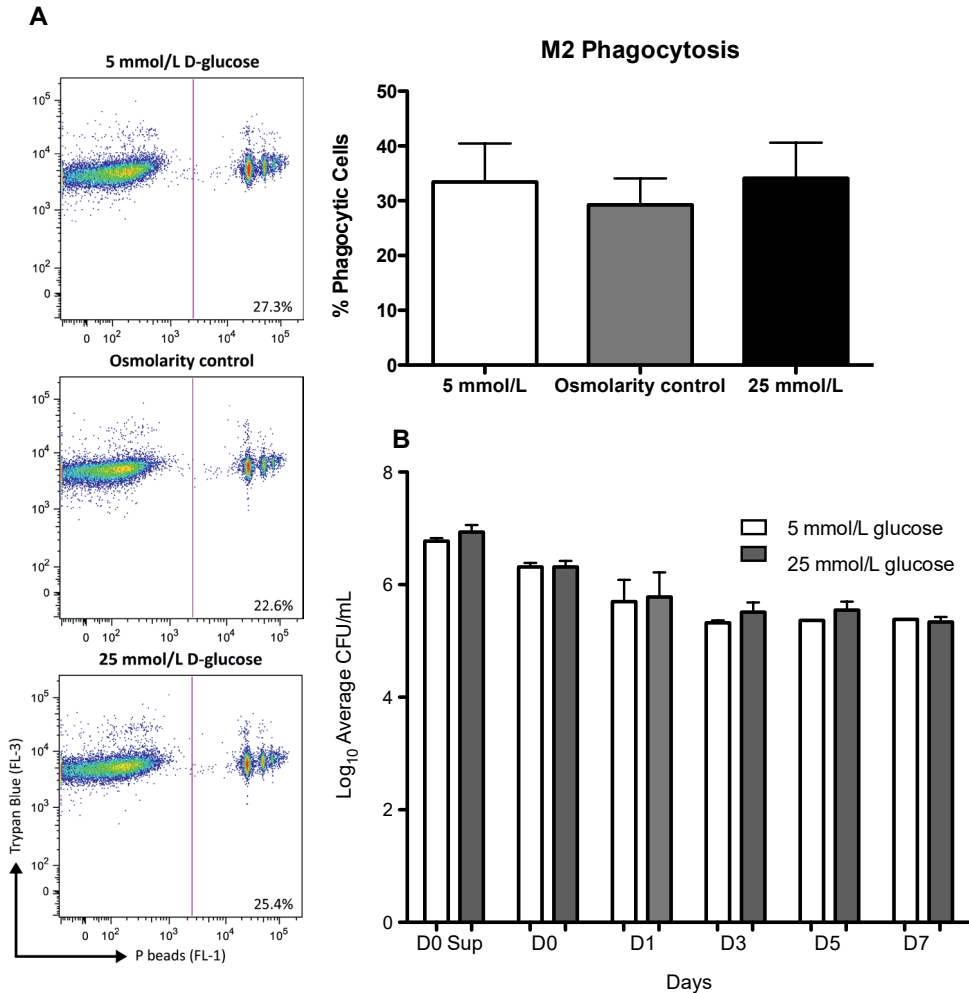


Figure 4: Effects of high glucose on phagocytic capacity of macrophages and infection with H37Rv.

M2 macrophages differentiated in the presence of 5 or 25 mmol/L glucose were either incubated with P-beads and subjected to flow cytometry measurements to determine the percentage of phagocytic cells (A) or were infected for 1 hour with H37Rv at an MOI of 10:1 (B). After infection macrophages were washed three times and fresh RPMI containing the different glucose media was added. The first wash (Day 0 Sup) of each infection was collected and plated in serial dilutions to determine whether different amounts of bacilli were taken up by euglycaemic or hyperglycaemic macrophages. Simultaneously macrophages (D0) were lysed and plated for CFU counts. Infected macrophages were also lysed on Day 1 (D1), Day 3 (D3), Day 5 (D5) and Day 7 (D7) after infection. CFUs were counted at once after 2-3 weeks of growth at 37°C. Data are shown as mean ± SEM (n=4).

Discussion

Type 2 diabetes mellitus confers a three-fold increased risk for active tuberculosis, but the underlying immunological mechanisms have not been identified ⁽¹⁾. In this study we investigated the effects of hyperglycaemia on *in vitro* cytokine production and mycobacterial infection. Hyperglycaemia altered cytokine production by PBMCs and macrophages stimulated with H37Rv lysate, although significant effects were mainly observed at the higher end of the glucose concentration range. Alternatively, hyperglycaemia did not affect the phagocytic capacity of macrophages or their ability to control outgrowth of H37Rv over a period of time.

PBMCs incubated in high glucose concentrations produced higher levels of TNF- α , IL-1 β and IL-6, whilst IFN- γ , IL-17A and IL-22 levels did not change. This suggests that hyperglycaemia mainly affects monocytes but not T cells. As a result, we investigated whether hyperglycaemia had a more specific effect on macrophage-derived cytokine production. An increase in IL-6, IL-10 and IL1RA levels was found when hyperglycaemic monocyte-derived macrophages were stimulated with MTB and LPS.

To our knowledge, no studies have presented data on the effects of high glucose levels on *in vitro* cytokine production in response to MTB. Previous studies that examined *ex vivo* cytokine production in diabetes patients with or without TB have provided conflicting results. Some studies have shown elevated production of pro-inflammatory cytokines from whole blood of patients with TB-DM whereas another study using whole blood and one using PBMCs reported defects in IFN- γ production in patients with TB-DM ^(19-21,26). Interestingly, both the increase and decrease of pro-inflammatory cytokines were correlated to increased HbA1c levels ^(19,26). Differences between studies can be explained by the use of different cell types and stimuli. In this study we chose to investigate M0 (serum derived) and M2 (M-CSF and serum derived) macrophages, as they most closely represent tissue resident macrophages such as alveolar macrophages, in which MTB dominantly resides. Furthermore, patient studies are often complicated by variations in age, HBA1c levels, metabolic perturbations, medication etc., making it difficult to specifically examine the effects of hyperglycaemia. For these reasons we chose to exclusively study the effects of hyperglycaemia *in vitro*.

In contrast to the effects on cytokine production, the capacity of macrophages to phagocytose P-beads remained unaltered under high glucose concentrations. In literature, several studies report findings that both support and contrast with our observations on the effects of hyperglycaemia or DM on the phagocytic capacity of macrophages. In a TB-DM animal model in particular no significant differences were found in the phagocytic capacity of alveolar macrophages from diabetic and non-diabetic rats subjected to aerosol infection with MTB ^(27,28). In patients with DM the phagocytic function of macrophages and polymorphonuclear cells (PMN) is even more unclear ^(14,29-31). In a recent study comparing patients with pulmonary TB, DM or the combination of TB and DM, no differences were found in the ability of PMNs to phagocytose, produce hydrogen

peroxide or reduce nitroblue tetrazolium. In contrast, two studies from the same group using monocytes from patients with diabetes⁽³²⁾ showed a reduced association of MTB bacilli and reduced phagocytosis via the complement or Fc- γ receptor pathway, although this was not demonstrated in the context of MTB itself⁽³³⁾.

Similar to phagocytosis, no differences were found in MTB killing or outgrowth between hyperglycaemic and euglycaemic macrophages. To our knowledge no other data have been published on outgrowth of MTB in hyperglycaemic macrophages or macrophages from patients with DM. Of interest however is one study showing increased tuberculosis susceptibility in mice with streptozotocin-induced diabetes. In line with our study no differences in CFU counts were found in the lungs of acute diabetic mice. These results may indicate that hyperglycaemia may have long-term effects on susceptibility that are difficult to emulate *in vitro*.^(27,34)

Several aspects and limitations of our studies should be considered when discussing the relatively mild effects of hyperglycaemia on the immune responses elicited by MTB. Firstly, although hyperglycaemia did not directly affect MTB survival in macrophages, it is possible that it does after longer periods of time, or contributes to increased susceptibility to infection indirectly through effects on other immune cells. Secondly, even though hyperglycaemia is regarded as a major hallmark of DM, the pathophysiology of the disease is not restricted to high glucose concentrations. Other physiological disturbances in DM such as hyperinsulinaemia, diabetic acidosis and metabolic changes have also been found to affect immune cell functions,^(35–37) and studies to assess their effects on MTB-induced immune responses are needed. Thirdly, DM is often associated with diet-induced conditions like dyslipidaemia. As MTB has been found to modulate host lipogenic pathways to survive in macrophages⁽³⁸⁾ it is possible that changes in blood lipid levels or composition contribute to the increased risk of active TB disease in DM patients. Furthermore we cannot exclude that the unidentified donors used in these experiments suffered from co-morbidities such as diabetes, although the chance of that are <1.5% as described above. Finally, it is unclear how accurately our *in vitro* model of hyperglycaemia reflects the *in vivo* situation during DM.

In short, these *in vitro* studies in PBMC and macrophages suggest that hyperglycaemia cannot fully explain the increased susceptibility to MTB in DM patients. Further studies that explore a broader range of metabolic parameters and cell types are needed to unravel the precise mechanisms underlying the effect of DM on TB.

Acknowledgments

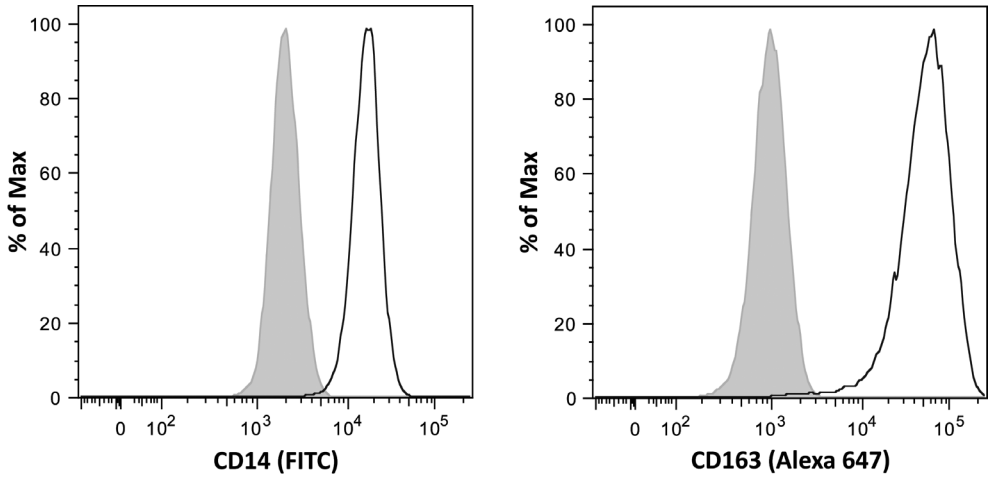
The authors have no acknowledgements.

Reference List

1. Jeon CY, Murray MB (2008) Diabetes mellitus increases the risk of active tuberculosis: a systematic review of 13 observational studies. *PLoS Med* 5: e152.
2. Ruslami R, Aarnoutse RE, Alisjahbana B, van der Ven AJ, van CR (2010) Implications of the global increase of diabetes for tuberculosis control and patient care. *Trop Med Int Health* 15: 1289-1299.
3. International Diabetes Federation (2013) *IDF Diabetes Atlas*. 6th ed., Brussels, Belgium.
4. van CR, Dockrell HM (2014) TANDEM: understanding diabetes and tuberculosis. *Lancet Diabetes Endocrinol* 2: 270-272.
5. Martinez N, Kornfeld H (2014) Diabetes and immunity to tuberculosis. *Eur J Immunol* 44: 617-626.
6. Ernst JD (2012) The immunological life cycle of tuberculosis. *Nat Rev Immunol* 12: 581-591.
7. Ottenhoff TH (2012) New pathways of protective and pathological host defense to mycobacteria. *Trends Microbiol* 20: 419-428.
8. Jouanguy E, Lamhamedi-Cherradi S, Altare F, Fondaneche MC, Tuerlinckx D et al. (1997) Partial interferon-gamma receptor 1 deficiency in a child with tuberculoid bacillus Calmette-Guerin infection and a sibling with clinical tuberculosis. *J Clin Invest* 100: 2658-2664.
9. Harris J, Keane J (2010) How tumour necrosis factor blockers interfere with tuberculosis immunity. *Clin Exp Immunol* 161: 1-9.
10. O'Garra A, Redford PS, McNab FW, Bloom CI, Wilkinson RJ et al. (2013) The immune response in tuberculosis. *Annu Rev Immunol* 31: 475-527.
11. Verreck FA, de BT, Langenberg DM, van der Zanden L, Ottenhoff TH (2006) Phenotypic and functional profiling of human proinflammatory type-1 and anti-inflammatory type-2 macrophages in response to microbial antigens and IFN-gamma- and CD40L-mediated costimulation. *J Leukoc Biol* 79: 285-293.
12. Redford PS, Boonstra A, Read S, Pitt J, Graham C et al. (2010) Enhanced protection to *Mycobacterium tuberculosis* infection in IL-10-deficient mice is accompanied by early and enhanced Th1 responses in the lung. *Eur J Immunol* 40: 2200-2210.
13. Gomez DI, Twahirwa M, Schlesinger LS, Restrepo BI (2013) Reduced *Mycobacterium tuberculosis* association with monocytes from diabetes patients that have poor glucose control. *Tuberculosis (Edinb)* 93: 192-197.
14. Lecube A, Pachon G, Petriz J, Hernandez C, Simo R (2011) Phagocytic activity is impaired in type 2 diabetes mellitus and increases after metabolic improvement. *PLoS One* 6: e23366.
15. Sun C, Sun L, Ma H, Peng J, Zhen Y et al. (2012) The phenotype and functional alterations of macrophages in mice with hyperglycemia for long term. *J Cell Physiol* 227: 1670-1679.
16. Liu HF, Zhang HJ, Hu QX, Liu XY, Wang ZQ et al. (2012) Altered polarization, morphology, and impaired innate immunity germane to resident peritoneal macrophages in mice with long-term type 2 diabetes. *J Biomed Biotechnol* 2012: 867023.

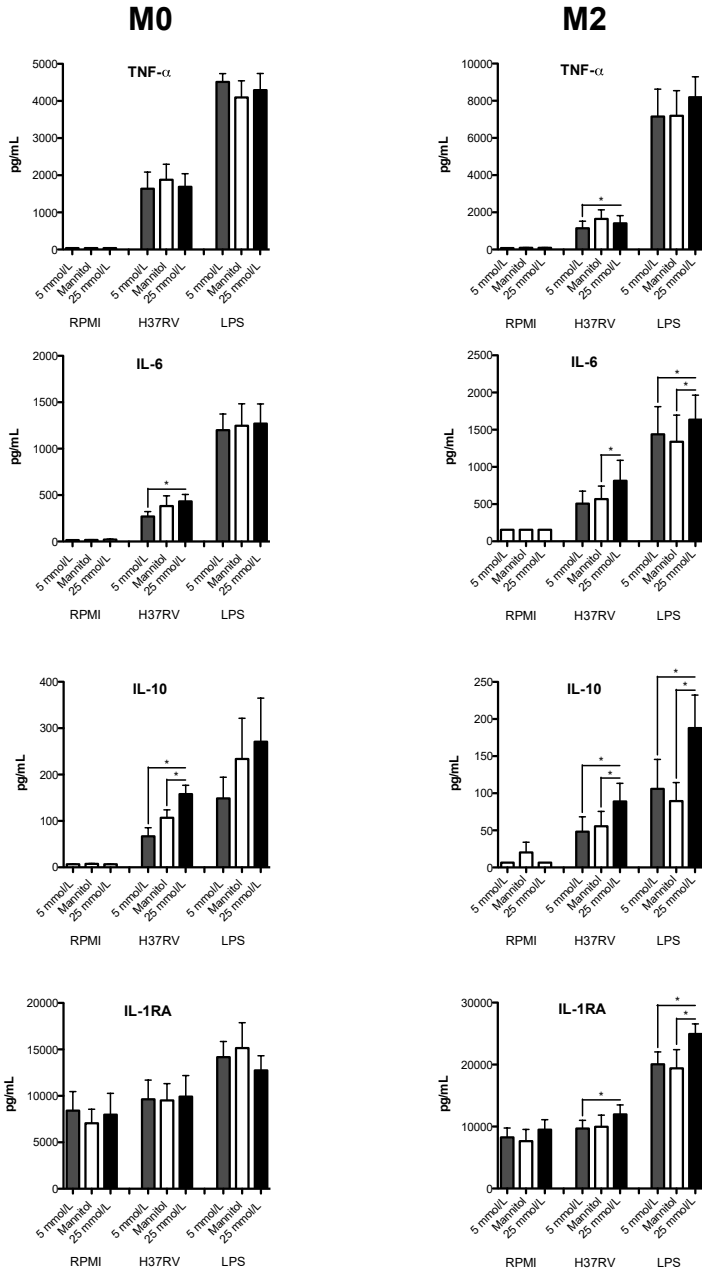
17. Mo Y, Wan R, Wang J, Chien S, Tollerud DJ et al. (2009) Diabetes is associated with increased sensitivity of alveolar macrophages to urban particulate matter exposure. *Toxicology* 262: 130-137.
18. Devaraj S, Venugopal SK, Singh U, Jialal I (2005) Hyperglycemia induces monocytic release of interleukin-6 via induction of protein kinase c- α and β . *Diabetes* 54: 85-91.
19. Restrepo BI, Fisher-Hoch SP, Pino PA, Salinas A, Rahbar MH et al. (2008) Tuberculosis in poorly controlled type 2 diabetes: altered cytokine expression in peripheral white blood cells. *Clin Infect Dis* 47: 634-641.
20. Stalenhoef JE, Alisjahbana B, Nelwan EJ, van d, V, Ottenhoff TH et al. (2008) The role of interferon-gamma in the increased tuberculosis risk in type 2 diabetes mellitus. *Eur J Clin Microbiol Infect Dis* 27: 97-103.
21. Kumar NP, Sridhar R, Banurekha VV, Jawahar MS, Fay MP et al. (2013) Type 2 diabetes mellitus coincident with pulmonary tuberculosis is associated with heightened systemic type 1, type 17, and other proinflammatory cytokines. *Ann Am Thorac Soc* 10: 441-449.
22. Atsma F, Veldhuizen I, de VF, Doggen C, de KW (2011) Cardiovascular and demographic characteristics in whole blood and plasma donors: results from the Donor InSight study. *Transfusion* 51: 412-420.
23. Statistics Netherlands (2010) Health, lifestyle, use of medical facilities, The Hague, The Netherlands.
24. Leclerc L, Boudard D, Pourchez J, Forest V, Sabido O et al. (2010) Quantification of micro-sized fluorescent particles phagocytosis to a better knowledge of toxicity mechanisms. *Inhal Toxicol* 22: 1091-1100.
25. Verreck FA, de BT, Langenberg DM, Hoeve MA, Kramer M et al. (2004) Human IL-23-producing type 1 macrophages promote but IL-10-producing type 2 macrophages subvert immunity to (myco)bacteria. *Proc Natl Acad Sci U S A* 101: 4560-4565.
26. Tan KS, Lee KO, Low KC, Gamage AM, Liu Y et al. (2012) Glutathione deficiency in type 2 diabetes impairs cytokine responses and control of intracellular bacteria. *J Clin Invest* 122: 2289-2300.
27. Sugawara I, Mizuno S (2008) Higher susceptibility of type 1 diabetic rats to *Mycobacterium tuberculosis* infection. *Tohoku J Exp Med* 216: 363-370.
28. Sugawara I, Yamada H, Mizuno S (2004) Pulmonary tuberculosis in spontaneously diabetic goto kakizaki rats. *Tohoku J Exp Med* 204: 135-145.
29. Marhoffer W, Stein M, Maeser E, Federlin K (1992) Impairment of polymorphonuclear leukocyte function and metabolic control of diabetes. *Diabetes Care* 15: 256-260.
30. Komura T, Sakai Y, Honda M, Takamura T, Matsushima K et al. (2010) CD14⁺ monocytes are vulnerable and functionally impaired under endoplasmic reticulum stress in patients with type 2 diabetes. *Diabetes* 59: 634-643.
31. Delamaire M, Maugeudre D, Moreno M, Le Goff MC, Allannic H et al. (1997) Impaired leucocyte functions in diabetic patients. *Diabet Med* 14: 29-34.
32. Restrepo BI, Schlesinger LS (2013) Host-pathogen interactions in tuberculosis patients with type 2 diabetes mellitus. *Tuberculosis (Edinb)* 93 Suppl: S10-S14.

33. Restrepo BI, Twahirwa M, Rahbar MH, Schlesinger LS (2014) Phagocytosis via complement or Fc-gamma receptors is compromised in monocytes from type 2 diabetes patients with chronic hyperglycemia. *PLoS One* 9: e92977.
34. Martens GW, Arikian MC, Lee J, Ren F, Greiner D et al. (2007) Tuberculosis susceptibility of diabetic mice. *Am J Respir Cell Mol Biol* 37: 518-524.
35. Lardner A (2001) The effects of extracellular pH on immune function. *J Leukoc Biol* 69: 522-530.
36. Han JM, Patterson SJ, Speck M, Ehses JA, Levings MK (2014) Insulin inhibits IL-10-mediated regulatory T cell function: implications for obesity. *J Immunol* 192: 623-629.
37. Tremaroli V, Backhed F (2012) Functional interactions between the gut microbiota and host metabolism. *Nature* 489: 242-249.
38. Mahajan S, Dkhar HK, Chandra V, Dave S, Nanduri R et al. (2012) Mycobacterium tuberculosis modulates macrophage lipid-sensing nuclear receptors PPARgamma and TR4 for survival. *J Immunol* 188: 5593-5603.



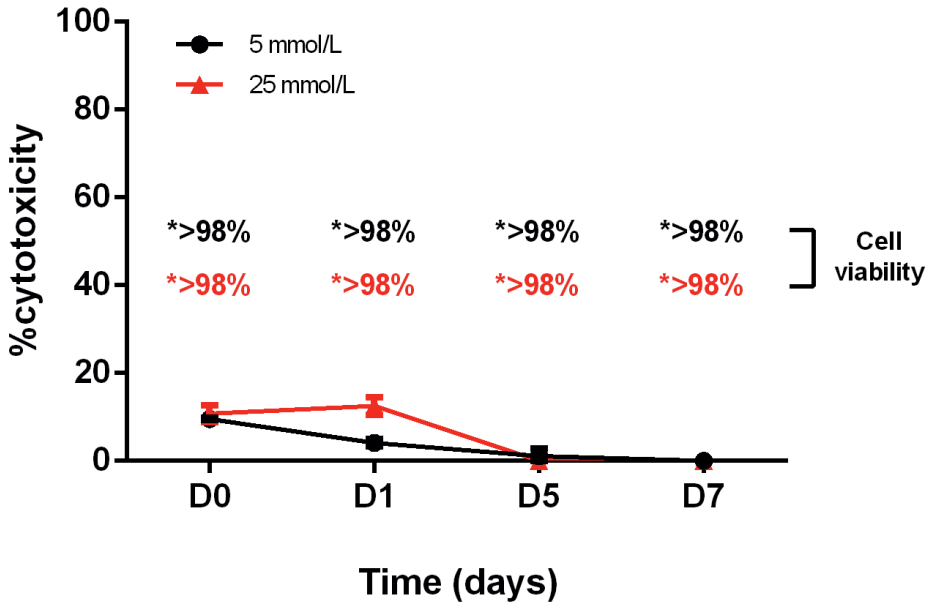
Supplementary Figure 1: M2 macrophage surface marker expression.

M2 macrophage differentiation was verified by analysing the cell surface expression of CD14 (FITC, clone HCD14) and CD163 (Alexa 647, clone RM3/1) by flow cytometry. The FACS plots display representative results for CD14⁺/CD163⁺ M2 macrophages (black) versus an unstained sample (grey).



Supplementary Figure 2: Effects of osmolarity on cytokine production from differentiated macrophages.

Monocytes were differentiated into M0 or M2 macrophages in the presence of 5 mmol/L glucose, 5 mmol/L glucose and 20 mmol/L mannitol, or 25 mmol/L glucose, and subsequently stimulated with RPMI, H37Rv lysate (1 μ g/mL) or LPS (10 ng/mL). Cell culture supernatants were collected after 24 h and the pro-inflammatory cytokines TNF- α and IL-6 were measured along with the anti-inflammatory cytokines IL-10 and IL-1RA (n=6). Data are shown as mean \pm SEM, *p<0.05, **p<0.01 and ***p<0.001.



Supplementary Figure 3: M2 macrophage viability during prolonged H37Rv infection.

M2 macrophages differentiated for 6 days in the presence of 5 or 25 mmol/L glucose were infected for 1 hour with H37Rv at an MOI of 10:1. After infection macrophages were washed three times and fresh RPMI containing the different glucose media was added. The percentage of cytotoxicity was assessed by measuring LDH release from day 0 to day 7 corrected using spontaneous and maximum LDH release controls per time point. Macrophages were additionally stained with Trypan Blue as a second measure of cell viability and the resulting percentage of viable cells is indicated in the graph with an * at each time point for both conditions (5 mmol/L: black; 25 mmol/L: red). Data are shown as mean \pm SD (n=2).

CHAPTER

4

Oxidized low-density lipoprotein (oxLDL) supports *Mycobacterium tuberculosis* survival in macrophages by inducing lysosomal dysfunction

Frank Vrieling¹, Louis Wilson¹, Patrick C.N. Rensen², Gerhard Walzl³, Tom H.M. Ottenhoff^{1#} and Simone A. Joosten^{1#*}

¹ Department of Infectious Diseases, Leiden University Medical Center, Albinusdreef 2, 2333 ZA Leiden, The Netherlands

² Department of Medicine, Division of Endocrinology, Leiden University Medical Center, Albinusdreef 2, 2333 ZA Leiden, The Netherlands

³ DST/NRF Center of Excellence for Biomedical Tuberculosis Research, SA MRC Center for TB Research, Division of Molecular Biology and Human Genetics, Department of Biomedical Sciences, Faculty of Medicine and Health Sciences Stellenbosch University, Francie van Zijl Drive, Tygerberg, 7505, Cape Town, South Africa

these authors contributed equally to this work

Type 2 diabetes mellitus (DM) is a major risk factor for developing tuberculosis (TB). TB-DM comorbidity is expected to pose a serious future health problem due to the alarming rise in global DM incidence. At present, the causal underlying mechanisms linking DM and TB remain unclear. DM is associated with elevated levels of oxidized low-density lipoprotein (oxLDL), a pathologically modified lipoprotein which plays a key role during atherosclerosis development through the formation of lipid-loaded foamy macrophages, an event which also occurs during progression of the TB granuloma. We therefore hypothesized that oxLDL could be a common factor connecting DM to TB. To study this, we measured oxLDL levels in plasma samples of healthy controls, TB, DM and TB-DM patients, and subsequently investigated the effect of oxLDL treatment on human macrophage infection with *Mycobacterium tuberculosis* (*Mtb*). Plasma oxLDL levels were significantly elevated in DM patients and associated with high triglyceride levels in TB-DM. Strikingly, incubation with oxLDL strongly increased macrophage *Mtb* load compared to native or acetylated LDL (acLDL). Mechanistically, oxLDL -but not acLDL- treatment induced macrophage lysosomal cholesterol accumulation and increased protein levels of lysosomal and autophagy markers, while reducing *Mtb* colocalization with lysosomes. Importantly, combined treatment of acLDL and intracellular cholesterol transport inhibitor (U18666A) mimicked the oxLDL-induced lysosomal phenotype and impaired macrophage *Mtb* control, illustrating that the localization of lipid accumulation is critical. Collectively, these results demonstrate that oxLDL could be an important DM-associated TB-risk factor by causing lysosomal dysfunction and impaired control of *Mtb* infection in human macrophages.

Introduction

Type 2 diabetes mellitus (DM) has been recognized as a major risk factor for tuberculosis (TB) for decades ⁽¹⁾. Recent epidemiological studies have demonstrated that DM triples the risk of developing active TB ⁽²⁾, and approximately 15% of global TB cases can be attributed to DM comorbidity ⁽³⁾. The precise mechanisms through which DM enhances the risk of active TB disease progression are unknown, however it has been hypothesized that metabolic changes associated with DM attenuate the immune response towards *Mycobacterium tuberculosis* (*Mtb*), the causative pathogen of TB. As the global incidence of DM has been rising at an alarming rate ⁽⁴⁾, including more recently in TB endemic regions of African and Asia, it is of great importance to identify the molecular and cellular mechanisms underlying TB-DM comorbidity.

DM patients often suffer from dyslipidemia and oxidative stress, conditions which can contribute to the formation of oxidized low density lipoprotein (oxLDL) ⁽⁵⁾. LDL can be oxidized by free radicals and reactive products of oxygenases, a process which has been mostly studied in the context of atherosclerosis during which oxLDL is generated in the subendothelial space of the arterial wall ^(6,7). High levels of circulating oxLDL were shown to be associated with DM, insulin resistance and decreased glucose tolerance ⁽⁸⁻¹¹⁾. oxLDL is recognized as a damage-associated molecular pattern (DAMP) by macrophages and is a ligand for various scavenger receptors on the cell surface, including CD36, scavenger receptor A (SR-A) and lectin-type oxidized LDL receptor 1 (LOX-1) ⁽¹²⁾. The uptake of oxLDL by macrophages plays a major role during the pathophysiology of atherosclerosis as it leads to the generation of pro-inflammatory lipid-loaded foam cells in the arterial vessel wall ^(13,14). These macrophages exhibit increased scavenger receptor expression, cytokine secretion and production of oxidizing agents, supporting both immune cell infiltration and further generation of oxLDL which can culminate in atherosclerotic plaque formation ⁽¹⁵⁾.

Foamy macrophages also occur during TB progression and are thought to be of great importance for the development of TB granulomas and persisting *Mtb* infection, since the bacterium relies on host-derived lipids and cholesterol as a source of carbon for its survival ⁽¹⁶⁻¹⁸⁾. Infection of alveolar macrophages with *Mtb* initiates the formation of the early TB granuloma, which progresses from a core of infected foam cells to an enclosed structure with a thick fibrous capsule and a lipid-rich caseous center of necrotic macrophages ⁽¹⁶⁾. Various studies have demonstrated that *Mtb* and other mycobacteria are able to utilize host-derived lipids and even reprogram lipid metabolism in infected macrophages to induce foam cell formation, in part through the effects of mycobacterial cell wall lipids ⁽¹⁹⁻²⁴⁾. Interestingly, oxLDL was also found to accumulate in granulomas and alveolar macrophages of *Mtb* infected guinea pigs and to enhance bacterial replication ⁽²⁵⁾, suggesting that local oxLDL production could play a role in foam cell formation and *Mtb* persistence during TB disease.

OxLDL-derived lipids have been demonstrated to be resistant to lysosomal esterases which are normally responsible for lipid breakdown. This results in lipid

accumulation inside lysosomes after initial uptake by macrophages^(26, 27), as well as to dysfunctions in the trafficking and efflux of intracellular cholesterol which mimic those observed in the lysosomal storage disorder Niemann Pick disease type C (NPC). During NPC disease, mutations in the lysosomal cholesterol transporters *NPC1* or *NPC2* result in severe neurological defects due to excessive intralysosomal storage of cholesterol and sphingolipids⁽²⁸⁾. Cholesterol accumulation due to oxLDL uptake or *NPC1*-deficiency induces lysosomal dysfunction in macrophages, as it can interfere with phagolysosomal trafficking, maturation and fusion^(29, 30); inhibit autophagy^(31, 32), an important cellular pathway which is simultaneously involved in lipid and cholesterol metabolism⁽³³⁾ and *Mtb* killing⁽³⁴⁾ in macrophages; increase lysosomal pH⁽³⁵⁾; directly damage lysosomal membranes^(36, 37); and trigger various downstream inflammatory pathways such as formation of the NLRP3 inflammasome⁽³⁸⁾. A recent paper demonstrated that both infection with live *M. smegmatis* or *M. bovis* BCG and treatment with mycobacterial cell wall lipids induced a NPC-like phenotype in macrophages with associated defects in lysosomal function⁽³⁹⁾, indicating that cholesterol accumulation could provide a permissive environment for mycobacteria in addition to being a nutritional source.

To investigate whether oxLDL is a molecular component in the interplay between TB and DM, we measured oxLDL concentrations in plasma samples of DM, TB and TB-DM patients and analyzed the effect of oxLDL on *in vitro* *Mtb* infection in primary human macrophages. We found that oxLDL is elevated in the plasma of DM patients and supported *Mtb* intracellular survival *in vitro* by inducing lysosomal dysfunction. Collectively, our findings provide a proof of concept for a contribution of oxLDL as a risk factor for TB during DM.

Results

Plasma oxLDL levels are increased in DM and TB-DM patients with dyslipidemia

First, we sought to confirm the presence of high levels of circulating oxLDL in DM patients from a TB endemic setting and to assess the relative impact of TB-DM comorbidity on circulating oxLDL levels. OxLDL concentrations were determined in plasma samples from healthy endemic controls (HC), TB, DM and TB-DM patients of a South-African cohort, previously used in a lipidomic biomarker analysis⁽⁴⁰⁾, by sandwich ELISA using a monoclonal antibody against a conformational epitope in oxidized ApoB-100⁽⁴¹⁾. Patient characteristics are described in Supplementary Table 1.

Plasma oxLDL levels were significantly higher in DM patients (median: 65.8 [interquartile range: 39.2 - 83.2] U/l) compared to both HC (42.3 [35.3 - 82.2] U/l, $p < 0.05$) and TB-DM patients (44.4 [30.3 - 56.7] U/l, $p < 0.05$) (Figure 1A), but not significantly different in patients with TB-DM compared to TB alone (44.3 [29.6 - 50.0] U/l). However, a clear dichotomy was distinguishable in the TB-DM patient group: our previous analysis of these samples⁽⁴⁰⁾ had demonstrated that both DM and TB-DM patients displayed characteristics of dyslipidemia, as evidenced by high levels of serum triglycerides (TG)

(Figure 1B). Furthermore, serum triglyceride levels were positively correlated with oxLDL across all measured samples ($r^2: 0.4189, p = 1.155 \times 10^{-10}$) (Figure 1C). To investigate whether oxLDL levels were related to the severity of dyslipidemia in TB-DM patients, we subdivided the groups according to serum TG-concentrations (TG-high and TG-low, Figure 1D). DM and TB-DM patients with TG-high had increased oxLDL levels compared to those with TG-low (DM: 72.0 [61.7 - 87.1] vs 46.8 [33.0 - 76.3] U/l, $p = 0.053$; TB-DM: 56.4 [52.1 - 59.4] vs 32.7 [27.2 - 39.2] U/l, $p < 0.05$). Taken together, the results validate that DM patients have increased levels of circulating oxLDL and that plasma oxLDL concentrations are elevated in DM and TB-DM patients with concomitant hypertriglyceridemia.

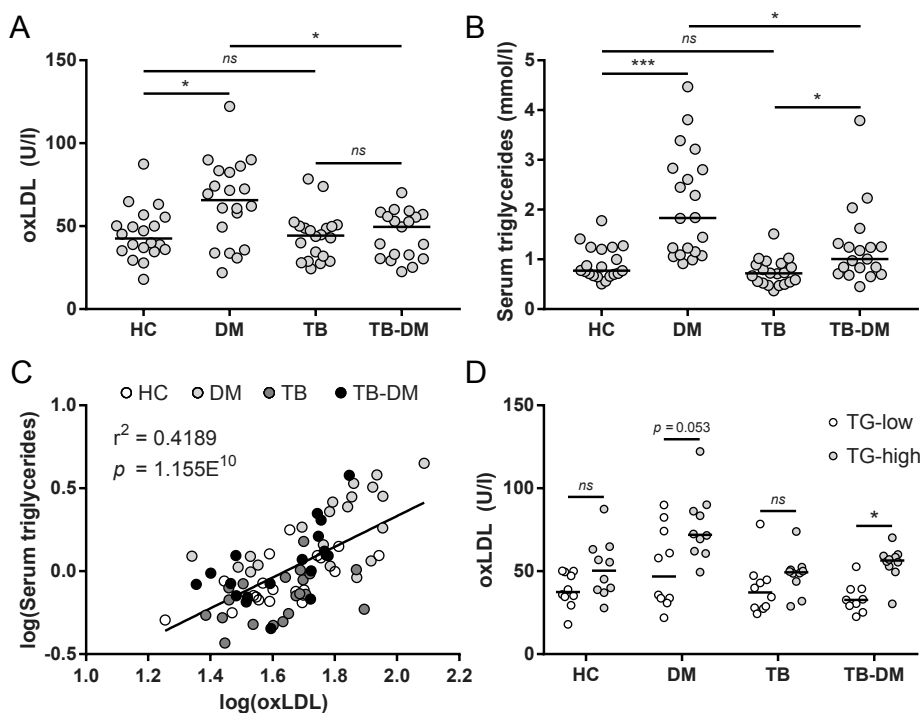


Figure 1: OxLDL levels are increased in DM and associated with triglyceride levels in TB-DM patients.

(A) OxLDL concentrations (U/l) were determined in plasma samples of healthy controls (HC) ($n = 20$), TB ($n = 20$), DM ($n = 20$) and TB-DM patients ($n = 19$) by ELISA. (B) Serum triglyceride (TG) levels (mmol/l) were determined by H^1 -NMR spectroscopy. (C) Linear correlation analysis of log-transformed serum triglyceride and oxLDL levels. (D) Plasma oxLDL concentrations in HC, TB, DM and TB-DM patients stratified by TG levels (TG-high vs TG-low; $n = 10$ /group except for TB-DM + TG-low: $n = 9$). Individual patients are depicted as dots with group medians. Statistical significance was determined by Kruskal-Wallis test with post-hoc Dunn's test. * = $p < 0.05$, *** = $p < 0.001$.

OxLDL treatment increases *Mtb* bacterial burden in infected human macrophages

As oxLDL was clearly elevated in DM patients and has been described to have profound effects on macrophage function, we hypothesized that oxLDL treatment could compromise the capacity of macrophages to control *Mtb* infection. To investigate this, macrophages were treated with 1, 10 or 25 $\mu\text{g/ml}$ oxLDL or native LDL overnight. Oil Red O staining indicated a dose-dependent increase in intracellular lipid levels after oxLDL treatment, while native LDL did not induce foam cells (Figure 2A, S1B). These macrophages were subsequently infected for 24 h with *Mtb* H37Rv and intracellular bacterial loads were assessed by bacterial colony forming unit (CFU) assay. OxLDL treatment significantly increased *Mtb* load compared to native LDL at all tested concentrations (1 $\mu\text{g/ml}$: 136% [113% - 171%] vs 97% [78% - 128%], $p < 0.01$; 10 $\mu\text{g/ml}$: 143% [115% - 167%] vs 110% [102% - 121%], $p < 0.01$; 25 $\mu\text{g/ml}$: 230% [179% - 248%] vs 115% [94.8% - 127%], $p < 0.01$), and this effect was dose-dependent (25 $\mu\text{g/ml}$ oxLDL vs 1 $\mu\text{g/ml}$: $p < 0.01$; vs 10 $\mu\text{g/ml}$: $p < 0.01$) (Figure 2B). The magnitude of the increase in bacterial load was not correlated with small fluctuations in infectious load (MOI) (Figure S1C).

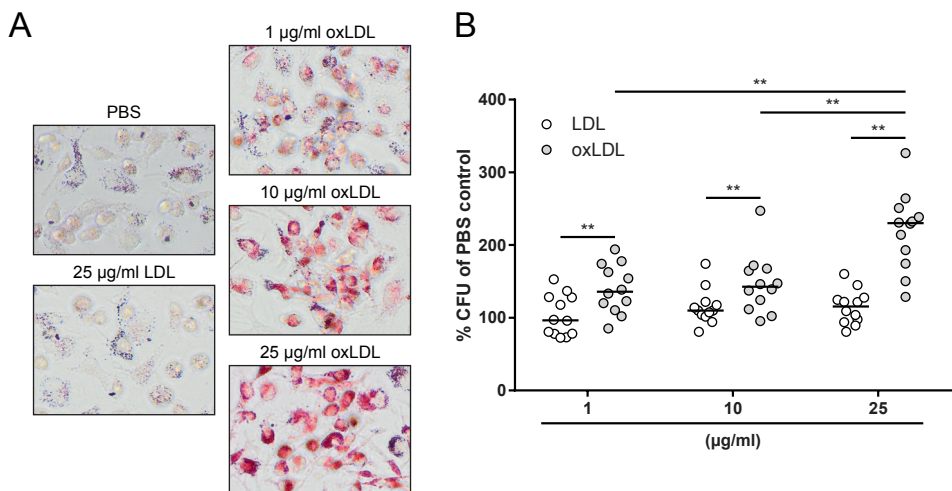


Figure 2: OxLDL-treated macrophages have an increased *Mtb* burden.

Primary human macrophages were treated with PBS control, native LDL or oxLDL (1, 10 or 25 $\mu\text{g/ml}$) overnight and subsequently infected with *Mtb* H37Rv at a MOI of 10:1. (A) Oil Red O staining of macrophages treated overnight with PBS, 25 $\mu\text{g/ml}$ LDL or 1, 10 and 25 $\mu\text{g/ml}$ oxLDL. Pictures were taken at a 20x magnification. (B) Macrophages were lysed at 24 h post-infection and bacterial load was determined by CFU assay. Results were normalized versus PBS control ($n = 8$). Individual donors are depicted as dots with group medians. Statistical significance was determined by Wilcoxon signed rank test with post-hoc FDR correction. ** = $p < 0.01$.

While these experiments demonstrated that oxLDL treatment supported *Mtb* persistence in human macrophages, it was unclear whether this was the result of increased phagocytosis, reduced intracellular mycobacterial control or enhanced replication. To gain a better understanding on the cellular processes affected by oxLDL treatment, we explored the functional consequences of oxLDL-induced foam cell formation. Firstly, the phagocytic capacity of oxLDL-treated macrophages was assessed to investigate whether the increased mycobacterial load might be related to enhanced *Mtb* uptake. Macrophages treated with either native LDL or oxLDL were incubated with fluorescent polystyrene beads and bead phagocytosis was quantified by flow cytometry (Figure 3A). Although a small but significant decrease in bead uptake was observed in macrophages incubated with 25 µg/ml oxLDL compared to LDL ($p < 0.05$) (Figure 3B), overall macrophage phagocytic capacity was unaffected by oxLDL treatment, indicating that the increased mycobacterial burden in oxLDL-derived foam cells was probably not the result of increased phagocytic uptake. To confirm this, we investigated the intracellular bacterial load of oxLDL-treated macrophages directly after 1 h of infection and found no significant differences compared to control conditions (Figure S2C).

Next, we explored the cytokine response of oxLDL-derived foam cells to *Mtb*-infection as earlier studies had reported potent oxLDL-induced pro-inflammatory cytokine production. In contrast to these studies, oxLDL-treatment in our experiments significantly decreased the secretion of TNF- α compared to treatment with LDL (47 [20 - 186] vs 128 [54 - 453] pg/ml, $p < 0.05$) or PBS (146 [62 - 466] pg/ml, $p < 0.05$). Similar results were obtained for IL-6 after oxLDL treatment versus LDL (11 [0 - 226] vs 66 [0 - 553] pg/ml, $p < 0.05$) or PBS (73 [0 - 412] pg/ml, $p < 0.05$), although some inter-individual variation was observed (Figure 3C). IL-10 levels were not significantly affected by oxLDL, while IL-1 β levels were very low.

Finally, oxLDL-derived macrophages were co-cultured with a HLA-DR2-restricted CD4⁺ T cell clone (R2F10) and its cognate peptide (*Mlep* hsp65 p418–427) and T cell proliferation was measured to determine macrophage dependent antigen presentation. OxLDL treatment dose-dependently diminished the antigen presentation capacity of macrophages, especially at suboptimal peptide concentrations (Figure 3D). Similar results were obtained using a second, HLA-DR3-restricted CD4⁺ T cell clone (Rp15 1-1) (Figure S2A), both after loading with its cognate peptide or purified protein derivative (PPD). This diminished antigen presentation capacity was independent of cell surface expression of HLA-DR and co-stimulatory molecules CD80 and CD86 (Figure S2B). Taken together, oxLDL treatment impaired several macrophage functions, including antigen presentation and pro-inflammatory cytokine secretion, but not their phagocytic capacity.

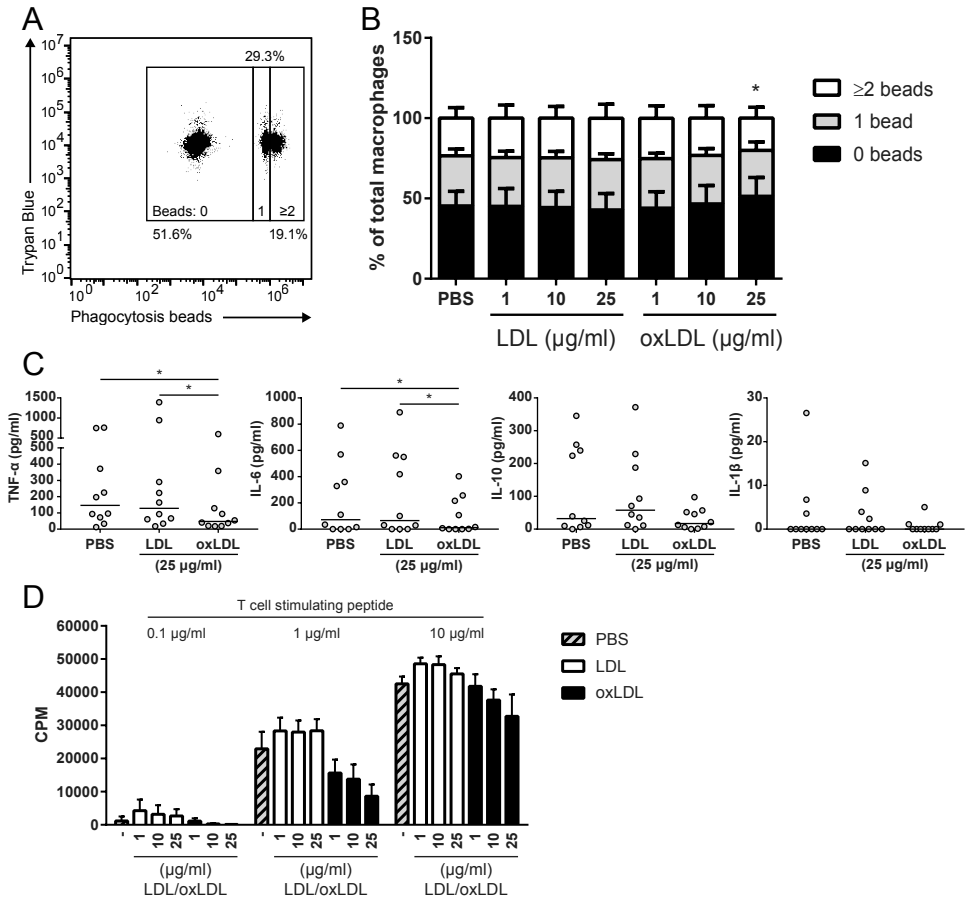


Figure 3: Functional analysis of oxLDL-treated macrophages.

Primary human macrophages were treated with PBS control, native LDL or oxLDL (1, 10 or 25 $\mu\text{g/ml}$) overnight. (A) Macrophages were incubated with fluorescent phagocytosis beads at a MOI of 10:1 and subsequently analyzed by flow cytometry. Fluorescence of extracellular beads was quenched with Trypan Blue. (B) Percentage of macrophages with 0, 1 or ≥ 2 beads internalized beads ($n = 6$). Data is represented as means with standard deviations. (C) Macrophages were infected with *Mtb* H37Rv at a MOI of 10:1 for 1 h. Supernatants were harvested at 24 h post-infection and concentrations of TNF- α , IL-6, IL-10 and IL-1 β were determined by ELISA ($n = 10$). Individual donors are depicted as dots with group medians. (D) Macrophages were co-cultured for four days with the HLA-DR2-restricted CD4 $^+$ T cell R2F10 at a ratio of 1:4 and 0.1, 1 or 10 $\mu\text{g/ml}$ of its cognate peptide. T cell proliferation was measured by tritium-thymidine incorporation during the last 24 h ($n = 3$). Data is represented as means with standard deviations. Statistical significance was determined by Wilcoxon signed rank test with post-hoc FDR correction. * = $p < 0.05$.

OxLDL supports *Mtb* intracellular survival through lysosomal cholesterol accumulation

OxLDL-derived free and esterified cholesterol have been demonstrated to be sequestered in lysosomes in macrophages^(26, 27), which potentially leads to lysosomal dysfunction. To investigate whether lysosomal localization of oxLDL lipids is required for its effect on *Mtb* load, oxLDL treatment was compared to acLDL, a non-naturally occurring modified lipoprotein which is endocytosed through identical scavenger receptor pathways as oxLDL, but does not induce lysosomal cholesterol accumulation^(26, 42). In resemblance to oxLDL, acLDL treatment of macrophages resulted in foam cell formation. However, while lipid staining intensities were similar (Figure S1B), clear differences in intracellular lipid localization and droplet structure were observed between both types of lipoproteins: in general, acLDL-induced intracellular lipid droplets were darker in color and appeared more granular than those resulting from oxLDL treatment (Figure 4A). Most importantly, however, acLDL did not affect macrophage *Mtb* load compared to untreated macrophages while oxLDL treatment significantly increased mycobacterial load (Figure 4B: oxLDL: 232% [194% – 278%] vs acLDL: 108% [88% - 126%]; $p < 0.0001$). This effect was not restricted to *Mtb*, as comparable results were obtained after macrophage infection with *Salmonella enterica* serovar Typhimurium (*Stm*) (Figure 4D: 179% [162% - 183%] vs 124% [88% - 136%]; $p < 0.05$) and *M. bovis* BCG (Figure 4C: 178% [133% - 254%] vs 97% [82% - 123%]; $p < 0.05$). To examine whether the observed difference between oxLDL and acLDL could be related to lysosomal function, their effect on lysosomal and autophagy markers during *Mtb* infection was analyzed by Western blot (Figure 4E). OxLDL treatment increased protein levels of lysosomal markers compared to PBS and acLDL, as demonstrated by higher levels of lysosomal membrane glycoproteins (LAMP1 & LAMP2) and proteases (Cathepsin D & L) (Figure 4F), also including the 48 kDa processing intermediate pro-cathepsin D (Figure S3A). Furthermore, oxLDL but not acLDL treatment led to an increased accumulation of LC3-II in the presence of vacuolar type H⁺-ATPase inhibitor bafilomycin A1 (10 nM) to block vesicle breakdown, indicative of increased autophagic flux. In contrast, levels of autophagosome cargo protein p62, a mediator of selective autophagy, were not elevated by oxLDL (Figure 4F). Collectively, these results indicate that oxLDL induces a general defect in macrophage antimicrobial function which is dependent on intracellular lipid localization.

To further substantiate this hypothesis, macrophages were treated with PBS, oxLDL or acLDL in the absence or presence of U18666A (3 µg/ml), an inhibitor of intracellular cholesterol transport⁽⁴³⁾. Lysosomal cholesterol sequestration was visualized using confocal microscopy by staining with fluorescent probes for neutral lipids (LipidTOX), lysosomes (LysoTracker) and cholesterol (filipin) (Figure 4G). OxLDL treatment induced a marked accumulation of cholesterol inside lysosomal vesicles as indicated by filipin and LysoTracker colocalization, which was not observed in macrophages treated with PBS or acLDL. Strikingly, when combined with U18666A, acLDL-treated macrophages

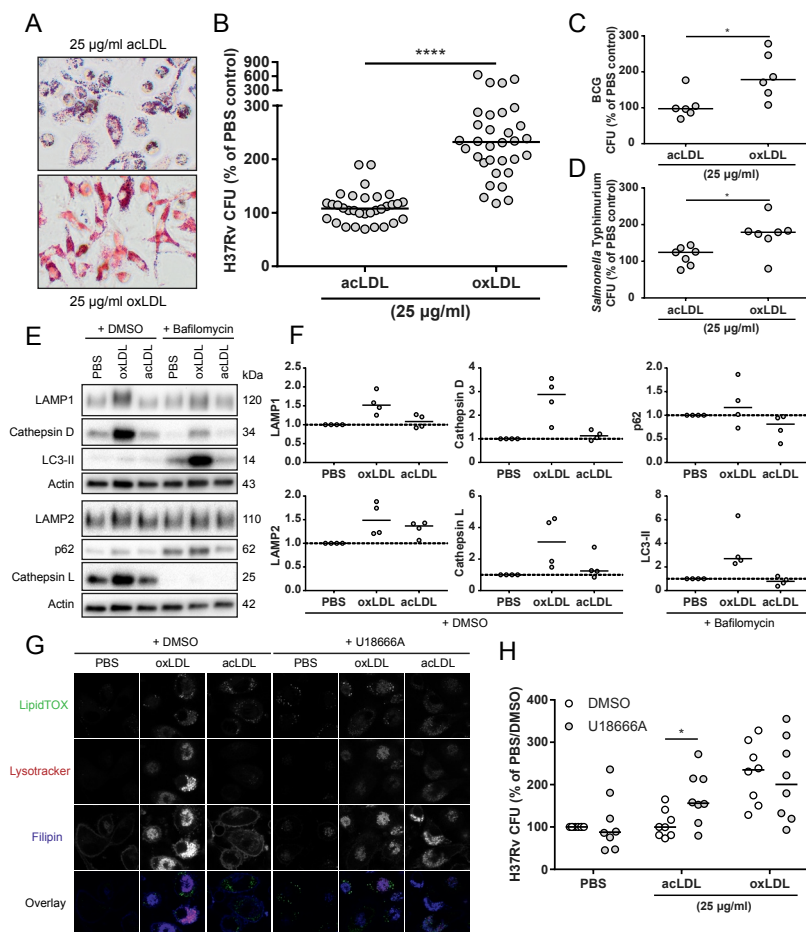


Figure 4: Lysosomal cholesterol accumulation attenuates macrophage *Mtb* control.

Primary human macrophages were treated with PBS control, acLDL or oxLDL (25 µg/ml) overnight. (A) Oil Red O staining of macrophages treated overnight with 25 µg/ml acLDL or oxLDL. Pictures were taken at a 20x magnification. Macrophages were infected with *Mtb* H37Rv (B) ($n = 32$), *M. bovis* BCG (C) ($n = 6$) or *Salmonella enterica* serovar Typhimurium (D) ($n = 6$) at a MOI of 10:1. Cells were lysed at 24 h post-infection and bacterial load was determined by CFU assay. Results were normalized versus PBS control. (E) Western blot analysis of lysosomal and autophagy markers in macrophages treated with bafilomycin A1 (10 nM) or DMSO control during 24 h of H37Rv *Mtb* infection. Data shown is from one representative donor ($n = 4$). (F) Quantification of LAMP1, LAMP2, Cathepsin D, Cathepsin L (+ DMSO), p62 and LC3-II (+ bafilomycin A1) protein levels. Protein levels were first normalized to actin and subsequently versus PBS control ($n = 4$). (G) Macrophages were co-treated with U18666A (3 µg/ml) or DMSO control for 24 h. Cells were subsequently stained for neutral lipids (LipidTOX, green), lysosomes (LysoTracker, red) and cholesterol (filipin, blue) and analyzed by confocal microscopy. Pictures were taken at a 63x magnification. Scale bars represent 5 µm. (H) Macrophages were co-treated with U18666A (3 µg/ml) or DMSO control for 24 h pre- and post-infection with *Mtb* H37Rv at a MOI of 10:1. Cells were lysed at 24 h post-infection and bacterial load was determined by CFU assay. Results were normalized versus PBS control (+ DMSO). Individual donors are depicted as dots with group medians. Statistical significance was determined by Wilcoxon signed rank test. * = $p < 0.05$, **** = $p < 0.0001$.

showed identical lysosomal cholesterol sequestration as oxLDL. The absence of an effect of acLDL treatment alone on *Mtb* load suggested that the localization of cholesterol inside lysosomes might be a causative factor in the increased *Mtb* growth phenotype of oxLDL-treated macrophages. To test this, we investigated whether combined treatment of acLDL with U18666A could mimic the effect of oxLDL on macrophage *Mtb* control. Indeed, while U18666A alone or in combination with oxLDL did not significantly alter macrophage phenotype (Figure 4G) and *Mtb* load, it increased mycobacterial burden when applied in conjunction with acLDL compared to DMSO control (Figure 4H: $169\% \pm 62\%$ vs $107\% \pm 32\%$; $p < 0.05$). Similar to oxLDL, U18666A treatment alone and in combination with acLDL increased protein levels of lysosome and autophagy markers in *Mtb*-infected macrophages, most notably Cathepsin L and when combined with bafilomycin A1 (10 nM), p62 and LC3-II (Figure S3B). Macrophage viability was unaffected by oxLDL and/or U18666A treatment in combination with *Mtb* infection as determined by combined Hoechst/propidium iodide (PI) staining (Figure S3C-D). Collectively, these results indicate that not simply the presence, but the specific accumulation of cholesterol inside lysosomes is crucial for the oxLDL- and U18666A-induced increase in *Mtb* survival in human macrophages.

While the above model proposes that oxLDL can interfere with macrophage mycobacterial control, we could not yet exclude whether oxLDL-induced foam cell formation also supported *Mtb* replication, possibly by providing increased nutrients. To gain a better understanding of overall kinetics of oxLDL-induced increased *Mtb* load and its associated cytokine response, infected macrophages treated with PBS control, oxLDL or acLDL were infected with *Mtb* and the intracellular bacterial load and concentrations of 29 cytokines and chemokines in supernatants were determined at 0 (uptake control), 4, 24, 48, 72 and 144 h post-infection. OxLDL treatment showed increased *Mtb* survival compared to PBS as early as 4 h post-infection, and versus both PBS and acLDL at all later time points (24 – 144 h) (Figure S4A). For all treatment conditions the intracellular *Mtb* load decreased with time, ranging from 1.3 to 12.4% of original bacterial uptake after 144 h of infection, which is supportive of a model in which the effect of oxLDL is the result of inhibited bacterial killing and not of increased bacterial outgrowth.

The multiplex results were congruent with the ELISA data from Figure 3C, as oxLDL-treated macrophages produced significantly lower levels of TNF- α and IL-6 after 24 h of *Mtb* infection compared to PBS control (Figure S4B). Many cyto- and chemokine concentrations were lower in oxLDL-treated macrophages between 4-48 h of *Mtb* infection, while supernatants from acLDL-treated macrophages often showed intermediate levels compared to PBS and oxLDL (IL-10, IL-6, TNF- α , IL-8, CCL3, CCL4, G-CSF, GM-CSF). We did not find significant differences at 72 and 144 h post-infection after FDR correction. IL-1RA was the only cytokine which showed increased production as a result of oxLDL, although the magnitude of this response varied between donors. Concentrations of CXCL10, IFN α 2, CCL2 and VEGF increased as a result of *Mtb* infection, however no differences were observed between treatment conditions for these factors. Levels of Epidermal Growth

Factor (EGF), Eotaxin, IFN γ , IL-12p40, IL-12p70, IL-1 β , IL-13, IL-15, IL-17A, IL-1 α , IL-2, IL-3, IL4, IL-5, IL-7 and TNF- β were measured but not shown as their concentrations were either very low in all samples (<100 pg/ml) or not detectable. Taken together, these experiments provide further evidence for an overall diminished cytokine response as a result of oxLDL treatment during *Mtb* infection.

OxLDL-inhibited mycobacterial killing is not rescued by small-molecules targeting known downstream signaling pathways

To identify the relevant molecular processes which are deregulated by lysosomal cholesterol accumulation, oxLDL-treated macrophages infected with *Mtb* were treated with compounds targeting various cell signaling pathways which are known to be affected by oxLDL in an attempt to rescue their antimicrobial capacity. Firstly, infected foamy macrophages were treated with rapamycin, an inhibitor of mammalian target of rapamycin complex 1 (mTORC1). mTOR is a master regulator of various cellular pathways including autophagy, and rapamycin-induced autophagy was reported to ameliorate foam cell formation^(44, 45). Rapamycin (2 μ M) slightly but significantly reduced *Mtb* load compared to DMSO in PBS-treated macrophages ($80 \pm 15\%$ of PBS/DMSO, $p < 0.05$), but did not affect bacterial burden in either oxLDL or acLDL-induced foamy macrophages (Figure 5A). Secondly, lysosomal storage disorders such as NPC disease are associated with defects in lysosomal Ca²⁺ homeostasis⁽⁴⁶⁾, and activation of the lysosomal ion channel transient receptor potential channel 1 (TRPML1) by small-molecule activator ML-SA1 was shown to rescue lysosomal trafficking in NPC1^{-/-}-macrophages⁽³⁰⁾. However, ML-SA1 treatment (10 μ M) did not affect *Mtb* infection in any of our conditions (Figure 5B). Finally, oxLDL can induce endoplasmic reticulum (ER) stress in macrophages⁽⁴⁷⁾, a state of disturbed ER homeostasis due to accumulation of unfolded proteins and/or disrupted Ca²⁺ handling which plays a role in the apoptotic response in atherosclerotic plaques and the TB granuloma^(48, 49). Treatment of *Mtb*-infected macrophages with three established reducers of the ER stress response, namely chemical chaperone 4-phenylbutyrate (4-PBA; 3 mM) and downstream kinase inhibitors 4 μ 8c (10 μ M) and GSK2656157 (10 μ M) (respectively targeting inositol-requiring enzyme 1- α (IRE1- α) and protein kinase RNA-like endoplasmic reticulum kinase (PERK)), did not alleviate the oxLDL-induced increase in mycobacterial survival (Figure 5C). In conclusion, chemical modulation of mTOR signaling, lysosomal Ca²⁺ homeostasis or ER stress did not reverse the oxLDL-induced increased mycobacterial load in human macrophages.

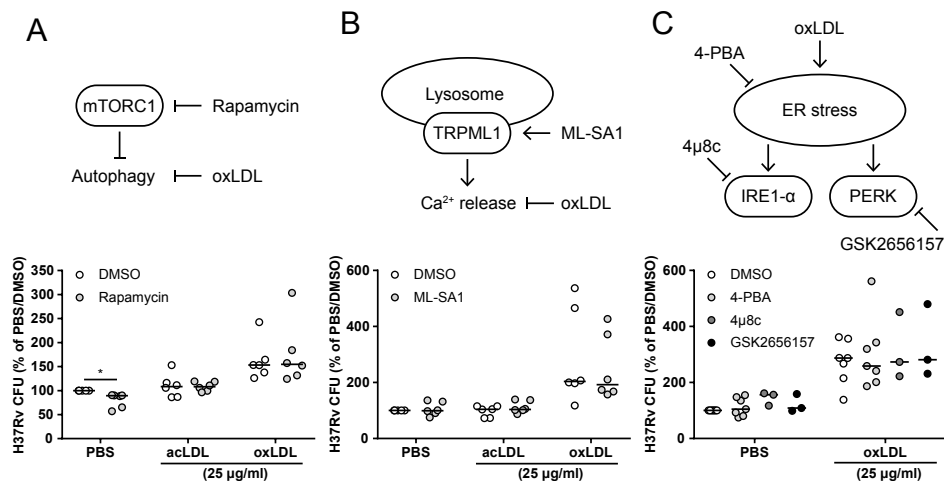


Figure 5: oxLDL-induced *Mtb* survival was not reversed by targeting known downstream pathways.

Primary human macrophages were treated with PBS control, acLDL or oxLDL (25 $\mu\text{g}/\text{ml}$) overnight and subsequently infected with *Mtb* H37Rv at a MOI of 10:1 and treated with compounds or DMSO control overnight. Cells were lysed at 24 h post-infection and bacterial load was determined by CFU assay. The following treatments were applied: (A) rapamycin (2 μM , $n = 6$) to induce mTORC1-regulated autophagy, (B) ML-SA1 (10 μM , $n = 6$) to stimulate lysosomal Ca^{2+} release and (C) 4-PBA (3 mM, $n = 7$), 4 μ 8c (10 μM , $n = 3$) and GSK2656157 (10 μM , $n = 3$) to inhibit the ER stress response. Individual donors are depicted as dots with group medians. Results were normalized versus PBS control (+ DMSO). Statistical significance was determined by Wilcoxon signed rank test. * = $p < 0.05$.

OxLDL inhibits *Mtb* localization to functional lysosomes in infected macrophages

The above experiments demonstrated that the endolysosomal system is pivotal for oxLDL-induced increased mycobacterial survival. As earlier studies have reported that cholesterol accumulation impaired proper lysosomal trafficking^(29, 30), we hypothesized that *Mtb* trafficking to functional lysosomes was inhibited by oxLDL treatment. To investigate this, oxLDL-treated macrophages infected with fluorescent DsRed-expressing H37Rv were stained for functional lysosomes with LysoTracker (Figure 6A), and lysosomal colocalization was determined for each intracellular mycobacterium individually (Figure 6B). OxLDL significantly decreased the average colocalization between *Mtb* and LysoTracker ($39 \pm 9\%$) compared to acLDL ($51 \pm 12\%$, $p < 0.05$) or PBS treatment ($60 \pm 6\%$, $p < 0.05$) (Figure 6C), indicating that oxLDL inhibits phagolysosomal fusion in *Mtb*-infected macrophages.

In an attempt to identify the specific lysosomal pathways affected by oxLDL treatment, we investigated colocalization of *Mtb* with galectin-3 and NDP52. Galectins are carbohydrate-binding proteins which play a role in targeting damaged endomembrane structures for autophagy⁽⁵⁰⁾, including phagolysosomes damaged by *Stm* or *Mtb*⁽⁵¹⁻⁵³⁾, and galectin-3 colocalization with lysosomes is an established measure of lysosomal damage⁽⁵⁴⁾. NDP52 is an autophagy adaptor which has previously been implicated in

the autophagic clearance of both *Stm* and *Mtb* ^(51, 55, 56). Although colocalization events with *Mtb* were observed for both galectin-3 and NDP52, this occurred for a minority of intracellular bacteria (range 2-8% of bacteria) and no significant differences were found between oxLDL and control conditions (Figure 6D-G).

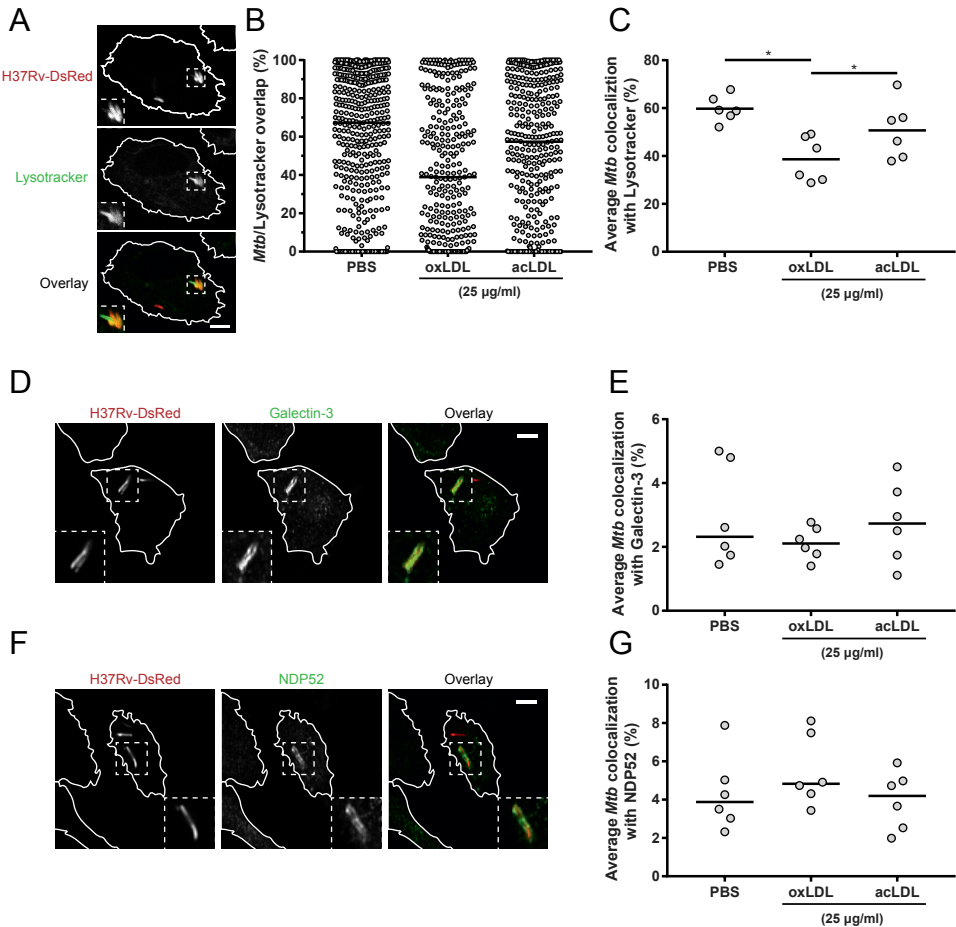


Figure 6: oxLDL impairs *Mtb* localization to lysosomes in macrophages.

Primary human macrophages were treated overnight with PBS control, acLDL or oxLDL (25 µg/ml) and subsequently infected with DsRed-*Mtb* H37Rv (red) at a MOI of 10:1. Cells were stained (green) for lysosomes (Lysotracker) (A), galectin-3 (D) or NDP52 (F) at 4 h post-infection and analyzed by confocal microscopy. Pictures were taken at a 63x magnification. Scale bars represent 5 µM. Percentage overlap of intracellular mycobacteria with staining was determined for 3 wells * 3 = 9 pictures per condition. (B) Results of a representative donor of *Mtb* overlap with Lysotracker. Individual mycobacteria are represented by dots with group medians. Average colocalization of *Mtb* with Lysotracker (C), galectin-3 (E) and NDP52 (G) are displayed for macrophages from six independent donors. Individual donors are depicted as dots with group medians. Statistical significance was determined by Wilcoxon signed rank test with post-hoc FDR correction. * = $p < 0.05$.

Discussion

The looming epidemic of concurrent TB-DM poses a serious global health problem. Identification of the causal molecular and cellular mechanisms underlying the increased risk of TB in DM patients is paramount for adequate treatment. Previously, we have demonstrated that TB-DM patients have a blood lipid profile with pro-atherogenic properties⁽⁴⁰⁾, which could have implications for TB-DM pathogenesis. We now identify oxLDL as a potential risk factor for TB. OxLDL levels were found to be increased in plasma samples of DM patients from a TB endemic region, who represent the specific population at increased risk for disease. Although both triglyceride and oxLDL levels were lower in the TB-DM group compared to DM, this might well be related to the duration and severity of DM disease as the majority of TB-DM patients were recently diagnosed diabetics compared to the DM alone group (Table S1). Furthermore, TB was associated with wasting syndrome and therefore with low levels of many circulating metabolites in this patient population, including LDL⁽⁴⁰⁾. As these patients were not merely at increased risk of TB at the moment of blood collection but had already developed active disease, it is not unlikely that oxLDL levels are decreased since onset of TB. Nonetheless, a clear dichotomy in oxLDL concentrations was visible based on triglyceride-status in TB-DM patients, implying that diabetes-associated dyslipidemia was a factor associated with increased oxLDL levels in this population.

Importantly, oxLDL-, but not acLDL-, induced foamy macrophage formation supported intracellular *Mtb* survival through lysosomal cholesterol accumulation and subsequent dysfunction. This effect was not limited to *Mtb* as similarly enhanced bacterial loads were observed for *Stm* and *M. bovis* BCG, which reside in different intracellular compartments compared to *Mtb*⁽⁵⁷⁾. Pharmacological manipulation of intracellular cholesterol transport with U18666A confirmed that subcellular localization of cholesterol to lysosomes was essential to lysosomal dysfunction. Since foamy macrophages play an important role during progression of the TB granuloma^(16, 18), our results suggest that increased levels of oxLDL could contribute to the enhanced TB susceptibility in DM patients.

Our findings are in line with earlier studies that reported increased levels of oxLDL in DM patients⁽⁸⁻¹¹⁾. Both hyperglycemia and dyslipidemia contribute to the generation of free radicals and oxidative stress during chronic DM^(58, 59), which can lead to the pathological modification of proteins and lipids involved in foam cell formation and atherosclerosis, such as oxLDL. Additionally, DM and hyperglycemia are associated with increased expression of oxLDL scavenger receptors CD36⁽⁶⁰⁻⁶²⁾, SR-A^(62, 63) and LOX-1^(62, 64), and macrophages from type 2 diabetics showed higher uptake of oxLDL⁽⁶⁵⁾. Similar to DM, TB has been demonstrated to result in increased oxidative stress and a systemic decrease in antioxidant capacity, e.g. reduced levels of glutathione⁽⁶⁶⁻⁶⁹⁾. *Mtb* infection increased CD36 expression *in vitro*⁽¹⁹⁾ and CD36-mediated uptake of surfactant lipids has been reported to support *Mtb* growth⁽²⁰⁾. In contrast, a recent paper did not find a role for CD36-

mediated macrophage lipid droplet formation in *Mtb* control ⁽⁷⁰⁾, which could indicate that not simply the presence of lipid droplets but rather the specific composition and/or localization of the intracellular lipids is most important for their effect on *Mtb* intracellular survival, similar to what we observed here when comparing acLDL and oxLDL.

At the functional level, oxLDL treatment displayed potential to inhibit macrophage antigen presentation to CD4⁺ T cells, which could in principal lead to impaired activation of adaptive immune responses. While their phagocytic capacity was largely unaffected, oxLDL-treatment macrophages showed an overall decreased cytokine production in response to *Mtb*. These results were somewhat surprising, as oxLDL has been associated with increased inflammation during atherosclerosis ⁽⁷¹⁾ and non-alcoholic steatohepatitis (NASH) ⁽⁷²⁻⁷⁴⁾, including activation of the NLRP3 inflammasome and subsequent secretion of IL-1 β by macrophages ^(38, 75). However, in these studies oxLDL treatment was often accompanied by secondary factors which may be required for the observed pro-inflammatory responses, such as macrophage apoptosis, circulating anti-oxLDL immune complexes or the formation of intralysosomal cholesterol crystals. In agreement with our own observations, several studies reported diminished inflammatory responses of oxLDL-treated macrophages after stimulation with TLR ligands ⁽⁷⁶⁻⁷⁸⁾. These divergent results could be related to study-specific differences in experimental setup, including variations in species, cell types, stimulations and degree of LDL oxidation. Additionally, oxLDL was reported to induce a long-lasting pro-inflammatory phenotype in monocytes through epigenetic changes, which possibly did not occur in our experiments due to their relatively short timeframe or lack of restimulation ^(79, 80).

Hypercholesterolemia has been implicated in increasing the risk of developing TB ⁽⁸¹⁻⁸³⁾, and cholesterol catabolism is needed for mycobacterial persistence and growth ^(84, 85). For this reason, most studies on foamy macrophage induction by mycobacteria have focused on the relatively long-term nutritional benefits of intracellular lipid accumulation ^(20, 86). The results presented in this manuscript demonstrate that pathologically modified lipids also directly interfere with macrophage antimicrobial capacities, providing a novel perspective on the importance of foam cell formation during TB. These findings are corroborated by a study which demonstrated that *M. smegmatis* and *M. bovis* BCG blocked phagolysosomal fusion by inducing an NPC-like phenotype in infected macrophages ⁽³⁹⁾. Additionally, macrophage cholesterol depletion restored halted phagosome maturation during *M. avium* infection ⁽⁸⁷⁾. Drugs which target host cholesterol metabolism can therefore have potential for TB host directed treatment, and *e.g.* statins have shown promise as adjunctive anti-mycobacterial therapy both *in vitro* and *in vivo* ⁽⁸⁸⁻⁹²⁾. Furthermore, our results suggest that oxLDL treatment supports mycobacterial survival through interference with phagolysosomal trafficking and/or fusion. Lysosomal lipid accumulation has been reported to influence these processes in several ways. Late endosomal transport is mediated by the lysosomal protein ORP1L, which modulates the interaction between Rab GTPases and their effectors, motor protein complexes and the

ER through conformational changes induced by fluctuations in intraluminal cholesterol levels^(93, 94). Furthermore, abnormal sphingolipid storage due to *NPC1*-deficiency or U18666A treatment was shown to disrupt lysosomal Ca²⁺ homeostasis, blocking vesicle transport and fusion^(30, 46). Finally, several studies have reported that lysosomal storage disorders interfere with the autophagic system^(31, 32), which might be reflected by the increased LC3-II levels detected in oxLDL- and U18666A-treated macrophages during *Mtb* infection. Although pharmacological modulation of these pathways did not ameliorate the oxLDL-induced effect on *Mtb* control, their involvement should not yet be excluded as the phenotype induced by oxLDL was practically irreversible in our experimental setup.

Our study might have had a number of limitations. Firstly, the oxLDL used throughout this manuscript was generated by copper-induced oxidation of native LDL, which is sometimes referred to as extensively oxidized LDL in literature due to its high oxidation grade⁽⁶⁾. It is generally believed that naturally occurring oxLDL is composed of less extensively oxidized variants as abundantly oxidized LDL would be rapidly cleared from the circulation. Therefore, it is possible that the phenotypes observed in our experiments are more extreme than would have occurred using naturally oxidized LDL. However, the precise composition of physiological oxLDL is still uncertain as accurate characterization of isolated oxLDL is technically challenging. As LDL oxidation mostly occurs in the subendothelial space during atherosclerosis, locally generated oxidized species might be of greater importance for disease than circulating oxLDL. Regardless, it would be of interest to investigate the effects of minimally modified LDL (mmLDL), a variant which is believed to be more similar to naturally occurring oxLDL⁽⁶⁾, on macrophage *Mtb* infection. Secondly, oxLDL was applied at a concentration of 25 µg/ml for the majority of the experiments, which is at the high end of what has been physiologically observed⁽⁹⁵⁻⁹⁷⁾. However, oxLDL treatment times were relatively short compared to what can be expected *in vivo*, and low levels of oxLDL (1 µg/ml) were already sufficient to increase mycobacterial load during this period. Thirdly, oxLDL is a complex particle consisting of hundreds of phospholipids, triglycerides and cholesteryl esters, which vary in terms of composition and susceptibility to oxidation and therefore have different intracellular effects⁽¹²⁾. It would be of great interest to study whether specific oxidized lipids or proteins are required for the observed oxLDL phenotype. Finally, although not within the scope of this study and technically challenging, it would be important to validate these findings in a disease model for translation to *in vivo* settings, e.g. using monocytes isolated from DM patients.

In conclusion, oxLDL treatment of human macrophages supports *Mtb* intracellular survival as a result of lysosomal dysfunction, providing a proof of concept for a contribution of increased levels of oxLDL as a potential risk factor for TB development during DM. While we previously demonstrated that hyperglycemia alone did not directly influence outcome of macrophage *Mtb* infection⁽⁹⁸⁾, we postulate that elevated lipid levels, which are associated with DM, can be involved in TB-DM pathogenesis⁽⁴⁰⁾. These

findings pave the way for further research, including the use of LDL-lowering drugs such as statins or antioxidant drugs as part of the DM-treatment regimen for the reduction of the risk of TB.

Materials and Methods

Ethics statement/Patient population and plasma oxLDL measurements

The patient population was previously used in an extensive lipid profiling analysis using ^1H -NMR spectroscopy as part of an EU-funded collaborative project, TANDEM⁽⁹⁹⁾, of which details regarding patient inclusion were reported earlier⁽⁴⁰⁾. From this population plasma samples of 20 healthy endemic controls, 20 TB patients, 20 DM patients and 20 TB-DM patients were selected at random for oxLDL determination. Plasma oxLDL levels were measured by sandwich ELISA according to manufacturer's instructions (Merckodia AB, Uppsala, Sweden). One TB-DM patient was excluded post-hoc due to the presence of clinical evidence suggestive of type 1 diabetes, while all other DM patients suffered from type 2 diabetes. This study was approved by the Health Research Ethics Committee of the University of Stellenbosch, and conducted according to the Helsinki Declaration and International Conference of Harmonization guidelines. Written informed consent was obtained from all participants.

Reagents and antibodies

Primary antibodies against LAMP1, LAMP2, Cathepsin D, Cathepsin L, p62, galectin-3 and secondary goat anti-mouse IgG (Alexa Fluor[®] 647) were purchased from Abcam (Cambridge, UK). LC3A/B was from Cell Signaling (Bioke, Leiden, The Netherlands), actin-HRP from Santa Cruz Biotechnology (Santa Cruz, CA, USA), CD86-Alexa700 and HLA-DR-PeCy5 from BD Biosciences (Erembodegem, Belgium) and CD80-BV650, CD14-FITC and CD163-Alexa647 were bought from Biolegend (ITK diagnostics, Uithoorn, The Netherlands). NDP52 (CALCOCO2), secondary goat anti-rabbit IgG (Alexa Fluor[®] 647) and HRP-conjugated antibodies reactive with mouse and rabbit were purchased from Thermo Fisher Scientific (Merelbeke, Belgium).

LDL isolation

LDL was isolated from the serum of healthy volunteers by density gradient ultracentrifugation⁽¹⁰⁰⁾. Blood was collected in clot activator tubes and clotted for 90 minutes at room temperature. Serum was obtained after 10 minutes of centrifugation at 1,500 *g*. EDTA was added to a final concentration of 1 mM, after which serum density was adjusted to 1.21 g/l by addition of solid potassium bromide and gentle stirring. The resulting serum solution was distributed over 13.7 ml UltraClear ultracentrifuge tubes (Beckman Coulter, Woerden, The Netherlands) and a density gradient was prepared by overlaying it with potassium bromide solutions of decreasing concentrations (1.063 g/l, 1.019 g/l, 1.0063 g/l) in PBS supplemented with 0.3 mM EDTA (pH 7.4) using a wide bore

pipette tip. The serum was then centrifuged at 40,000 RPM for 20 h at 4°C in a SW41 Ti swinging bucket rotor (Optima™ LE-80K, Beckman Coulter). After centrifugation the tubes were carefully removed from the rotor and the LDL fraction was aspirated using a glass Pasteur pipette. The LDL was dialyzed against PBS at 4°C for 16 h during which the buffer was refreshed three times. The protein concentration of LDL was determined using a BCA kit according to the manufacturer's instructions (Pierce, Thermo Fisher Scientific).

Generation of oxLDL and acetylated LDL (acLDL)

OxLDL was generated by copper oxidation of native LDL. Copper sulfate was added to 200 µg/ml LDL in PBS at a final concentration of 5 µM and incubated for 20 h at 37°C in the dark. The reaction was stopped by addition of 0.2 mM EDTA and oxLDL was then dialyzed against PBS containing 1 mM EDTA at 4°C for 24 h during which the buffer was refreshed three times. To produce acLDL, LDL was acetylated according to the protocol by Fraenkel-Conrat *et al.* ⁽¹⁰¹⁾. An equal volume of saturated sodium acetate was added to 1 mg/ml of LDL and stirred at 4°C until cold. During the following hour acetic anhydride was added in 2 µl aliquots until 1.5x the mass of LDL was added in total. The mixture was stirred for another 30 minutes after the last aliquot was added. The acLDL was then dialyzed against PBS containing 1 mM EDTA at 4°C for 24 h during which the buffer was refreshed three times. Finally, the modified lipoproteins were concentrated to 1 mg/ml using 100 kDa Amicon Ultracel centrifugal filter units (Merck Millipore, Amsterdam, The Netherlands).

Macrophage differentiation and foam cell generation

CD14⁺ monocytes were isolated from buffy coats of healthy blood bank donors by positive selection using an autoMACS Pro Separator (Miltenyi Biotec BV, Leiden, The Netherlands). Donors were not part of an already-existing collection. Monocytes were differentiated into macrophages by addition of 50 ng/ml macrophage-colony stimulating factor (M-CSF) (Miltenyi Biotec) during culture for 6 days at 37°C/5% CO₂ ⁽¹⁰²⁾. Cells were cultured in RPMI-1640 medium with L-glutamine, without glucose and sodium bicarbonate (Sigma-Aldrich Chemie BV, Zwijndrecht, the Netherlands), supplemented with 5 mM D-glucose, 2 g/l sodium bicarbonate, 10% fetal bovine serum, 100 units/ml penicillin and 100 µg/ml streptomycin. After differentiation macrophages were harvested by trypsinization and seeded in multi-well plates. As a quality control, macrophages were stained for surface expression of CD14 and CD163 and acquired on a BD LSRFortessa flow cytometer (BD Biosciences) (Figure S1A). To generate foam cells, macrophages were treated with various concentrations of oxLDL overnight. PBS, native LDL and/or acLDL were used as controls. Foam cell formation was confirmed by Oil Red O staining. Macrophages were fixed for 30 minutes in 4% paraformaldehyde and subsequently stained with a filtered work solution of Oil Red O (Sigma-Aldrich) in isopropanol (0.3% Oil Red O in 60% isopropanol) for 20 minutes. Afterwards, the red stain was dissolved in 4% NP-40 in isopropanol and quantified

by measuring the optical density (OD) at 520 nm using a iMark Microplate Absorbance Reader (Bio-Rad, Veenendaal, The Netherlands).

Mtb H37Rv infection and cytokine measurements

Mtb H37Rv cultures were grown to mid-log phase in Middlebrook 7H9 liquid medium (Difco, BD Biosciences) supplemented with albumin/dextrose/catalase (ADC) (BBL, BD Biosciences). Bacterial concentrations were determined by measuring culture optical density at 600 nm. Macrophages were infected with H37Rv at a multiplicity of infection (MOI) of 10:1 for 1 h at 37°C, after which the cells were washed twice with medium containing 30 µg/ml gentamicin and cultured overnight in fresh medium containing 5 µg/ml gentamicin. Infected cells were lysed either directly after infection or at 4, 24, 48, 72 or 144 h post-infection using 0.05% Triton X-100 and a dilution series of the lysates was plated on 7H10 square agar plates (Difco, BD Biosciences) supplemented with oleate/albumin/dextrose/catalase (OADC) (BBL, BD Biosciences). Colony-forming units (CFU) were determined after 2-3 weeks of incubation at 37°C. From some experiments supernatants were harvested and filtered for determination of IL-1β, IL-6, TNF-α (Invitrogen, Thermo Fisher Scientific) and IL-10 (Sanquin, Amsterdam, The Netherlands) by ELISA or for testing using a Human Cytokine/Chemokine Immunology Multiplex Assay (Merck Millipore, Amsterdam, the Netherlands) according to their manufacturers' instructions.

Phagocytosis assay

To quantify phagocytic capacity, fluorescent polystyrene particles (Fluoresbrite YG carboxylate microspheres) (Polysciences, Hirschberg an der Bergstrasse, Germany) were used as described by Leclerc *et al* ⁽¹⁰³⁾. Macrophages were incubated with fluorescent beads in a ratio of 10 beads to 1 cell for 90 min at 37°C. Cells were subsequently harvested by gentle scraping and resuspended in a 1:1 mixture of culture medium and Trypan Blue, and internalization of the beads was quantified by acquisition on a BD Accuri C6 flow cytometer (BD Biosciences). Non-internalized bead fluorescence was quenched by Trypan Blue and detected in the FL-3 channel (red), whereas internalized beads were detected in the FL-1 channel (green). Analysis was performed using Flowjo software (version 10.1, Tree Star Inc, Ashland, OR).

Antigen presentation assay

HLA-DR2/HLA-DR3-positive macrophages were harvested, seeded in 96-well plates at 2,500 cells/wells and treated with PBS, 25 µg/ml oxLDL or native LDL. The following day the cells were washed once in assay medium (IMDM with 10% human serum) and HLA class II restricted CD4⁺ T cell clones were added at a ratio of 4:1 together with a dilution series of their specific cognate peptide (R2F10 clone: HLA-DR2 restricted, reactive with *Mycobacterium leprae* (*Mlep*) hsp65; Rp15 1-1: HLA-DR3 restricted, reactive with *Mtb* and *Mlep* hsp65) or 1.25 µg/ml purified protein derivative (PPD) (Staten Serum Institute,

Copenhagen, Denmark) ^(104, 105). Medium was used as negative control. Macrophages and T cells were co-cultured for 3 days at 37°C/5% CO₂, and tritium-thymidine was added for the last 16 h of culture after which the cells were harvested and tritium-thymidine incorporation was measured using a Microbeta plate counter (Wallac, Turku, Finland). Furthermore, macrophages were stained for surface expression of CD86, CD80 and HLA-DR and analyzed on a BD LSRFortessa flow cytometer (BD Biosciences).

Western blotting

For analysis of lysosomal and autophagy-related proteins, (*Mtb*-infected) macrophages were lysed for 5 minutes using a buffer containing 3% SDS, 4 mm glycerol, 100 mM Tris-HCl (pH 6.8) containing protease inhibitors (Roche, Woerden, The Netherlands) and the resulting lysates were boiled for 10 min at 95°C. Protein concentrations were determined by bicinchoninic acid assay (Pierce, Thermo Fisher Scientific) and equal amounts were mixed with 4x Laemmli buffer before loading on a 4–20% Mini-PROTEAN TGX™ precast protein gel (Bio-Rad). After separation, proteins were transferred onto a polyvinylidene fluoride membrane and blocked for 1 h in Tris-buffered saline/2.5% Tween-20 containing 5% non-fat dry milk and subsequently probed with primary antibodies overnight at 4°C. Membranes were incubated with horseradish peroxidase-conjugated secondary antibodies (reactive against mouse or rabbit) for 2 h at room temperature before visualization by Amersham Enhanced Chemiluminescence Western Blotting Detection kit (GE Healthcare, Hoevelaken, The Netherlands). Blots were quantified using Image J (NIH, Bethesda, MD, USA) and proteins were normalized versus actin.

Confocal microscopy

For confocal microscopy, macrophages were seeded in black poly-d-lysine coated glass 96-well plates (MatTek Corporation, Ashland, MA, USA). To stain lysosomes, macrophages were incubated with 75 nM LysoTracker Red or Deep Red (Thermo Fisher Scientific) at 37°C/5%CO₂ for 1 h before fixation. Cells were fixed for 1 h in 1% EM-grade formaldehyde, followed by quenching with PBS/1.5 mg/ml glycine for 10 min and blocking in 5% human serum for 45 min, all at room temperature. For immunostaining, cells were permeabilized for 10 minutes with 0.1% Triton X-100 before blocking and subsequently stained with primary and secondary antibodies for 30 minutes each in the dark at room temperature. Finally, cells were stained with phalloidin-Alexa488 (Thermo Fisher Scientific) and/or LipidTOX Green (Thermo Fisher Scientific) for 30 min according to the manufacturer's instructions, and/or 50 µg/ml Filipin complex from *Streptomyces filipinensis* (Sigma-Aldrich) for 2 h at room temperature in the dark. LysoTracker and filipin pictures were taken using a SP8WLL confocal microscope (Leica, Amsterdam, The Netherlands). Galectin-3 and NDP52 colocalization was visualized using a Dragonfly spinning-disk confocal microscope (Andor Technologies, Belfast, UK) equipped with 405, 488, 561 and 640nm lasers and a Zyla 4.2 sCMOS camera.

Colocalization analysis

Macrophages were infected for 4 h with a DsRed-expressing *Mtb* H37Rv strain at a MOI of 10:1 and stained with LysoTracker Deep Red or primary antibodies for galectin 3 and NDP52 as described above. LysoTracker channel background was subtracted by rolling ball algorithm (20 pixel radius). All images were analyzed using CellProlifer 3.0.0⁽¹⁰⁶⁾. First, pictures were corrected for non-homogenous illumination if necessary. DsRed-*Mtb* were segmented by manual global thresholding with intensity-based declumping, and stained objects were segmented by adaptive two-class Otsu thresholding with upper and lower bounds to correct for individual cell-specific differences in background signal with intensity-based declumping. Then, the percentage of staining object overlap with individual DsRed-*Mtb* was calculated for each image and the average colocalization was calculated for each treatment condition.

Macrophage viability assay

To assess cell viability after treatment and infection with H37Rv *Mtb*, macrophages were stained with 2 µg/ml propidium iodide (PI) (Sigma-Aldrich) and 2 µg/ml Hoechst 33342 (Sigma-Aldrich) in RPMI without phenol red and FCS for 5 min in the dark. Cells were subsequently imaged on a AF6000 fluorescence microscope (Leica) and pictures were taken at a 20x magnification. Pictures were processed and analyzed in Image J. First, the background was subtracted by rolling ball algorithm (20 pixel radius). Then, Hoechst- or PI-positive nuclei were segmented by Otsu thresholding and counted, from which the percentages of viable macrophages were calculated. Staurosporin (5 µM) (Sigma-Aldrich) was used as a positive control for cell death.

Statistical analysis

Statistical significance was assessed by Kruskal-Wallis test with post-hoc Dunn's test, or Wilcoxon signed rank test using GraphPad software (version 7.02, Prism, La Jolla, CA, USA) with post-hoc false discovery rate (FDR) correction for multiple comparisons when necessary. Statistical analysis of patients characteristics was performed in SPSS 23 (IBM, Armonk, NY, USA) by one-way ANOVA (reported *p*-values are the outcome of the *F*-test), independent samples *t*-test or chi-squared test.

Acknowledgements

We are grateful to Prof. dr. Ronit Shiri-Sverdlov and Dr. Sofie Walenbergh, Departments of Molecular Genetics, Human Biology and Surgery, School of Nutrition and Translational Research in Metabolism (NUTRIM), Maastricht University, for their helpful suggestions regarding acLDL treatment, to Dr. Yanan Wang, Department of Medicine, Division of Endocrinology, Leiden University Medical Center, for providing the relevant protocols for LDL isolation and modification, to the Molecular Biology Clinical Research team at Stellenbosch University for characterizing the participants and for collecting the samples and to all the study participants and blood donors.

References

1. Morton R. *Phthisiologia: or a treatise of consumptions*. London: Smith and Walford; 1694.
2. Jeon CY, Murray MB. Diabetes mellitus increases the risk of active tuberculosis: a systematic review of 13 observational studies. *PLoS Med*. 2008;5(7):e152. doi: 10.1371/journal.pmed.0050152.
3. World Health Organization. *Diabetes & TB - fact sheet*. Geneva, Switzerland 2016
4. International Diabetes Federation. *Diabetes Atlas*. 8th edn. Brussels, Belgium 2017
5. Singh R, Devi S, Gollen R. Role of free radical in atherosclerosis, diabetes and dyslipidaemia: larger-than-life. *Diabetes/metabolism research and reviews*. 2015;31(2):113-26. doi: 10.1002/dmrr.2558. PMID: 24845883
6. Levitan I, Volkov S, Subbaiah PV. Oxidized LDL: diversity, patterns of recognition, and pathophysiology. *Antioxidants & redox signaling*. 2010;13(1):39-75. doi: 10.1089/ars.2009.2733. PMID: 19888833
7. Yoshida H, Kisugi R. Mechanisms of LDL oxidation. *Clin Chim Acta*. 2010;411(23-24):1875-82. doi: 10.1016/j.cca.2010.08.038. PMID: 20816951
8. Toshima S, Hasegawa A, Kurabayashi M, Itabe H, Takano T, Sugano J, et al. Circulating oxidized low density lipoprotein levels. A biochemical risk marker for coronary heart disease. *Arteriosclerosis, thrombosis, and vascular biology*. 2000;20(10):2243-7. PMID: 11031210
9. Park K, Gross M, Lee DH, Holvoet P, Himes JH, Shikany JM, et al. Oxidative stress and insulin resistance: the coronary artery risk development in young adults study. *Diabetes Care*. 2009;32(7):1302-7. doi: 10.2337/dc09-0259. PMID: 19389821
10. Njajou OT, Kanaya AM, Holvoet P, Connelly S, Strotmeyer ES, Harris TB, et al. Association between oxidized LDL, obesity and type 2 diabetes in a population-based cohort, the Health, Aging and Body Composition Study. *Diabetes/metabolism research and reviews*. 2009;25(8):733-9. doi: 10.1002/dmrr.1011. PMID: 19780064
11. Marin MT, Dasari PS, Tryggstad JB, Aston CE, Teague AM, Short KR. Oxidized HDL and LDL in adolescents with type 2 diabetes compared to normal weight and obese peers. *Journal of diabetes and its complications*. 2015;29(5):679-85. doi: 10.1016/j.jdiacomp.2015.03.015. PMID: 25881918
12. Miller YI, Shyy JY. Context-Dependent Role of Oxidized Lipids and Lipoproteins in Inflammation. *Trends in endocrinology and metabolism: TEM*. 2016. doi: 10.1016/j.tem.2016.11.002. PMID: 27931771
13. Moore KJ, Freeman MW. Scavenger receptors in atherosclerosis: beyond lipid uptake. *Arteriosclerosis, thrombosis, and vascular biology*. 2006;26(8):1702-11. doi: 10.1161/01.ATV.0000229218.97976.43. PMID: 16728653
14. Miller YI, Choi SH, Wiesner P, Fang L, Harkewicz R, Hartvigsen K, et al. Oxidation-specific epitopes are danger-associated molecular patterns recognized by pattern recognition receptors of innate immunity. *Circulation research*. 2011;108(2):235-48. doi: 10.1161/CIRCRESAHA.110.223875. PMID: 21252151

15. Park YM. CD36, a scavenger receptor implicated in atherosclerosis. *Exp Mol Med*. 2014;46:e99. doi: 10.1038/emm.2014.38. PMID: 24903227
16. Russell DG, Cardona PJ, Kim MJ, Allain S, Altare F. Foamy macrophages and the progression of the human tuberculosis granuloma. *Nature immunology*. 2009;10(9):943-8. doi: 10.1038/ni.1781. PMID: 19692995
17. Santucci P, Bouzid F, Smichi N, Poncin I, Kremer L, De Chastellier C, et al. Experimental Models of Foamy Macrophages and Approaches for Dissecting the Mechanisms of Lipid Accumulation and Consumption during Dormancy and Reactivation of Tuberculosis. *Frontiers in cellular and infection microbiology*. 2016;6:122. doi: 10.3389/fcimb.2016.00122. PMID: 27774438
18. Peyron P, Vaubourgeix J, Poquet Y, Levillain F, Botanch C, Bardou F, et al. Foamy macrophages from tuberculous patients' granulomas constitute a nutrient-rich reservoir for *M. tuberculosis* persistence. *PLoS pathogens*. 2008;4(11):e1000204. doi: 10.1371/journal.ppat.1000204. PMID: 19002241
19. Mahajan S, Dkhar HK, Chandra V, Dave S, Nanduri R, Janmeja AK, et al. Mycobacterium tuberculosis modulates macrophage lipid-sensing nuclear receptors PPARgamma and TR4 for survival. *Jimmunol*. 2012;188(11):5593-603. doi: jimmunol.1103038 [pii];10.4049/jimmunol.1103038 [doi].
20. Dodd CE, Pyle CJ, Glowinski R, Rajaram MV, Schlesinger LS. CD36-Mediated Uptake of Surfactant Lipids by Human Macrophages Promotes Intracellular Growth of Mycobacterium tuberculosis. *Journal of immunology*. 2016;197(12):4727-35. doi: 10.4049/jimmunol.1600856. PMID: 27913648
21. Ouimet M, Koster S, Sakowski E, Ramkhelawon B, van Solingen C, Oldebeken S, et al. Mycobacterium tuberculosis induces the miR-33 locus to reprogram autophagy and host lipid metabolism. *Nature immunology*. 2016;17(6):677-86. doi: 10.1038/ni.3434. PMID: 27089382
22. Singh V, Jamwal S, Jain R, Verma P, Gokhale R, Rao KV. Mycobacterium tuberculosis-driven targeted recalibration of macrophage lipid homeostasis promotes the foamy phenotype. *Cell host & microbe*. 2012;12(5):669-81. doi: 10.1016/j.chom.2012.09.012. PMID: 23159056
23. Mattos KA, Oliveira VC, Berredo-Pinho M, Amaral JJ, Antunes LC, Melo RC, et al. Mycobacterium leprae intracellular survival relies on cholesterol accumulation in infected macrophages: a potential target for new drugs for leprosy treatment. *Cell Microbiol*. 2014. doi: 10.1111/cmi.12279 [doi].
24. Kim MJ, Wainwright HC, Lockett M, Bekker LG, Walther GB, Dittrich C, et al. Caseation of human tuberculosis granulomas correlates with elevated host lipid metabolism. *EMBO molecular medicine*. 2010;2(7):258-74. doi: 10.1002/emmm.201000079. PMID: 20597103
25. Palanisamy GS, Kirk NM, Ackart DF, Obregon-Henao A, Shanley CA, Orme IM, et al. Uptake and accumulation of oxidized low-density lipoprotein during Mycobacterium tuberculosis infection in guinea pigs. *PLoSOne*. 2012;7(3):e34148. doi: 10.1371/journal.pone.0034148 [doi];PONE-D-11-17086 [pii].

26. Yancey PG, Jerome WG. Lysosomal sequestration of free and esterified cholesterol from oxidized low density lipoprotein in macrophages of different species. *Journal of lipid research*. 1998;39(7):1349-61. PMID: 9684737
27. Brown AJ, Mander EL, Gelissen IC, Kritharides L, Dean RT, Jessup W. Cholesterol and oxysterol metabolism and subcellular distribution in macrophage foam cells. Accumulation of oxidized esters in lysosomes. *Journal of lipid research*. 2000;41(2):226-37. PMID: 10681406
28. Platt N, Speak AO, Colaco A, Gray J, Smith DA, Williams IM, et al. Immune dysfunction in Niemann-Pick disease type C. *Journal of neurochemistry*. 2016;136 Suppl 1:74-80. doi: 10.1111/jnc.13138. PMID: 25946402
29. Huynh KK, Gershenzon E, Grinstein S. Cholesterol accumulation by macrophages impairs phagosome maturation. *The Journal of biological chemistry*. 2008;283(51):35745-55. doi: 10.1074/jbc.M806232200. PMID: 18955491
30. Shen D, Wang X, Li X, Zhang X, Yao Z, Dibble S, et al. Lipid storage disorders block lysosomal trafficking by inhibiting a TRP channel and lysosomal calcium release. *Nature communications*. 2012;3:731. doi: 10.1038/ncomms1735. PMID: 22415822
31. Schwerd T, Pandey S, Yang HT, Bagola K, Jameson E, Jung J, et al. Impaired antibacterial autophagy links granulomatous intestinal inflammation in Niemann-Pick disease type C1 and XIAP deficiency with NOD2 variants in Crohn's disease. *Gut*. 2016. doi: 10.1136/gutjnl-2015-310382. PMID: 26953272
32. Sarkar S, Carroll B, Buganim Y, Maetzel D, Ng AH, Cassady JP, et al. Impaired autophagy in the lipid-storage disorder Niemann-Pick type C1 disease. *Cell reports*. 2013;5(5):1302-15. doi: 10.1016/j.celrep.2013.10.042. PMID: 24290752
33. Ouimet M, Franklin V, Mak E, Liao X, Tabas I, Marcel YL. Autophagy regulates cholesterol efflux from macrophage foam cells via lysosomal acid lipase. *Cell Metab*. 2011;13(6):655-67. doi: 10.1016/j.cmet.2011.03.023. PMID: 21641547
34. Chandra P, Kumar D. Selective autophagy gets more selective: Uncoupling of autophagy flux and xenophagy flux in *Mycobacterium tuberculosis*-infected macrophages. *Autophagy*. 2016;12(3):608-9. doi: 10.1080/15548627.2016.1139263. PMID: 27046255
35. Emanuel R, Sergin I, Bhattacharya S, Turner JN, Epelman S, Settembre C, et al. Induction of lysosomal biogenesis in atherosclerotic macrophages can rescue lipid-induced lysosomal dysfunction and downstream sequelae. *Arteriosclerosis, thrombosis, and vascular biology*. 2014;34(9):1942-52. doi: 10.1161/ATVBAHA.114.303342. PMID: 25060788
36. Li W, Yuan XM, Olsson AG, Brunk UT. Uptake of oxidized LDL by macrophages results in partial lysosomal enzyme inactivation and relocation. *Arteriosclerosis, thrombosis, and vascular biology*. 1998;18(2):177-84. PMID: 9484981
37. Li W, Dalen H, Eaton JW, Yuan XM. Apoptotic death of inflammatory cells in human atheroma. *Arteriosclerosis, thrombosis, and vascular biology*. 2001;21(7):1124-30. PMID: 11451740
38. Duewell P, Kono H, Rayner KJ, Sirois CM, Vladimer G, Bauernfeind FG, et al. NLRP3 inflammasomes are required for atherogenesis and activated by cholesterol crystals. *Nature*. 2010;464(7293):1357-61. doi: 10.1038/nature08938. PMID: 20428172

39. Fineran P, Lloyd-Evans E, Lack NA, Platt N, Davis LC, Morgan AJ, et al. Pathogenic mycobacteria achieve cellular persistence by inhibiting the Niemann-Pick Type C disease cellular pathway. *Wellcome open research*. 2016;1:18. doi: 10.12688/wellcomeopenres.10036.1. PMID: 28008422
40. Vrieling F, Ronacher K, Kleynhans L, van den Akker E, Walzl G, Ottenhoff THM, et al. Patients with Concurrent Tuberculosis and Diabetes Have a Pro-Atherogenic Plasma Lipid Profile. *EBioMedicine*. 2018. doi: 10.1016/j.ebiom.2018.05.011. PMID: 29779698
41. Holvoet P, Donck J, Landeloos M, Brouwers E, Luijckens K, Arnout J, et al. Correlation between oxidized low density lipoproteins and von Willebrand factor in chronic renal failure. *Thrombosis and haemostasis*. 1996;76(5):663-9. PMID: 8950769
42. Loughheed M, Moore ED, Scriven DR, Steinbrecher UP. Uptake of oxidized LDL by macrophages differs from that of acetyl LDL and leads to expansion of an acidic endolysosomal compartment. *Arteriosclerosis, thrombosis, and vascular biology*. 1999;19(8):1881-90. PMID: 10446066
43. Liscum L, Faust JR. The intracellular transport of low density lipoprotein-derived cholesterol is inhibited in Chinese hamster ovary cells cultured with 3-beta-[2-(diethylamino)ethoxy] androst-5-en-17-one. *The Journal of biological chemistry*. 1989;264(20):11796-806. PMID: 2745416
44. Zhang Y, Han Q, You S, Cao Y, Zhang X, Liu H, et al. Rapamycin Promotes the Autophagic Degradation of Oxidized Low-Density Lipoprotein in Human Umbilical Vein Endothelial Cells. *J Vasc Res*. 2015;52(3):210-9. doi: 10.1159/000441143. PMID: 26623657
45. Liu X, Tang Y, Cui Y, Zhang H, Zhang D. Autophagy is associated with cell fate in the process of macrophage-derived foam cells formation and progress. *J Biomed Sci*. 2016;23(1):57. doi: 10.1186/s12929-016-0274-z. PMID: 27473161
46. Lloyd-Evans E, Morgan AJ, He X, Smith DA, Elliot-Smith E, Sillence DJ, et al. Niemann-Pick disease type C1 is a sphingosine storage disease that causes deregulation of lysosomal calcium. *Nature medicine*. 2008;14(11):1247-55. doi: 10.1038/nm.1876. PMID: 18953351
47. Yao S, Miao C, Tian H, Sang H, Yang N, Jiao P, et al. Endoplasmic reticulum stress promotes macrophage-derived foam cell formation by up-regulating cluster of differentiation 36 (CD36) expression. *The Journal of biological chemistry*. 2014;289(7):4032-42. doi: 10.1074/jbc.M113.524512. PMID: 24366867
48. Myoishi M, Hao H, Minamino T, Watanabe K, Nishihira K, Hatakeyama K, et al. Increased endoplasmic reticulum stress in atherosclerotic plaques associated with acute coronary syndrome. *Circulation*. 2007;116(11):1226-33. doi: 10.1161/CIRCULATIONAHA.106.682054. PMID: 17709641
49. Seimon TA, Kim MJ, Blumenthal A, Koo J, Ehrt S, Wainwright H, et al. Induction of ER stress in macrophages of tuberculosis granulomas. *PloS one*. 2010;5(9):e12772. doi: 10.1371/journal.pone.0012772. PMID: 20856677
50. Jia J, Abudu YP, Claude-Taupin A, Gu Y, Kumar S, Choi SW, et al. Galectins Control mTOR in Response to Endomembrane Damage. *Mol Cell*. 2018;70(1):120-35 e8. doi: 10.1016/j.molcel.2018.03.009. PMID: 29625033

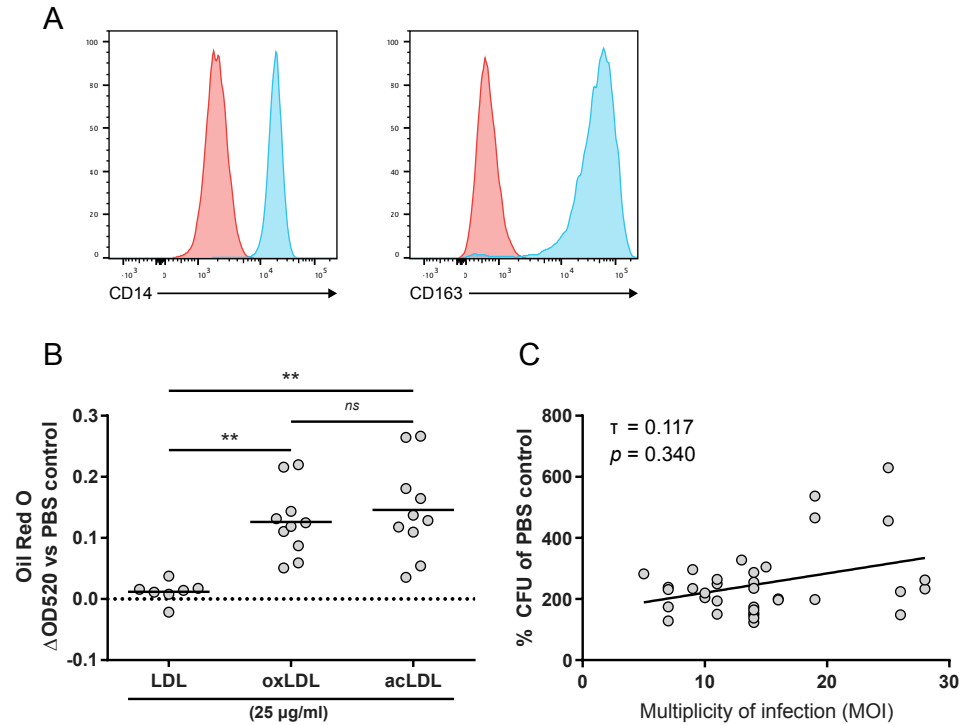
51. Thurston TL, Wandel MP, von Muhlinen N, Foeglein A, Randow F. Galectin 8 targets damaged vesicles for autophagy to defend cells against bacterial invasion. *Nature*. 2012;482(7385):414-8. doi: 10.1038/nature10744. PMID: 22246324
52. Weng IC, Chen HL, Lo TH, Lin WH, Chen HY, Hsu DK, et al. Cytosolic galectin-3 and -8 regulate antibacterial autophagy through differential recognition of host glycans on damaged phagosomes. *Glycobiology*. 2018;28(6):392-405. doi: 10.1093/glycob/cwy017. PMID: 29800364
53. Mittal E, Skowrya ML, Uwase G, Tinaztepe E, Mehra A, Koster S, et al. *Mycobacterium tuberculosis* Type VII Secretion System Effectors Differentially Impact the ESCRT Endomembrane Damage Response. *MBio*. 2018;9(6). doi: 10.1128/mBio.01765-18. PMID: 30482832
54. Aits S, Krickler J, Liu B, Ellegaard AM, Hamalisto S, Tvingsholm S, et al. Sensitive detection of lysosomal membrane permeabilization by lysosomal galectin puncta assay. *Autophagy*. 2015;11(8):1408-24. doi: 10.1080/15548627.2015.1063871. PMID: 26114578
55. Watson RO, Manzanillo PS, Cox JS. Extracellular *M. tuberculosis* DNA targets bacteria for autophagy by activating the host DNA-sensing pathway. *Cell*. 2012;150(4):803-15. doi: 10.1016/j.cell.2012.06.040. PMID: 22901810
56. Manzanillo PS, Ayres JS, Watson RO, Collins AC, Souza G, Rae CS, et al. The ubiquitin ligase parkin mediates resistance to intracellular pathogens. *Nature*. 2013;501(7468):512-6. doi: 10.1038/nature12566. PMID: 24005326
57. Mitchell G, Chen C, Portnoy DA. Strategies Used by Bacteria to Grow in Macrophages. *Microbiol Spectr*. 2016;4(3). doi: 10.1128/microbiolspec.MCHD-0012-2015. PMID: 27337444
58. Ceriello A, Taboga C, Tonutti L, Quagliaro L, Piconi L, Bais B, et al. Evidence for an independent and cumulative effect of postprandial hypertriglyceridemia and hyperglycemia on endothelial dysfunction and oxidative stress generation: effects of short- and long-term simvastatin treatment. *Circulation*. 2002;106(10):1211-8. PMID: 12208795
59. Giacco F, Brownlee M. Oxidative stress and diabetic complications. *Circulation research*. 2010;107(9):1058-70. doi: 10.1161/CIRCRESAHA.110.223545. PMID: 21030723
60. Griffin E, Re A, Hamel N, Fu C, Bush H, McCaffrey T, et al. A link between diabetes and atherosclerosis: Glucose regulates expression of CD36 at the level of translation. *Nature medicine*. 2001;7(7):840-6. doi: 10.1038/89969. PMID: 11433350
61. Sampson MJ, Davies IR, Braschi S, Ivory K, Hughes DA. Increased expression of a scavenger receptor (CD36) in monocytes from subjects with Type 2 diabetes. *Atherosclerosis*. 2003;167(1):129-34. PMID: 12618277
62. Lu H, Yao K, Huang D, Sun A, Zou Y, Qian J, et al. High glucose induces upregulation of scavenger receptors and promotes maturation of dendritic cells. *Cardiovascular diabetology*. 2013;12:80. doi: 10.1186/1475-2840-12-80. PMID: 23718574
63. Fukuhara-Takaki K, Sakai M, Sakamoto Y, Takeya M, Horiuchi S. Expression of class A scavenger receptor is enhanced by high glucose in vitro and under diabetic conditions in vivo: one mechanism for an increased rate of atherosclerosis in diabetes. *The Journal of biological chemistry*. 2005;280(5):3355-64. doi: 10.1074/jbc.M408715200. PMID: 15556945

64. Chen M, Nagase M, Fujita T, Narumiya S, Masaki T, Sawamura T. Diabetes enhances lectin-like oxidized LDL receptor-1 (LOX-1) expression in the vascular endothelium: possible role of LOX-1 ligand and AGE. *Biochem Biophys Res Commun*. 2001;287(4):962-8. doi: 10.1006/bbrc.2001.5674. PMID: 11573959
65. Balderas FL, Quezada-Larios M, Garcia Latorre EA, Mendez JD. Increased uptake of oxidized LDL by macrophages from type 2 diabetics is inhibited by polyamines. *Biomedicine & pharmacotherapy = Biomedecine & pharmacotherapie*. 2016;77:59-64. doi: 10.1016/j.biopha.2015.11.006. PMID: 26796266
66. Palanisamy GS, Kirk NM, Ackart DF, Shanley CA, Orme IM, Basaraba RJ. Evidence for oxidative stress and defective antioxidant response in guinea pigs with tuberculosis. *PLoS one*. 2011;6(10):e26254. doi: 10.1371/journal.pone.0026254. PMID: 22028843
67. Torun E, Gedik AH, Cakir E, Umutoglu T, Gok O, Kilic U. Serum paraoxonase 1 activity and oxidative stress in pediatric patients with pulmonary tuberculosis. *Medical principles and practice : international journal of the Kuwait University, Health Science Centre*. 2014;23(5):426-31. doi: 10.1159/000363700. PMID: 25034194
68. Jack CI, Jackson MJ, Hind CR. Circulating markers of free radical activity in patients with pulmonary tuberculosis. *Tubercle and lung disease : the official journal of the International Union against Tuberculosis and Lung Disease*. 1994;75(2):132-7. doi: 10.1016/0962-8479(94)90042-6. PMID: 8032046
69. Venketaraman V, Millman A, Salman M, Swaminathan S, Goetz M, Lardizabal A, et al. Glutathione levels and immune responses in tuberculosis patients. *Microbial pathogenesis*. 2008;44(3):255-61. doi: 10.1016/j.micpath.2007.09.002. PMID: 17959342
70. Knight M, Braverman J, Asfaha K, Gronert K, Stanley S. Lipid droplet formation in *Mycobacterium tuberculosis* infected macrophages requires IFN-gamma/HIF-1alpha signaling and supports host defense. *PLoS pathogens*. 2018;14(1):e1006874. doi: 10.1371/journal.ppat.1006874. PMID: 29370315
71. Seimon TA, Nadolski MJ, Liao X, Magallon J, Nguyen M, Feric NT, et al. Atherogenic lipids and lipoproteins trigger CD36-TLR2-dependent apoptosis in macrophages undergoing endoplasmic reticulum stress. *Cell Metab*. 2010;12(5):467-82. doi: 10.1016/j.cmet.2010.09.010. PMID: 21035758
72. Yimin, Furumaki H, Matsuoka S, Sakurai T, Kohanawa M, Zhao S, et al. A novel murine model for non-alcoholic steatohepatitis developed by combination of a high-fat diet and oxidized low-density lipoprotein. *Lab Invest*. 2012;92(2):265-81. doi: 10.1038/labinvest.2011.159. PMID: 22064320
73. Bieghs V, van Gorp PJ, Walenbergh SM, Gijbels MJ, Verheyen F, Buurman WA, et al. Specific immunization strategies against oxidized low-density lipoprotein: a novel way to reduce nonalcoholic steatohepatitis in mice. *Hepatology*. 2012;56(3):894-903. doi: 10.1002/hep.25660. PMID: 22334337
74. Bieghs V, Walenbergh SM, Hendriks T, van Gorp PJ, Verheyen F, Olde Damink SW, et al. Trapping of oxidized LDL in lysosomes of Kupffer cells is a trigger for hepatic inflammation.

- Liver international : official journal of the International Association for the Study of the Liver. 2013;33(7):1056-61. doi: 10.1111/liv.12170. PMID: 23617943
75. Sheedy FJ, Grebe A, Rayner KJ, Kalantari P, Ramkhelawon B, Carpenter SB, et al. CD36 coordinates NLRP3 inflammasome activation by facilitating intracellular nucleation of soluble ligands into particulate ligands in sterile inflammation. *Nature immunology*. 2013;14(8):812-20. doi: 10.1038/ni.2639. PMID: 23812099
 76. Ohlsson BG, Englund MC, Karlsson AL, Knutsen E, Erixon C, Skribeck H, et al. Oxidized low density lipoprotein inhibits lipopolysaccharide-induced binding of nuclear factor-kappaB to DNA and the subsequent expression of tumor necrosis factor-alpha and interleukin-1beta in macrophages. *The Journal of clinical investigation*. 1996;98(1):78-89. doi: 10.1172/JCI118780. PMID: 8690807
 77. Chung SW, Kang BY, Kim SH, Pak YK, Cho D, Trinchieri G, et al. Oxidized low density lipoprotein inhibits interleukin-12 production in lipopolysaccharide-activated mouse macrophages via direct interactions between peroxisome proliferator-activated receptor-gamma and nuclear factor-kappa B. *The Journal of biological chemistry*. 2000;275(42):32681-7. doi: 10.1074/jbc.M002577200. PMID: 10934192
 78. Jongstra-Bilen J, Zhang CX, Wisnicki T, Li MK, White-Alfred S, Ilaalagan R, et al. Oxidized Low-Density Lipoprotein Loading of Macrophages Downregulates TLR-Induced Proinflammatory Responses in a Gene-Specific and Temporal Manner through Transcriptional Control. *Journal of immunology*. 2017;199(6):2149-57. doi: 10.4049/jimmunol.1601363. PMID: 28784845
 79. Bekkering S, Quintin J, Joosten LA, van der Meer JW, Netea MG, Riksen NP. Oxidized low-density lipoprotein induces long-term proinflammatory cytokine production and foam cell formation via epigenetic reprogramming of monocytes. *Arteriosclerosis, thrombosis, and vascular biology*. 2014;34(8):1731-8. doi: 10.1161/ATVBAHA.114.303887. PMID: 24903093
 80. Christ A, Gunther P, Lauterbach MAR, Duewell P, Biswas D, Pelka K, et al. Western Diet Triggers NLRP3-Dependent Innate Immune Reprogramming. *Cell*. 2018;172(1-2):162-75 e14. doi: 10.1016/j.cell.2017.12.013. PMID: 29328911
 81. Soh AZ, Chee CB, Wang YT, Yuan JM, Koh WP. Dietary Cholesterol Increases the Risk whereas PUFAs Reduce the Risk of Active Tuberculosis in Singapore Chinese. *J Nutr*. 2016;146(5):1093-100. doi: 10.3945/jn.115.228049. PMID: 27075903
 82. Martens GW, Arikian MC, Lee J, Ren F, Vallerkog T, Kornfeld H. Hypercholesterolemia impairs immunity to tuberculosis. *Infection and immunity*. 2008;76(8):3464-72. doi: 10.1128/IAI.00037-08. PMID: 18505807
 83. Martens GW, Vallerkog T, Kornfeld H. Hypercholesterolemic LDL receptor-deficient mice mount a neutrophilic response to tuberculosis despite the timely expression of protective immunity. *J Leukoc Biol*. 2012;91(6):849-57. doi: 10.1189/jlb.0311164. PMID: 22227965
 84. Pandey AK, Sasseti CM. *Mycobacterial persistence requires the utilization of host cholesterol*. *Proceedings of the National Academy of Sciences of the United States of America*. 2008;105(11):4376-80. doi: 10.1073/pnas.0711159105. PMID: 18334639

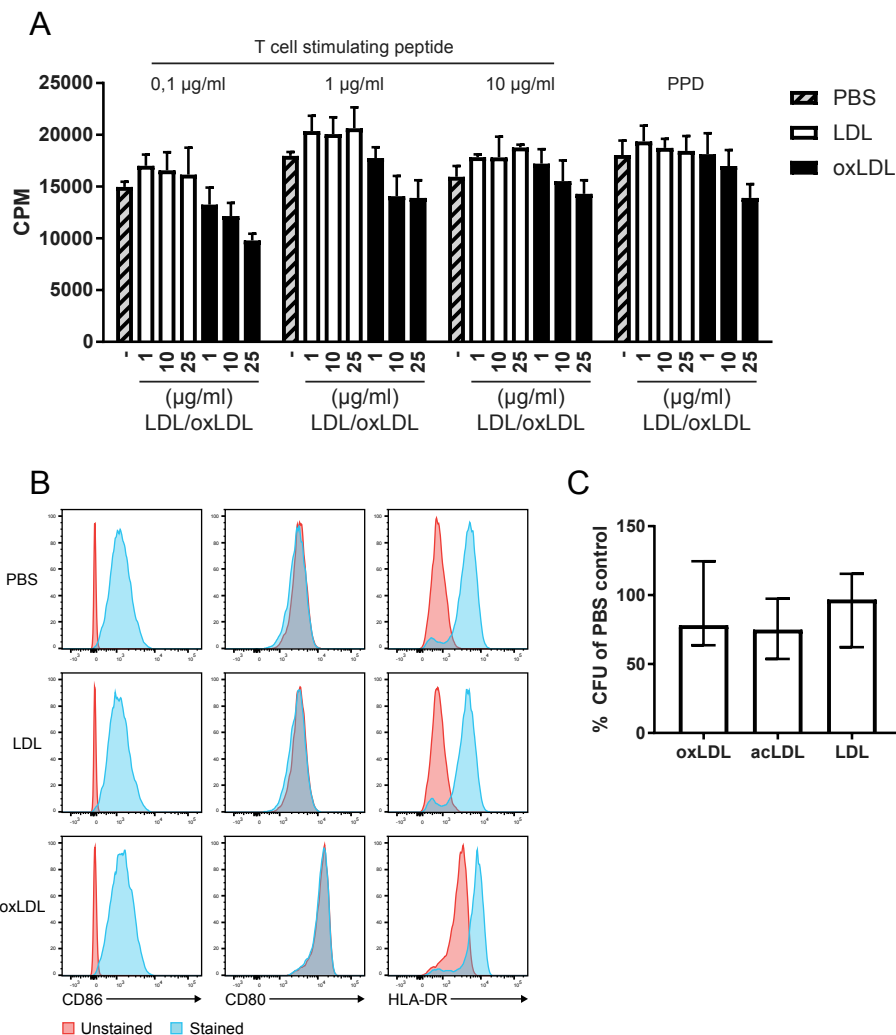
85. Brzostek A, Pawelczyk J, Rumijowska-Galewicz A, Dziadek B, Dziadek J. Mycobacterium tuberculosis is able to accumulate and utilize cholesterol. *J Bacteriol.* 2009;191(21):6584-91. doi: 10.1128/JB.00488-09. PMID: 19717592
86. Genoula M, Marin Franco JL, Dupont M, Kviatcovsky D, Milillo A, Schierloh P, et al. Formation of Foamy Macrophages by Tuberculous Pleural Effusions Is Triggered by the Interleukin-10/Signal Transducer and Activator of Transcription 3 Axis through ACAT Upregulation. *Frontiers in immunology.* 2018;9:459. doi: 10.3389/fimmu.2018.00459. PMID: 29593722
87. de Chastellier C, Thilo L. Cholesterol depletion in Mycobacterium avium-infected macrophages overcomes the block in phagosome maturation and leads to the reversible sequestration of viable mycobacteria in phagolysosome-derived autophagic vacuoles. *Cellular microbiology.* 2006;8(2):242-56. doi: 10.1111/j.1462-5822.2005.00617.x. PMID: 16441435
88. Parihar SP, Guler R, Khutlang R, Lang DM, Hurdalay R, Mhlanga MM, et al. Statin therapy reduces the mycobacterium tuberculosis burden in human macrophages and in mice by enhancing autophagy and phagosome maturation. *J Infect Dis.* 2014;209(5):754-63. doi: 10.1093/infdis/jit550. PMID: 24133190
89. Lai CC, Lee MT, Lee SH, Hsu WT, Chang SS, Chen SC, et al. Statin treatment is associated with a decreased risk of active tuberculosis: an analysis of a nationally representative cohort. *Thorax.* 2016;71(7):646-51. doi: 10.1136/thoraxjnl-2015-207052. PMID: 26941271
90. Dutta NK, Bruiners N, Pinn ML, Zimmerman MD, Prideaux B, Dartois V, et al. Statin adjunctive therapy shortens the duration of TB treatment in mice. *J Antimicrob Chemother.* 2016;71(6):1570-7. doi: 10.1093/jac/dkw014. PMID: 26903278
91. Su VY, Su WJ, Yen YF, Pan SW, Chuang PH, Feng JY, et al. Statin Use Is Associated With a Lower Risk of TB. *Chest.* 2017;152(3):598-606. doi: 10.1016/j.chest.2017.04.170. PMID: 28479115
92. Lobato LS, Rosa PS, Ferreira Jda S, Neumann Ada S, da Silva MG, do Nascimento DC, et al. Statins increase rifampin mycobactericidal effect. *Antimicrob Agents Chemother.* 2014;58(10):5766-74. doi: 10.1128/AAC.01826-13. PMID: 25049257
93. Rocha N, Kuijl C, van der Kant R, Janssen L, Houben D, Janssen H, et al. Cholesterol sensor ORP1L contacts the ER protein VAP to control Rab7-RILP-p150 Glued and late endosome positioning. *J Cell Biol.* 2009;185(7):1209-25. doi: 10.1083/jcb.200811005. PMID: 19564404
94. van der Kant R, Fish A, Janssen L, Janssen H, Krom S, Ho N, et al. Late endosomal transport and tethering are coupled processes controlled by RILP and the cholesterol sensor ORP1L. *Journal of cell science.* 2013;126(Pt 15):3462-74. doi: 10.1242/jcs.129270. PMID: 23729732
95. Holvoet P, Vanhaecke J, Janssens S, Van de Werf F, Collen D. Oxidized LDL and malondialdehyde-modified LDL in patients with acute coronary syndromes and stable coronary artery disease. *Circulation.* 1998;98(15):1487-94. PMID: 9769301
96. Brinkley TE, Nicklas BJ, Kanaya AM, Satterfield S, Lakatta EG, Simonsick EM, et al. Plasma oxidized low-density lipoprotein levels and arterial stiffness in older adults: the health, aging, and body composition study. *Hypertension.* 2009;53(5):846-52. doi: 10.1161/HYPERTENSIONAHA.108.127043. PMID: 19332658

97. Hamed S, Brenner B, Abassi Z, Aharon A, Daoud D, Roguin A. Hyperglycemia and oxidized-LDL exert a deleterious effect on endothelial progenitor cell migration in type 2 diabetes mellitus. *Thrombosis research*. 2010;126(3):166-74. doi: 10.1016/j.thromres.2010.03.002. PMID: 20347119
98. Lachmandas E, Vrieling F, Wilson LG, Joosten SA, Netea MG, Ottenhoff TH, et al. The effect of hyperglycaemia on in vitro cytokine production and macrophage infection with *Mycobacterium tuberculosis*. *PLoSOne*. 2015;10(2):e0117941. doi: 10.1371/journal.pone.0117941 [doi];PONE-D-14-29657 [pii].
99. van Crevel R, Dockrell HM. TANDEM: understanding diabetes and tuberculosis. *Lancet Diabetes Endocrinol*. 2014;2(4):270-2. doi: S2213-8587(14)70011-7 [pii];10.1016/S2213-8587(14)70011-7 [doi].
100. Redgrave TG, Roberts DC, West CE. Separation of plasma lipoproteins by density-gradient ultracentrifugation. *Anal Biochem*. 1975;65(1-2):42-9. PMID: 165752
101. Fraenkel-Conrat H. [11] Methods for investigating the essential groups for enzyme activity. *Methods in Enzymology*. Volume 4: Academic Press; 1957. p. 247-69.
102. Verreck FA, de BT, Langenberg DM, Hoeve MA, Kramer M, Vaisberg E, et al. Human IL-23-producing type 1 macrophages promote but IL-10-producing type 2 macrophages subvert immunity to (myco)bacteria. *ProcNatlAcadSciUSA*. 2004;101(13):4560-5. doi: 10.1073/pnas.0400983101 [doi];0400983101 [pii].
103. Leclerc L, Boudard D, Pourchez J, Forest V, Sabido O, Bin V, et al. Quantification of micro-sized fluorescent particles phagocytosis to a better knowledge of toxicity mechanisms. *InhalToxicol*. 2010;22(13):1091-100. doi: 10.3109/08958378.2010.522781 [doi].
104. Haanen JB, de Waal Malefijt R, Res PC, Kraakman EM, Ottenhoff TH, de Vries RR, et al. Selection of a human T helper type 1-like T cell subset by mycobacteria. *The Journal of experimental medicine*. 1991;174(3):583-92. PMID: 1831489
105. Ottenhoff TH, Haanen JB, Geluk A, Mutis T, Ab BK, Thole JE, et al. Regulation of mycobacterial heat-shock protein-reactive T cells by HLA class II molecules: lessons from leprosy. *Immunol Rev*. 1991;121:171-91. PMID: 1937531
106. Carpenter AE, Jones TR, Lamprecht MR, Clarke C, Kang IH, Friman O, et al. CellProfiler: image analysis software for identifying and quantifying cell phenotypes. *Genome Biol*. 2006;7(10):R100. doi: 10.1186/gb-2006-7-10-r100. PMID: 17076895



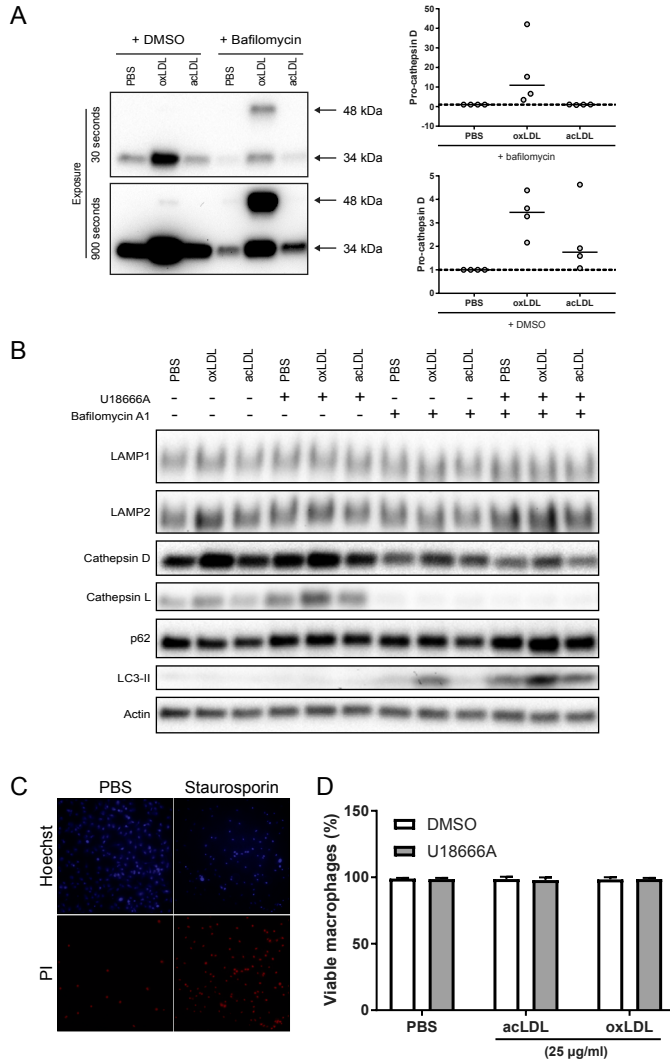
Supplementary Figure 1: Macrophage phenotype and Oil Red O staining.

Monocyte-derived macrophages were differentiated using M-CSF (50 ng/ml) for 6 days. (A) Histograms of the cell surface expression of CD14 and CD163 as determined by flow cytometry. Stained (blue) and unstained (blue) samples are displayed. Data shown are from one representative donor. (B) Macrophages were treated overnight with PBS control, LDL, acLDL or oxLDL at 25 μ g/ml and stained for neutral lipids with Oil Red O. Staining was dissolved and quantified by measuring OD at 520 nm. Data are displayed as Δ OD520 versus PBS control. Individual donors are depicted as dots with group medians. Statistical significance was determined by Kruskal-Wallis test with post-hoc Dunn's test. ** = $p < 0.01$. (C) Macrophages were treated with 25 μ g/ml oxLDL or PBS control overnight and infected with *Mtb* H37Rv for 24 h. OxLDL-induced increased *Mtb* loads were normalized to PBS control and plotted versus the infectious load (MOI) as determined by CFU assay ($n=34$; each dot represents one individual donor). Kendall tau correlation and associated two-sided p -value are displayed.



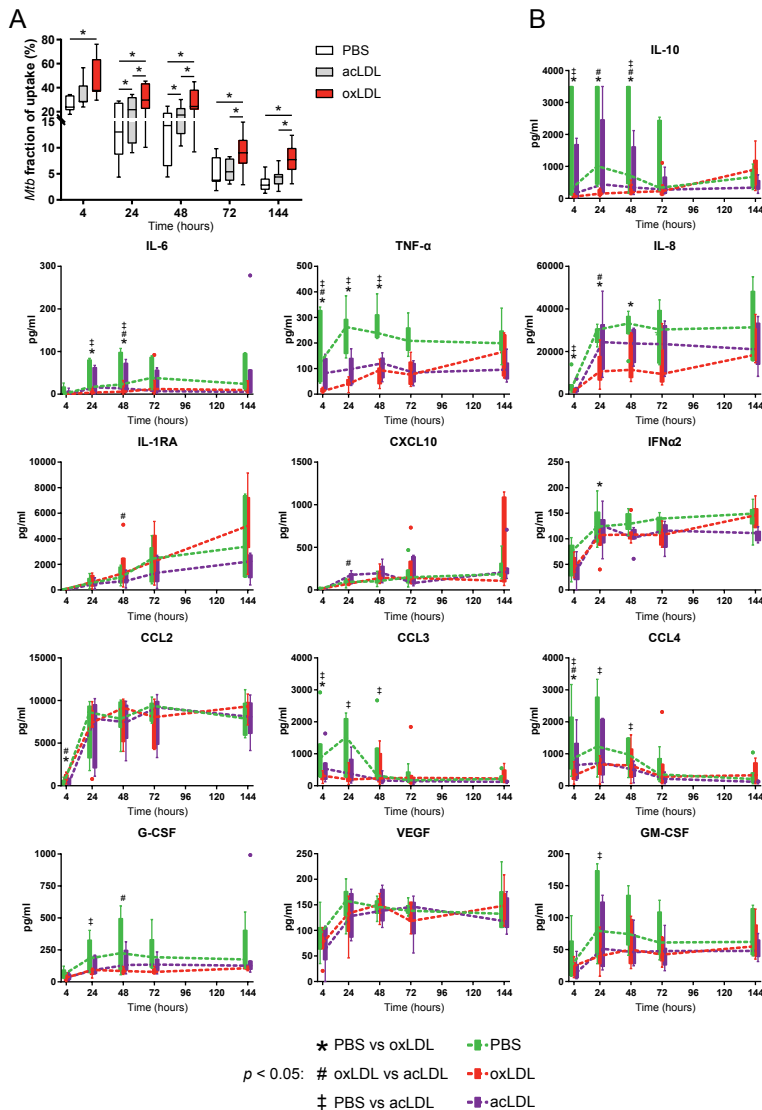
Supplementary Figure 2: oxLDL treatment diminished macrophage antigen presentation to a second CD4+ T cell clone and this was independent of cell surface expression of CD86, CD80 and HLA-DR.

Primary human macrophages were treated with PBS control, native LDL or oxLDL (1, 10 or 25 $\mu\text{g/ml}$) overnight. (A) Macrophages were co-cultured for four days with the HLA-DR3-restricted CD4+ T cell Rp15 1-1 at a ratio of 1:4 and 0.1, 1 or 10 $\mu\text{g/ml}$ of its cognate peptide or 1.25 $\mu\text{g/ml}$ PPD. T cell proliferation was measured by tritium-thymidine incorporation during the last 24 h ($n = 3$). Data is represented as means with standard deviations. (B) Cell surface expression of CD86, CD80 and HLA-DR as determined by flow cytometry of macrophages treated overnight with PBS, native LDL or oxLDL (25 $\mu\text{g/ml}$). Stained (blue) and unstained (blue) samples are displayed. Data shown are from one representative donor ($n = 3$). (C) Primary human macrophages were treated overnight with PBS control ($n = 15$), acLDL ($n = 9$), oxLDL ($n = 15$) or native LDL ($n = 6$) (25 $\mu\text{g/ml}$) and subsequently infected with *Mtb* H37Rv at a MOI of 10:1. Cells were lysed directly after 1 h of infection and bacterial load was determined by CFU assay to determine *Mtb* uptake. Results were normalized versus PBS control and depicted as group medians with 95% confidence intervals.



Supplementary Figure 3: U18666A and oxLDL increased protein markers of lysosomes and autophagy in *Mtb*-infected macrophages without affecting cell viability.

Primary human macrophages were treated with PBS control, acLDL or oxLDL (25 µg/ml) for 24 h prior to infection with *Mtb* H37Rv at a MOI of 10:1. (A) Representative Western Blot result of Cathepsin D protein levels from macrophages treated with bafilomycin A1 (10 nM) or DMSO, showing protein bands of both the mature heavy chain (34 kDa) and the processing intermediate pro-cathepsin D (48 kDa) after 30 and 900 seconds of exposure time. Pro-cathepsin D levels were first normalized to actin and subsequently versus PBS control (n = 4). (B) Western blot analysis of lysosomal and autophagy markers in macrophages co-treated with PBS, oxLDL or acLDL (25 µg/ml) and U18666A (3 µg/ml), bafilomycin A1 (10 nM) or DMSO control during 24 h of H37Rv *Mtb* infection. Data shown is from one representative donor (n = 2). (C) *Mtb*-infected macrophages were stained with Hoechst and PI to determine cell viability. Staurosporin (5 µM) and PBS were used as positive and negative control for cell death. (D) Percentages of viable cells (Hoechst+/PI-). Data are displayed as means with standard deviations (n = 4).



Supplementary Figure 4: Kinetic analysis of intracellular *Mtb* survival and associated cytokine responses in human macrophages.

Primary human macrophages were treated with PBS control, acLDL or oxLDL (25 μ g/ml) overnight and subsequently infected with *Mtb* H37Rv at a MOI of 10:1. Cells were lysed at 0 (uptake), 4, 24, 48, 72 and 144 h post-infection for CFU analysis (n = 7). (A) Intracellular *Mtb* loads are depicted as fraction of uptake in Tukey's boxplots for each time point and condition: PBS (white), acLDL (grey) and oxLDL (red). (B) Supernatants were harvested at each time point post-infection and cytokine concentrations were determined by multiplex assay. Levels of IL-10, IL-6, TNF- α , IL-8, IL-1RA, CXCL10, IFN α 2, CCL2, CCL3, CCL4, G-CSF, VEGF and GM-CSF (pg/ml) are depicted in Tukey's boxplots for each time point and condition: PBS (green), acLDL (purple) and oxLDL (red). Group medians are shown as dashed lines. Statistical significance was determined by Wilcoxon signed rank test with post-hoc FDR correction. $p < 0.05$ for * = PBS vs oxLDL, # = oxLDL vs acLDL, ‡ = PBS vs acLDL.

Supplementary Table 1: Patient clinical characteristics according to disease group (n = 79).

Data is presented as percentage of total (%) or mean \pm SD, *Point-of-care measurements, †lab measurements, 1 data available from 12/19 patients, 2 data available from 12/20 patients, 3 data available from 16/19 patients

	HC n=20	DM n=20	TB n=20	TB-DM n=19	p-value
Ethnicity: Coloured	20/20 (100%)	20/20 (100%)	19/20 (95%)	19/19 (100%)	0.394
Sex (male/female)	10/10	7/13	11/9	11/8	0.482
Age (years)	37.3 \pm 9.7	49.8 \pm 12.4	45.7 \pm 8.5	44.8 \pm 10.3	0.003
BMI (kg/m ²)	23.6 \pm 7.0	31.2 \pm 6.7	19.4 \pm 3.0	20.7 \pm 4.4	< 0.001
HbA1c (%)	5.2 \pm 0.3*	10.0 \pm 2.3*	5.6 \pm 0.3†	8.8 \pm 2.6†	< 0.001
Random blood glucose (mmol/l)	4.8 \pm 1.0	14.3 \pm 5.2	5.8 \pm 1.3	8.6 \pm 4.91	< 0.001
Previous TB (>1 year ago)	na	3/20 (15%)	11/20 (55%)	5/19 (26.3%)	0.021
Smoking (currently)	na	5/20 (25%)	17/20 (85%)	14/19 (73.7%)	< 0.001
Quantiferon positive	13/19 (68.4%)	15/19 (78.9%)	na	na	0.461
Time to positivity (days)	na	na	8.3 \pm 5.62	7.8 \pm 4.83	0.794
DM medication	na	20/20 (100%)	na	7/19 (36.8%)	0.001
Insulin		12/20 (60%)		2/19 (10.5%)	0.003
Metformin		16/20 (80%)		6/19 (31.6%)	0.002
Statins		6/20 (30%)		1/19 (5.3%)	0.044
Other		4/20 (20%)		2/19 (10.5%)	0.412
Years since DM diagnosis	na		na		
<1		0/20 (0%)		14/19 (73.7%)	< 0.001
1-5		6/20 (30%)		1/19 (5.3%)	0.044
6-15		8/20 (40%)		3/19 (20.8%)	0.093
>15		6/20 (30%)		1/19 (5.3%)	0.044

CHAPTER

5

Patients with Concurrent Tuberculosis and Diabetes Have a Pro-Atherogenic Plasma Lipid Profile

Frank Vrieling¹, Katharina Ronacher^{2,3}, Léanie Kleynhans², Erik van den Akker^{4,5}, Gerhard Walzl², Tom H. M. Ottenhoff¹ and Simone A. Joosten¹

¹ Department of Infectious Diseases, Leiden University Medical Center, Leiden, The Netherlands

² DST/NRF Centre of Excellence for Biomedical Tuberculosis Research, SA MRC Center for TB Research, Division of Molecular Biology and Human Genetics, Department of Biomedical Sciences, Faculty of Medicine and Health Sciences Stellenbosch University, Cape Town, South Africa

³ Mater Research Institute, The University of Queensland, Translational Research Institute, Brisbane, Australia

⁴ Department of Biomedical Data Sciences, Leiden University Medical Center, Leiden, The Netherlands

⁵ Pattern Recognition & Bioinformatics, Delft University of Technology, Delft, The Netherlands

BACKGROUND: Type 2 diabetes mellitus (DM) is a major risk factor for development of tuberculosis (TB), however the underlying molecular foundations are unclear. Since lipids play a central role in the development of both DM and TB, lipid metabolism may be important for TB-DM pathophysiology.

METHODS: A $^1\text{H-NMR}$ spectroscopy-based platform was used to determine 225 lipid and other metabolic intermediates in plasma samples of healthy controls (n=50) and patients with TB (n=50), DM (n=50) or TB-DM (n=27).

RESULTS: TB patients presented with wasting disease, represented by decreased amino acid levels including histidine and alanine. Conversely, DM patients were dyslipidemic as evidenced by high levels of very low-density lipoprotein triglycerides and low high-density lipoprotein cholesterol. TB-DM patients displayed metabolic characteristics of both wasting and dyslipidemia combined with disease interaction-specific increases in phospholipid metabolites (e.g. sphingomyelins) and atherogenic remnant-like lipoprotein particles. Biomarker analysis identified the ratios of phenylalanine/histidine and esterified cholesterol/sphingomyelin as markers for TB classification regardless of DM-status.

CONCLUSIONS: TB-DM patients possess a distinctive plasma lipid profile with pro-atherogenic properties. These findings support further research on the benefits of improved blood lipid control in the treatment of TB-DM.

Introduction

Type 2 diabetes mellitus (DM) is a major risk factor for tuberculosis (TB) and triples the risk of developing active TB disease ⁽¹⁾. At present approximately 15% of global TB cases can be attributed to DM comorbidity ⁽²⁾. Clinically, DM increases TB severity and impairs TB treatment ⁽³⁾, while conversely TB hampers glycemic control ⁽⁴⁾. DM impacts both susceptibility to infection and progression towards active disease ^(1, 5), however the immunological processes involved are unclear ⁽⁶⁾. The number of DM patients in TB-endemic regions of Africa and Asia is predicted to rise significantly during the coming decades ⁽⁷⁾, and TB-DM comorbidity is estimated to seriously affect TB and consequently general global health. Therefore the TANDEM project seeks to optimize treatment and diagnosis of comorbid TB-DM and to understand its causal mechanisms ⁽⁸⁾.

While DM is primarily characterized by hyperglycemia and insulin resistance, it is often also associated with severe dyslipidemia as a result of high dietary fat intake and deregulated hepatic lipid metabolism ⁽⁹⁾. DM-associated high insulin levels stimulate *de novo* lipogenesis in hepatocytes while failing to suppress lipolysis in insulin-resistant adipocytes of DM patients, leading to increased free fatty acid flux to the liver and overproduction of large triglyceride-rich very low-density lipoprotein (VLDL) particles ⁽¹⁰⁾. Diabetic dyslipidemia is defined as having high levels of plasma triglycerides and/or cholesterol in combination with low levels of high-density lipoprotein (HDL) cholesterol and is a major risk factor for cardiovascular disease and atherosclerosis, which often complicate DM.

In contrast to DM, TB is often associated with malnutrition and wasting syndrome ⁽¹¹⁾, and a low bodyweight is a risk factor for TB disease ^(12, 13). Additionally, TB leads to decreased body fat mass and levels of the adipocyte hormone leptin ⁽¹⁴⁾. Interestingly, the causative agent of TB, *Mycobacterium tuberculosis* (*Mtb*), has been shown to rely heavily on host-derived lipids for its survival ⁽¹⁵⁻¹⁷⁾. *Mtb* induces the formation of lipid-loaded foamy macrophages, similar to the ones found in atherosclerotic lesions, and exploits these cells as its primary niche for replication. Several studies have identified high cholesterol levels as risk factor for TB ⁽¹⁸⁻²⁰⁾, and reducing cholesterol levels using statins was beneficial in *Mtb*-infected macrophages, mice and patients through enhancing the bactericidal effect of first-line antibiotics and phagosome maturation ⁽²¹⁻²⁵⁾.

To identify potential differences in lipid metabolism, we compared plasma lipid profiles of patients with TB-DM to those of patients with TB or DM. To this end we determined plasma metabolic profiles ⁽²⁶⁾ in healthy controls (HC) and patients with TB, DM or TB-DM. We hypothesized that the combination of these two diseases on seemingly opposite sides of the metabolic spectrum would result in distinctive plasma lipid profiles, as well as novel biomarkers.

Materials & methods

Ethics statement/Patient inclusion

This study was undertaken as part of a EU-funded collaborative project (TANDEM)⁽⁸⁾. Patients (18-70 years) were enrolled in Cape Town, South-Africa from six public health care clinics around Tygerberg Academic Hospital (Elsies River, Ravensmead, Uitsig, Adriaanse, Durbanville, Fisantekraal). In total, 177 participants were included: 50 healthy community controls, 50 DM patients, 50 TB patients and 27 TB-DM patients. DM patients without TB were recruited from community health centers/day hospitals in Elsies River and Durbanville and previously diagnosed with DM according to WHO-criteria⁽²⁷⁾. TB patients were screened for DM and classification was based on hyperglycaemia (random plasma glucose ≥ 200 mg/dl), HbA1c $\geq 6.5\%$ and/or self-reported DM, in which case previous determination of random plasma glucose levels was not repeated. From the patients included in this study there is clinical evidence suggesting that one participant has type 1 diabetes, whereas all other patients suffered from type 2 diabetes. TB patients were identified based on positive Xpert *Mtb*/RIF assay (Cepheid Inc, Sunnyvale, CA, USA), MGIT culture and *Mtb* confirmation. Participants were excluded if they were HIV-positive, pregnant, on steroid therapy (in the last 6 months), had a hemoglobin < 10 g/L, presented with emphysema, chronic bronchitis, asthma, steroid-induced DM, cancer or known alcohol abuse. The study was approved by the Health Research Ethics Committee of the University of Stellenbosch, and conducted according to the Helsinki Declaration and International Conference of Harmonization guidelines. Written informed consent was obtained from all participants.

Metabolic profile quantification by ¹H-Nuclear Magnetic Resonance (NMR) spectroscopy

A high-throughput ¹H-NMR spectroscopy platform was used to determine plasma metabolic profiles consisting of 225 parameters (Nightingale Health, Helsinki, Finland), including detailed concentrations and compositions of 14 lipoprotein subclasses, fatty acids & glycerides, amino acids and glycolytic molecules⁽²⁸⁾. Methods regarding sample preparation and measurement procedures were described previously⁽²⁶⁾.

Statistical analysis

For multivariate analysis, metabolite ratios were excluded. Metabolites were log-transformed to correct for skewed distributions, with the exception of lipoprotein particle concentrations for regression analysis due to a substantial amount of zero measurements. Partial least squares discriminant analysis (PLS-DA) modelling and hierarchical clustering was used to visualize metabolic differences between the groups. Only samples and measurements with $\leq 10\%$ missing or zero values were considered for PLS-DA modelling. The optimal number of components was determined based on estimated classification error rates calculated by fivefold cross validation, which was repeated ten times. To

illustrate the differences between our individual groups (HC, TB, DM and TB-DM patients), separate linear regression models were fitted for each pairwise combination of groups while adjusting for age and sex. 98 measures of specific particle concentrations and compositions of 14 lipoprotein subclasses were analysed distinctly from the remaining parameters (44 metabolite subset, Supplementary Table 1). Next, interaction-specific effects of TB-DM comorbidity were investigated by fitting the following linear model:

$$\text{Metabolite: } \beta_0 + \beta_1\text{TB} + \beta_2\text{DM} + \beta_3\text{TB*DM} + \beta_4\text{Age} + \beta_5\text{Sex} + \epsilon$$

where TB = TB-status (true/false), DM = DM-status (true/false), TB*DM = disease interaction effect, Age = age (years) and Sex = sex (male/female).

Univariate biomarker analysis was performed to identify metabolic measures with potential for TB diagnosis. Analysis was stratified by DM-status (HC vs. TB, DM vs. TB-DM). Log-transformed data of the 44 metabolite subset was mean-centred, scaled to standard deviation (SD) units and top 20 metabolite ratios based on *p*-values were calculated and added to the analysis. For each biomarker receiver operating characteristic (ROC) curves were plotted and area under the curve (AUC) values with 95% confidence interval (CI) determined. Biomarker analysis was performed using the online tool MetaboAnalyst 3.5 and methodological details were published previously ⁽²⁹⁾.

Statistical analysis of clinical characteristics was performed in SPSS 23 (IBM) by one-way ANOVA (reported *p*-values are the outcome of the *F*-test), independent samples t-test or chi-squared test. Univariate analysis of absolute metabolite concentrations was done in Graphpad Prism 7 by Kruskal-Wallis test with post-hoc Dunn's test. PLS-DA and multiple linear regression analysis were performed using R version 3.3.2. including the following packages: mixOmics ⁽³⁰⁾ version 6.3.0, limma ⁽³¹⁾ version 3.30.13 and phenotypicForest ⁽³²⁾ version 0.3.

Table 1: Patient clinical characteristics according to disease group (n = 177).

	HC n=50	DM n=50	TB n=50	TB-DM n=50	p-value
Ethnicity: Colored	48/50 (96%)	50/50 (100%)	47/50 (94%)	26/27 (96.3%)	0.414
Sex (male/female)	25/25	23/27	33/17	13/14	0.186
Age (years)	37.7 ± 9.2	51.6 ± 11.2	46.3 ± 9.3	44.4 ± 9.5	< 0.001
BMI (kg/m ²)	24.2 ± 6.4	29.1 ± 5.8	19.1 ± 2.6	22.2 ± 5.2	< 0.001
HbA1c (%)	5.3 ± 0.4*	10.1 ± 2.6**	5.5 ± 0.4 [†]	9.5 ± 2.5 [†]	< 0.001
Random blood glucose (mmol/l)	5.1 ± 1.2	13.3 ± 5.1	6.1 ± 1.6	8.6 ± 4.9 [§]	< 0.001
Previous TB (>1 year ago)	na	13/50 (26%)	26/50 (52%)	7/27 (25.9%)	0.012
Smoking (currently)	na	20/50 (40%)	47/50 (94%)	18/27 (66.7%)	< 0.001
Quantiferon positive	35/46 (76%)	41/48 (85%)	na	na	0.250
Time to positivity (days)	na	na	7.3 ± 4.5	7.1 ± 4.4 ^{**}	0.612
DM medication	na	50/50 (100%)	na	15/27 (55.6%)	< 0.001
Insulin		28/50 (56%)		5/27 (18.5%)	0.002
Metformin		45/50 (90%)		11/27 (40.7%)	< 0.001
Other		12/50 (24%)		5/27 (18.5%)	0.580
Statins		18/50 (36%)		4/27 (14.8%)	0.050
Years since DM diagnosis	na		na		
<1		0/49 (0%)		14/27 (51.2%)	< 0.001
1-5		16/49 (32.7%)		3/27 (11.1%)	0.038
6-15		19/49 (38.3%)		7/27 (25.9%)	0.258
>15		14/49 (28.6%)		3/27 (11.1%)	0.080

Data is presented as percentage of total (%) or mean ± SD, *Point-of-care measurements, [†]lab measurements, [‡]data available from 48/50 patients, [§]data available from 12/27 patients, ^{||}data available from 35/50 patients, ^{**}data available from 21/27 patients, na = not available.

Results

Clinical and metabolic characteristics of the study population

Patient characteristics are shown in Table 1. On average, DM patients were older and had a higher BMI compared to the other groups. TB patients had a relatively low BMI, while this was comparable for TB-DM patients and HC. All (non-TB) DM patients were on anti-diabetic drugs, while this was the case for 55.6% of TB-DM patients. TB-DM patients not on treatment were newly diagnosed DM cases. In total, 177 participants were included in the study and their plasma metabolic profiles were determined using ¹H-NMR spectroscopy. Metabolite ratios were excluded in the multivariate analysis to limit parameter interdependence, resulting in a total of 142 variables.

Partial least square discriminant analysis (PLS-DA) (Figure 1a) was performed to visualize the metabolic differences between the four groups based on the complete metabolic signature. The score plot of the first two principal components (explaining

42% and 16% of total variance, respectively) is depicted in Figure 1a. TB-DM patients appeared largely scattered over both single disease groups, implying significant metabolic heterogeneity. To explore this further we compared TB, DM and TB-DM patients by hierarchical clustering analysis (Figure 1b). While the majority of TB and DM patients each clustered together, TB-DM patients were again dispersed throughout the two single disease groups, further illustrating high inter-individual variation.

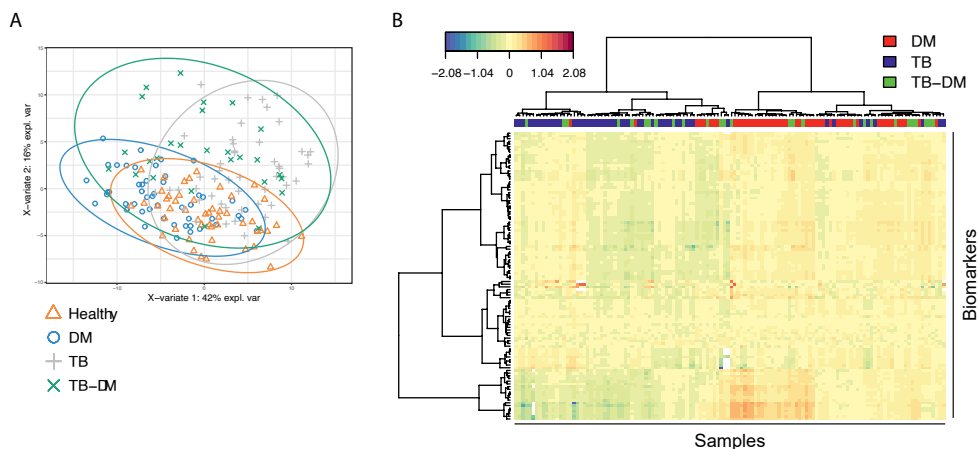


Figure 1: Discrimination of patient groups based on biomarkers.

PLS-DA was used for discrimination of patient groups based on ¹H-NMR-spectroscopy plasma biomarkers. Only samples and variables with $\leq 10\%$ missing or zero values were included, resulting in 107 biomarkers and 175 individuals (healthy = 49, DM = 49, TB = 50, TB-DM = 27). (a) Score plot of the first two components of a PLS-DA model obtained from healthy controls (orange triangles), DM-only (blue circles), TB-only (grey pluses) and TB-DM patients (green crosses). (b) Two-way hierarchical clustering analysis using Euclidean distance and Ward's method of a PLS-DA model of DM-only (red), TB-only (blue) and TB-DM (green) patients.

DM is associated with dyslipidemia while TB is associated with wasting

We performed pairwise comparisons of all groups by multiple linear regression analysis adjusting for age and sex. For each comparison the FDR-corrected $-\log(p)$ values of 44 metabolic parameters are plotted in circular histograms (Figure 2a-e). Measures of size-specific (XS, S, M, L, XL) lipoprotein particle concentrations (Figure 2f-j), lipid composition (Figure S1b) and average lipoprotein diameter (Figure S1a) were analyzed separately. Absolute concentrations or ratios of a subset of metabolites are plotted in Figure 3 (a-l). Metabolite means, standard deviations and numbers of successful measurements are presented in Supplementary Table 1, and raw measurement data can be found in Supplementary Table 2.

Table 2: Univariate biomarker analysis.

Biomarker	TB vs HC			TB-DM vs DM			
	AUC	T-test	95% CI	Biomarker	AUC	T-test	95% CI
His/Gp	0.934	2.97E-17	0.888 – 0.971	His/Phe	0.957	3.88E-17	0.895 – 0.993
His/Phe	0.903	2.81E-14	0.846 – 0.955	EstC/SM	0.933	1.44E-12	0.870 – 0.983
His	0.888	8.52E-14	0.805 – 0.941	Serum-C/FreeC	0.903	2.10E-10	0.832 – 0.964
Serum-C/EstC	0.885	8.15E-11	0.821 – 0.943	EstC/FreeC	0.902	4.13E-10	0.828 – 0.963
Serum-C/FreeC	0.885	5.96E-12	0.809 – 0.942	Serum-C/EstC	0.902	1.82E-09	0.830 – 0.961
EstC/FreeC	0.885	1.38E-11	0.815 – 0.938	His	0.901	1.22E-12	0.823 – 0.971
Ala/Gp	0.876	9.02E-13	0.811 – 0.944	ApoB/Gp	0.897	2.79E-11	0.819 – 0.958
ApoB/Gp	0.871	1.20E-12	0.788 – 0.933	Ala/Gp	0.896	2.43E-12	0.803 – 0.967
EstC/SM	0.854	2.34E-10	0.776 – 0.928	His/Gp	0.895	3.97E-12	0.800 – 0.973
Ile/Gp	0.850	2.14E-10	0.771 – 0.922	Ile/Gp	0.894	1.42E-10	0.782 – 0.975

First, we wanted to define the metabolic effects of DM and TB vs. HC (Figure 2b and c). As expected, the primary parameter associated with DM was increased plasma glucose ($p = 1.83E^{-16}$; p -values reported here are from multivariate analyses) (Figure 2b). DM patients showed major hallmarks of dyslipidemia, namely high levels of VLDL-triglycerides (VLDL-TG) ($p = 5.72E^{-7}$) (Figure 3a), VLDL-cholesterol (VLDL-C) ($p = 6.66E^{-4}$) and ApoB ($p = 0.017$), with low levels of HDL-C ($p = 4.34E^{-5}$) (Figure 3b) and ApoA1 ($p = 1.82E^{-3}$), resulting in an increased ApoB/ApoA1 ratio (Figure 3d). Correspondingly, DM patients displayed elevated plasma concentrations of VLDL particles (XXL to S) and lower numbers of HDL particles (XL to M) (Figure 2g). Furthermore, DM patients had increased amounts of branched-chain amino acids (valine ($p = 0.011$), leucine ($p = 0.093$), isoleucine ($p = 1.29E^{-4}$) (Figure 3h)), a subclass of amino acids associated with insulin resistance⁽³³⁾, while glutamine levels were lower ($p = 5.50E^{-4}$) (Figure 3g).

In contrast, TB patients presented with signs of wasting disease as the majority of metabolites were decreased compared to HC (Figure 2c). Most notably, TB patients had low levels of amino acids (e.g. histidine ($p = 5.36E^{-10}$) (Figure 3e), glutamine ($p = 7.38E^{-4}$) (Figure 3g), alanine ($p = 1.29E^{-4}$)), serum cholesterol ($p = 1.72E^{-4}$) and total fatty acids ($p = 1.32E^{-3}$), including a prominent reduction in polyunsaturated fatty acids ($p = 3.36E^{-6}$), as well as decreased amounts of phospholipid metabolites. Except for inflammation marker Gp (glycoprotein acetylation) ($p = 4.12E^{-8}$) (Figure 3l), TB patients only displayed elevated levels of two metabolites: phenylalanine ($p = 3.07E^{-4}$) (Figure 3f), an aromatic amino acid, and β -hydroxybutyrate ($p = 0.017$) (Figure 3k), a ketone body. Intriguingly, the average low-density lipoprotein (LDL) particle diameter was very significantly increased as a result of TB (Figure S1a) through a relative decrease in smaller (sizes M to S) LDL and HDL particles (Figure 2h).

TB-DM patients display the most prominent metabolic characteristics of both diseases

As DM and TB displayed divergent effects on plasma metabolite concentrations, we next compared the effect of TB-DM comorbidity with the single disease states. Compared to DM (Figure 2e), TB-DM patients showed a similar metabolic signature as TB vs. HC, i.e. reduced levels of amino acids (e.g. histidine ($p = 8.87E^{-11}$) (Figure 3e), alanine ($p = 6.02E^{-8}$) combined with increased concentrations of phenylalanine ($p = 8.57E^{-8}$) (Figure 3f) and β -hydroxybutyrate ($p = 0.013$) (Figure 3k). Although serum cholesterol and total fatty acids were unaffected ($p = 0.738$ and 0.692 respectively), VLDL-TG levels were lower in TB-DM compared to DM patients ($p = 6.40E^{-3}$) (Figure 3a), which is consistent with a decreased amount of VLDL particles (XL to M) (Figure 2j). Similar to the TB group, the average LDL diameter was significantly larger (Figure S1a), which was also the case for HDL due to a relative increase in larger (L to XL) vs. smaller (S to M) particles (Figure 2j).

Importantly, TB-DM patients displayed major hallmarks of DM when compared to the TB group (Figure 2a), namely elevated plasma concentrations of glucose ($p = 6.21E^{-9}$),

VLDL-TG ($p = 5.37E^{-4}$) (Figure 3a), ApoB ($p = 8.06E^{-3}$), VLDL-C ($p = 4.43E^{-4}$), total fatty acids ($p = 5.37E^{-4}$) and branched-chain amino acids (valine ($p = 0.016$), leucine ($p = 0.016$), isoleucine ($p = 3.41E^{-3}$) (Figure 3h)). Moreover, TB-DM comorbidity reduced glutamine levels even further compared to either TB or DM alone ($p = 0.036$ and $7.19E^{-4}$ respectively) (Figure 3g). Similar to DM, VLDL particle levels were elevated, accompanied by an additional increase in LDL particles (M to S) (Figure 2f).

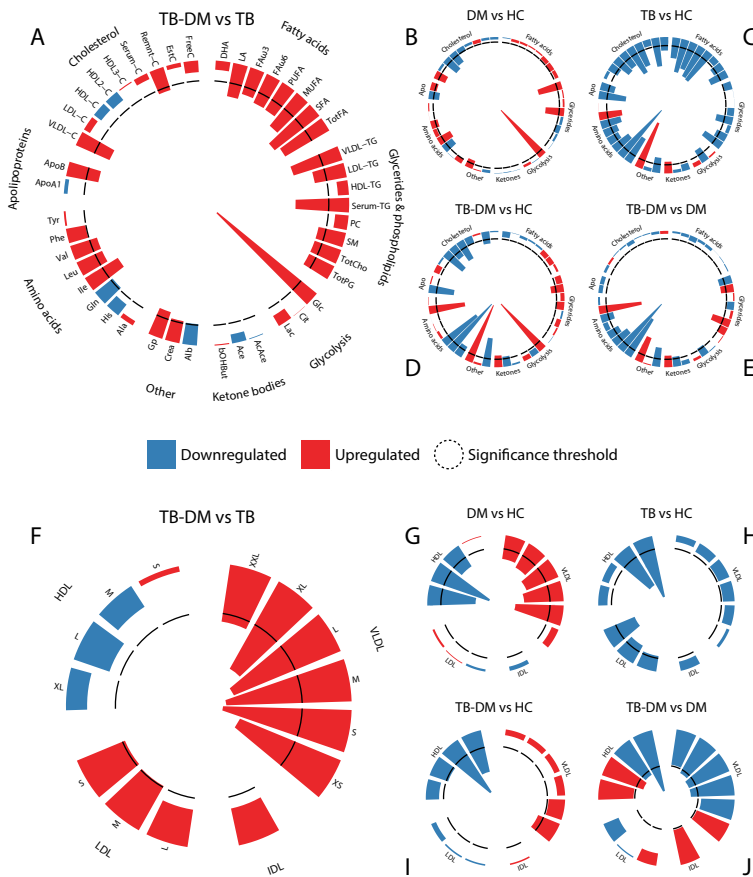


Figure 2: Pairwise comparisons of biomarker profiles and specific lipoprotein particle concentrations.

$^1\text{H-NMR}$ -spectroscopy plasma biomarkers were analyzed by multiple linear regression and the resulting $-\log$ -transformed FDR-corrected p -values (t-test) are displayed as circular histograms for a subset of 44 metabolic biomarkers (a-e) and for the particle concentrations of 14 lipoprotein subclasses (f-j). Biomarkers are grouped by metabolite family and lipoproteins by density. The following comparisons are plotted: TB-DM vs. TB (a & f), DM vs. healthy controls (b & g), TB vs. healthy controls (c & h), TB-DM vs. healthy controls (d & i) and TB-DM vs. DM (e & j). Detailed legends given in the larger plots also apply for the corresponding smaller plots. Up- and downregulated biomarkers are indicated by red and blue bars, respectively, and the significance threshold ($p = 0.05$) is indicated by a dashed line.

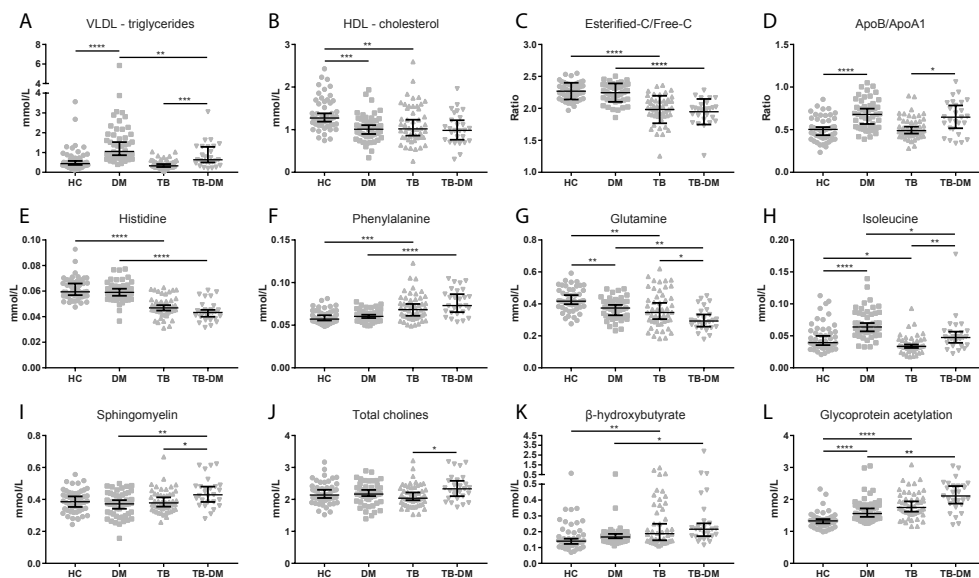


Figure 3: Absolute values for a subset of biomarkers.

(A-L) Concentrations (mmol/L), or ratios of 12 selected important biomarkers. Data are displayed as scatter plots with median and 95% CI, with each dot representing one individual. HC (n=50) and TB-DM (n=27) were compared to TB-only (n=50) and DM-only (n=50) by Kruskal-Wallis test with post-hoc Dunn's test. * $p = 0.05$, ** $p = 0.01$, *** $p = 0.001$, **** $p = 0.0001$.

TB-DM interaction increased levels of phospholipid metabolites and atherogenic lipoprotein remnants

In addition to the pairwise comparison of all disease groups, we investigated whether TB-DM comorbidity resulted in disease interaction-specific effects by adding an interaction term (TB*DM) to the multiple linear regression model. Resulting FDR-corrected p -values (Figure 4) reflect changes in metabolite levels which were not explained by the effects of TB or DM alone. We identified a TB-DM interaction-specific increase in phospholipid metabolite levels (Figure 4a), i.e. sphingomyelins ($p = 5.57E^{-3}$) (Figure 3i), phosphatidylcholine ($p = 0.054$), total cholines ($p = 0.017$) (Figure 3j) and phosphoglycerides ($p = 0.079$). Furthermore, TB-DM interaction trended towards increased atherogenic lipoprotein remnants, XS VLDL ($p = 0.115$) and IDL ($p = 0.072$), while decreasing the concentrations of larger VLDL particles (Figure 4b). This relative increase in remnant-like particles is also apparent from our pairwise comparisons (Figure 2f: TB-DM vs TB – XS VLDL: $p = 1.34E^{-3}$, IDL: $p = 0.101$; Figure 2j: TB-DM vs DM – XS VLDL: $p = 0.055$, IDL: $p = 0.055$). Finally, the data suggest TB-DM is associated with elevated LDL-TG concentrations when compared to HC, TB or DM patients (Figure 2d, 2a, 2e: $p = 7.80E^{-3}$, $8.40E^{-3}$ and $7.18E^{-3}$, respectively), which could be driven by a relative enrichment of LDL particle TG content (Figure S1c) due to diminished LDL lipolysis.

reflects mycobacterial load. Univariate analysis showed a trending inverse correlation between TTP and levels of individual and total branched-chain amino acids, as well as the ketone bodies acetoacetate and β -hydroxybutyrate (Figure S2a-f). However, these findings need to be corroborated in follow-up studies with greater power.

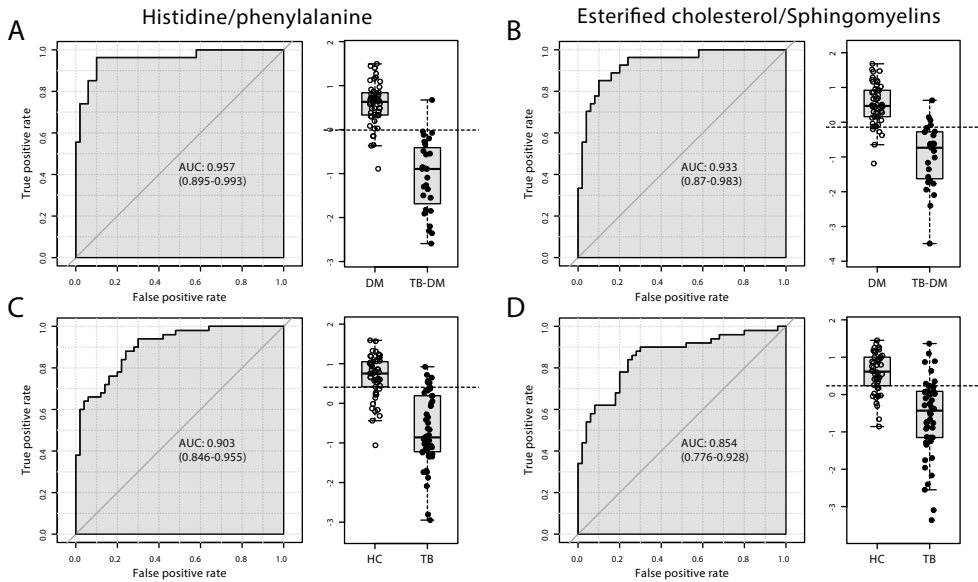


Figure 5: TB biomarker analysis.

Biomarkers and ratios from the 44 metabolite set were used to identify TB status in DM-only (n=50) vs. TB-DM (n=27) (a, b) and in HC (n=50) vs. TB-only (n=50) (c, d) patients. ROC curves for the histidine/phenylalanine (a, c) and esterified cholesterol/sphingomyelins (b, d) ratios are plotted. Individual patients are shown as dots in accompanying boxplots with cut-off (dashed line).

Discussion

Although accumulating epidemiological evidence from recent and older studies indicates a link between TB and DM, the underlying pathophysiological mechanisms remain elusive. Since lipids play important roles in both diseases, we studied the impact of TB disease on host lipid metabolism and analyzed how this relates to TB-DM comorbidity. Our results show that plasma from patients with TB displayed signatures of extensive wasting, represented by lower levels of amino acids, cholesterol, fatty acids and phospholipid metabolites, while conversely DM was associated with dyslipidemia. Plasma from TB-DM patients showed the most prominent metabolic characteristics of both diseases, i.e. wasting, exemplified by reduced concentrations of amino acids (histidine, alanine, glutamine), and dyslipidemia in the form of high levels of VLDL-TG and low HDL cholesterol. Although TB-DM-associated dyslipidemia was less severe than that of DM, the inter-individual heterogeneity was high. This could suggest that there are TB-DM patients

in whom the effects of wasting dominate over the DM-associated dyslipidemia, as well as patients with the opposite metabolic phenotype. Alternatively, it is possible that this inter-individual variation is the result of differences in DM-duration, as the TB-DM group comprised a mix of long-term diabetics and patients who were recently diagnosed with DM (Table 1).

In addition to its overlapping effects with either TB or DM metabolic profiles, we find that TB-DM comorbidity leads to a relative increase in remnant-like plasma lipoprotein particles (XS-VLDL, IDL) which are strongly associated with cardiovascular disease and atherosclerosis⁽³⁴⁾. The formation of remnant-like particles depends on the relative contributions of lipoprotein lipase (LPL) and hepatic triglyceride lipase (HTGL) to lipoprotein hydrolysis: the former initiates the cascade through lipolysis of chylomicrons and nascent VLDL while the latter preferentially converts smaller VLDL and IDL particles to LDL⁽³⁵⁾. Furthermore, both play roles in HDL metabolism and have been shown to have opposing effects on HDL size⁽³⁶⁾. The elevated amount of remnant-like particles and LDL TG-enrichment indicate relatively decreased HTGL/LPL activity in TB-DM patients. This is further supported by a reduction in smaller HDL particles (sizes M to S) in plasma from both TB and TB-DM patients and the relative increase in LDL diameter in both groups as a result of TB. Additionally, TB-DM interaction leads to a specific increase in sphingomyelins and related phospholipid metabolites. It has been demonstrated that hepatic sphingolipid synthesis is increased under inflammatory conditions⁽³⁷⁾, specifically through increased levels of the rate-limiting enzyme serine palmitoyltransferase (SPT). High levels of circulating sphingomyelin are associated with coronary artery disease as they increase the atherogenic potential of lipoproteins⁽³⁸⁾ and also function as a physiological inhibitor of HTGL activity⁽³⁹⁾.

The ratio of histidine/phenylalanine in plasma was a potential biomarker for TB irrespective of DM-status. This result is congruent with earlier metabolomic profiling of TB which reported changes in histidine and/or phenylalanine metabolism in plasma⁽⁴⁰⁾ and urine⁽⁴¹⁾, and will require further validation in independent cohorts with larger sample sizes. It is possible that a decreased histidine/phenylalanine ratio reflects non-specific oxidative stress and/or inflammation as similar changes were demonstrated in other inflammatory conditions, including rheumatoid arthritis⁽⁴²⁾, sepsis⁽⁴³⁾, obesity⁽⁴⁴⁾ and cancer⁽⁴⁵⁾. Furthermore, TB disease status was associated with a decreased ratio of esterified to free cholesterol in plasma. Cholesterol esterification is regulated by lecithin-cholesterol acyltransferase (LCAT), a liver-produced enzyme which is bound to HDL particles in plasma. A possible explanation for this shift is the ability of sphingomyelin to inhibit LCAT activity^(46, 47) as the esterified cholesterol/sphingomyelin ratio also showed strong predictive power, particularly in TB-DM patients. Furthermore, LCAT and HTGL levels were shown to be decreased during the acute phase response, the early reaction of the body to infection or inflammation, strengthening the notion that these enzymes could be deregulated during TB. Taken together, our results support a model in which

the unique lipid profile of TB-DM patients is the outcome of the interaction between DM-induced dyslipidemia and TB-induced changes in lipoprotein metabolism.

We postulate that the pro-atherogenic phenotype of TB-DM patients might contribute to TB susceptibility or reactivation. Some striking similarities exist between the progression of TB and atherosclerosis. Pivotal in both pathologies is the formation of lipid-loaded foamy macrophages⁽¹⁵⁾. *Mtb* has been demonstrated to reprogram macrophage lipid metabolism for its own benefit as it requires host-derived lipids as nutrient source for survival and replication⁽⁴⁸⁻⁵¹⁾. Interestingly, we find that TB leads to increased plasma levels of β -hydroxybutyrate, a ketone body which has been implicated in *Mtb*-induced intracellular lipid droplet formation⁽⁵⁰⁾. A recent study showed that DM-associated dyslipidemia exacerbates the severity of caseous lung necrosis in TB patients⁽⁵²⁾, supporting the hypothesis that aberrant lipid levels negatively affect TB outcome. Paradoxically, others reported a DM-independent protective effect of high BMI on the risk of TB^(13, 53), however it has been suggested that this association depends on the local TB incidence⁽⁵⁴⁾. Regardless, it would be of great interest to compare lipid profiles in obese TB patients with or without DM.

Some inherent weaknesses in study design will have to be addressed in future follow-up studies as the overall statistical power was inadequate to control for all possible confounding factors. Firstly, differences in both the DM and TB-DM populations could be related to the use of anti-diabetic medication such as insulin, metformin or statins, all of which affect glucose and lipid metabolism. Secondly, some of the observed effects of TB and/or DM could have been driven by differences in BMI and not by disease state as such. However, correcting for this could obscure genuine metabolic effects induced by TB, DM or both which are (partially) mediated through changes in energy expenditure or storage and therefore reflected by the patients' BMI. Thirdly, it was not possible to correctly control for differences in smoking habits as this information was not available for the HC group. Finally, the studied patient population was ethnically uniform, the majority being from the Colored population of South Africa. It will be important to explore how the results of this study translate to patient populations with different ethnic backgrounds.

In conclusion, TB-DM comorbidity results in a distinctive lipid profile with pro-atherogenic properties, including significantly elevated levels of sphingomyelins and remnant-like lipoprotein particles. These results will have to be validated in independent cohort studies, and simultaneous investigation of HTGL, LPL, SPT and LCAT activity is warranted. Our findings may have therapeutic implications and encourage more extensive studies into the possible beneficial effects of lipid-lowering drugs on TB outcome in TB-DM patients. We suggest that after initiation of antibiotic treatment TB-DM patients should receive life-style change counseling, and it may be valuable to determine blood lipid profiles. Statin or other lipid-lowering treatments could be started in case of aberrant lipid levels or existing cardiovascular malconditions. Furthermore, systematically determining TG and/or cholesterol levels at TB diagnosis could help identifying patients at risk.

Acknowledgements

We thank the members of the TANDEM consortium for discussion of the data. We are grateful to all study participants, to the clinical team Stephanus T. Malherbe, Elizna Maasdorp, Charmaine Abrahams and Shriley McAnda as well as to the database manager Kim Stanley.

Funding Sources

This study was supported by the TANDEM (Tuberculosis and Diabetes Mellitus) Grant of the ECFP7 (European Union's Seventh Framework Programme) under Grant Agreement No. 305279 for patient recruitment, data collection and analysis; and by TBVAC2020 Grant of EC HOR2020 (Grant Agreement No. 643381) for analysis.

Conflicts of Interest

All authors: no reported conflicts.

Author Contributions

Conceived and designed the study: SAJ THMO GW. Supervised sample collection and selection: KR, LK, GW. Analyzed the data: FV EvdA SAJ. Wrote the paper: FV SAJ THMO.

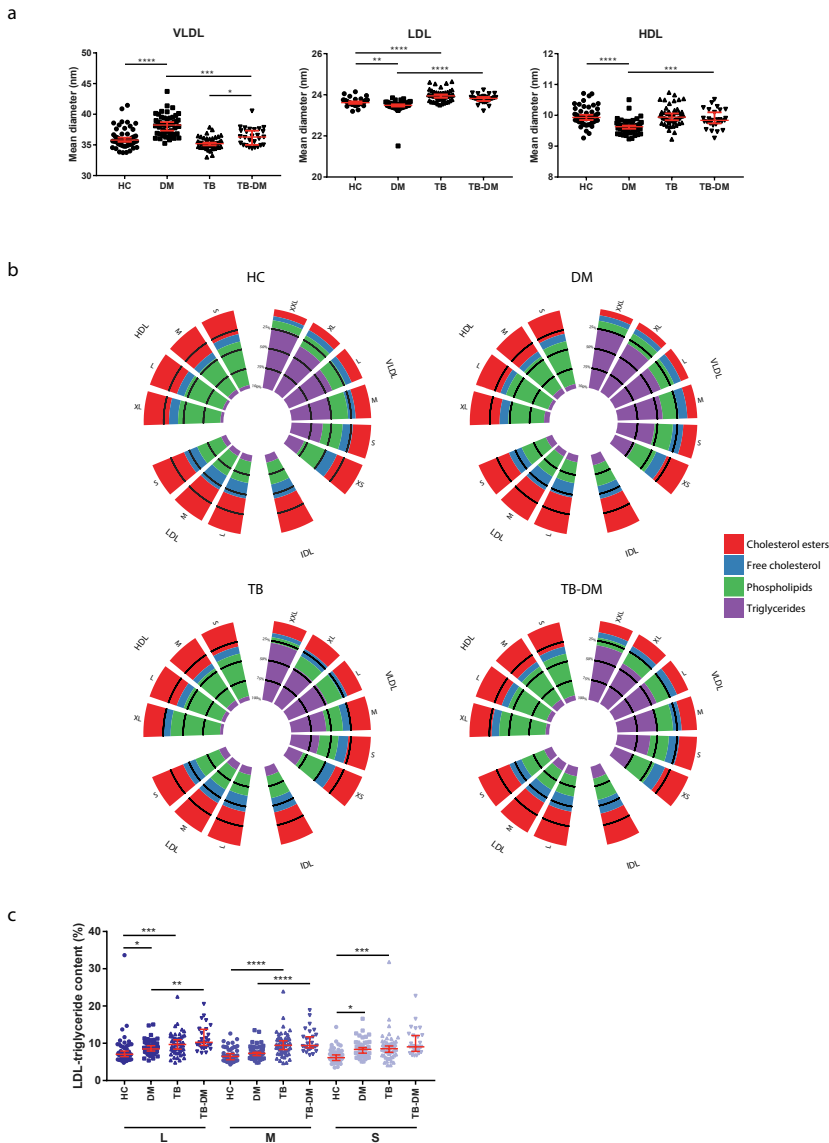
References

- 1 Jeon CY, Murray MB. Diabetes mellitus increases the risk of active tuberculosis: a systematic review of 13 observational studies. *PLoS Med*. 2008;5(7):e152.
- 2 World Health Organization. Diabetes & TB - fact sheet. Geneva, Switzerland 2016.
- 3 Baker MA, Harries AD, Jeon CY, Hart JE, Kapur A, Lonnroth K, et al. The impact of diabetes on tuberculosis treatment outcomes: a systematic review. *BMC Med*. 2011;9:81.
- 4 Niazi AK, Kalra S. Diabetes and tuberculosis: a review of the role of optimal glycemic control. *J Diabetes Metab Disord*. 2012;11(1):28.
- 5 Hensel RL, Kempker RR, Tapia J, Oladele A, Blumberg HM, Magee MJ. Increased risk of latent tuberculous infection among persons with pre-diabetes and diabetes mellitus. *Int J Tuberc Lung Dis*. 2016;20(1):71-8.
- 6 Kumar Nathella P, Babu S. Influence of diabetes mellitus on immunity to human tuberculosis. *Immunology*. 2017;152(1):13-24.
- 7 International Diabetes Federation. Diabetes Atlas. 8th edn. Brussels, Belgium 2017 2013. Report No.
- 8 van Crevel R, Dockrell HM, Consortium T. TANDEM: understanding diabetes and tuberculosis. *Lancet Diabetes Endocrinol*. 2014;2(4):270-2.
- 9 Taskinen MR, Boren J. New insights into the pathophysiology of dyslipidemia in type 2 diabetes. *Atherosclerosis*. 2015;239(2):483-95.
- 10 Haas ME, Attie AD, Biddinger SB. The regulation of ApoB metabolism by insulin. *Trends in endocrinology and metabolism: TEM*. 2013;24(8):391-7.
- 11 Schwenk A, Macallan DC. Tuberculosis, malnutrition and wasting. *Curr Opin Clin Nutr Metab Care*. 2000;3(4):285-91.
- 12 Khan A, Sterling TR, Reves R, Vernon A, Horsburgh CR. Lack of weight gain and relapse risk in a large tuberculosis treatment trial. *Am J Respir Crit Care Med*. 2006;174(3):344-8.
- 13 Lonnroth K, Williams BG, Cegielski P, Dye C. A consistent log-linear relationship between tuberculosis incidence and body mass index. *Int J Epidemiol*. 2010;39(1):149-55.
- 14 van Crevel R, Karyadi E, Netea MG, Verhoef H, Nelwan RH, West CE, et al. Decreased plasma leptin concentrations in tuberculosis patients are associated with wasting and inflammation. *The Journal of clinical endocrinology and metabolism*. 2002;87(2):758-63.
- 15 Russell DG, Cardona PJ, Kim MJ, Allain S, Altare F. Foamy macrophages and the progression of the human tuberculosis granuloma. *Nature immunology*. 2009;10(9):943-8.
- 16 Lee W, VanderVen BC, Fahey RJ, Russell DG. Intracellular Mycobacterium tuberculosis exploits host-derived fatty acids to limit metabolic stress. *The Journal of biological chemistry*. 2013;288(10):6788-800.
- 17 Kim MJ, Wainwright HC, Locketz M, Bekker LG, Walther GB, Dittrich C, et al. Caseation of human tuberculosis granulomas correlates with elevated host lipid metabolism. *EMBO molecular medicine*. 2010;2(7):258-74.

- 18 Soh AZ, Chee CB, Wang YT, Yuan JM, Koh WP. Dietary Cholesterol Increases the Risk whereas PUFAs Reduce the Risk of Active Tuberculosis in Singapore Chinese. *J Nutr.* 2016;146(5):1093-100.
- 19 Martens GW, Arikan MC, Lee J, Ren F, Vallerskog T, Kornfeld H. Hypercholesterolemia impairs immunity to tuberculosis. *Infection and immunity.* 2008;76(8):3464-72.
- 20 Martens GW, Vallerskog T, Kornfeld H. Hypercholesterolemic LDL receptor-deficient mice mount a neutrophilic response to tuberculosis despite the timely expression of protective immunity. *J Leukoc Biol.* 2012;91(6):849-57.
- 21 Parihar SP, Guler R, Khutlang R, Lang DM, Hurdayal R, Mhlanga MM, et al. Statin therapy reduces the mycobacterium tuberculosis burden in human macrophages and in mice by enhancing autophagy and phagosome maturation. *J Infect Dis.* 2014;209(5):754-63.
- 22 Lai CC, Lee MT, Lee SH, Hsu WT, Chang SS, Chen SC, et al. Statin treatment is associated with a decreased risk of active tuberculosis: an analysis of a nationally representative cohort. *Thorax.* 2016;71(7):646-51.
- 23 Dutta NK, Bruiners N, Pinn ML, Zimmerman MD, Prideaux B, Dartois V, et al. Statin adjunctive therapy shortens the duration of TB treatment in mice. *J Antimicrob Chemother.* 2016;71(6):1570-7.
- 24 Su VY, Su WJ, Yen YF, Pan SW, Chuang PH, Feng JY, et al. Statin Use Is Associated With a Lower Risk of TB. *Chest.* 2017;152(3):598-606.
- 25 Lobato LS, Rosa PS, Ferreira Jda S, Neumann Ada S, da Silva MG, do Nascimento DC, et al. Statins increase rifampin mycobactericidal effect. *Antimicrob Agents Chemother.* 2014;58(10):5766-74.
- 26 Soinenen P, Kangas AJ, Wurtz P, Suna T, Ala-Korpela M. Quantitative serum nuclear magnetic resonance metabolomics in cardiovascular epidemiology and genetics. *Circulation Cardiovascular genetics.* 2015;8(1):192-206.
- 27 Definition and diagnosis of diabetes mellitus and intermediate hyperglycemia: report of a WHO/IDF consultation. Geneva: 2006.
- 28 Wurtz P, Kangas AJ, Soinenen P, Lawlor DA, Davey Smith G, Ala-Korpela M. Quantitative Serum Nuclear Magnetic Resonance Metabolomics in Large-Scale Epidemiology: A Primer on -Omic Technologies. *American journal of epidemiology.* 2017;186(9):1084-96.
- 29 Xia J, Wishart DS. Using MetaboAnalyst 3.0 for Comprehensive Metabolomics Data Analysis. *Current protocols in bioinformatics.* 2016;55:14 0 1- 0 91.
- 30 Lê Cao KA, Rohart F, Gonzalez I, Déjean S, Gautier B, Bartolo F. mixOmics: Omics Data Integration Project 2017. Available from: <https://CRAN.R-project.org/package=mixOmics>.
- 31 Ritchie ME, Phipson B, Wu D, Hu Y, Law CW, Shi W, et al. limma powers differential expression analyses for RNA-sequencing and microarray studies. *Nucleic acids research.* 2015;43(7):e47.
- 32 Ladroue C. phenotypicForest. R package version 0.3 2015. Available from: <https://github.com/chrislad/phenotypicForest>.
- 33 Newgard CB. Interplay between lipids and branched-chain amino acids in development of insulin resistance. *Cell Metab.* 2012;15(5):606-14.

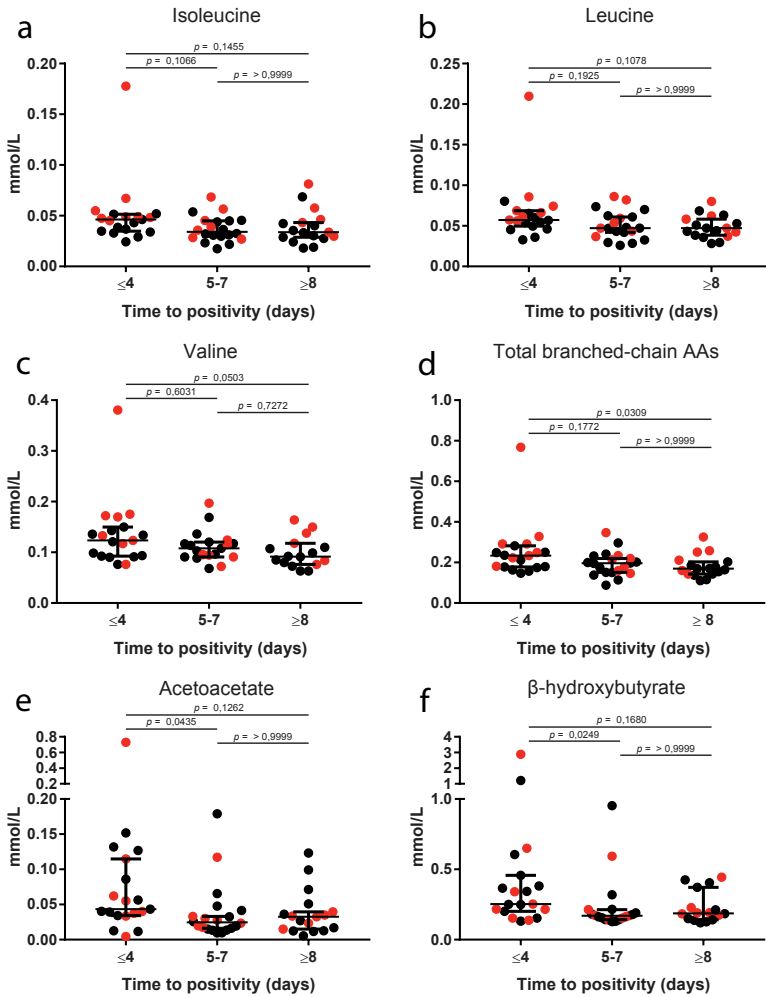
- 34 Varbo A, Benn M, Nordestgaard BG. Remnant cholesterol as a cause of ischemic heart disease: evidence, definition, measurement, atherogenicity, high risk patients, and present and future treatment. *Pharmacol Ther.* 2014;141(3):358-67.
- 35 Goldberg IJ, Le NA, Paterniti JR, Jr., Ginsberg HN, Lindgren FT, Brown WV. Lipoprotein metabolism during acute inhibition of hepatic triglyceride lipase in the cynomolgus monkey. *The Journal of clinical investigation.* 1982;70(6):1184-92.
- 36 Tani M, Horvath KV, Lamarche B, Couture P, Burnett JR, Schaefer EJ, et al. High-density lipoprotein subpopulation profiles in lipoprotein lipase and hepatic lipase deficiency. *Atherosclerosis.* 2016;253:7-14.
- 37 Memon RA, Holleran WM, Moser AH, Seki T, Uchida Y, Fuller J, et al. Endotoxin and cytokines increase hepatic sphingolipid biosynthesis and produce lipoproteins enriched in ceramides and sphingomyelin. *Arteriosclerosis, thrombosis, and vascular biology.* 1998;18(8):1257-65.
- 38 Dong J, Liu J, Lou B, Li Z, Ye X, Wu M, et al. Adenovirus-mediated overexpression of sphingomyelin synthases 1 and 2 increases the atherogenic potential in mice. *Journal of lipid research.* 2006;47(6):1307-14.
- 39 Yang P, Subbaiah PV. Regulation of hepatic lipase activity by sphingomyelin in plasma lipoproteins. *Biochimica et biophysica acta.* 2015;1851(10):1327-36.
- 40 Weiner J, 3rd, Parida SK, Maertzdorf J, Black GF, Repsilber D, Telaar A, et al. Biomarkers of inflammation, immunosuppression and stress with active disease are revealed by metabolomic profiling of tuberculosis patients. *PloS one.* 2012;7(7):e40221.
- 41 Luies L, Loots D. Tuberculosis metabolomics reveals adaptations of man and microbe in order to outcompete and survive (vol 12, 40, 2016). *Metabolomics.* 2016;12(3).
- 42 Gerber DA. Low free serum histidine concentration in rheumatoid arthritis. A measure of disease activity. *The Journal of clinical investigation.* 1975;55(6):1164-73.
- 43 Su L, Li H, Xie A, Liu D, Rao W, Lan L, et al. Dynamic changes in amino acid concentration profiles in patients with sepsis. *PloS one.* 2015;10(4):e0121933.
- 44 Niu YC, Feng RN, Hou Y, Li K, Kang Z, Wang J, et al. Histidine and arginine are associated with inflammation and oxidative stress in obese women. *Br J Nutr.* 2012;108(1):57-61.
- 45 Neurauter G, Grahmann AV, Klieber M, Zeimet A, Ledochowski M, Sperner-Unterweger B, et al. Serum phenylalanine concentrations in patients with ovarian carcinoma correlate with concentrations of immune activation markers and of isoprostane-8. *Cancer Lett.* 2008;272(1):141-7.
- 46 Subbaiah PV, Liu M. Role of sphingomyelin in the regulation of cholesterol esterification in the plasma lipoproteins. Inhibition of lecithin-cholesterol acyltransferase reaction. *The Journal of biological chemistry.* 1993;268(27):20156-63.
- 47 Subbaiah PV, Jiang XC, Belikova NA, Aizezi B, Huang ZH, Reardon CA. Regulation of plasma cholesterol esterification by sphingomyelin: effect of physiological variations of plasma sphingomyelin on lecithin-cholesterol acyltransferase activity. *Biochimica et biophysica acta.* 2012;1821(6):908-13.

- 48 Peyron P, Vaubourgeix J, Poquet Y, Levillain F, Botanch C, Bardou F, et al. Foamy macrophages from tuberculous patients' granulomas constitute a nutrient-rich reservoir for *M. tuberculosis* persistence. *PLoS pathogens*. 2008;4(11):e1000204.
- 49 Mahajan S, Dkhar HK, Chandra V, Dave S, Nanduri R, Janmeja AK, et al. *Mycobacterium tuberculosis* modulates macrophage lipid-sensing nuclear receptors PPARgamma and TR4 for survival. *Journal of immunology*. 2012;188(11):5593-603.
- 50 Singh V, Jamwal S, Jain R, Verma P, Gokhale R, Rao KV. *Mycobacterium tuberculosis*-driven targeted recalibration of macrophage lipid homeostasis promotes the foamy phenotype. *Cell host & microbe*. 2012;12(5):669-81.
- 51 Ouimet M, Koster S, Sakowski E, Ramkhelawon B, van Solingen C, Oldebeken S, et al. *Mycobacterium tuberculosis* induces the miR-33 locus to reprogram autophagy and host lipid metabolism. *Nature immunology*. 2016;17(6):677-86.
- 52 Dong Z, Shi J, Dorhoi A, Zhang J, Soodeen-Lalloo AK, Chen W, et al. Hemostasis and lipoprotein indices signify exacerbated lung injury in tuberculosis with diabetes comorbidity. *Chest*. 2017.
- 53 Lin HH, Wu CY, Wang CH, Fu H, Lonroth K, Chang YC, et al. Association of obesity, diabetes, and risk of tuberculosis: two population-based cohorts. *Clin Infect Dis*. 2017.
- 54 Zhang H, Li X, Xin H, Li H, Li M, Lu W, et al. Association of Body Mass Index with the Tuberculosis Infection: a Population-based Study among 17796 Adults in Rural China. *Sci Rep*. 2017;7:41933.



Supplementary Figure 1: Lipoprotein diameter and lipid compositions.

(A) Mean diameters (nm) of VLDL, LDL and HDL particles. Data are displayed as scatter plots with median and 95% CI, with each dot representing one individual. HC (n=50) and TB-DM (n=27) were compared to TB-only (n=50) and DM-only (n=50) by Kruskal-Wallis test with post-hoc Dunn's test. * $p = 0,05$, ** $p = 0,01$, *** $p = 0,001$, **** $p = 0,0001$. (B) Lipid compositions of 14 lipoprotein subclasses. Each bar represents the total composition (100%) of a specific particle. Cholesterol ester (red), free cholesterol (blue), phospholipid (green) and triglyceride (purple) content are shown. (C) Relative triglyceride content of different LDL particles (%). Data are displayed as scatter plots with median and 95% CI, with each dot representing one individual. HC (n=50) and TB-DM (n=27) were compared to TB-only (n=50) and DM-only (n=50) by Kruskal-Wallis test with post-hoc Dunn's test. * $p = 0,05$, ** $p = 0,01$, *** $p = 0,001$, **** $p = 0,0001$.



Supplementary Figure 2: Biomarker correlation with TTP.

TB and TB-DM patients were grouped according to TTP: ≤ 4 days ($n=19$), 5-7 days ($n=20$) and ≥ 8 days ($n=17$). Absolute concentrations of isoleucine (A), leucine (B), valine (C), total branched-chain amino acids (D), acetoacetate (E) and β -hydroxybutyrate (F) are shown. Data are displayed as scatter plots with median and 95% CI, with each dot representing one individual. Black and red dots represent TB and TB-DM patients, respectively. Groups were compared by Kruskal-Wallis test with post-hoc Dunn's test.

CHAPTER

6

Plasma metabolomics in tuberculosis patients with and without concurrent type 2 diabetes at diagnosis and during antibiotic treatment

Frank Vrieling¹, Bacht Alisjahbana^{2,3}, Edhyana Sahiratmadja³, Reinout van Crevel⁴, Amy C. Harms⁵, Thomas Hankemeier⁵, Tom H. M. Ottenhoff¹ and Simone A. Joosten¹

¹ Department of Infectious Diseases, Leiden University Medical Center, Leiden, The Netherlands

² Department of Internal Medicine, Hasan Sadikin General Hospital, Bandung, Indonesia

³ Infectious Disease Research Center, Faculty of Medicine, Universitas Padjadjaran, Bandung

⁴ Department of Internal Medicine and Radboud Center for Infectious Diseases, Radboud Institute for Health Sciences (RIHS), Radboud University Medical Center, Nijmegen, the Netherlands

⁵ Systems Biomedicine and Pharmacology, Leiden Academic Center for Drug Research, Leiden University, Leiden, The Netherlands

Tuberculosis (TB) and type 2 diabetes mellitus (DM), a major TB risk factor, are both accompanied by marked alterations in metabolic processes. Dissecting the specific metabolic changes induced by disease through metabolomics has shown potential to improve our understanding of relevant pathophysiological mechanisms of disease, which could lead to improved treatment. Targeted tandem liquid chromatography–mass spectrometry (LC-MS/MS) was used to compare amine and acylcarnitine levels in plasma samples of patients with TB or TB-DM from Indonesia at time of diagnosis and during antibiotic treatment. Partial least squares discrimination analysis (PLS-DA) showed good separation of patient groups. Amine levels were strongly altered in both disease groups compared to healthy controls, including low concentrations of citrulline and ornithine. Several amino acid ratios discriminated TB from controls (phenylalanine/histidine; citrulline/arginine; kynurenine/tryptophan), possibly reflecting changes in indoleamine-pyrrole 2,3-dioxygenase (IDO) and nitric oxide synthase (NOS) activity. Choline, glycine, serine, threonine and homoserine levels were lower in TB-DM compared to TB, and, in contrast to other analytes, did not normalize to healthy control levels during antibiotic treatment. Our results not only provide important validation of previous studies but also identify novel biomarkers, and significantly enhance our understanding of metabolic changes in human TB and TB-DM.

Introduction

Tuberculosis (TB) is a severe infectious disease which mostly affects the lungs and is caused by *Mycobacterium tuberculosis*. In 2016, 10.4 million people were newly diagnosed with TB and 1.7 million individuals died as a result of TB, ranking TB as the 10th leading cause of death worldwide⁽¹⁾. Over recent years, type 2 diabetes mellitus (DM) has been recognized as an important risk factor for TB development and reduced success of TB treatment⁽²⁻⁴⁾. It is currently estimated that 15% of global TB cases can be attributed to concurrent TB-DM⁽⁵⁾. The number of people living with DM worldwide is estimated to increase by 48% in 2045, especially in low- and middle-income countries, where TB is endemic, due to changes in lifestyle associated with economic development and urbanization⁽⁶⁾. Therefore a better understanding of the characteristics governing TB in the context of DM comorbidity is crucial for deciphering their combined pathophysiology and ultimately improved treatment.

Both TB and DM are accompanied by marked metabolic changes: TB progression is associated with the development of wasting syndrome, a nutritional state during which the combination of increased energy expenditure necessary to combat the infection and decreased food-intake leads to severe weight loss and wasting of muscle tissue, whereas hyperglycemia and hyperlipidemia are major hallmarks of DM. We recently showed that TB-DM patients display metabolic characteristics of both diseases as determined by ¹H-Nuclear Magnetic Resonance (NMR) plasma lipid profiling⁽⁷⁾. Metabolomics, defined as the comprehensive analysis of small molecule intermediates of metabolism within a biological system which together form the metabolome, has developed into a powerful approach to study potential perturbations of metabolic homeostasis caused by disease. The use of metabolomics has resulted in the successful identification of small molecule metabolite biomarkers for various illnesses, including Alzheimer's disease⁽⁸⁾, various forms of cancer⁽⁹⁾, and diabetes⁽¹⁰⁾. A number of studies have used metabolomics to identify biomarkers for TB in both serum and urine⁽¹¹⁾. More recently, a prognostic metabolic biosignature with good predictive power for TB progression was developed⁽¹²⁾. However, further validation of many of these biomarker candidates has not been performed in independent studies or in the presence of clinically relevant comorbidities such as DM.

Here, we performed targeted metabolomics to investigate amine and acylcarnitine levels in plasma samples of TB patients with or without DM and healthy endemic controls. Acylcarnitines are intermediates of fatty acid and amino acid oxidation which may be involved in early insulin resistance⁽¹⁰⁾. Furthermore, the metabolic profiles of both TB and TB-DM patients were followed longitudinally during TB treatment to analyze possible effects of antibiotic TB treatment on metabolite biomarkers. We find that TB and TB-DM have both shared and unique effects on patient plasma metabolic profiles, including marked changes in metabolites involved in the urea cycle, indoleamine 2,3-dioxygenase (IDO) signaling and liver function, of which the majority normalized to healthy control levels during the course of antibiotic treatment. The results of this study

not only confirm and validate key findings from previous metabolomics studies on TB in a geographically and genetically distinct population, but also propose novel biomarker candidates for TB and TB-DM.

Results

Study population

In total, metabolite concentrations were measured in plasma samples from 48 TB patients, 20 TB-DM patients and 48 healthy controls (HC). HC had a similar age but higher body weight compared to TB patients without DM; diabetic TB patients were older and had a higher BMI compared with non-diabetic TB patients (Table 1). No significant differences were present between the groups based on sex, ethnicity, current smoking status or severity of TB scored on chest x-rays (CXR).

Table 1: Patients' clinical characteristics according to disease group (n = 116).

	HC n=48	HC n=48	TB-DM n=19	p-value
Sex (male/female)	24/24	23/26	13/6	0.269
Age (years)	29.0 ± 9.1	29.4 ± 9.1	48.3 ± 8.5	< 0.001
BMI (kg/m ²)	22.9 ± 4.0	17.3 ± 2.1	20.5 ± 2.9	< 0.001
Fasting blood glucose (mg/dl)	80.2 ± 9.1	80.7 ± 13.6	218.5 ± 76.8	< 0.001
Smoking (currently)	20/48 (41.7%)	19/49 (38.8%)	9/19 (47.4%)	0.811
CXR score (mild/advanced)	na	21/28	10/9	0.468
Ethnicity:				0.650
Betawi	10/48 (20.8%)	11/49 (22.4%)	3/19 (15.8%)	
Jawa	17/48 (35.4%)	13/49 (26.5%)	6/19 (31.6%)	
Sunda	8/48 (16.7%)	12/49 (24.5%)	4/19 (21.1%)	
Mixed	10/48 (20.8%)	11/49 (22.4%)	3/19 (15.8%)	
Other	3/48 (6.3%)	2/49 (4.1%)	3/19 (15.8%)	

Data is presented as percentage of total (%) or mean ± SD. BMI = Body Mass Index, CXR = Chest X-ray Radiograph.

First, a principal component analysis (PCA) model was built to visualize differences between disease groups based on the entire dataset, which consisted of four components explaining 54% of total variance. The score plot of the first two components (explaining 25% and 13% of total variance, respectively) is displayed in Figure 1A. While disease status (HC, TB or TB-DM) accounted for a proportion of the total variance, no complete separation was observed between the three groups. However, sex differences also comprised a considerable source of data variance (Figure S1A). These results were corroborated by hierarchical clustering analysis which showed incomplete clustering based on either

sex or disease group status (Figure 1B). To correct for the effect of sex, a multilevel PCA model was built¹³ to separate the “within-sex” from the “between-sex” data variation. The multilevel model improved the discriminatory capacity based on disease group (Figure S1B), while neither sex nor smoking status contributed to data variance. Finally, partial-least squares discrimination analysis (PLS-DA) models were fitted for each disease group comparison and the resulting score plots and cross-validated quality metrics for model predictive ability (Q2) and explained variance (R2X & R2Y) are displayed in Figure 1C-E. All models showed high goodness of fit and predictive ability as indicated by R2Y and Q2 scores of >0.5, and the resulting score plots showed relatively good clustering and separation of samples based on disease group. Taken together, TB and TB-DM status were found to be major contributors to data variance based on the entire metabolomic dataset, and adjusting for differences in sex was of importance for further analysis.

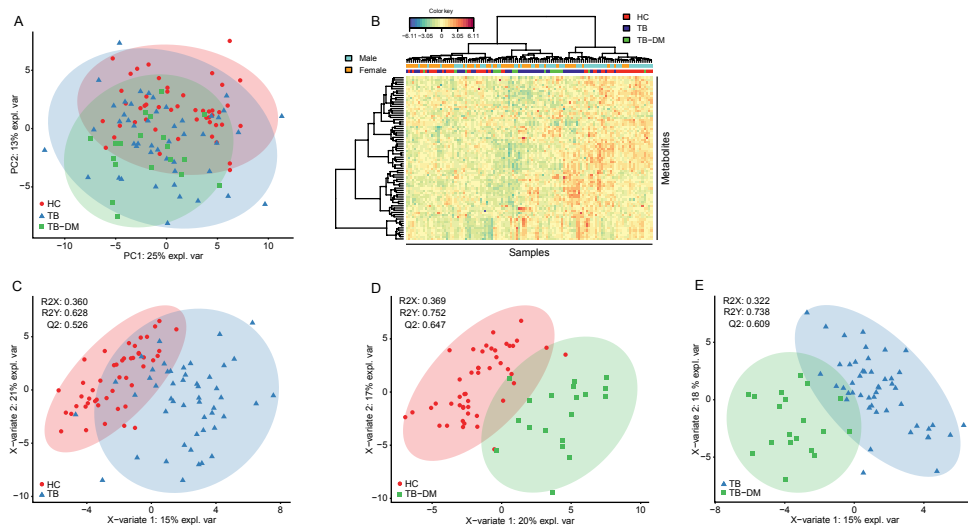


Figure 1: TB/TB-DM status result in distinct metabolic profiles.

(A) Score plot of the first two principal components of a PCA model built on the entire dataset and color coded by group with confidence ellipses. HC are displayed as red dots, TB patients as blue triangles and TB-DM patients as green squares. (B) Two-way hierarchical clustering analysis by Euclidean distance with Ward's method. Samples are annotated by disease group and sex: HC (red), TB patients (blue) and TB-DM patients (green), male (cyan), female (orange). (C-E) Score plots of PLS-DA models for TB vs HC (C), TB-DM vs HC (D) and TB-DM vs TB (E). HC are displayed as red dots, TB patients as blue triangles and TB-DM patients as green squares. PLS-DA evaluation criteria (R2X, R2Y, Q2) are displayed for each model.

Patients with TB and TB-DM have distinct metabolic profiles

In total, levels of 31/53 amines (58.5%) and 5/21 acylcarnitines (23.8%) were significantly different in TB patients compared to HC based on a linear regression model (Figure 2A). Medians with interquartile ranges of all measurements and their resulting q -values can be found in Supplementary Table 1. Volcano plots of regression model statistics versus metabolite log₂-transformed fold changes are depicted in Figure S2. TB was strongly associated with low levels of citrulline and ornithine, both central amino acids of the urea cycle (Figure 2D), whereas levels of arginine and aspartic acid, two other important intermediates in the urea cycle, were higher in TB patients. Furthermore, levels of histidine were significantly reduced, while those for phenylalanine were increased in TB patients, a finding which is congruent with previous metabolomics analyses⁽⁷⁾. The metabolite with the strongest positive association with TB was 3-methoxytyrosine, a metabolite of levodopa which is mostly associated with aromatic L-amino acid decarboxylase (AADC) deficiency. Other notable changes included significantly lower levels of tryptophan and higher plasma concentrations of kynurenine, two metabolites which are part of the immunoregulatory enzyme IDO pathway.

The metabolite profile of TB-DM patients (Figure 2B) was mostly characterized by low levels of amines when compared to HC, while only two metabolites, putrescine and glycylglycine, were significantly elevated. Similar to TB patients, TB-DM was associated with low levels of citrulline, histidine, ornithine and tryptophan, among others. However, the most notable difference was the exceptionally low average concentration of choline compared to HC ($q = 6.45E^{-19}$), an effect which was magnitudes stronger than observed in TB patients without DM (Figure 2C). Similarly, levels of serine, homoserine, glycine and threonine, were significantly lower in TB-DM patient plasma compared to TB patients, as well as to HC. These results are congruent with earlier studies describing decreased glycine, serine and threonine levels during DM^(14,15).

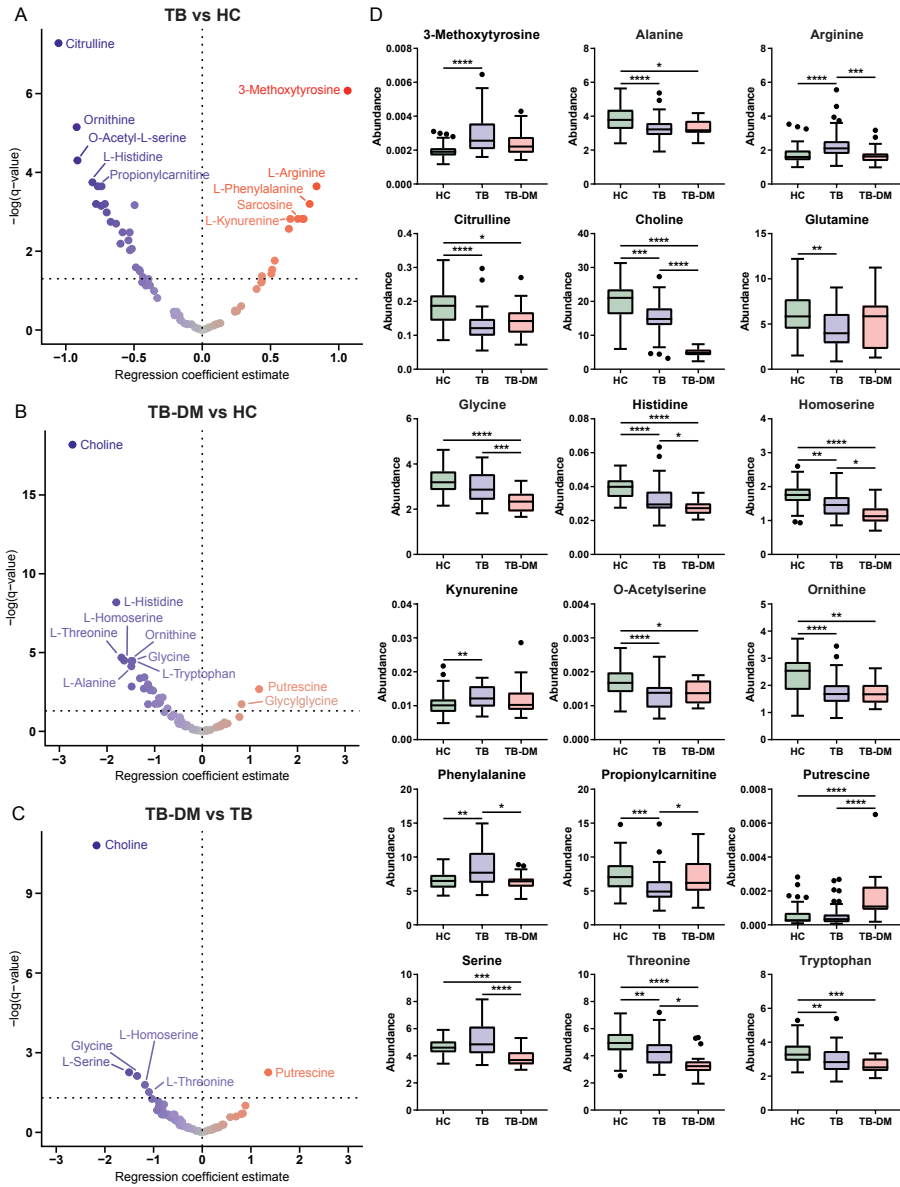


Figure 2: TB and TB-DM greatly impact patient plasma metabolite levels.

Multiple linear regression models were fitted for each between disease group comparison, and resulting $-\log$ -transformed p -values (q -values) are plotted against the regression coefficient estimate for each metabolite: TB vs HC (A), TB-DM vs HC (B), TB-DM vs TB (C). Each dot represents an individual metabolite. Dot color represents direction and size of the regression coefficient. The significance threshold ($q = 0.05$) is displayed as a horizontal dotted line. (D) Absolute abundance of individual metabolites per group displayed as Tukey's boxplots. Significance differences between HC ($n = 48$), TB ($n = 48$) and TB-DM ($n = 20$) groups were determined by Kruskal-Wallis test with post-hoc Dunn's test. * $p = 0.05$, ** $p = 0.01$, *** $p = 0.001$, **** $p = 0.0001$.

Metabolite ratios show potential for TB and TB-DM classification

In order to evaluate their potential as metabolic biomarkers for TB or TB-DM, receiver operating characteristic (ROC) curves were plotted per metabolite for each disease group comparison and the resulting AUC values were calculated (Supplementary Table 1). The three metabolites with the highest AUC values were subsequently incorporated into multivariate signatures and their classification effectiveness was tested by a linear support vector machines (SVM) machine learning algorithm (Figure 3A). Citrulline, 3-methoxytyrosine and arginine were the individual metabolites with the best classification capacity for TB versus HC, which was further improved by their inclusion in a multivariate signature (AUC: 0.913 [0.818 – 0.978]). As expected, choline was the superior biomarker for TB-DM versus HC from our dataset (AUC: 0.991 [0.977 – 1.000]), followed by histidine and glycine. Choline, serine and putrescine showed the highest potential for discriminating TB-DM from TB patients. Incorporation into cross-validated multivariate models in these cases resulted in similar AUC values (TB-DM vs HC: 0.995 [0.981 – 1.000]; TB-DM vs TB: 0.967 [0.940 – 0.998]). While some of our data validate published findings from African cohorts in an Asian cohort, the new TB-DM biomarker results reported here for the first time will need to be validated, including in age-matched cohorts as this was not corrected for in this analysis.

We previously identified the ratio of phenylalanine over histidine (Phe/His) as a promising biomarker for TB classification and diagnosis irrespective of DM-status in a South-African patient cohort⁽⁷⁾. This finding is corroborated independently in the current study in a genetically and geographically completely different cohort (Figure 3B): the Phe/His ratio demonstrated a superior classification capacity for TB versus HC compared to any individual metabolite (AUC: 0.912 [0.850 – 0.974]), and similar values were obtained for TB-DM patients vs HC (AUC: 0.908 [0.807 – 1.000]). Furthermore, multiple linear regression analyses showed a relative increase in kynurenine accompanied with decreased tryptophan in TB patients. The ratio between these amino acids (Kyn/Trp) reflects the activity of IDO, which catalyzes the rate-limiting step in the kynurenine pathway of tryptophan catabolism. The results (Figure 3C) showed that both TB and TB-DM were associated with an increased Kyn/Trp ratio (AUC: 0.838 [0.755 – 0.922]; AUC: 0.802 [0.682 – 0.921] respectively), indicative of increased IDO activity. Finally, various amino acids from the urea cycle were found to be divergently affected during TB, including citrulline and arginine (Cit/Arg) which are essential for nitric oxide (NO) production by NO synthase (NOS). TB but not TB-DM was associated with a decreased Cit/Arg ratio compared to HC (AUC: 0.895 [0.834 – 0.955]), possibly reflecting diminished NO production through NOS in these patients.

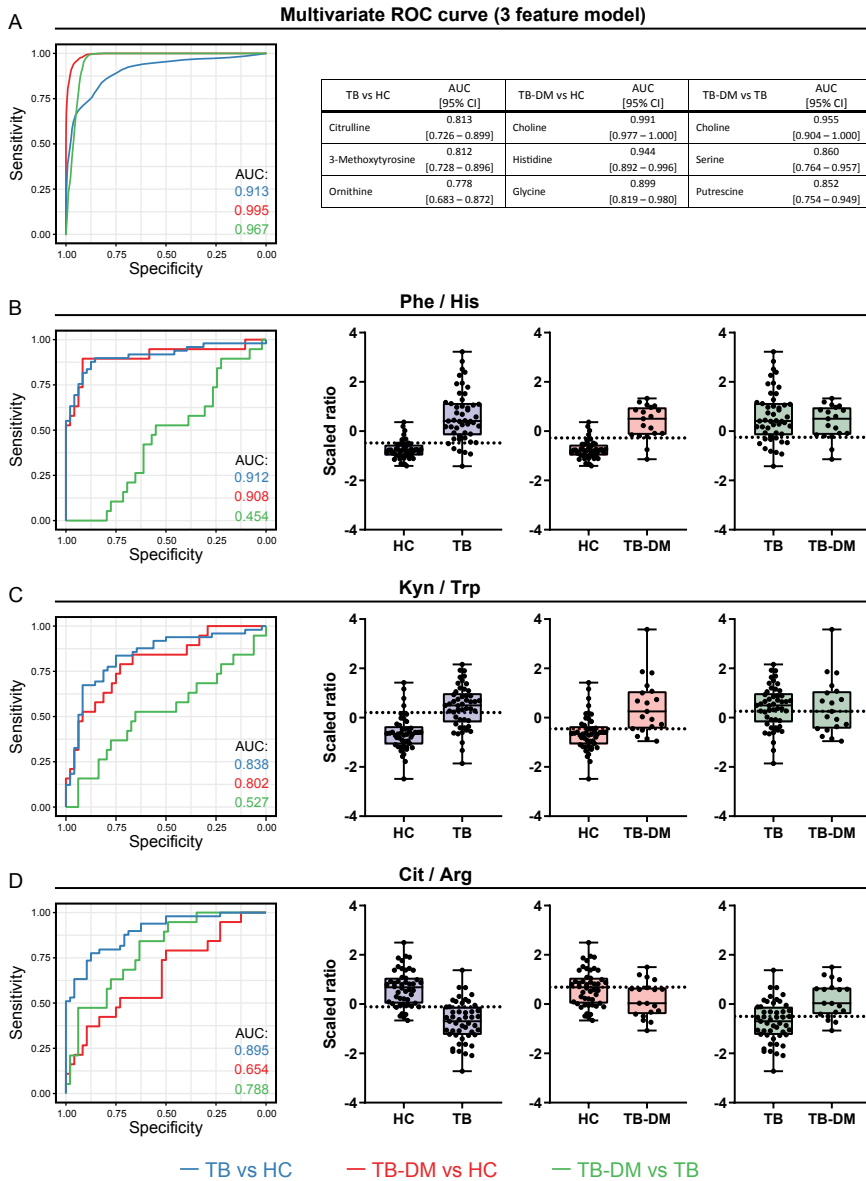


Figure 3: Biomarker analysis.

ROC curves and AUCs were determined for each metabolite and disease group comparison: TB vs HC (blue), TB-DM vs HC (red) and TB-DM vs TB (green). (A) The three metabolites with the highest AUCs per comparison were combined in a 3-feature model and corresponding multivariate ROC curves were fitted by linear support vector machine algorithm. (B-D) ROC curves and boxplots of the following metabolite ratios are shown: phenylalanine/histidine (Phe/His) (B), kynurenine/tryptophan (Kyn/Trp) (C) and citrulline/arginine (Cit/Arg) (D). Each dot represents an individual patient and the optimal cut-off as determined by Youden's statistic is displayed as a horizontal dotted line.

Anti-TB treatment resulted in normalization of diverging metabolites to healthy levels

Next, we sought to investigate the effect of anti-TB treatment on the metabolic profiles of TB and TB-DM patients. Plasma samples collected at both ~8 weeks and ~26 weeks after initiation of antibiotic treatment were available and measured for 45/49 TB and 18/19 TB-DM patients, respectively. Successful TB treatment was associated with a significant linear positive effect for 29 metabolites in TB patients (Figure 4A), while 4 metabolites were downregulated during anti-TB therapy. Many metabolites which were lower in TB patients at diagnosis normalized to HC levels during treatment duration, including citrulline, glutamine, tryptophan, histidine and ornithine, while glycylglycine and phenylalanine were decreased as a result of therapy after previously being upregulated in TB patients' plasma. Interestingly, 3-methoxytyrosine did not normalize to HC levels during treatment ($q = 0.928$), and could therefore represent a long-lasting TB-associated biomarker.

The metabolic effects of treatment in TB and TB-DM patients showed strong similarities (Figure 4B-C) as demonstrated by significant positive correlations of metabolite regression coefficients ($r^2: 0.528, p = 2.35E^{-13}$). Metabolites with significant treatment-associated effects in both groups were glutamine, gamma-glutamylglutamine, gamma-glutamylalanine, histidine, citrulline, proline, O-acetylserine and glutamate. Interestingly, the levels of glutamine and gamma-glutamylglutamine were significantly higher in TB-DM patients compared to HC at the end of treatment ($p < 0.01$), while glutamate was simultaneously decreased ($p < 0.0001$) (Figure 4D). Although treatment resulted in normalization of choline to HC levels in TB patients ($q = 9.40E^{-3}$), choline concentrations remained very low in TB-DM patients ($q = 0.756$). In addition, levels of glycine, serine, threonine and homoserine did not increase with treatment, further establishing their association with DM in these patients.

As the 2HRZE/4H3R3 treatment regimen is more intensive during the first two months compared to the last four, it is reasonable to expect that a subset of metabolites would react to treatment in a non-linear fashion. Therefore, separate mixed models were fitted for time periods 0 to 8 weeks and 8 to 26 weeks in both disease groups (Figure S3A-B). Similar to the general linear treatment model, the effects of treatment in TB and TB-DM patients were positively correlated during both 0 to 8 weeks ($r^2: 0.739, p = 1.04E^{-22}$) and 8 to 26 weeks ($r^2: 0.532, p = 1.67E^{-13}$). When comparing changes in metabolite levels between both time periods, some inverse relationships were observed in both TB and TB-DM patients (Figure S3C-E). Two metabolites were strongly increased during the first 8 weeks of treatment in both patient populations, namely methionine sulfone and putrescine, while their levels had significantly receded at the end of treatment. In TB patients, 7 metabolites followed an opposite trend with decreased levels at 8 weeks followed by a rise at 26 weeks post-treatment (Figure S3C), i.e. methionine, glycylproline, asparagine, octenoylcarnitine, lysine, phenylalanine and serine; similar effects were observed in TB-DM patients for all but the latter (Figure S3D).

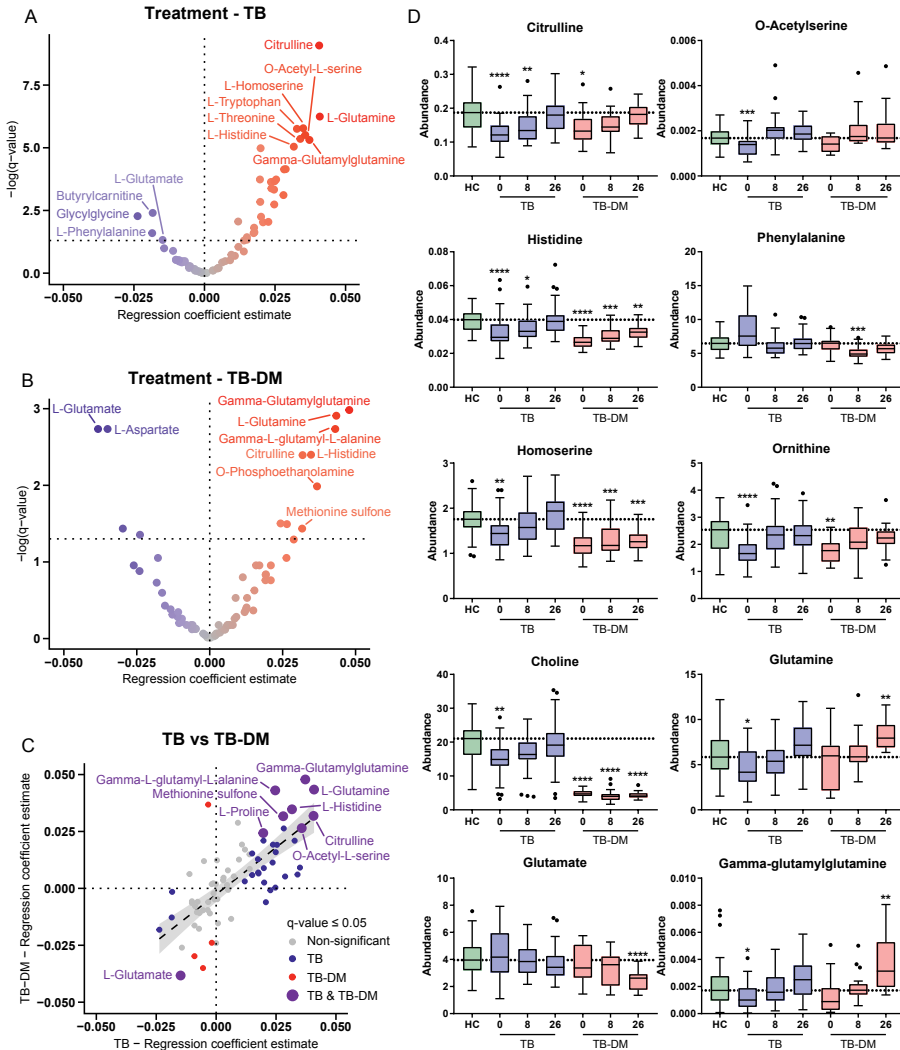


Figure 4: Anti-TB treatment leads to normalization of patient plasma metabolic profiles to HC levels.

Linear mixed models were fitted for the effect of antibiotic treatment on metabolite levels in TB patients (A) and TB-DM patients (B) separately. Resulting $-\log$ -transformed p -values (q -values) are plotted against the regression coefficient estimate for each metabolite. Each dot represents an individual metabolite. Dot color represents direction and size of the regression coefficient. The significance threshold ($q = 0.05$) is displayed as a horizontal dotted line. (C) Beta-beta plot of metabolite regression coefficients for the effect of anti-TB treatment in TB patients (x-axis) versus TB-DM patients (y-axis). Each dot represents an individual metabolite. Dot color represents whether the metabolite was significantly affected by anti-TB treatment in TB patients (blue), TB-DM patients (red), both (purple) or not at all (grey). Regression line is displayed as a dashed line with 95% confidence interval. (D) Absolute abundance of individual metabolites per group displayed as Tukey's boxplots. For TB and TB-DM patients metabolite levels are displayed at 0, 8 and 26 weeks post-treatment. Significance differences between HC ($n = 48$) versus TB ($n = 44$) or TB-DM ($n = 19$) patients were determined by Kruskal-Wallis test with post-hoc Dunn's test. * $p = 0.05$, ** $p = 0.01$, *** $p = 0.001$, **** $p = 0.0001$.

Metabolite associations with TB severity

Finally, we wondered whether some metabolites could be related to TB severity as quantified by CXR score (mild or advanced lesions). To investigate this, CXR was added as a covariate to our initial regression model which was subsequently fitted on TB and TB-DM patients combined. Eleven metabolites showed a significant association with CXR score, however none of these survived FDR-correction, indicating that the statistical power of this dataset was insufficient to accurately assess this question. Nonetheless, to highlight possible trends of metabolic associations with TB severity, we performed classical biomarker analysis using CXR score as identifier and only selected metabolites with univariate t-test statistic p -values < 0.01 . This resulted in five metabolites with a potential positive association with advanced CXR lesions (Figure S4), including four acylcarnitines (hexanoylcarnitine, 3-methoxytyrosine, hexadecenoylcarnitine, dodecenoylcarnitine, tetradecenoylcarnitine). These results suggest that while acylcarnitine levels were not strongly associated with TB or TB-DM in the initial regression analysis, some could specifically be affected in individuals with severe disease. These results will have to be validated in studies with more statistical power.

Discussion

Here, we applied plasma metabolomics to identify differences in amine and acylcarnitine levels associated with TB or TB-DM in a cohort of Indonesian patients at the time of diagnosis as well as during longitudinal follow-up over the course of antibiotic treatment. We identified several potential biomarkers with high AUC values for TB and/or TB-DM diagnosis, which included ratios of citrulline, arginine, phenylalanine and histidine among others. Overall, levels of many amines were decreased in both TB and TB-DM patients at diagnosis compared to HC, while relatively few acylcarnitines were affected. TB patients were further characterized by relatively high levels of several metabolites including the L-DOPA metabolite 3-methoxytyrosine, whereas only putrescine, a polyamine associated with DM⁽¹⁶⁾, was found to be specifically elevated in TB-DM. This lack of positively correlated metabolites in the TB-DM group was surprising to some extent, as DM is often linked to overnutrition and our previous results have demonstrated that TB-DM patients from a South-African cohort displayed major hallmarks of DM, *e.g.* hyperglycemia, dyslipidemia and elevated branched-chain amino acids⁽⁷⁾. TB-DM patients were further characterized by lower levels of glycine, serine, threonine and homoserine compared to TB patients, which were similarly unaffected by TB treatment. These amino acids are part of the same biosynthetic pathway and have been implicated in the development of non-alcoholic fatty liver disease (NAFLD)^(17,18), a liver disorder commonly associated with DM and insulin resistance⁽¹⁹⁾.

Importantly, the majority of TB-related metabolites normalized towards HC levels during antibiotic treatment, substantiating their association with active disease. Exceptions to this included choline, which was dramatically lowered in plasma of patients

with TB-DM compared to both HC and TB patients and did not change in response to treatment in these patients. We consider it unlikely that this effect is an artifact introduced during measurement or blood collection, as all samples were randomized and blinded before technical analysis and the results were very consistent over multiple independent time points. Decreased choline bioavailability due to reduced intake or gut microbiome dysbiosis have been linked to NAFLD^(20,21) and therefore align with the detected low levels of glycine, serine, threonine and homoserine, all of which similarly did not normalize to HC levels during treatment. However, this result should be interpreted with some caution as similar levels of choline deficiency during either TB or DM have not been reported before to the best of our knowledge.

Our results are in concordance with -and independently validate- earlier metabolic biomarker studies for TB, currently in a cohort from Indonesia. We previously found reduced concentrations of histidine, glutamine, alanine and valine in TB patients from South-Africa combined with high phenylalanine levels⁽⁷⁾, and the described high predictive capacity of the Phe/His ratio as a biomarker for TB regardless of DM-status was confirmed in this current cohort. Similarly, Weiner *et al.* reported lower serum levels of histidine, citrulline, glutamine, gamma-glutamylglutamine, alanine and threonine in active TB patients, while phenylalanine, 3-methoxytyrosine and aspartic acid were elevated^(12, 22). Low levels of tryptophan and/or high concentrations of kynurenine have been demonstrated in both TB patients' sera⁽²²⁻²⁴⁾ and pleural fluids⁽²⁵⁾. An increased Kyn/Trp ratio is an estimate of enhanced activity of the immunoregulatory enzyme IDO, which was found to benefit *Mtb* infection both *in vitro* and *in vivo*⁽²⁶⁾, and showed potential as a biomarker for TB diagnosis in our analysis. This striking agreement between TB metabolomics studies performed using diverse technical platforms as well as patient cohorts from different geographical regions confirms and highlights the robustness of the platforms and resulting data, as well as its potential for diagnosis and prognosis of TB⁽¹²⁾.

TB patients showed decreased levels of citrulline and ornithine, whereas arginine and aspartic acid concentrations were elevated. Furthermore, the Cit/Arg ratio displayed good predictive capacity for TB vs HC, but not for TB-DM vs HC. Citrulline, ornithine, arginine and aspartic acid are important intermediates of the urea cycle, which is responsible for the majority of nitrogen excretion through conversion of toxic ammonia to urea in the liver⁽²⁷⁾. At the beginning of the cycle, citrulline is formed from ornithine and ammonia, which subsequently reacts with aspartic acid to form arginine through arginosuccinate. Arginine can then be hydrolyzed by arginase to form urea and ornithine, or be used by NOS leading to the production of NO and citrulline, a balance which has shifted in TB patients as reflected by their relatively decreased Cit/Arg ratio. In mouse models of TB disease, arginase 1 (Arg1) expression in myeloid cells from TB granulomas has been demonstrated to exacerbate disease through substrate competition with NOS^(28,29). Citrulline, however, was shown to fuel antimycobacterial mechanisms of murine macrophages^(30,31) and T-cells⁽²³⁾ as an alternative source of intracellular arginine, implying that decreased citrulline

levels could be detrimental for TB patients. Although the importance of arginase and NO production for the antimycobacterial response in humans remains controversial, *ARG1* was found to be expressed in granulomatous tissue of TB patients^(33,34) and could therefore play a role in TB pathophysiology. Whether the observed changes in arginine, citrulline and ornithine are caused by changes in expression or activity of these enzymes cannot be ascertained from these results, and will have to be addressed in future studies.

Antibiotic treatment led to normalization to HC levels for the majority of TB-associated metabolites in both TB and TB-DM patients, including citrulline, ornithine, histidine and phenylalanine. In contrast, a subset of metabolites specifically changed during the first 2 months of intensive treatment, of which the strongly increased concentrations of methionine sulfone and putrescine were especially striking. Methionine is susceptible to oxidative modification by reactive oxygen species (ROS), and high levels of oxidized methionine are therefore regarded as a marker of oxidative stress⁽³⁵⁾. While initial oxidation of methionine leads to the reversible formation of methionine sulfoxide, the second oxidation step to form methionine sulfone is effectively irreversible. Methionine oxidation was found to be associated with drug-induced liver injury⁽³⁶⁾, which could be the cause of the observed elevation of methionine sulfone during intensive antibiotic treatment. Surprisingly, although plasma methionine concentrations were appropriately decreased, levels of methionine sulfoxide were not affected by antibiotic treatment in either TB or TB-DM patients. In addition to oxidized methionine, the authors reported elevated levels of gamma-glutamyl dipeptides during various types of liver injury⁽³⁶⁾. Gamma-glutamyl dipeptides are formed by gamma-glutamyltransferase (GGT) as byproducts of anti-oxidative glutathione synthesis and therefore reflect oxidative stress. GGT is widely used as a diagnostic marker for hepatic disease and alcohol consumption⁽³⁷⁾, and high circulating GGT levels are a risk factor for DM development⁽³⁸⁾. Correspondingly, we found that gamma-glutamylalanine and gamma-glutamylglutamine increased with antibiotic treatment, even to levels above HC in TB-DM patients for the latter, which could be indicative of enhanced GGT activity as a result of treatment. Additionally, high levels of putrescine were similarly shown to be associated with hepatotoxicity and antibiotic treatment in animal models^(39,40). Taken together, anti-TB therapy correlated with increased levels of metabolic biomarkers associated with liver injury and oxidative stress, especially during early intensive antibiotic treatment, emphasizing the necessity of liver function monitoring during this period. Since the final blood samples were collected at the end of treatment, it would be informative to measure the abundance of these metabolites sometime after end of therapy in the future to possibly study liver function recovery.

As a result of limitations in patient sampling, several possible confounders of the study need to be discussed. Firstly, TB-DM patients were significantly older compared to both HC and TB patients. Although we attempted to correct for this by including age as a covariate in the regression analyses, it cannot be fully excluded that differences in age explain a proportion of the data variance in TB-DM patients, as levels of threonine,

histidine, glycine and serine, for instance, have been demonstrated to decrease with age⁽⁴¹⁾. Secondly, the average BMI was significantly different between the three groups, which could be correlated with changes in metabolite levels. However, we purposefully chose not to adjust for BMI in our analysis as it is intrinsically associated with the pathophysiology of both TB and DM and consequently its possible effect on patients' metabolic profiles. Similarly, we could not control for differences in factors such as nutrition and microbiome composition which could also have caused certain specific metabolite alterations. Thirdly, as these measurements were performed on a historic patient cohort no additional control groups could be included. In order to confirm the specificity of the reported metabolic changes for disease, future studies should include DM patients without TB and compare TB to other respiratory or infectious diseases. A recent paper which compared circulating amine and acylcarnitines levels of lung cancer patients to healthy controls reported increased plasma arginine levels while citrulline and glycine were decreased, similar to what we observed for TB, indicating that these could potentially be a reflection of general lung pathology⁽⁴²⁾. In contrast, no consistent changes were observed for the other TB-associated amines such as histidine and phenylalanine that we identified. Additionally, a metabolomics study on chronic obstructive pulmonary disease (COPD) showed little overlap with our observations⁽⁴³⁾, supporting the specificity of these results for TB. Finally, the use of anti-diabetic medication could have influenced the concentrations of metabolites in the TB-DM group.

In conclusion, TB and TB-DM are associated with marked changes in plasma levels of amine metabolites, which normalize during anti-TB therapy. The presence of TB-DM-specific changes indicates that this comorbidity needs to be considered for the development of diagnostic tests for TB based on levels of metabolic intermediates. This study supports the use of relevant metabolite ratios as potential biomarkers for TB, and it would be of great interest to investigate their possible relation with TB disease progression, severity and treatment outcome in future studies.

Materials & Methods

Study subjects

Patients plasma samples included in this study were randomly selected, based on sample availability, from a previously described cohort from Indonesia⁽⁴⁴⁾. In brief, newly diagnosed active pulmonary TB patients were recruited from January 2002 to December 2004 at an outpatient TB treatment center in Jakarta. TB diagnosis was established according to World Health Organization (WHO) criteria, on the basis of clinical presentation and a chest X-ray radiograph (CXR) and confirmed by microscopic detection of acid-fast bacilli in Ziehl-Nielsen-stained sputum smears and positive culture of *Mtb*. Human immunodeficiency virus (HIV)-seropositive patients, patients with cardiac diseases and patients with incomplete data records were excluded. TB patients were classified as having mild-to-moderate TB or advanced TB on the basis of the extent of

lesions on CXR. CXR results were divided into lower, middle and upper lung regions, left and right, and abnormalities were scored as 'mild' (1 of 6 areas involved), 'moderate' (2 or 3 out of 6 areas) or advanced (more than 3 areas involved)⁽⁴⁵⁾. Diabetes was diagnosed if fasting blood glucose (FBG) was >126 mg/dl, in accordance with WHO criteria at time of recruitment, or by self-reported diabetes. In the same period, healthy individuals matched for sex and age ($\pm 10\%$) and living within the same rukun tetangga (consisting of 15-30 households) were included as control subjects. Controls with diabetes, signs, symptoms, and CXR results suggestive of active TB, a history of anti-TB treatment or incomplete data entry were excluded. HIV status was not tested in the control group, however Indonesia was classified as a country with a low HIV prevalence of $\leq 0.1\%$ at time of study subject recruitment. Free anti-TB drug treatment was provided to all patients, which consisted of a standard regimen of isoniazid, rifampin, pyrazinamide, and ethambutol (2HRZE/4H3R3) according to the Indonesian national TB program guideline. A subgroup of patients was followed longitudinally, from which blood samples were collected at two and six months after start of treatment. This study was approved by the Ethical Committee of the Faculty of Medicine, University of Indonesia, Jakarta, and by the Eijkman Institute Research Ethics Committee, Jakarta, and written informed consent was voluntarily signed by all patients and control subjects. All research was performed in accordance with relevant guidelines and regulations at time of recruitment.

LC-MS/MS

Metabolite levels in plasma were measured in individual replicates using two targeted LC-MS/MS platforms. Subject numbers were randomized and run in 5 batches which included a calibration line, QC samples and blanks. QC samples were analyzed every 10 samples, they are used to assess data quality and to correct for instrument response. Blanks are used to check for blank effects.

The amine platform covers amino acids and biogenic amines employing an Accq-Tag derivatization strategy adapted from the protocol supplied by Waters⁽⁴⁶⁾. 5.0 μL of each sample was spiked with an internal standard solution. Then proteins were precipitated by the addition of MeOH. The supernatant was taken to dryness in a speedvac. The residue was reconstituted in borate buffer (pH 8.5) with AQC reagent. 1.0 μL of the reaction mixture was injected into the UPLC-MS/MS system. Chromatographic separation was achieved by an Agilent 1290 Infinity II LC System on an Accq-Tag Ultra column (Waters). The UPLC was coupled to electrospray ionization on a triple quadrupole mass spectrometer (AB SCIEX Qtrap 6500). Analytes were detected in the positive ion mode and monitored in Multiple Reaction Monitoring (MRM) using nominal mass resolution. Acquired data were evaluated using MultiQuant Software for Quantitative Analysis (AB SCIEX, Version 3.0.2).

The acylcarnitine platform covers acylcarnitines as well as Trimethylamine-N-oxide, Choline, Betaine, Deoxycarnitine and Carnitine. 10 μL of each sample was spiked with an internal standard solution. Then proteins were precipitated by the addition

of MeOH. 1.0 μL of the reaction mixture was injected into the UPLC-MS/MS system. Chromatographic separation was achieved by UPLC (Agilent 1290, San Jose, CA, USA) on an Accq-Tag Ultra column (Waters). The UPLC was coupled to electrospray ionization on a triple quadrupole mass spectrometer (Agilent 6460, San Jose, CA, USA). Analytes were detected in the positive ion mode and monitored in Multiple Reaction Monitoring (MRM) using nominal mass resolution. Acquired data were evaluated using Agilent MassHunter Quantitative Analysis software (Agilent, Version B.05.01).

The data are expressed as relative response ratios (target area/ISTD area; unit free) using proper internal standards. For analysis of amino acids their $^{13}\text{C}^{15}\text{N}$ -labeled analogs were used. For other metabolites, the closest-eluting internal standard was employed. All internal standards are listed in Supplementary Table 2. In-house developed algorithms were applied using the pooled QC samples to compensate for shifts in the sensitivity of the mass spectrometer over the batches. After quality control correction, metabolite targets complied with the acceptance criteria of $\text{RSD}_{\text{qc}} < 15\%$.

Statistical analysis

For multivariate analysis, metabolite measurements were log transformed, mean centered and scaled to standard deviation units. After preprocessing, the data variance associated with disease or sex were investigated by principal component analysis (PCA) and hierarchical clustering. Differences between disease groups were further visualized by fitting three component partial least squares discriminant analysis (PLS-DA) models for each disease group comparison. PLS-DA model evaluation criteria (Q^2 , R^2X , R^2Y) were determined after leave-one-out cross validation.

To identify significant differences in metabolite levels between the three groups at diagnosis while correcting for age and sex, the following multiple linear regression model was fitted for each metabolite in separate two-level disease group comparisons (TB vs HC, TB-DM vs HC and TB-DM vs TB):

$$\text{Metabolite} = \beta_0 + \beta_1 \text{ Disease} + \beta_2 \text{ Age} + \beta_3 \text{ Sex} + \varepsilon$$

where *Disease* = disease group (HC, TB or TB-DM), *Age* = age (years) and *Sex* = sex (male/female).

CXR score was consequently added to the model as a covariate to investigate possible metabolite associations with TB severity.

To analyze and compare the effect of anti-TB treatment on metabolite levels in TB and TB-DM patients, the following linear mixed effect model with random intercept for each individual study participant (u_0 *Subject*) was fitted for the TB and TB-DM groups separately:

$$\text{Metabolite} = (\beta_0 + u_0 \text{ Subject}) + \beta_1 \text{ Treatment} + \beta_2 \text{ Age} + \beta_3 \text{ Sex} + \varepsilon$$

where *Treatment* = duration of treatment (weeks), *Age* = age (years) and *Sex* = sex (male/female).

Resulting *p*-values were corrected by False Discovery Rate (FDR) using the Benjamini–Hochberg procedure to obtain *q*-values, which were subsequently $-\log$ transformed and plotted versus the regression coefficient estimate (β_1) to generate metabolite volcano plots. Alternatively, regression coefficient estimates of two comparisons were plotted against each other (beta-beta plots).

For univariate biomarker analysis, metabolite receiver operating characteristic (ROC) plots and area under the curves (AUCs) were generated for each disease group comparison based on the optimal cut-off as calculated by Youden's J statistic⁴⁷, defined as the value for which the distance to the diagonal line is maximal. AUC 95% confidence intervals (CI) were computed using 2000 stratified bootstrapping samples. Furthermore, for each group comparison the three metabolites with the highest univariate AUCs were combined in a three parameter metabolic signature. Multivariate ROC curves and AUCs were calculated using a linear SVM algorithm included in the MetaboAnalyst R package (version 1.01.)⁽⁴⁸⁾ after hundredfold repeated random sub-sampling cross validation, during which 2/3 of the samples were used for model training and the remaining 1/3 for model testing.

Statistical analysis of clinical characteristics was performed in SPSS 23 (IBM) by one-way ANOVA (reported *p*-values are the outcome of the F-test) or chi-squared test. Analysis of absolute metabolite concentrations was done in Graphpad Prism 7 by Kruskal-Wallis test with post-hoc Dunn's test. PCA, PLS-DA, hierarchical clustering, multiple linear regression and linear mixed modeling were performed using R version 3.5.0. and the following packages: mixOmics version 6.3.2⁽⁴⁹⁾, lme4 version 1.1.17⁽⁵⁰⁾, lmerTest version 3.0.1⁽⁵¹⁾ and ggplot2 version 3.1.0⁽⁵²⁾

Data availability statement

All data underlying this study are included within the manuscript and its Supporting Information files.

Acknowledgements

Not applicable.

Author Contributions

Conceived and designed the study: SAJ, THMO. Supervised sample collection and selection: BA, ES, RvC. Performed analytical measurements: ACH, TH. Analyzed the data: FV, SAJ, THMO. Wrote the paper: FV, SAJ, THMO.

Funding Sources

This study was supported by the TANDEM (Tuberculosis and Diabetes Mellitus) Grant of the ECFP7 (European Union's Seventh Framework Programme) under Grant Agreement No. 305279 and by TBVAC2020 Grant of EC HOR2020 (Grant Agreement No. 643381) for data analysis and interpretation.

Competing Interests Statement

All authors: no reported conflicts.

References

- 1 World Health Organization. Global Tuberculosis Report. (Geneva, Switzerland, 2018).
- 2 Nijland, H. M. *et al.* Exposure to rifampicin is strongly reduced in patients with tuberculosis and type 2 diabetes. *Clin Infect Dis* **43**, 848-854, doi:10.1086/507543 (2006).
- 3 Koesoemadinata, R. C. *et al.* Latent TB infection and pulmonary TB disease among patients with diabetes mellitus in Bandung, Indonesia. *Trans R Soc Trop Med Hyg* **111**, 81-89, doi:10.1093/trstmh/trx015 (2017).
- 4 Ugarte-Gil, C. *et al.* Diabetes mellitus among pulmonary tuberculosis patients from four TB-endemic countries: the TANDEM study. *Clin Infect Dis*, doi:10.1093/cid/ciz284 (2019).
- 5 World Health Organization. Diabetes & TB - fact sheet. (Geneva, Switzerland 2016).
- 6 International Diabetes Federation. Diabetes Atlas. 8th edn., (Brussels, Belgium 2017).
- 7 Vrieling, F. *et al.* Patients with Concurrent Tuberculosis and Diabetes Have a Pro-Atherogenic Plasma Lipid Profile. *EBioMedicine*, doi:10.1016/j.ebiom.2018.05.011 (2018).
- 8 Varma, V. R. *et al.* Brain and blood metabolite signatures of pathology and progression in Alzheimer disease: A targeted metabolomics study. *PLoS Med* **15**, e1002482, doi:10.1371/journal.pmed.1002482 (2018).
- 9 Armitage, E. G. & Ciborowski, M. Applications of Metabolomics in Cancer Studies. *Adv Exp Med Biol* **965**, 209-234, doi:10.1007/978-3-319-47656-8_9 (2017).
- 10 Pallares-Mendez, R., Aguilar-Salinas, C. A., Cruz-Bautista, I. & Del Bosque-Plata, L. Metabolomics in diabetes, a review. *Ann Med* **48**, 89-102, doi:10.3109/07853890.2015.1137630 (2016).
- 11 Salgado-Bustamante, M. *et al.* Metabolomics applied to the discovery of tuberculosis and diabetes mellitus biomarkers. *Biomark Med* **12**, 1001-1013, doi:10.2217/bmm-2018-0050 (2018).
- 12 Weiner, J. *et al.* Metabolite changes in blood predict the onset of tuberculosis. *Nature communications* **9**, 5208, doi:10.1038/s41467-018-07635-7 (2018).
- 13 Westerhuis, J. A., van Velzen, E. J., Hoefsloot, H. C. & Smilde, A. K. Multivariate paired data analysis: multilevel PLSDA versus OPLSDA. *Metabolomics* **6**, 119-128, doi:10.1007/s11306-009-0185-z (2010).
- 14 Adeva-Andany, M. *et al.* Insulin resistance and glycine metabolism in humans. *Amino Acids* **50**, 11-27, doi:10.1007/s00726-017-2508-0 (2018).
- 15 Berteau, M. *et al.* Deoxysphingoid bases as plasma markers in diabetes mellitus. *Lipids Health Dis* **9**, 84, doi:10.1186/1476-511X-9-84 (2010).
- 16 Fernandez-Garcia, J. C. *et al.* Type 2 Diabetes Is Associated with a Different Pattern of Serum Polyamines: A Case(-)Control Study from the PREDIMED-Plus Trial. *J Clin Med* **8**, doi:10.3390/jcm8010071 (2019).
- 17 Mardinoglu, A. *et al.* Personal model-assisted identification of NAD(+) and glutathione metabolism as intervention target in NAFLD. *Mol Syst Biol* **13**, 916, doi:10.15252/msb.20167422 (2017).

- 18 Gaggini, M. *et al.* Altered amino acid concentrations in NAFLD: Impact of obesity and insulin resistance. *Hepatology* **67**, 145-158, doi:10.1002/hep.29465 (2018).
- 19 Tilg, H., Moschen, A. R. & Roden, M. NAFLD and diabetes mellitus. *Nat Rev Gastroenterol Hepatol* **14**, 32-42, doi:10.1038/nrgastro.2016.147 (2017).
- 20 Sharpton, S. R., Ajmera, V. & Loomba, R. Emerging Role of the Gut Microbiome in Nonalcoholic Fatty Liver Disease: From Composition to Function. *Clin Gastroenterol Hepatol* **17**, 296-306, doi:10.1016/j.cgh.2018.08.065 (2019).
- 21 Leermakers, E. T. *et al.* Effects of choline on health across the life course: a systematic review. *Nutr Rev* **73**, 500-522, doi:10.1093/nutrit/nuv010 (2015).
- 22 Weiner, J., 3rd *et al.* Biomarkers of inflammation, immunosuppression and stress with active disease are revealed by metabolomic profiling of tuberculosis patients. *PLoS one* **7**, e40221, doi:10.1371/journal.pone.0040221 (2012).
- 23 Suzuki, Y. *et al.* Serum indoleamine 2,3-dioxygenase activity predicts prognosis of pulmonary tuberculosis. *Clin Vaccine Immunol* **19**, 436-442, doi:10.1128/CVI.05402-11 (2012).
- 24 Feng, S. *et al.* Analysis of serum metabolic profile by ultra-performance liquid chromatography-mass spectrometry for biomarkers discovery: application in a pilot study to discriminate patients with tuberculosis. *Chin Med J (Engl)* **128**, 159-168, doi:10.4103/0366-6999.149188 (2015).
- 25 Suzuki, Y. *et al.* Indoleamine 2,3-dioxygenase in the pathogenesis of tuberculous pleurisy. *Int J Tuberc Lung Dis* **17**, 1501-1506, doi:10.5588/ijtld.13.0082 (2013).
- 26 Gautam, U. S. *et al.* In vivo inhibition of tryptophan catabolism reorganizes the tuberculoma and augments immune-mediated control of Mycobacterium tuberculosis. *Proceedings of the National Academy of Sciences of the United States of America* **115**, E62-E71, doi:10.1073/pnas.1711373114 (2018).
- 27 Morris, S. M., Jr. Regulation of enzymes of the urea cycle and arginine metabolism. *Annu Rev Nutr* **22**, 87-105, doi:10.1146/annurev.nutr.22.110801.140547 (2002).
- 28 El Kasmi, K. C. *et al.* Toll-like receptor-induced arginase 1 in macrophages thwarts effective immunity against intracellular pathogens. *Nature immunology* **9**, 1399-1406, doi:10.1038/ni.1671 (2008).
- 29 Monin, L. *et al.* Helminth-induced arginase-1 exacerbates lung inflammation and disease severity in tuberculosis. *The Journal of clinical investigation* **125**, 4699-4713, doi:10.1172/JCI77378 (2015).
- 30 Rapovy, S. M. *et al.* Differential Requirements for L-Citrulline and L-Arginine during Antimycobacterial Macrophage Activity. *Journal of immunology* **195**, 3293-3300, doi:10.4049/jimmunol.1500800 (2015).
- 31 Lange, S. M. *et al.* L-Arginine Synthesis from L-Citrulline in Myeloid Cells Drives Host Defense against Mycobacteria In Vivo. *Journal of immunology*, doi:10.4049/jimmunol.1801569 (2019).
- 32 Lange, S. M. *et al.* L-Citrulline Metabolism in Mice Augments CD4(+) T Cell Proliferation and Cytokine Production In Vitro, and Accumulation in the Mycobacteria-Infected Lung. *Frontiers in immunology* **8**, 1561, doi:10.3389/fimmu.2017.01561 (2017).

- 33 Pessanha, A. P., Martins, R. A., Mattos-Guaraldi, A. L., Vianna, A. & Moreira, L. O. Arginase-1 expression in granulomas of tuberculosis patients. *FEMS Immunol Med Microbiol* **66**, 265-268, doi:10.1111/j.1574-695X.2012.01012.x (2012).
- 34 Mattila, J. T. *et al.* Microenvironments in tuberculous granulomas are delineated by distinct populations of macrophage subsets and expression of nitric oxide synthase and arginase isoforms. *Journal of immunology* **191**, 773-784, doi:10.4049/jimmunol.1300113 (2013).
- 35 Suzuki, S. *et al.* Methionine sulfoxides in serum proteins as potential clinical biomarkers of oxidative stress. *Sci Rep* **6**, 38299, doi:10.1038/srep38299 (2016).
- 36 Soga, T. *et al.* Serum metabolomics reveals gamma-glutamyl dipeptides as biomarkers for discrimination among different forms of liver disease. *J Hepatol* **55**, 896-905, doi:10.1016/j.jhep.2011.01.031 (2011).
- 37 Whitfield, J. B. Gamma glutamyl transferase. *Critical reviews in clinical laboratory sciences* **38**, 263-355, doi:10.1080/20014091084227 (2001).
- 38 Kunutsor, S. K., Abbasi, A. & Adler, A. I. Gamma-glutamyl transferase and risk of type II diabetes: an updated systematic review and dose-response meta-analysis. *Ann Epidemiol* **24**, 809-816, doi:10.1016/j.annepidem.2014.09.001 (2014).
- 39 Bunes, A. *et al.* Identification of metabolites, clinical chemistry markers and transcripts associated with hepatotoxicity. *PLoS one* **9**, e97249, doi:10.1371/journal.pone.0097249 (2014).
- 40 Yu, M. *et al.* Marked Response in Microbial Community and Metabolism in the Ileum and Cecum of Suckling Piglets After Early Antibiotics Exposure. *Frontiers in microbiology* **9**, 1166, doi:10.3389/fmicb.2018.01166 (2018).
- 41 Kouchiwa, T. *et al.* Age-related changes in serum amino acids concentrations in healthy individuals. *Clin Chem Lab Med* **50**, 861-870, doi:10.1515/cclm-2011-0846 (2012).
- 42 Ni, J., Xu, L., Li, W., Zheng, C. & Wu, L. Targeted metabolomics for serum amino acids and acylcarnitines in patients with lung cancer. *Exp Ther Med* **18**, 188-198, doi:10.3892/etm.2019.7533 (2019).
- 43 Novotna, B. *et al.* A pilot data analysis of a metabolomic HPLC-MS/MS study of patients with COPD. *Advances in clinical and experimental medicine : official organ Wroclaw Medical University* **27**, 531-539, doi:10.17219/acem/68763 (2018).
- 44 Sahiratmadja, E. *et al.* Dynamic changes in pro- and anti-inflammatory cytokine profiles and gamma interferon receptor signaling integrity correlate with tuberculosis disease activity and response to curative treatment. *Infection and immunity* **75**, 820-829, doi:10.1128/IAI.00602-06 (2007).
- 45 Falk, A. Classification of pulmonary tuberculosis. *Diagnostic standards and classification of tuberculosis*, 68-76 (1969).
- 46 Noga, M. J. *et al.* Metabolomics of cerebrospinal fluid reveals changes in the central nervous system metabolism in a rat model of multiple sclerosis. *Metabolomics* **8**, 253-263, doi:10.1007/s11306-011-0306-3 (2012).
- 47 Youden, W. J. Index for rating diagnostic tests. *Cancer* **3**, 32-35 (1950).

- 48 Chong, J. & Xia, J. MetaboAnalystR: an R package for flexible and reproducible analysis of metabolomics data. *Bioinformatics* **34**, 4313-4314, doi:10.1093/bioinformatics/bty528 (2018).
- 49 Rohart, F., Gautier, B., Singh, A. & Le Cao, K. A. mixOmics: An R package for 'omics feature selection and multiple data integration. *PLoS Comput Biol* **13**, e1005752, doi:10.1371/journal.pcbi.1005752 (2017).
- 50 Bates, D., Mächler, M., Bolker, B. & Walker, S. Fitting Linear Mixed-Effects Models Using lme4. *2015* **67**, 48, doi:10.18637/jss.v067.i01 (2015).
- 51 Kuznetsova, A., Brockhoff, P. B. & Christensen, R. H. B. lmerTest Package: Tests in Linear Mixed Effects Models. *2017* **82**, 26, doi:10.18637/jss.v082.i13 (2017).
- 52 Wickham, H. *ggplot2: elegant graphics for data analysis*. (Springer, 2016).

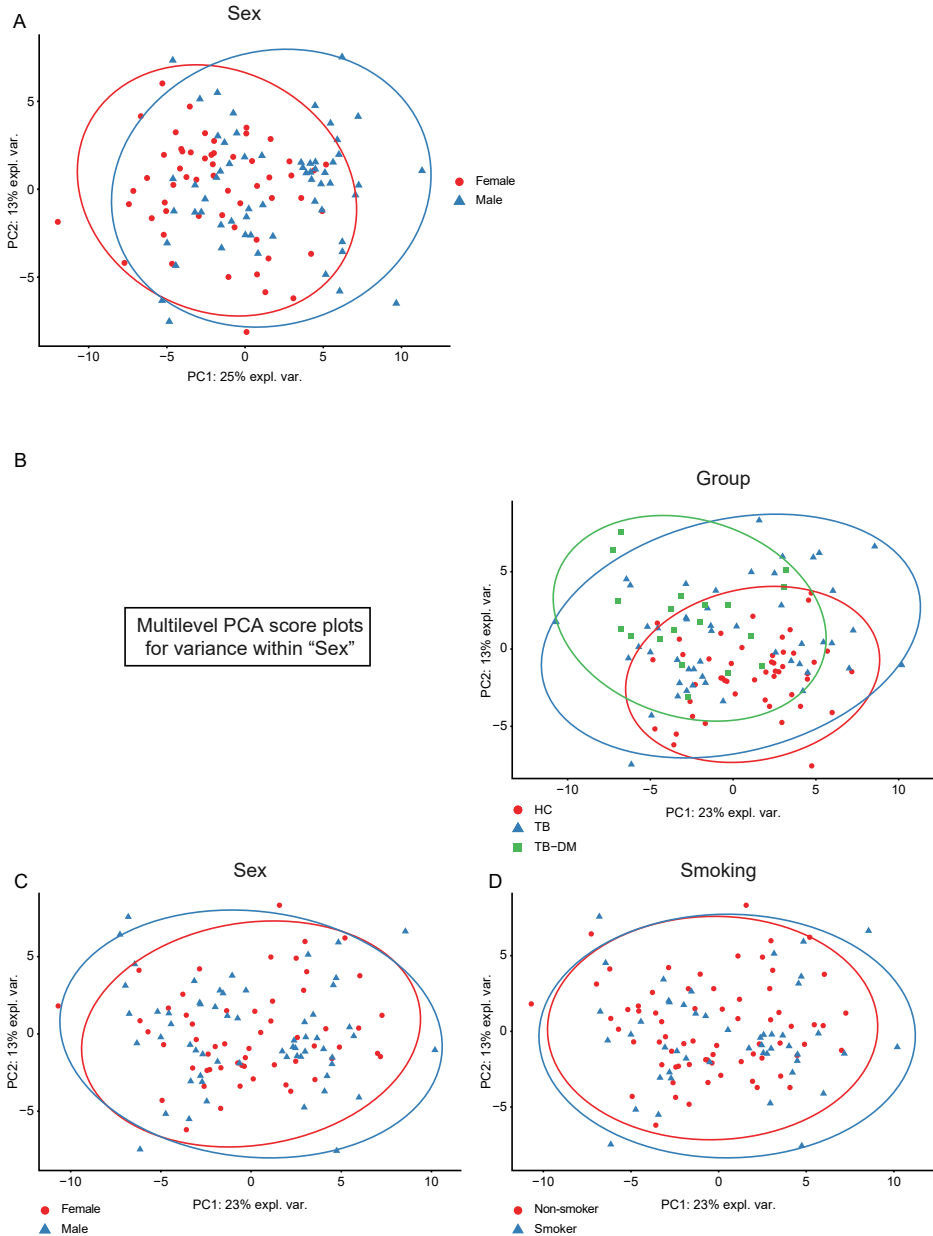


Figure S1: Multilevel PCA for metabolomics data variance within subjects with the same sex improves disease group separation.

(A) Score plot of the first two principal components of a PCA model built on the entire dataset and colored for sex with confidence ellipses. Females are displayed as red dots and males as blue triangles. (B-E) Score plots of the first two principal components of a multilevel PCA model for data variance within "Sex", colored for disease group membership (B), sex (C) or smoking status (D).

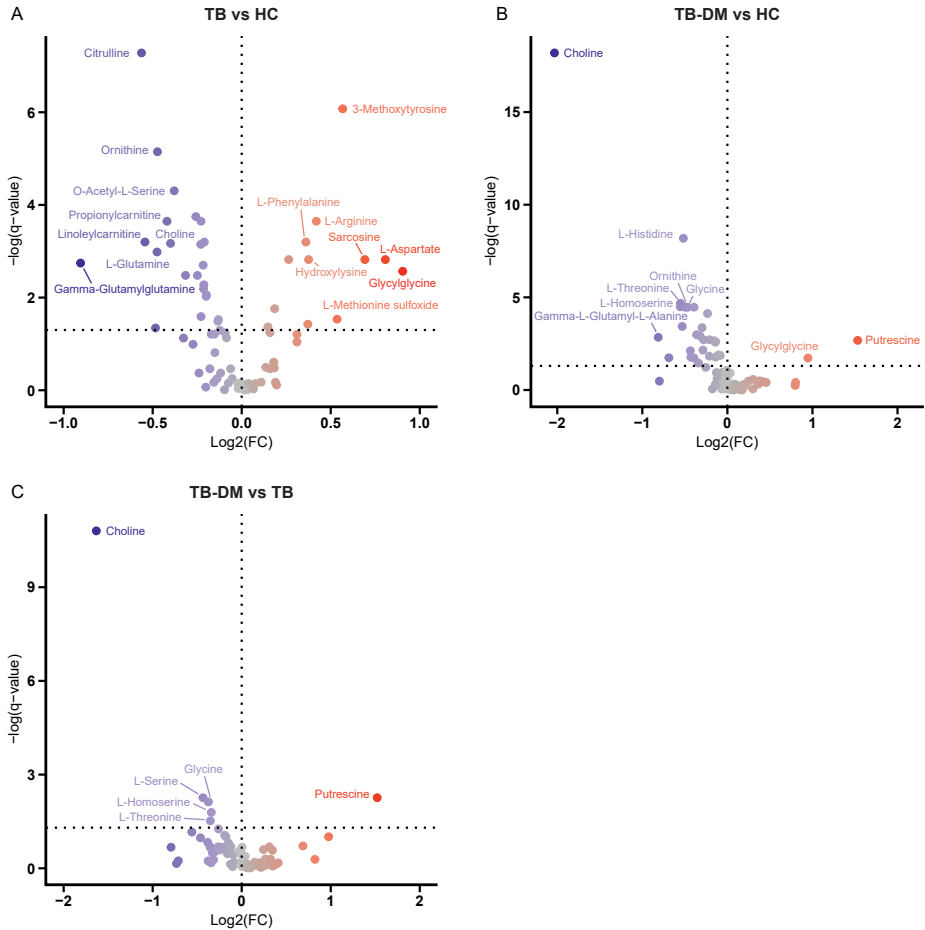


Figure S2: Volcano plots of linear regression models versus metabolite fold changes.

Multiple linear regression models were fitted for each between disease group comparison, and resulting $-\log$ -transformed p -values (q -values) are plotted against \log_2 -transformed fold changes for each metabolite: TB vs. HC (A), TB-DM vs. HC (B), TB-DM vs. TB (C). Each dot represents an individual metabolite. Dot color represents direction and size of the fold change. The significance threshold ($q = 0.05$) is displayed as a horizontal dotted line.

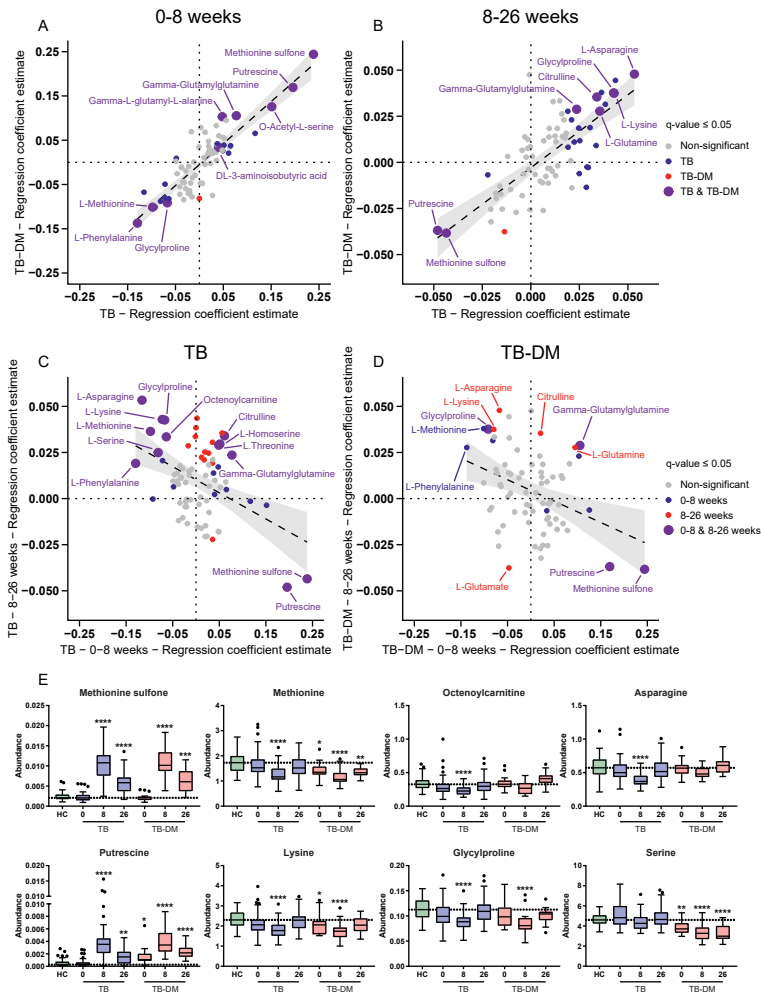


Figure S3: Differences between the effect of early (0-8 weeks) versus late (8-26 weeks) anti-TB treatment on patient plasma metabolic profiles.

Linear mixed models were fitted for the effect of 0-8 weeks or 8-26 weeks of anti-TB treatment on metabolite levels in TB patients and TB-DM patients separately. (A-B) Beta-beta plots of metabolite regression coefficients for the effect of anti-TB treatment in TB patients (x-axis) versus TB-DM patients (y-axis) for 0-8 weeks (A) and 8-26 weeks (B) of treatment. Each dot represents an individual metabolite. Dot color indicates whether the metabolite was significantly affected by anti-TB treatment in TB patients (blue), TB-DM patients (red), both (purple) or not at all (grey). Regression line with is displayed as a dashed line with 95% confidence interval. (C-D) Beta-beta plots of metabolite regression coefficients for the effect of anti-TB treatment during 0-8 weeks (x-axis) versus 8-26 weeks of anti-TB treatment (y-axis) in TB patients (C) and TB-DM patients (D). Each dot represent an individual metabolite. Dot color represents whether the metabolite was significantly affected by anti-TB treatment during weeks 0-8 (blue), 8-26 (red), both (purple) or not at all (grey). (E) Absolute abundance of individual metabolites per group displayed as Tukey's boxplots. For TB and TB-DM patients metabolite levels are displayed at 0, 8 and 26 weeks post-treatment. Significant differences between HC (n = 48) versus TB (n = 44) or TB-DM (n = 19) patients were determined by Kruskal-Wallis test with post-hoc Dunn's test. * $p = 0.05$, *** $p = 0.001$, **** $p = 0.0001$.

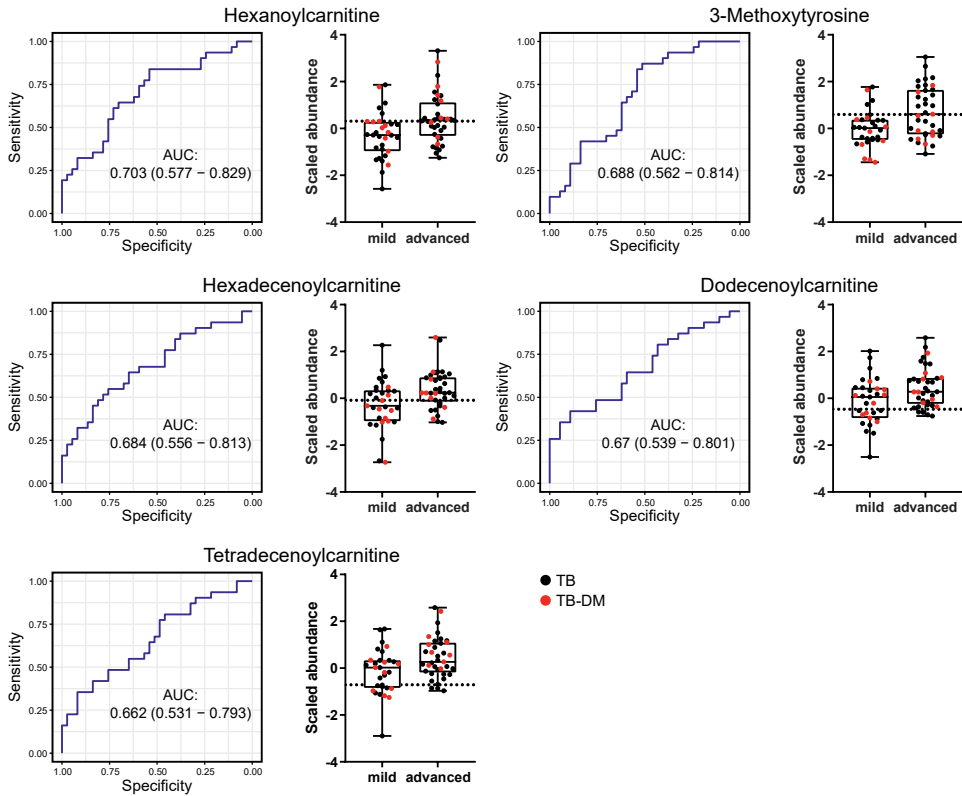


Figure S4: Metabolite association with CXR score.

ROC curves and AUCs of CXR score classification (mild/advanced lesions) for hexanoylcarnitine, 3-methoxytyrosine, hexadecenylcarnitine, dodecenylcarnitine and tetradecenylcarnitine. Log-transformed and standard deviation unit scaled metabolite abundances are displayed in boxplots. Each dot represents an individual patient (black = TB, red = TB-DM) and the optimal cut-off as determined by Youden's statistic is displayed as a horizontal dotted line.

Supplementary Table 2:

Internal standards: amines
Asn_C13N15
Asp_C13N15
L-ornithine-3,3,4,4,5,5,-d6
L-NT-methyl-d3-L-histidine
Glu_C13N15
Lys_C13N15
Ser_C13N15
Beta-alanine-2,2,3,3,-d4
Tyr_C13N15
Gln_C13N15
Thr_C13N15
L-Methionine_C13N15
Arg_C13N15
Ala_C13N15
Val_C13N15
Gly_C13N15
Phe_C13N15
Trp_C13N15
Histamine- $\alpha,\alpha,\beta,\beta$ -d4 2HCl
L-2-aminobutyric acid-d6 acid
2-(4-hydroxy-3-methoxyphenyl) ethyl-1,1,2,2-d4-amine
L-Ile_C13N15
Leu_C13N15
Internal standards: acylcarnitines
Carnitine-d3 HCl
Betaine-d3 HCl
Deoxycarnitine-d9 HCl
Acetyl-L-carnitine-d3 HCl
Butyryl-L-carnitine-d3 HCl
Octanoyl-L-carnitine-d3 HCl
Octadecanoyl-L-carnitine-d3 HCl

CHAPTER

7

Analyzing the impact of *Mycobacterium tuberculosis* infection on primary human macrophages by combined exploratory and targeted metabolomics

Frank Vrieling¹, Sarantos Kostidis², Herman P. Spaink³, Mariëlle C. Haks¹, Oleg Mayboroda², Tom H. M. Ottenhoff¹, Simone A. Joosten^{1*}

¹ Department of Infectious Diseases, Leiden University Medical Center, Leiden, The Netherlands

² Center for Proteomics and Metabolomics, Leiden University Medical Center, Leiden, The Netherlands

³ Institute of Biology, Leiden University, Leiden, The Netherlands

The pathogenic success of *Mycobacterium tuberculosis* (*Mtb*) is tightly linked to its ability to recalibrate host metabolic processes in infected host macrophages. Since changes in cellular metabolic intermediates or pathways also affect macrophage function in response to pathogens, we sought to analyse specific metabolic alterations induced by *Mtb* infection. Stimulation of macrophages with *Mtb* lysate or lipopolysaccharide (LPS) induced a relative increase in glycolysis versus oxidative phosphorylation. Cellular metabolomics revealed that *Mtb* infection induced a distinct metabolic profile compared to LPS in both M1 and M2 macrophages. Specifically, *Mtb* infection resulted in elevated intracellular levels of nicotinamide adenine dinucleotide (NAD⁺), creatine, creatine phosphate and glutathione compared to uninfected control macrophages. Correspondingly, RNA-sequencing datasets showed altered gene expression of key metabolic enzymes involved in NAD⁺, creatine, glucose and glutamine metabolism (e.g. *NAMPT*, *SLC6A8*, *HK2*) in *Mtb*-infected M2 macrophages. These findings demonstrate clear modulation of host macrophage metabolic pathways by *Mtb* infection.

Introduction

Mycobacterium tuberculosis (*Mtb*) is the causative pathogen of tuberculosis (TB) and responsible for over a million deaths annually⁽¹⁾. *Mtb* is transmitted through inhalation of aerosol particles and transported to the lungs, where it infects alveolar macrophages and avoids eradication through interfering with innate antimicrobial mechanisms. Infected cells are sequestered at the core of the TB granuloma as part of the host immune response, a confined niche where *Mtb* can reside in a dormant state for decades before potential disease reactivation^(2,3). However, in order to persist *Mtb* must overcome the limitations set by the anti-mycobacterial microenvironment of the granuloma, which include hypoxia⁽⁴⁾ and nutrient scarcity⁽⁵⁾. These conditions compel *Mtb* to switch from using carbohydrates to lipids and cholesterol as primary carbon source during later stages of infection, as part of its transition to a dormant state⁽⁶⁻⁹⁾. Several studies have demonstrated that *Mtb* is able to reprogram macrophage metabolism, and these adaptations are thought to be essential for its pathogenic success⁽¹⁰⁻¹²⁾.

Besides providing the necessary nutrients, metabolic changes induced by *Mtb* could also rewire the activation state and anti-microbial effector functions of infected macrophages. Over recent years many studies in the emerging field of immunometabolism have attempted to define the associations between macrophage metabolic states and their immunological responses⁽¹³⁾. The outcome of macrophage immunometabolism is largely determined by the balance between glycolysis and mitochondrial metabolism through oxidative phosphorylation (OXPHOS) of tricarboxylic acid cycle (TCA) intermediates^(14,15). Glycolysis is associated with classical pro-inflammatory macrophages activated with IFN γ and/or the Toll-like receptor (TLR) 4 ligand lipopolysaccharide (LPS)⁽¹⁶⁾, and OXPHOS with the alternatively activated anti-inflammatory phenotype induced by the T $_H$ 2 cytokines interleukin-(IL)-4 and IL-13⁽¹⁷⁾. Activation of myeloid and T cells has been demonstrated to enhance aerobic glycolysis^(18,19), resembling a process first observed in cancer cells by Otto Warburg and therefore known as the Warburg effect⁽²⁰⁾. The Warburg effect supports pro-inflammatory effector functions through rapid production of ATP and other necessary metabolic intermediates. Several studies reported increased lactate production or glycolytic enzyme expression in human and murine macrophages or lung tissue after *Mtb* infection⁽²¹⁻²⁴⁾, implying that glycolysis is induced as part of the host anti-mycobacterial response. However, stimulation with different pathogens or TLR ligands has since been shown to lead to more complex metabolic phenotypes in myeloid cells than what simply can be explained by the Warburg effect, including changes in lipid, cholesterol and amino acid metabolism⁽²⁵⁾. Importantly, *Mtb* and other mycobacteria have been shown to manipulate macrophage lipid metabolism, leading to the formation of lipid-loaded foam cells which constitute a preferred niche for mycobacterial persistence^(8, 11, 26-28).

Considering the importance of metabolic adaptations for *Mtb* killing and survival, several studies aimed to dissect the precise impact of the bacterium on macrophage

metabolism by cellular metabolomics⁽²⁹⁻³¹⁾. However, these relied on phorbol 12-myristate 13-acetate (PMA)-activated macrophage-like THP-1 cells as a model for macrophage infection, which significantly differ from primary macrophages in terms of polarization and response to stimuli^(32, 33). To address this critical gap in knowledge, we have here studied the effect of *Mtb* infection on primary human macrophage metabolism using not only untargeted liquid chromatography-mass spectrometry (LC-MS) metabolomics but also targeted ¹H-nuclear magnetic resonance (NMR) spectroscopy⁽³⁴⁾.

Results

***Mtb* lysate and LPS induced glycolytic metabolism in human macrophages**

In vitro stimulation with TLR ligands or whole pathogen lysates is commonly used to model immune cell activation in response to bacterial infection, and has previously been demonstrated to modulate myeloid cell metabolism^(18, 25). To validate whether primary human macrophage metabolism was truly affected by *Mtb* stimulation, macrophage colony-stimulating factor (M-CSF)-derived primary human macrophages (M2) were stimulated with *Mtb* lysate (10 µg/ml) as a model for *Mtb* infection and their metabolic activity was analyzed using a Seahorse XF Analyzer. LPS (100 ng/ml), a TLR4 ligand which is known to induce glycolysis in macrophages, and culture medium were used as a positive and negative control for metabolic skewing, respectively. Cellular glycolysis (Figure 1A), OXPHOS and spare respiratory capacity (SRC) (Figure 1B) were determined after a series of injections with D-glucose, ATP synthase inhibitor oligomycin and mitochondrial uncoupling agent FCCP. As expected, LPS stimulation showed a trend towards increased glycolysis-related acidification, while simultaneously decreasing macrophage mitochondrial respiration compared to medium control (Figure 1C&D), albeit with a greater SRC (Figure 1E). *Mtb* lysate induced similar tendencies for both extracellular acidification rate (ECAR)/oxygen consumption rate (OCR) ratio (Figure 1C&D) and SRC (Figure 1E), although the magnitude of this effect was less pronounced compared to LPS. Taken together, both stimulation with *Mtb* and LPS seem to result in metabolic skewing towards increased glycolysis while simultaneously decreasing OXPHOS in primary human macrophages.

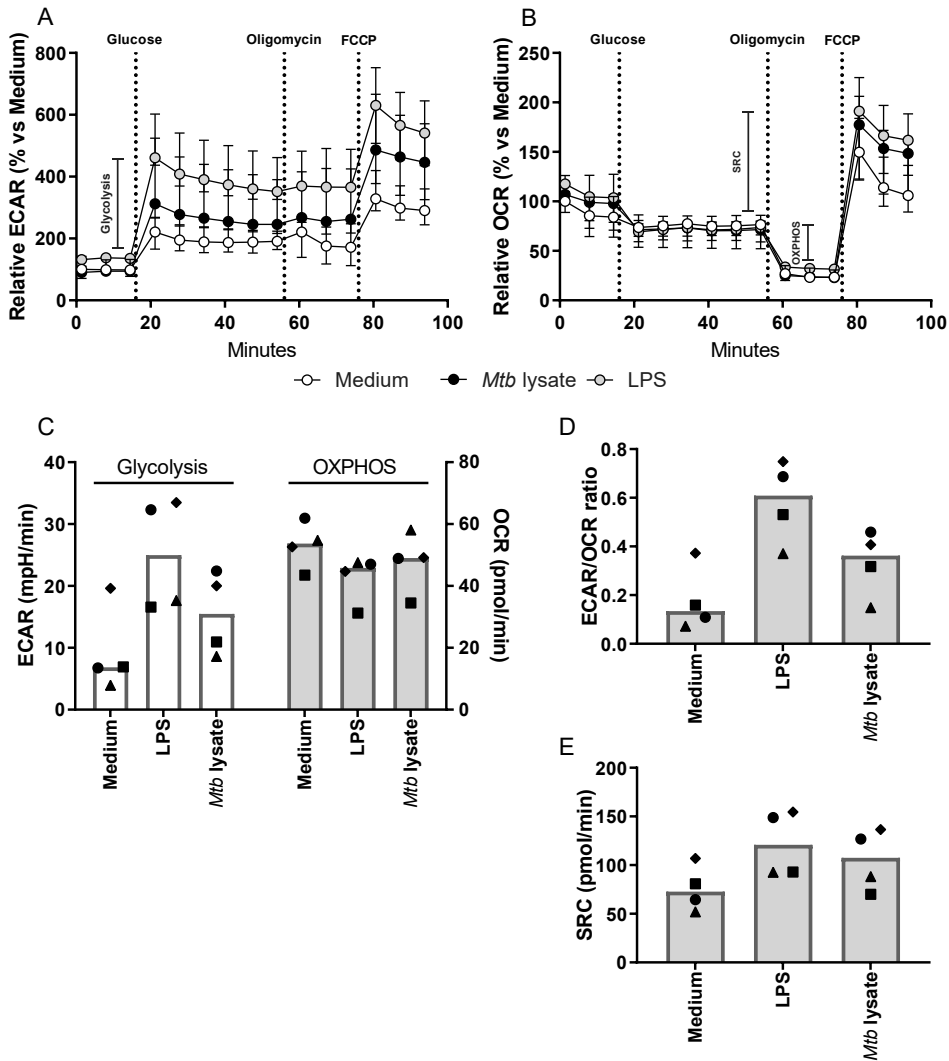


Figure 1: Stimulation with LPS or *Mtb* lysate induced a glycolytic shift in primary human macrophages.

M2 macrophages were stimulated with medium (white circles), *Mtb* lysate (10 µg/ml; black circles) or LPS (100 ng/ml; grey circles) for 24 hs. (A) Macrophage extracellular acidification rate (ECAR) and (B) oxygen-consumption rate (OCR) were measured during sequential injections of D-glucose (10 mM), oligomycin (1 µM) and FCCP (2 µM). (C) Glycolysis (white bars) as determined by the difference in ECAR pre- and post-glucose injection, and OXPHOS (grey bars) as the difference in OCR pre- and post-oligomycin injection. (D) ECAR/OCR ratio. (E) Spare respiratory capacity as determined by the difference in OCR pre-oligomycin and post-FCCP injection. Each symbol represents an individual donor, and bars represent group medians (n=4). Data is depicted as medians with ranges (n = 4).

Exploratory metabolomics of *Mtb*-infected macrophages

Since mycobacterial products are able to redirect macrophage metabolism, we sought to further characterize the effects of live *Mtb* infection on macrophage metabolism using exploratory metabolomics. Therefore, we generated a set consisting of granulocyte-macrophage colony-stimulating factor (GM-CSF) (M1) and M-CSF (M2) differentiated macrophages from six healthy blood bank donors which were either infected with *Mtb*-H37Rv, stimulated with lipopolysaccharide (LPS) or left untreated and subsequently harvested at either 4 or 24 h post-infection for metabolite extraction. Supplementary figure 1 (Figure S1A-D) shows an exploratory analysis of the resulting dataset (peak intensities of 270 masses) by Principal Component Analysis (PCA); the resulting score plot is colored according to main possible sources of variance in the LC-MS data. A dichotomy in cell type indicating metabolic differences between M1 and M2 macrophages was observed in the first two principal components, explaining 24% of total variance (Fig S1B). However, high inter individual heterogeneity also strongly contributed to the variance explained by the first two components. Therefore, a multilevel PCA model was fitted on the dataset to separate the between-donor and within-donor data variation⁽³⁵⁾ (Figure S1E-G). This model successfully reduced the donor related variability (Figure S1E), while retaining the metabolic effects of cell type (Figure S1F) within the first two components, explaining 19% of total variance. To compensate for this difference in metabolic profile at baseline between M1 and M2 macrophages, distinct multilevel PCA models were fitted for both cell types (Figure S2) to visualize potential effects of *Mtb* infection or LPS stimulation. The resulting score plots showed improved separation based on infection/treatment status in M2 macrophages (Figure S2F), however this was not clearly observable in M1 macrophages (Figure S2C).

For a more focused analysis of the effect of *Mtb* infection or LPS stimulation on macrophage metabolism, we performed group separation at specific time points per stimulation using Partial Least Squares Discrimination Analysis (PLS-DA) and extracted Variable Importance in Projection (VIP) scores from the resulting models to identify which masses carried the highest classification weight for each individual comparison. Separate multilevel PLS-DA models were built for each combination of cell type and time point using treatment group status as class variable. Resulting score plots and cross-validated model quality characteristics are displayed in Figure 2. All models showed good predictive capabilities as evidenced by high Q2 and R2Y scores (> 0.5 and > 0.8 respectively), signifying clear metabolic effects of both *Mtb* infection and LPS stimulation for each cell type and time point compared to untreated control. Next, VIP scores were extracted from the first component of each PLS-DA model to examine which measured variables explained the largest proportion of data variance in each model. Volcano plots of metabolite VIP scores versus their respective regression coefficients for each individual PLS-DA model are displayed in Supplementary Figure S3. In total, 46 masses reached a combined high VIP score of ≥ 2 and associated regression coefficient of ≥ 0.1 or ≤ -0.1 in at least one model.

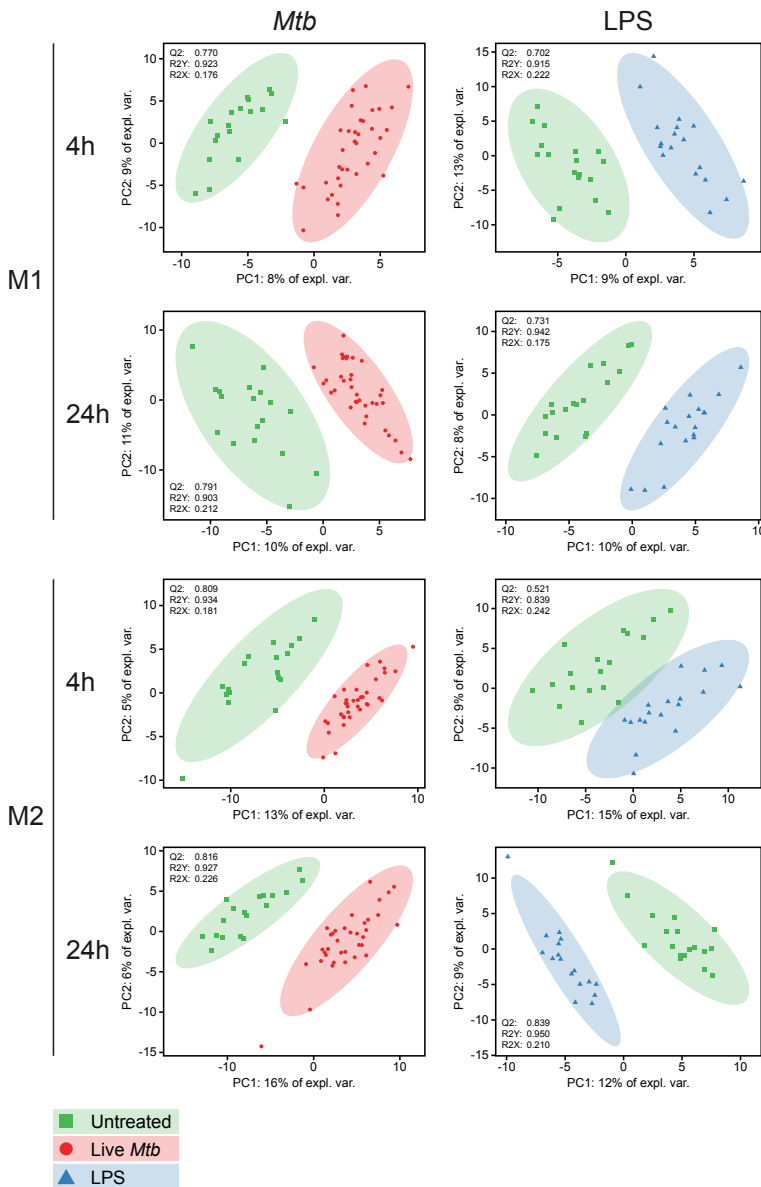


Figure 2: PLS-DA models of M1 and M2 macrophages after 4 h or 24 h of *Mtb* infection or LPS stimulation.

M1 and M2 macrophages were either infected with *Mtb* at a MOI of 10:1, stimulated with LPS (100 ng/ml) or left untreated. Cells were lysed at 4 h and 24 h post-infection/stimulation and intracellular metabolites were subsequently extracted and measured by LC-MS. Multilevel PLS-DA models were fitted for each group/time point comparison in M1 and M2 macrophages and score plots of the resulting eight models with associated quality metrics (Q2/R2Y/R2X) are displayed. Each point represents one technical replicate derived from six biological blood bank donors. Untreated samples are depicted as green squares, LPS stimulated samples as blue triangles and *Mtb* infected samples as red dots.

To verify the discriminatory capacity of this selection of masses, separate PLS-DA models were fitted on all combined samples derived from either M1 or M2 macrophages using only these 46 variables (Figure 3A&C). Both cell type models still showed good class separation of *Mtb*-infected cells at 4 and 24 h and LPS-treated cells at 24 h compared to untreated controls samples based on the first two components. Circle correlation plots visualizing the correlation between individual variables and the first components revealed 20 and 12 metabolites in M1 (Figure 3B) and M2 (Figure 3D) macrophages, respectively, with relatively good correlation scores (≥ 0.5), which combined constituted a total of 21 unique masses. Tentative annotations of these masses with degree of certainty are shown in Table 1, and boxplots of metabolite peak areas are displayed in Supplementary Figure S4. In both cell types, LPS treatment was associated with increased levels of masses annotated as adenosine (X265, $m/z = 269.104$), nicotinamide (X32, $m/z = 123.055$) and propionylcarnitine (X166, $m/z = 218.138$), while *Mtb* infection showed high correlation with relatively large masses (X489, $m/z = 382.189$; X579, $m/z = 458.249$; X586, $m/z = 470.241$) which could not be annotated based on database searches. These unknown structures are fragments of either proteins or lipids for which the number of possible assignments cannot be reduced to a minimum required for tentative annotation.

Table 1: Tentative annotation of selected masses.

Nr.	m/z	ID	Adduct	Error (ppm)	ID level
X14	104.107	Choline	H+	6	3
X23	116.071	Proline	H+	1	2
X32	123.055	Nicotinamide	H+	1	2
X44	133.061	L-Asparagine	H+	2	2
X53	142.026	Dimethylglycine	K+	3	2
X59	146.996	NA	-	-	4
X66	149.063	Glutamate	H+	1	2
X113	184.073	3-Dehydroxycarnitine	K+	1	3
X166	218.138	Propionylcarnitine	H+	1	3
X225	249.045	Unknown peptide	H+	-	4
X243	258.110	Glycerophosphocholine	H+	1	3
X254	263.086	Hydroxysebacate	2Na-H	3	3
X265	268.104	Adenosine	H+	1	3
X292	280.092	Glycerophosphocholine	Na+	1	3
X489	382.189	Unknown peptide	-	-	4
X491	383.101	NA	-	-	-
X494	385.175	NA	-	-	-
X502	388.269	NA	-	-	-
X525	415.224	NA	-	-	-
X579	459.249	NA	-	-	-
X586	470.241	NA	-	-	-

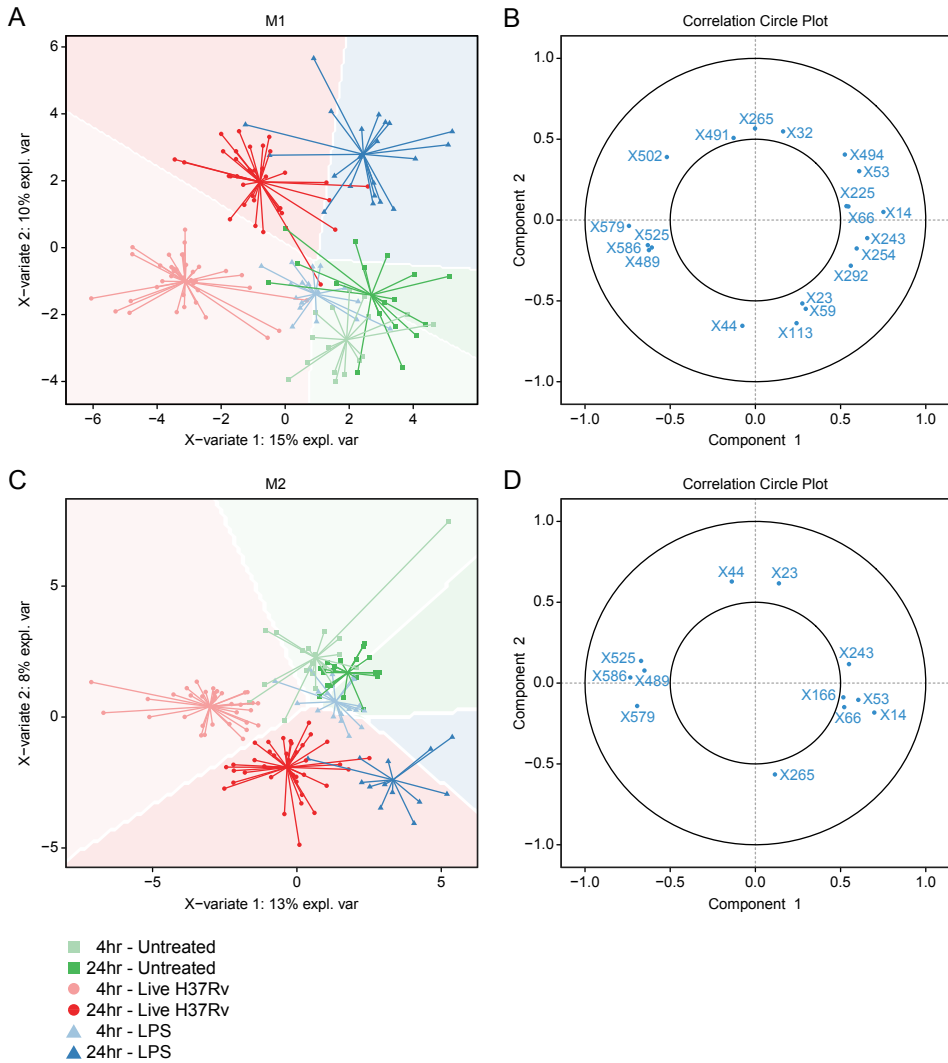


Figure 3: Group separation by selected metabolites with high Variable Importance for Projection (VIP) scores.

Multilevel PLS-DA models were fitted on all samples using a selection of 46 metabolites which reached VIP scores of ≥ 2 and associated regression coefficients of ≤ -0.1 or ≥ 0.1 in any pairwise PLS-DA model described in Figure 2. Score plots of the resulting model for M1 (A) and M2 (C) macrophages (M2) are displayed. Untreated samples are depicted as green squares, LPS stimulated samples as blue triangles and *Mtb* infected samples as red dots. Shade of symbol color reflects time point (4 h = light, 24 h = dark). Strongly correlated metabolites (threshold: ≥ 0.5) are displayed in circle plots for both the M1 (B) and the M2 (C) PLS-DA model.

Targeted metabolomics of *Mtb*-infected macrophages by ¹H-NMR spectroscopy

While the LC-MS approach clearly demonstrated that *Mtb* infection greatly impacts the metabolome of infected macrophages beyond the increase in glycolysis, the untargeted metabolic profiling often enables only a tentative structural annotation. Therefore, to complement our untargeted dataset, we employed ¹H-nuclear magnetic resonance (NMR) spectroscopy to further dissect the metabolic effects of *Mtb* infection in M2 macrophages compared to uninfected control samples at 4 h and 24 h post-infection. While not as sensitive as mass spectrometry, ¹H-NMR spectroscopy is nonetheless quantitative and known for its robustness (34).

Separate linear random intercept models were fitted for each individual metabolite to model the interaction between infection status (*Mtb* vs uninfected) and time (24 h vs 4 h) (Figure 4A). Significant interactions were detected for four metabolites, creatine ($q = 9.09E^{-3}$), glutathione ($q = 0.014$), nicotinamide-adenine-dinucleotide (NAD⁺) ($q = 0.029$) and taurine ($q = 0.029$), all of which increased between 4 and 24 h in infected macrophages but either decreased or did not change in uninfected controls (Fig, 4E). Together with creatine-phosphate and myo-inositol, these metabolites constituted the top six most elevated factors in *Mtb*-infected versus uninfected macrophages according to median log₂-transformed fold changes (Figure 4D&E). Next, we fitted linear mixed models without interaction term to analyze the fixed effects of infection and time. The disaccharide trehalose, an important component of mycobacterial cell-wall glycolipids (35), was only detected in infected macrophages and therefore significantly associated with *Mtb* infection ($q = 2.26E^{-3}$) (Figure 4B). Various metabolites showed a significant positive association with time (Figure 4C), including sn-glycero-3-phosphocholine ($q = 4.50E^{-3}$), choline ($q = 0.023$), creatine phosphate ($q = 0.032$), pyroglutamate ($q = 0.032$) and lactate ($q = 0.033$), although the magnitude of this increase could vary based on infection status (Figure 4E).

As macrophage activation with *Mtb* lysate induced a relative increase in extracellular acidification indicative of anaerobic glycolysis, we wondered whether live *Mtb* infection would also trigger similar changes in glycolytic intermediates. While glucose levels were lower in *Mtb*-infected macrophages in 3/4 donors at both 4 h and 24 h, the lactate/glucose ratio was increased in all donors at 24 h (median increase of 81%) (Figure 4F), indicative of increased glucose utilization for ATP production by anaerobic glycolysis⁽³⁶⁾, which is congruent with the results from Figure 1. Additionally, extracellular lactate concentrations were elevated in all donors at 24 h post-infection (Figure 4F). As only one intermediate of the TCA cycle was detected (succinate) which in itself did not show obvious modulation by *Mtb* infection, the relative mitochondrial activity could not be assessed in a similar fashion. However, we did observe a decreased glutamine (Gln) to glutamate (Glu) ratio (Figure 4F), reflecting increased glutamine catabolism.

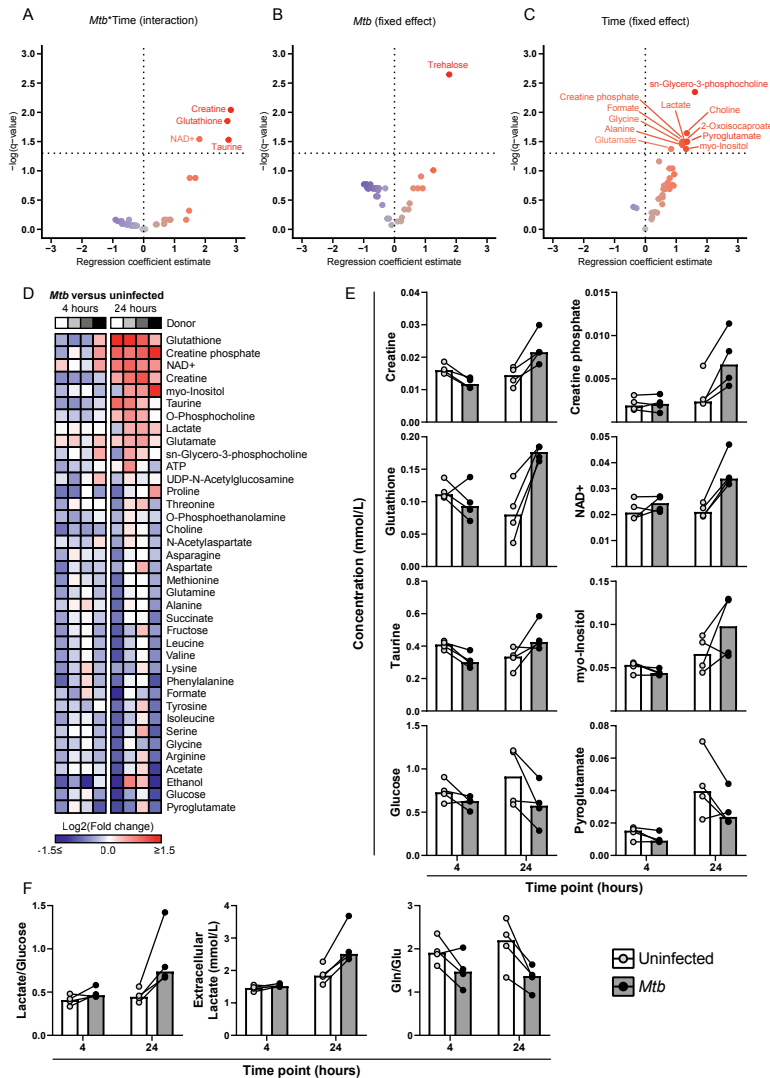


Figure 4: Targeted ¹H-NMR spectroscopy analysis of *Mtb*-infected M2 macrophages.

M2 macrophages were infected with *Mtb* at a MOI of 10:1 or left uninfected. Cells were lysed at 4 h and 24 h post-infection and intracellular metabolites were subsequently extracted and measured by ¹H-NMR spectroscopy. Linear random intercept models were fitted for each metabolite to investigate: (A) the interaction between infection and time (*Mtb*:Time), or the separate fixed effects of (B) *Mtb* infection or (C) time. Resulting $-\log$ -transformed FDR-corrected p -values (q -values) are plotted against the regression coefficient estimate for each metabolite in volcano plots. (D) Heatmap of \log_2 -transformed metabolite fold changes (*Mtb* / uninfected). Metabolites are sorted by average median fold change at 24 h. Individual donors are presented in greyscale. (E) Absolute levels of creatine, creatine phosphate, glutathione, NAD⁺, taurine, myo-inositol, glucose and pyroglutamate (mmol/L) in *Mtb*-infected macrophages (grey bars) or uninfected controls (white bars) at 4 h and 24 h. (F) Extracellular lactate concentrations and relative ratios of lactate/glucose and glutamate/glutamine (Glu/Gln). Each dot represents an individual donor, and measurements from matching donors are connected by black lines. Bars represent group medians.

***Mtb*-induced metabolic changes are reflected by the macrophage transcriptome**

Finally, we wondered whether the observed metabolic changes induced by *Mtb* infection were reflected by alterations in macrophage gene expression levels. To study this, we analysed the results of previously published expression profiling of M2 macrophages infected with *Mtb*-H37Rv (n = 6) performed by Blischak *et al.* (37) for differentially expressed genes involved in glycolysis, NAD⁺, creatine and glutamine metabolism, and compared their expression profiles to an exploratory RNA-seq dataset of *Mtb*-infected M1 and M2 macrophages acquired using our own specific *Mtb* infection model. Gene expression profiles showed significant linear correlation between both datasets, especially for M2 macrophages at 24 h (Figure S5). In both sets, *Mtb* infection was associated with differential expression of NAD⁺-consuming enzymes, such as cyclic ADP ribose hydrolase (*CD38*) and various members of the poly (ADP-ribose) polymerase (PARP) and sirtuin (SIRT) protein families (Figure 5A). Congruent with the observed increase in intracellular NAD⁺ levels, genes involved in NAD⁺ biosynthesis were strongly upregulated during *Mtb* infection, including nicotinamide phosphoribosyltransferase (*NAMPT*) and indoleamine 2,3-dioxygenase 1 (*IDO1*), rate-limiting enzymes of the NAD⁺ salvage and kynurenine pathway respectively. In contrast, expression of quinolate phosphoribosyltransferase (*QPRT*), which catalyzes quinolinic acid conversion downstream of *IDO1*, was decreased. With regard to creatine metabolism, expression of creatine synthesis enzyme genes *GATM* and *GAMT* decreased as a result of *Mtb* infection, while the creatine transporter *SLC6A8* and creatine kinase (brain-type, *CKB*) were increased, most notably in our M2 infection model (Figure 5B). Furthermore, *Mtb* infection induced expression of genes known to control glycolytic flux (38), namely glucose transporter 1 (*GLUT1*) and 3 (*GLUT3*), hexokinase 2 (*HK2*), 6-phosphofructo-2-kinase/fructose-2,6-biphosphatase 3 (*PFKFB3*) and monocarboxylate transporter 4 (*MCT4*) (Figure 5C), which is again in agreement with the NMR metabolic data. Finally, *Mtb* modulated expression of various genes involved in glutamine metabolism in both datasets, including members of the hexosamine (*GFPT1* and *GPFT2*) and glutathione synthesis (*GCLC* and *GCLM*) pathways (Figure 5D), corresponding with the increased levels of intracellular glutathione after *Mtb* infection. Taken together, we find that *Mtb* infection results in clear metabolic changes in macrophages, including alterations in NAD⁺, creatine, glucose and glutamine metabolism, which can be connected to corresponding changes in metabolic gene expression patterns.

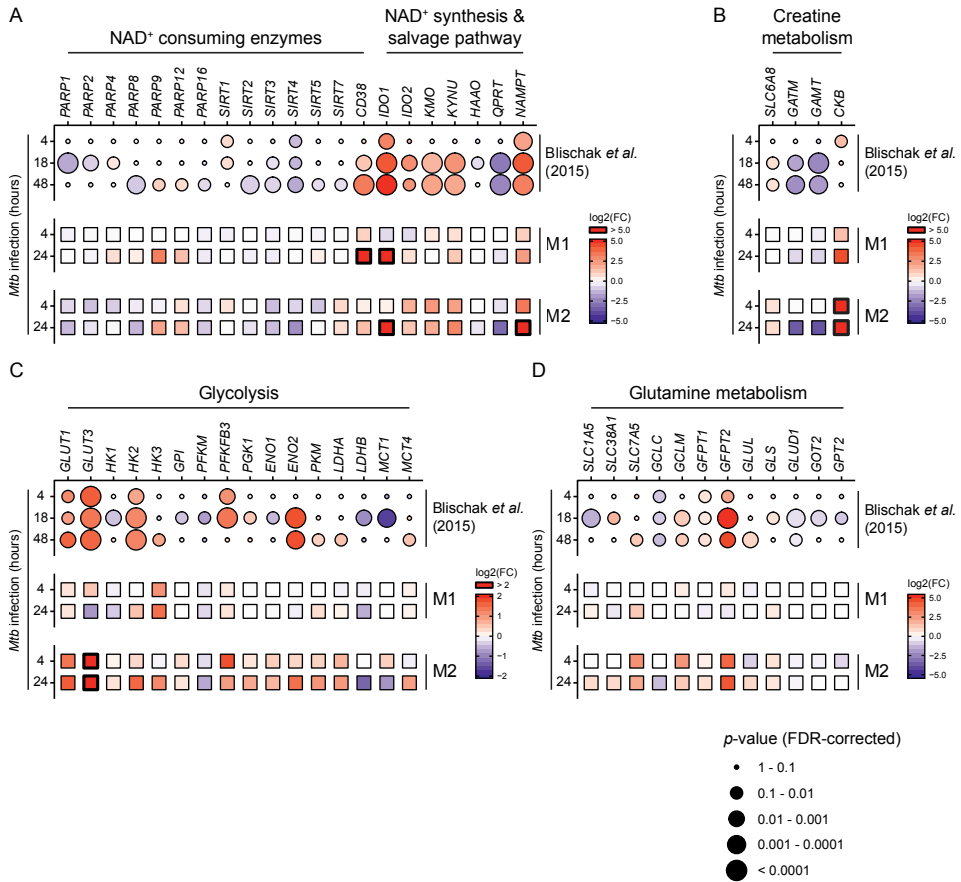


Figure 5: *Mtb* modulates gene expression of key metabolic enzymes in infected macrophages.

Expression profiles of genes involved in (A) NAD⁺ consumption and synthesis, (B) creatine metabolism, (C) glycolysis and (D) glutamine metabolism from a previously published RNA-seq dataset (Blischak *et al.* 2015) (37) of M2 macrophages at 4, 18 and 48 h post-*Mtb* infection and an exploratory RNA-seq dataset derived from our M1/M2 *Mtb* infection model. Expression data is displayed as log₂-transformed fold changes of *Mtb* infected vs non-infected macrophages. Up- and downregulation of genes is displayed by a color gradient (up = red, down = blue). Differential expression results (FDR-corrected *p*-values) from Blischak *et al.* are reflected by circle size.

Discussion

Since the emergence of the multidisciplinary field of immunometabolism, a growing body of evidence has accumulated connecting specific aspects of cellular metabolism to macrophage activation and functions in response to danger signals or microbes. While we were able to validate that LPS and activation with *Mtb* lysate resulted in a relative shift toward increased glycolysis in primary macrophages, many of the published findings in the literature have yet to be translated to infections of primary human cells with live pathogens. Here, we contribute to this knowledge gap by employing both untargeted LC-MS metabolomics and targeted ¹H-NMR spectroscopy to investigate the effect of live *Mtb* infection on macrophage metabolism. PLS-DA modeling of untargeted metabolomics data demonstrated that both *Mtb* infection and LPS stimulation were associated with marked changes in the cellular metabolome in both M1 and M2 macrophages. Tentative annotation of changed metabolites indicate increased levels of adenosine, nicotinamide and propionylcarnitine in LPS-stimulated M1 and M2 macrophages. *Mtb* infection was strongly associated with increased levels of relatively large masses, however these could not be annotated based on current metabolite databases and potentially constitute *Mtb*-derived protein fragments or lipids, one of which was identified as trehalose using quantitative ¹H-NMR measurements. The latter also revealed various changes in specific metabolites in *Mtb*-infected versus uninfected macrophages, including NAD⁺, creatine and glutathione, which could be linked to changes in gene expression as determined by analysis of RNA-seq datasets.

Levels of NAD⁺, an important cofactor in many cellular pathways, were elevated in *Mtb*-infected macrophages. *Mtb* has been demonstrated to secrete toxins which can induce macrophage necrosis through NAD⁺-depletion^(39, 40). In addition, recent studies have highlighted the importance of sustaining adequate NAD⁺ levels for pro-inflammatory macrophage function. Reactive oxygen species (ROS) produced during inflammatory activation were shown to induce DNA damage in macrophages, leading to PARP activation and depletion of NAD⁺ pools (41). NAD⁺ salvage through activation of NAMPT was required for maintaining glycolytic flux and inflammatory functions. Furthermore, NAD⁺ synthetic capacity was reduced in aged mice compared to young controls, indicating that changes in NAD⁺ metabolism could play a role during aging-associated immune dysregulation⁽⁴²⁾. Our results imply increased activity of NAD⁺ biosynthesis pathways as a result of *Mtb* infection. This result is corroborated by analysis of independent RNA-seq datasets, which showed increased expression of genes involved in NAD⁺ synthesis and salvage, including IDO1 and NAMPT. Interestingly, expression of QPRT was decreased in M2 macrophages, an effect which was found to limit *de novo* NAD⁺ synthesis through the kynurenine pathway in LPS-stimulated macrophages⁽⁴²⁾. As the general interest in the therapeutic potential of NAD⁺-boosting drugs is on the rise⁽⁴³⁾, these results call for further studies on the importance of macrophage NAD⁺ metabolism during *Mtb* infection, in view also of potential application in host-directed therapeutic strategies.

Besides NAD^+ , intracellular levels of the anti-oxidant glutathione (GSH; reduced form) also increased during macrophage *Mtb* infection. Glutathione is produced as part of the cellular redox response to increased levels of ROS and regulates macrophage anti-mycobacterial functions both through direct anti-microbial effects and by serving as a carrier of nitric oxide (NO) ⁽⁴⁴⁾. Furthermore, *Mtb*-infected cells showed an increase in glutamine catabolism via its conversion to glutamate. The latter is a precursor for the *de novo* synthesis of glutathione and together with the increased intracellular GSH, point to a metabolic switch caused by *Mtb* infection towards the synthesis of glutathione ⁽⁴⁵⁾. As glutamine has been reported to regulate macrophage cytokine production ⁽⁴⁶⁾ and support M2 polarization ⁽⁴⁷⁾, increased glutamine catabolism could potentially modulate macrophage cytokine responses to *Mtb*, although the resulting net effect on mycobacterial bacterial survival is unclear. Intracellular levels of creatine and creatine phosphate were also increased after 24 h of *Mtb* infection. The creatine phosphate system constitutes a spatiotemporal buffer for intracellular ATP concentrations, mostly in tissues with high energy consumption such as skeletal muscle and brain ⁽⁴⁸⁾. Creatine phosphate was also shown to be involved in cytoskeletal dynamics ^(49, 50) and macrophage phagocytosis ⁽⁵¹⁾, possibly through increased localization of CKB to nascent phagosomes ⁽⁵²⁾. The observed increase in creatine phosphate and CKB expression could therefore be a reflection of macrophage phagocytic activity. Additionally, creatine is synthesized from arginine, and increased creatine production could reduce intracellular availability of arginine for anti-bacterial NO production ⁽⁵³⁾. However, as creatine synthesis *in vivo* occurs through respective actions of GATM of GAMT in the kidneys and liver, the elevated creatine levels could also be the result of increased expression of the creatine transporter SLC6A8, as was observed in the RNA-seq analysis. Finally, the intracellular lactate/glucose ratio was elevated during *Mtb* infection, further evidencing an increased glycolytic flux from glucose to lactate. These findings are corroborated by a recent study which also reported increased levels of lactate and glutamine-derived metabolites in *Mtb* lysate-stimulated peripheral blood mononuclear cells ⁽⁵⁴⁾. Interestingly, while increased glycolysis has been linked to improved *Mtb* clearance ⁽²¹⁾, a recent paper demonstrated that *Mtb* can utilize lactate as a source of carbon for intracellular replication in macrophages ⁽⁵⁵⁾, calling for more extensive studies on the role of lactate production during macrophage *Mtb* infection.

Our study has several limitations that need to be discussed. Firstly, it was not possible to differentiate whether metabolites were of mycobacterial or human host origin in our experimental setup, with the exception of metabolites such as trehalose that can only be of mycobacterial origin, and were only detected in *Mtb* infected macrophages. However, we consider major mycobacterial contributions to metabolite levels unlikely due to the large difference in cell volume between macrophages and infecting *Mtb*. Furthermore, the majority of our observed changes (e.g. elevated creatine, glutathione, NAD^+) manifested predominantly with prolonged infection time, which could be considered an argument against being mycobacterial metabolites as these were also

present and likely measurable at 4h, in a similar fashion to trehalose. Secondly, we were unable to perform extracellular flux analysis during live *Mtb* infection due to biosafety restrictions and therefore used *Mtb* lysate as a model for infection. While the observed increase in ECAR/OCR ratio is corroborated by other studies using γ -irradiated *Mtb* ^(21, 56), this result was contradicted by a recent paper which reported an overall decrease in macrophage bioenergetic profile during live *Mtb* infection ⁽⁵⁷⁾. Although we find that a potential role of toxicity on these results is not conclusively excluded by the authors, it would still be important to compare the effects of *Mtb* lysate stimulation to those of live *Mtb* infection in future experiments. Lastly, it is unclear how accurately the observed metabolic responses of human monocyte-derived macrophages reflect those of alveolar macrophages *in vivo*. Results from mouse studies are suggestive of a model in which the metabolic response of macrophages to *Mtb* infection is largely dependent on their ontology (58). Therefore, it would be of great interest to study whether our results are reproducible using primary tissue-resident macrophage populations.

In conclusion, live *Mtb* infection induces pronounced metabolic changes in primary human macrophages, including activation of NAD⁺ and glutathione synthesis, glycolysis, glutaminolysis and the creatine phosphate pathway. Whether these changes benefit the host or the bacterium could not directly be inferred from these experiments and needs to be studied further: follow-up experiments using small-molecule inhibitors or small interfering RNAs (siRNAs) which target key enzymes of these pathways will be necessary to gauge their exact involvement in the macrophage anti-mycobacterial immune response.

Materials & Methods

Study design and sample collection

All experimental procedures were performed according to local and national guidelines on the work with pathogenic mycobacteria. Infection experiments with *Mycobacterium tuberculosis* H37Rv were performed as approved by the local biosafety officer and following the BSLIII permit granted to LUMC by the Dutch government.

Monocytes were isolated from buffy coats obtained from Sanquin blood products (Amsterdam, The Netherlands). The medical ethical review board of LUMC has approved use of buffy coats, remaining after blood donation, for scientific purposes. Healthy donors donating their blood have provided written informed consent for scientific use of their blood products.

Monocyte isolation and differentiation

CD14⁺ monocytes were isolated from buffy coats of healthy blood bank donors by positive selection using an autoMACS Pro Separator (Miltenyi Biotec BV, Leiden, The Netherlands). Monocytes were differentiated into macrophages using 50 ng/ml M-CSF (Miltenyi Biotec) or 5 ng/ml GM-CSF (Miltenyi Biotec) for six days at 37°C/5%CO₂. Cells were cultured in RPMI-1640 medium supplemented with 10% fetal calf serum (FCS), 100 units/ml penicillin and 100 µg/ml streptomycin and GlutaMAX (Gibco, Thermo Fisher, Merelbeke, Belgium). After differentiation macrophages were harvested by trypsinization and seeded in multiwell plates. As a quality control, macrophages were stained for surface expression of CD14 and CD163 and acquired on a BD LSRFortessa flow cytometer (BD Biosciences, Erembodegem, Belgium).

Seahorse extracellular flux (XF) analysis

For cellular metabolic flux analysis, macrophages were stimulated overnight with either medium, 100 ng/ml LPS or H37Rv *Mtb* lysate (10 µg/ml) and measured on a Seahorse XF96 Analyzer (Seahorse Bioscience, North Billerica, MA, USA). Cell culture medium was replaced with RPMI without buffer and glucose supplemented with 5% FCS and L-glutamine and macrophages were incubated in a 37°C dry incubator for one hour before start of measurements. Macrophage oxygen consumption rates (OCR) and extracellular acidification rates (ECAR) were determined in real-time throughout consecutive injections of D-glucose (10 mM), oligomycin (1 µM) and FCCP (2 µM). Acidification due to glycolysis was calculated as the difference in highest ECAR measurements pre- and post-glucose injection. Oxygen consumed for ATP production by oxidative phosphorylation was calculated as the difference between highest OCR measurements pre- and post-oligomycin injection. In case of obvious injection errors the affected measurements were excluded from the analysis.

***Mtb* H37Rv culture and infection**

Mtb H37Rv cultures were grown to mid-log phase in Middlebrook 7H9 liquid medium (Difco, BD Biosciences) supplemented with albumin/dextrose/catalase (ADC) (BBL, BD Biosciences). Bacterial concentrations were determined by measuring the culture optical density at 600nm⁽⁵⁹⁾. Macrophages were infected with H37Rv at a multiplicity of infection (MOI) of 10:1 for 1 hour at 37°C, after which the cells were washed twice with medium containing 30 µg/ml gentamicin and further cultured for 4 or 24 h in fresh medium containing 5 µg/ml gentamicin. MOI was confirmed by plating a dilution series of the inoculum on 7H10 square agar plates supplemented with oleate/albumin/dextrose/catalase (OADC) (BBL, BD Biosciences)⁽⁵⁹⁾.

Sample preparation for LC-MS

Macrophages were seeded in 24-well plates at a density of 300,000 cells/well and either infected with *Mtb*, stimulated with LPS (100 ng/ml; Thermo Fisher) or left untreated. At 4 and 24 h post-infection/stimulation, macrophages were washed with ice-cold 1% NaCl and subsequently lysed in water by osmotic pressure for 15 minutes at 4°C. Lysates were thoroughly resuspended and mixed with pre-heated 80% ethanol at a 1:3 ratio (end concentration: 60% ethanol) in polypropylene screwcap tubes and subsequently heated for 10 min at 90°C. Samples were chilled for 10 minutes on ice before centrifugation at 13.2×1000 rpm for 10 minutes at 4°C, after which the supernatants were harvested and stored at -80°C for subsequent LC-MS analysis.

LC-MS/MS measurements and metabolite annotation

Samples were randomized before the analysis. The acquisition sequence was designed using a standard block structure: the material was injected by the blocks of five samples flanked by the QC pool samples. Fifty μ L of each sample or QC pool were injected into the RPLCQ-TOF system (Ultimate 3000RS tandem Ultra High Performance Chromatography system, Thermo Scientific/Dionex, Amsterdam, Netherlands; Electrospray Ionization – Ultra High Resolution - Time of Flight mass spectrometer maXis, Bruker Daltonics, Bremen, Germany). The details of the RPLC-Q-TOF method have previously been reported (60). Pre-processing of the raw data (alignment of retention time, peak picking, filtering and normalization) was performed on the files converted into mzxml format. Retention time was aligned using the msalign package⁽⁶¹⁾ keeping the mass error parameter at 5 ppm. Peak picking and grouping were done within the XCMS package using centWave function⁽⁶²⁾. A final data matrix included only the features with a relative standard deviation ≤ 0.3 within the QC pool. Finally, we manually removed the signals corresponding to the HEPES clusters and anticipating the potential difficulties with structural annotation, which are known for the of the untargeted profiling data, we filtered out the last quarter of the chromatogram.

Metabolite annotation was carried out according to the minimal reporting standards (63). The Smart Formula tool within the Data Analysis software (version 4.1) as used for the initial ion annotation based on accurate mass (mass error < 5 ppm) and isotopic distribution (sigma value < 20). The results were matched against online metabolomics databases (METLIN, Human Metabolome Database, MassBank). When possible the hits were confirmed with MS–MS experiments of the sample with the highest intensity for each of the putative metabolites and the reference standards. MS–MS experiments were performed on the same RPLC-Q-TOF instrument in auto MS–MS mode.

Sample preparation for ¹H-NMR spectroscopy

Macrophages were seeded in 24-well plates with 300,000 cells/well and either infected with H37Rv or left untreated. At 4 and 24 h post-infection, supernatants were harvested

and the cells were washed once quickly with ice-cold PBS. Macrophages were rapidly quenched with liquid nitrogen and the plates were stored at -80°C . Supernatants were filter-sterilized using $2\ \mu\text{m}$ filter plates, mixed with methanol chilled at -80°C at a ratio of 1:3 and subsequently stored at -80°C . On the day of metabolite extraction, plates were put on ice and $300\ \mu\text{l}$ 90% methanol/chloroform 9:1 was added to each well and cells were scraped thoroughly with a pipette tip before transferring of samples to eppendorf tubes. Samples were chilled for 10 minutes on ice before centrifugation at 13.2×1000 rpm for 15 minutes at 4°C , after which the supernatants were harvested and put on ice. Dry protein pellets were stored at -20°C and protein concentrations were determined by bicinchoninic acid assay (BCA) (Pierce, Thermo Fisher) according to manufacturer's instructions. Supernatant/methanol samples from the -80°C were centrifuged at 13.2×1000 rpm for 30 minutes at 4°C , after which supernatants were collected and also put on ice. Both cellular- and supernatant- extracts were then dried by nitrogen stream and stored at -80°C until day of measurement.

$^1\text{H-NMR}$ spectroscopy

NMR analysis of the intracellular metabolites was carried out as described previously ⁽³⁴⁾. Briefly, the dried extracts were reconstituted in $250\ \mu\text{l}$ of $0.15\ \text{M}\ \text{K}_2\text{HPO}_4/\text{KH}_2\text{PO}_4$ buffer (pH = 7.4) in 99.9% deuterated water (D_2O), including $0.2\ \text{mM}\ \text{NaN}_3$ and $0.4\ \text{mM}$ trimethylsilylpropionic acid sodium salt ($\text{TSP-}d_4$), and transferred to 3-mm NMR tubes. NMR data were recorded on a 14.1 T NMR spectrometer (600 MHz for ^1H ; Bruker Avance II) under standardized conditions for all samples. All spectra were processed for phase and baseline correction and referenced to $\text{TSP-}d_4$. One-dimensional (1D) spectra were imported into Chenomx NMR suit 8 (Chenomx Edmonton, Canada) for quantification. Metabolites were identified based on the Bbioefcode (Bruker Biospin) and the Chenomx databases as well as in-house reference spectra. The concentrations of the quantified metabolites (mM) were normalized to the protein mass per sample.

RNA-sequencing

Total RNA was extracted from of M1 and M2 macrophages either uninfected or infected with *Mtb* in triplicate from a single blood bank donor using TRIzol Reagent (Thermo Fisher) at 4 and 24 h post-infection and purified using RNeasy MinElute Cleanup Kit (Qiagen, The Netherlands). The concentration and purity of RNA was evaluated by NanoDrop 2000 (Thermo Fisher). RNA-seq was performed using an Illumina Hi-Seq 2500 as previously described ⁽⁶⁴⁾. The RNA-seq data were mapped versus the human genome (version GRCH38) and tag counts were performed by Bowtie 2 using GeneTiles software (<http://www.genetiles.com>) ⁽⁶⁵⁾. Normalization and gene expression analysis was performed using the R package DESeq2 ⁽⁶⁶⁾.

Statistical analysis

All statistical methods were performed in R (version 3.5.0) or GraphPad software (version 7.02, Prism, La Jolla, CA, USA). Morpheus (<https://software.broadinstitute.org/morpheus>) was used to generate the NMR metabolite heatmap. The following R packages were used: (multilevel) PCA and PLS-DA modeling was performed using mixOmics version 6.3.2 ⁽⁶⁷⁾, linear mixed models were fitted using lme4 version 1.1.17 ⁽⁶⁸⁾ and lmerTest ⁽⁶⁹⁾ version 3.0.1, and graphical output was constructed using ggplot2 version 3.1.0 ⁽⁷⁰⁾.

Acknowledgements

Not applicable.

Funding Sources

This study was supported by the TANDEM (Tuberculosis and Diabetes Mellitus) Grant of the ECFP7 (European Union's Seventh Framework Programme) under Grant Agreement No. 305279 and by TBVAC2020 Grant of EC HOR2020 (Grant Agreement No. 643381) for data analysis and interpretation.

Competing Interests Statement

All authors: no reported conflicts.

References

1. World Health Organization. Global Tuberculosis Report. Geneva, Switzerland; 2018.
2. Ramakrishnan L. Revisiting the role of the granuloma in tuberculosis. *Nature reviews Immunology*. 2012;12(5):352-66.
3. Russell DG, Cardona PJ, Kim MJ, Allain S, Altare F. Foamy macrophages and the progression of the human tuberculosis granuloma. *Nature immunology*. 2009;10(9):943-8.
4. Belton M, Brilha S, Manavaki R, Mauri F, Nijran K, Hong YT, et al. Hypoxia and tissue destruction in pulmonary TB. *Thorax*. 2016;71(12):1145-53.
5. Berney M, Berney-Meyer L. *Mycobacterium tuberculosis* in the Face of Host-Imposed Nutrient Limitation. *Microbiol Spectr*. 2017;5(3).
6. Shi L, Sohaskey CD, Pheiffer C, Datta P, Parks M, McFadden J, et al. Carbon flux rerouting during *Mycobacterium tuberculosis* growth arrest. *Mol Microbiol*. 2010;78(5):1199-215.
7. Lee W, VanderVen BC, Fahey RJ, Russell DG. Intracellular *Mycobacterium tuberculosis* exploits host-derived fatty acids to limit metabolic stress. *The Journal of biological chemistry*. 2013;288(10):6788-800.
8. Peyron P, Vaubourgeix J, Poquet Y, Levillain F, Botanch C, Bardou F, et al. Foamy macrophages from tuberculous patients' granulomas constitute a nutrient-rich reservoir for *M. tuberculosis* persistence. *PLoS pathogens*. 2008;4(11):e1000204.
9. Deb C, Lee CM, Dubey VS, Daniel J, Abomoelak B, Sirakova TD, et al. A novel in vitro multiple-stress dormancy model for *Mycobacterium tuberculosis* generates a lipid-loaded, drug-tolerant, dormant pathogen. *PloS one*. 2009;4(6):e6077.
10. Singh V, Jamwal S, Jain R, Verma P, Gokhale R, Rao KV. *Mycobacterium tuberculosis*-driven targeted recalibration of macrophage lipid homeostasis promotes the foamy phenotype. *Cell host & microbe*. 2012;12(5):669-81.
11. Ouimet M, Koster S, Sakowski E, Ramkhelawon B, van Solingen C, Oldebeken S, et al. *Mycobacterium tuberculosis* induces the miR-33 locus to reprogram autophagy and host lipid metabolism. *Nature immunology*. 2016;17(6):677-86.
12. Mahajan S, Dkhar HK, Chandra V, Dave S, Nanduri R, Janmeja AK, et al. *Mycobacterium tuberculosis* modulates macrophage lipid-sensing nuclear receptors PPARgamma and TR4 for survival. *Jimmunol*. 2012;188(11):5593-603.
13. Van den Bossche J, O'Neill LA, Menon D. Macrophage Immunometabolism: Where Are We (Going)? *Trends Immunol*. 2017;38(6):395-406.
14. Pearce EL, Pearce EJ. Metabolic pathways in immune cell activation and quiescence. *Immunity*. 2013;38(4):633-43.
15. O'Neill LA, Pearce EJ. Immunometabolism governs dendritic cell and macrophage function. *The Journal of experimental medicine*. 2016;213(1):15-23.
16. Tan Z, Xie N, Cui H, Moellering DR, Abraham E, Thannickal VJ, et al. Pyruvate dehydrogenase kinase 1 participates in macrophage polarization via regulating glucose metabolism. *Journal of immunology*. 2015;194(12):6082-9.

17. Vats D, Mukundan L, Odegaard JI, Zhang L, Smith KL, Morel CR, et al. Oxidative metabolism and PGC-1beta attenuate macrophage-mediated inflammation. *Cell Metab.* 2006;4(1):13-24.
18. Lachmandas E, Boutens L, Ratter JM, Hijmans A, Hooiveld GJ, Joosten LA, et al. Microbial stimulation of different Toll-like receptor signalling pathways induces diverse metabolic programmes in human monocytes. *Nature microbiology.* 2016;2:16246.
19. Chang CH, Curtis JD, Maggi LB, Jr., Faubert B, Villarino AV, O'Sullivan D, et al. Posttranscriptional control of T cell effector function by aerobic glycolysis. *Cell.* 2013;153(6):1239-51.
20. Warburg O. On the origin of cancer cells. *Science.* 1956;123(3191):309-14.
21. Gleeson LE, Sheedy FJ, Palsson-McDermott EM, Triglia D, O'Leary SM, O'Sullivan MP, et al. Cutting Edge: Mycobacterium tuberculosis Induces Aerobic Glycolysis in Human Alveolar Macrophages That Is Required for Control of Intracellular Bacillary Replication. *Journal of immunology.* 2016;196(6):2444-9.
22. Shi L, Salamon H, Eugenin EA, Pine R, Cooper A, Gennaro ML. Infection with Mycobacterium tuberculosis induces the Warburg effect in mouse lungs. *Sci Rep.* 2015;5:18176.
23. Shin JH, Yang JY, Jeon BY, Yoon YJ, Cho SN, Kang YH, et al. (1)H NMR-based metabolomic profiling in mice infected with Mycobacterium tuberculosis. *J Proteome Res.* 2011;10(5):2238-47.
24. Lachmandas E, Beigier-Bompadre M, Cheng SC, Kumar V, van Laarhoven A, Wang X, et al. Rewiring cellular metabolism via the AKT/mTOR pathway contributes to host defence against Mycobacterium tuberculosis in human and murine cells. *Eur J Immunol.* 2016;46(11):2574-86.
25. Stienstra R, Netea-Maier RT, Riksen NP, Joosten LAB, Netea MG. Specific and Complex Reprogramming of Cellular Metabolism in Myeloid Cells during Innate Immune Responses. *Cell Metab.* 2017;26(1):142-56.
26. Fineran P, Lloyd-Evans E, Lack NA, Platt N, Davis LC, Morgan AJ, et al. Pathogenic mycobacteria achieve cellular persistence by inhibiting the Niemann-Pick Type C disease cellular pathway. *Wellcome open research.* 2016;1:18.
27. Dkhar HK, Nanduri R, Mahajan S, Dave S, Saini A, Somavarapu AK, et al. Mycobacterium tuberculosis keto-mycolic acid and macrophage nuclear receptor TR4 modulate foamy biogenesis in granulomas: a case of a heterologous and noncanonical ligand-receptor pair. *Journal of immunology.* 2014;193(1):295-305.
28. Vermeulen I, Baird M, Al-Dulayymi J, Smet M, Verschoor J, Grooten J. Mycolates of Mycobacterium tuberculosis modulate the flow of cholesterol for bacillary proliferation in murine macrophages. *Journal of lipid research.* 2017;58(4):709-18.
29. Cheng J, Che N, Li H, Ma K, Wu S, Fang J, et al. Extraction, derivatization, and determination of metabolome in human macrophages. *J Sep Sci.* 2013;36(8):1418-28.
30. Zimmermann M, Kogadeeva M, Gengenbacher M, McEwen G, Mollenkopf HJ, Zamboni N, et al. Integration of Metabolomics and Transcriptomics Reveals a Complex Diet of Mycobacterium tuberculosis during Early Macrophage Infection. *mSystems.* 2017;2(4).

31. Beste DJ, Noh K, Niedenfuhr S, Mendum TA, Hawkins ND, Ward JL, et al. 13C-flux spectral analysis of host-pathogen metabolism reveals a mixed diet for intracellular *Mycobacterium tuberculosis*. *Chem Biol*. 2013;20(8):1012-21.
32. Bosshart H, Heinzemann M. THP-1 cells as a model for human monocytes. *Ann Transl Med*. 2016;4(21):438.
33. Shiratori H, Feinweber C, Luckhardt S, Linke B, Resch E, Geisslinger G, et al. THP-1 and human peripheral blood mononuclear cell-derived macrophages differ in their capacity to polarize in vitro. *Mol Immunol*. 2017;88:58-68.
34. Kostidis S, Addie RD, Morreau H, Mayboroda OA, Giera M. Quantitative NMR analysis of intra- and extracellular metabolism of mammalian cells: A tutorial. *Anal Chim Acta*. 2017;980:1-24.
35. Kalscheuer R, Koliwer-Brandl H. Genetics of *Mycobacterial* Trehalose Metabolism. *Microbiol Spectr*. 2014;2(3).
36. Meiser J, Kramer L, Sapcariu SC, Battello N, Ghelfi J, D'Herouel AF, et al. Pro-inflammatory Macrophages Sustain Pyruvate Oxidation through Pyruvate Dehydrogenase for the Synthesis of Itaconate and to Enable Cytokine Expression. *The Journal of biological chemistry*. 2016;291(8):3932-46.
37. Blischak JD, Tailleux L, Mitrano A, Barreiro LB, Gilad Y. *Mycobacterial* infection induces a specific human innate immune response. *Sci Rep*. 2015;5:16882.
38. Tanner LB, Goglia AG, Wei MH, Sehgal T, Parsons LR, Park JO, et al. Four Key Steps Control Glycolytic Flux in Mammalian Cells. *Cell Syst*. 2018;7(1):49-62 e8.
39. Pajuelo D, Gonzalez-Juarbe N, Tak U, Sun J, Orihuela CJ, Niederweis M. NAD(+) Depletion Triggers Macrophage Necroptosis, a Cell Death Pathway Exploited by *Mycobacterium tuberculosis*. *Cell reports*. 2018;24(2):429-40.
40. Freire DM, Gutierrez C, Garza-Garcia A, Grabowska AD, Sala AJ, Ariyachaokun K, et al. An NAD(+) Phosphorylase Toxin Triggers *Mycobacterium tuberculosis* Cell Death. *Mol Cell*. 2019;73(6):1282-91 e8.
41. Cameron AM, Castoldi A, Sanin DE, Flachsmann LJ, Field CS, Puleston DJ, et al. Inflammatory macrophage dependence on NAD(+) salvage is a consequence of reactive oxygen species-mediated DNA damage. *Nature immunology*. 2019;20(4):420-32.
42. Minhas PS, Liu L, Moon PK, Joshi AU, Dove C, Mhatre S, et al. Macrophage de novo NAD(+) synthesis specifies immune function in aging and inflammation. *Nature immunology*. 2019;20(1):50-63.
43. Rajman L, Chwalek K, Sinclair DA. Therapeutic Potential of NAD-Boosting Molecules: The In Vivo Evidence. *Cell Metab*. 2018;27(3):529-47.
44. Morris D, Khurasany M, Nguyen T, Kim J, Guilford F, Mehta R, et al. Glutathione and infection. *Biochimica et biophysica acta*. 2013;1830(5):3329-49.
45. Bansal A, Simon MC. Glutathione metabolism in cancer progression and treatment resistance. *J Cell Biol*. 2018;217(7):2291-8.
46. Wallace C, Keast D. Glutamine and macrophage function. *Metabolism*. 1992;41(9):1016-20.

47. Jha AK, Huang SC, Sergushichev A, Lampropoulou V, Ivanova Y, Loginicheva E, et al. Network integration of parallel metabolic and transcriptional data reveals metabolic modules that regulate macrophage polarization. *Immunity*. 2015;42(3):419-30.
48. Greenhaff PL. The creatine-phosphocreatine system: there's more than one song in its repertoire. *J Physiol*. 2001;537(Pt 3):657.
49. O'Connor RS, Steeds CM, Wiseman RW, Pavlath GK. Phosphocreatine as an energy source for actin cytoskeletal rearrangements during myoblast fusion. *J Physiol*. 2008;586(12):2841-53.
50. Kuiper JW, van Horssen R, Oerlemans F, Peters W, van Dommelen MM, te Lindert MM, et al. Local ATP generation by brain-type creatine kinase (CK-B) facilitates cell motility. *PloS one*. 2009;4(3):e5030.
51. Loike JD, Kozler VF, Silverstein SC. Increased ATP and creatine phosphate turnover in phagocytosing mouse peritoneal macrophages. *The Journal of biological chemistry*. 1979;254(19):9558-64.
52. Kuiper JW, Pluk H, Oerlemans F, van Leeuwen FN, de Lange F, Fransen J, et al. Creatine kinase-mediated ATP supply fuels actin-based events in phagocytosis. *PLoS Biol*. 2008;6(3):e51.
53. Karamat FA, van Montfrans GA, Brewster LM. Creatine synthesis demands the majority of the bioavailable L-arginine. *J Hypertens*. 2015;33(11):2368.
54. Koeken V, Lachmandas E, Riza A, Matzaraki V, Li Y, Kumar V, et al. Role of Glutamine Metabolism in Host Defense Against Mycobacterium tuberculosis Infection. *J Infect Dis*. 2019;219(10):1662-70.
55. Billig S, Schneefeld M, Huber C, Grassl GA, Eisenreich W, Bange FC. Lactate oxidation facilitates growth of Mycobacterium tuberculosis in human macrophages. *Sci Rep*. 2017;7(1):6484.
56. Hackett EE, Charles-Messance H, O'Leary SM, Gleeson LE, Munoz-Wolf N, Case S, et al. Mycobacterium tuberculosis Limits Host Glycolysis and IL-1beta by Restriction of PFK-M via MicroRNA-21. *Cell reports*. 2020;30(1):124-36 e4.
57. Cumming BM, Addicott KW, Adamson JH, Steyn AJ. Mycobacterium tuberculosis induces decelerated bioenergetic metabolism in human macrophages. *Elife*. 2018;7.
58. Huang L, Nazarova EV, Tan S, Liu Y, Russell DG. Growth of Mycobacterium tuberculosis in vivo segregates with host macrophage metabolism and ontogeny. *The Journal of experimental medicine*. 2018;215(4):1135-52.
59. Vrieling F, Wilson L, Rensen PCN, Walzl G, Ottenhoff THM, Joosten SA. Oxidized low-density lipoprotein (oxLDL) supports Mycobacterium tuberculosis survival in macrophages by inducing lysosomal dysfunction. *PLoS pathogens*. 2019;15(4):e1007724.
60. Nevedomskaya E, Mayboroda OA, Deelder AM. Cross-platform analysis of longitudinal data in metabolomics. *Mol Biosyst*. 2011;7(12):3214-22.
61. Nevedomskaya E, Derks R, Deelder AM, Mayboroda OA, Palmblad M. Alignment of capillary electrophoresis-mass spectrometry datasets using accurate mass information. *Anal Bioanal Chem*. 2009;395(8):2527-33.

62. Smith CA, Want EJ, O'Maille G, Abagyan R, Siuzdak G. XCMS: processing mass spectrometry data for metabolite profiling using nonlinear peak alignment, matching, and identification. *Anal Chem.* 2006;78(3):779-87.
63. Sumner LW, Amberg A, Barrett D, Beale MH, Beger R, Daykin CA, et al. Proposed minimum reporting standards for chemical analysis Chemical Analysis Working Group (CAWG) Metabolomics Standards Initiative (MSI). *Metabolomics.* 2007;3(3):211-21.
64. Marin-Juez R, Jong-Raadsen S, Yang S, Spaik HP. Hyperinsulinemia induces insulin resistance and immune suppression via Ptpn6/Shp1 in zebrafish. *The Journal of endocrinology.* 2014;222(2):229-41.
65. Veneman WJ, de Sonnevile J, van der Kolk KJ, Ordas A, Al-Ars Z, Meijer AH, et al. Analysis of RNAseq datasets from a comparative infectious disease zebrafish model using GeneTiles bioinformatics. *Immunogenetics.* 2015;67(3):135-47.
66. Love MI, Huber W, Anders S. Moderated estimation of fold change and dispersion for RNA-seq data with DESeq2. *Genome Biol.* 2014;15(12):550.
67. Rohart F, Gautier B, Singh A, Le Cao KA. mixOmics: An R package for 'omics feature selection and multiple data integration. *PLoS Comput Biol.* 2017;13(11):e1005752.
68. Bates D, Mächler M, Bolker B, Walker S. Fitting Linear Mixed-Effects Models Using lme4. 2015. 2015;67(1):48.
69. Kuznetsova A, Brockhoff PB, Christensen RHB. lmerTest Package: Tests in Linear Mixed Effects Models. 2017. 2017;82(13):26.
70. Wickham H. ggplot2: elegant graphics for data analysis: Springer; 2016.

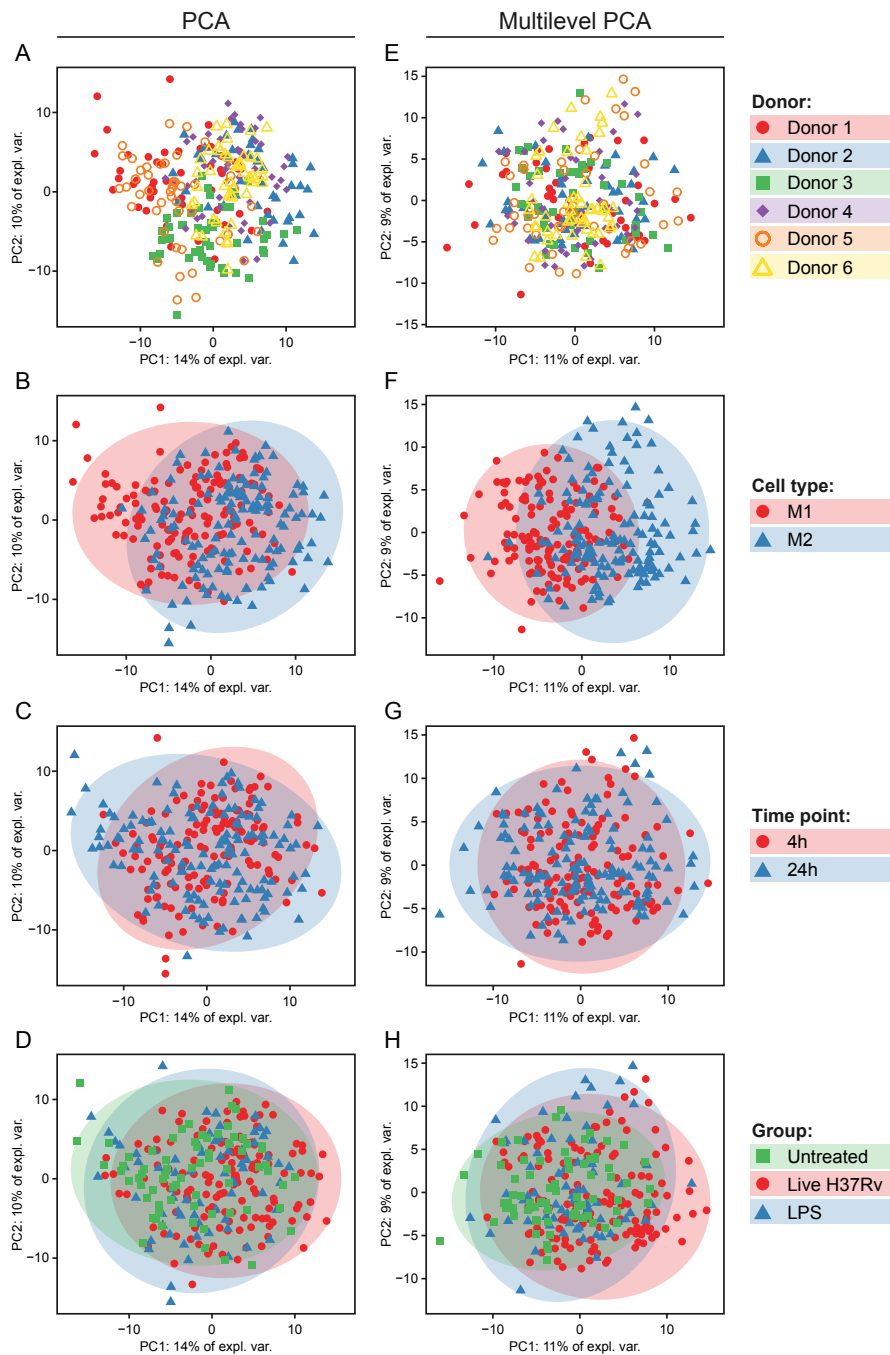


Figure S1: PCA models of untargeted LC-MS metabolomics.

Score plots of the first two components of a standard (A-D) and a multilevel PCA (E-H) model built on the entire dataset. Samples are color coded by donor (A&E), cell type (B&F), time point (C&G) or group membership (D&H).

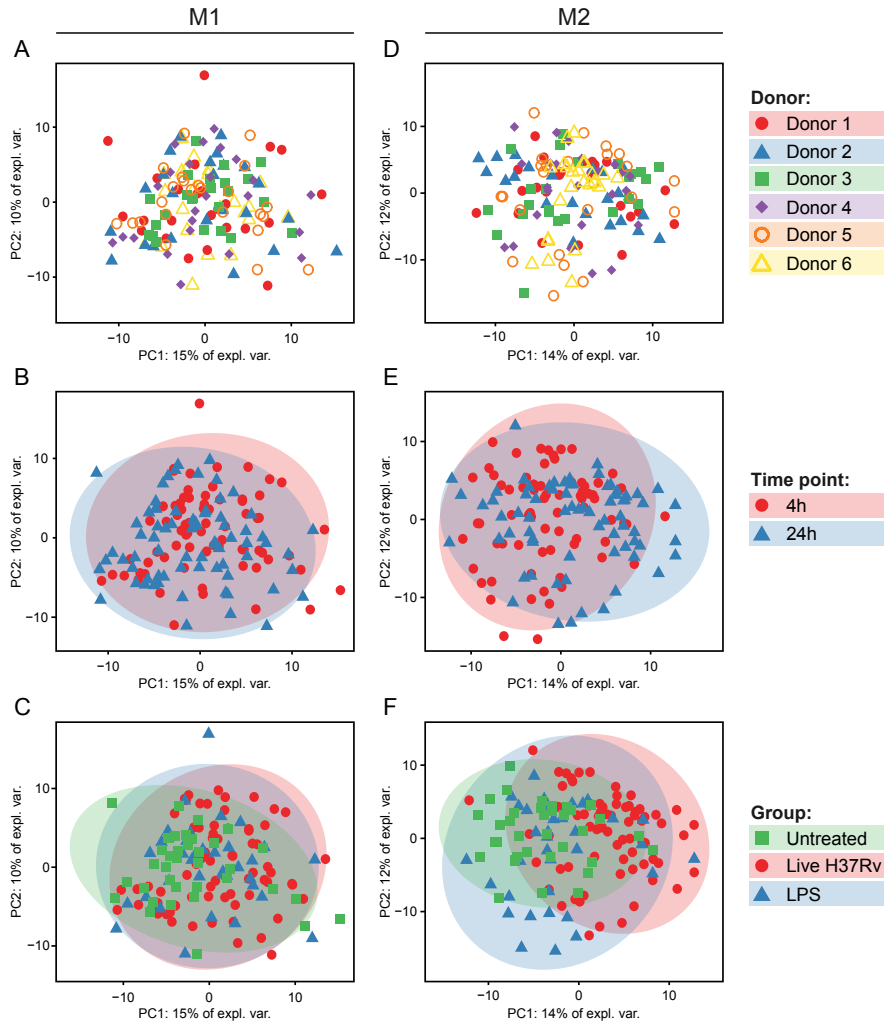


Figure S2: Separate multilevel PCA models by cell type.

Score plots of the first two components of multilevel PCA models built for M1 (A-C) or M2 macrophages (D-F). Samples are color coded by donor (A&D), time point (B&E) or group membership (C&F).

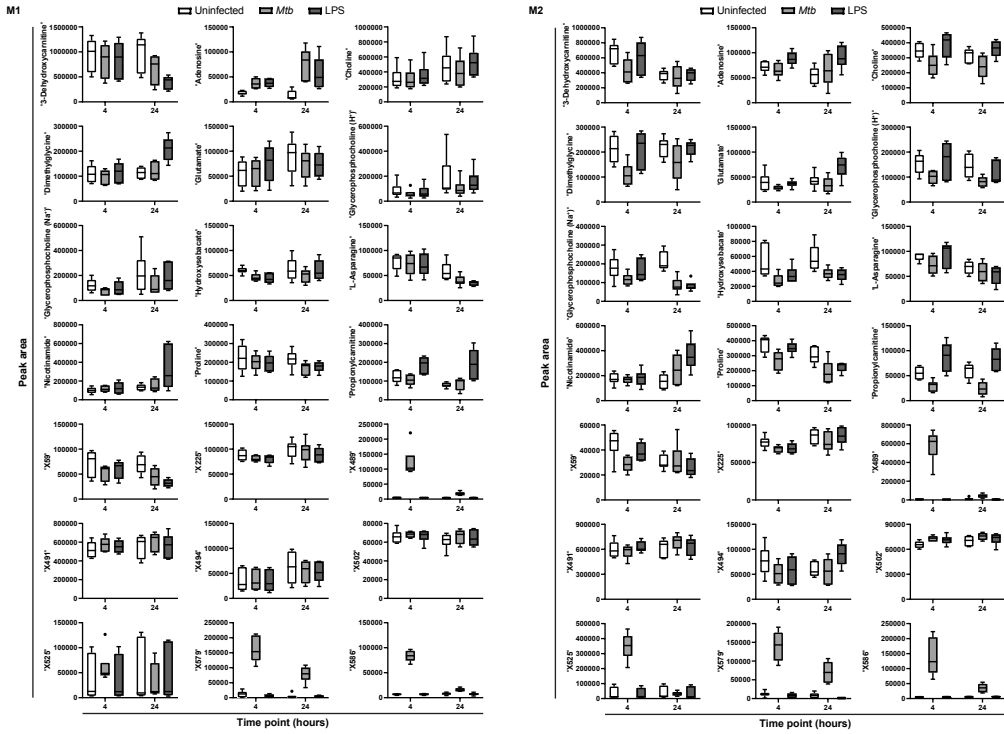


Figure S4: Abundance of selected metabolites in M1 and M2 macrophages.

Peak area results of 21 masses with high correlation scores (≥ 0.5) in the final M1 and M2 PLS-DA models. Results are displayed in Tukey's boxplots for untreated (white), *Mtb*-infected (light gray) and LPS-stimulated (dark gray) M1 or M2 macrophages at 4 and 24 h.

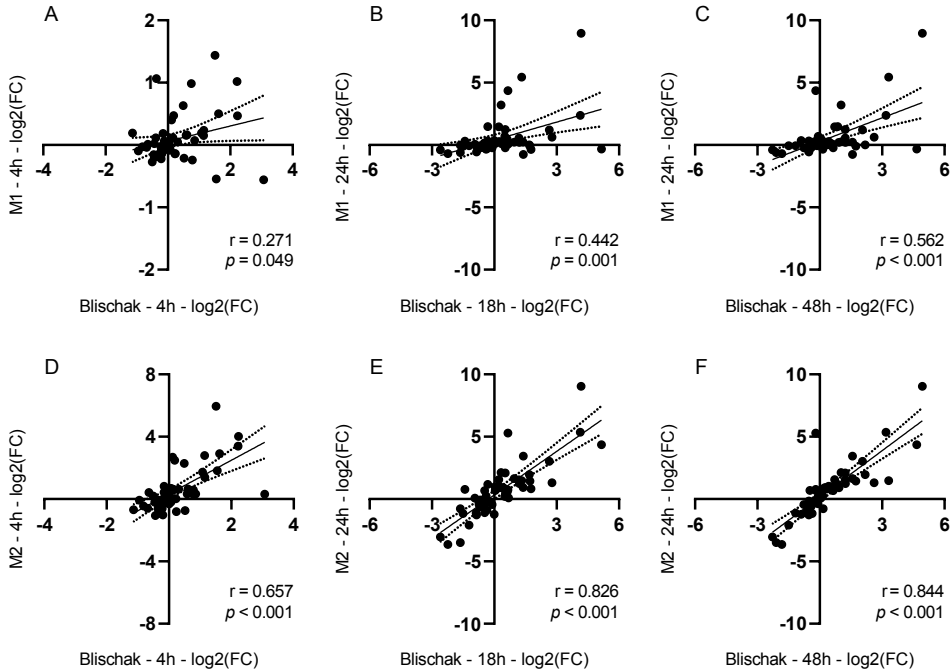


Figure S5: Metabolic gene expression profiles of Blischak *et al.* and exploratory M1/M2 RNA-seq data showed high positive correlation.

Comparison of macrophage gene expression profiles of 53 metabolic genes during *Mtb* infection between Blischak *et al.* (37) and the exploratory M1/M2 RNA-seq dataset. Correlation between: (A) M1 macrophages (4 h) versus Blischak *et al.* (4 h), (B) M1 macrophages (24 h) versus Blischak *et al.* (18 h), (C) M1 macrophages (24 h) versus Blischak *et al.* (48 h), (D) M2 macrophages (4 h) versus Blischak *et al.* (4 h), (E) M2 macrophages (24 h) versus Blischak *et al.* (18 h) and (F) M2 macrophages (24 h) versus Blischak *et al.* (48 h). Expression data is plotted as \log_2 -transformed fold changes of *Mtb* infected vs non-infected macrophages with linear regression line and 95% confidence interval. Individual genes are depicted as dots. Pearson correlation coefficient (r) and associated p-value are displayed for each comparison.

CHAPTER

8

Summarizing Discussion

Frank Vrieling¹

¹ Department of Infectious Diseases, Leiden University Medical Center, Leiden, The Netherlands



Introduction

Diabetes mellitus type 2 (DM) is a major risk factor for developing active tuberculosis (TB) disease, yet the causal mechanisms driving this association remain largely elusive. As the incidence of DM is rising, especially in TB endemic countries, it is important to identify the relevant immunological and metabolic processes that underlie TB-DM comorbidity, because such insights will facilitate optimal treatment, diagnosis and prevention. In this thesis, we have started to unravel key factors underlying the association between TB and DM using two approaches. Firstly, we identified and analyzed human macrophage subsets and studied the interactions between these human cells and a major pathogen, *Mycobacterium tuberculosis* (*Mtb*), and the specific metabolic changes involved using well-controlled *in vitro* systems. Next, we employed metabolomics to determine the impact of concurrent TB-DM on circulating metabolites in patient cohorts *ex vivo*. Here we discuss and synthesize these results (summarized in **Figure 1**) and discuss their implications for TB-DM biology, treatment, diagnosis and prevention.

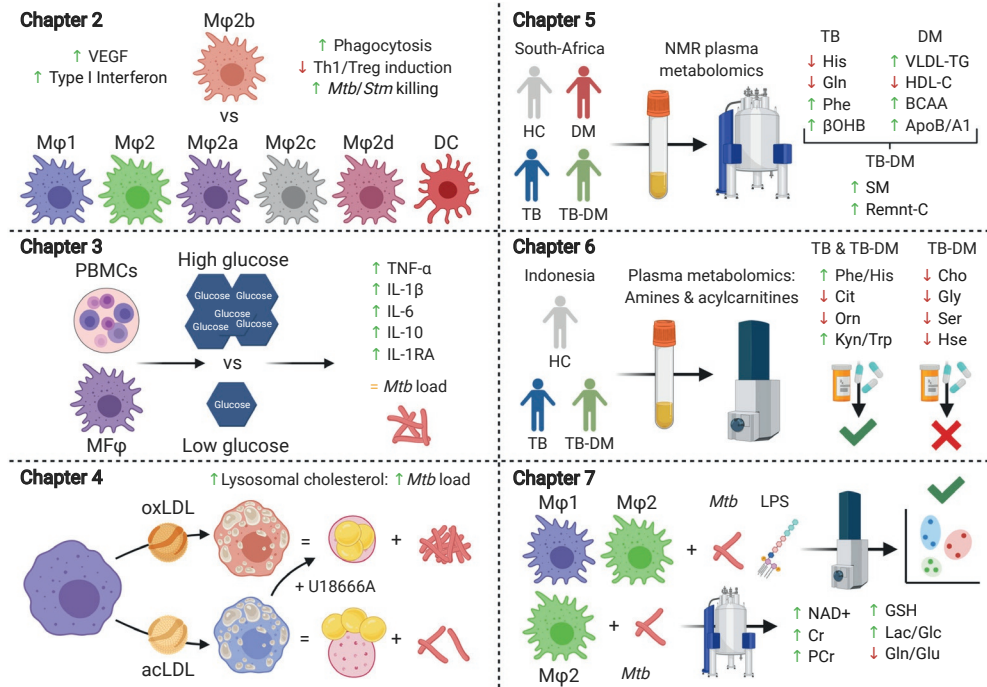


Figure 1: Schematic overview of thesis results by chapter.

Human macrophages and macrophage subsets as a model for TB(-DM)

Macrophages are key players during the *Mtb* infection cycle as they are the preferential habitat of *Mtb*. For this reason, many TB researchers use primary macrophages as a model to study *Mtb* infection dynamics *in vitro*. An important hallmark of macrophages is their high functional plasticity, which also governs their capacity to eradicate intracellular pathogens such as *Mtb*. While originally classified as either pro-inflammatory M ϕ 1 or anti-inflammatory M ϕ 2, there has recently been increasing appreciation of higher diversity within the macrophage activation spectrum (1, 2). As imbalances in tissue macrophage polarization have been demonstrated to exacerbate various diseases including TB (3), targeting macrophage differentiation holds merit as a potential therapeutic approach. The importance of macrophage function in the infectious process of *Mtb* is illustrated in **Chapter 2**, in which we characterized various M ϕ 2 subsets. We identified M ϕ 2b macrophages (induced by combined exposure to lipopolysaccharide (LPS) and IgG + ovalbumin immune complexes) as a polarized subset with potent antimicrobial activity against both *Mtb* and *Salmonella* Typhimurium, and unexpectedly, with a relatively poor capacity to induce Th1 and Treg responses compared to M ϕ 2a/c/d. The observed reduced bacterial load was not the result of diminished phagocytosis. Proteomics and transcriptomics analyses both showed that M ϕ 2b macrophages were characterized by a marked type I interferon signature, and they secreted relatively high levels of vascular endothelial growth factor (VEGF), an important mediator of granulomatous inflammation and angiogenesis in both mice (4) and zebrafish (5), in response to stimulation with a mixture of LPS, interferon- γ (IFN- γ) and *Mtb* lysate. Moreover, repolarization of M ϕ 2 subsets towards M ϕ 2b successfully induced an anti-mycobacterial phenotype, indicating that M ϕ 2b polarization could potentially be targeted as host-directed treatment of infectious diseases.

As macrophage polarization is strongly intertwined with cellular metabolism, this also provides an interesting model for studying TB-DM interactions. First, we examined whether hyperglycemia, the major hallmark of DM, could directly modulate functional macrophage cytokine responses to, or macrophage infection by *Mtb* (**Chapter 3**). Fasting blood glucose levels normally range between 4.4-6.6 mM in non-diabetics, but can reach levels as high as 25 mM during diabetic hyperglycemia. Many DM-associated complications can be attributed to hyperglycemia, including diabetic ketoacidosis and micro- and macrovascular disease (6). We found that *in vitro* differentiation of human macrophages under high glucose conditions (25 mM D-glucose) increased M ϕ 2 cytokine production (TNF- α , IL-6, IL-10, IL-1RA) in response to stimulation with LPS or *Mtb* lysate. Similar results have been obtained by other groups using both primary macrophages (7) and THP-1 cells (8). However, high glucose levels did not affect macrophage cytokine production or mycobacterial outgrowth after live *Mtb* infection. Furthermore, while several studies previously reported impaired macrophage phagocytosis as a result of hyperglycemia (9, 10), we did not observe significant differences in uptake of fluorescent

beads or mycobacteria when comparing macrophages cultured in hyperglycemic to euglycemic conditions.

Taken together, these results do not support a direct role for hyperglycemia during DM-associated TB. However, as is intrinsic to all *in vitro* research, our model of DM-associated hyperglycemia is reductionist in nature, calling for careful interpretation of its results. Firstly, only the direct effect of high glucose levels on macrophages was assessed, while other cell types and cell-cell interactions involved in TB immunity were not taken into account. Hyperglycemia has previously been shown to hamper neutrophil mobilization (11) and antibacterial activity (12), reduce immunoglobulin production by B cells (13) and induce T cell hyperresponsiveness (14). Secondly, it can be questioned whether a relatively short term incubation under hyperglycemic conditions accurately mimics the metabolic complexities of chronic DM *in vivo*, which also elicit changes in epigenetics (15). It would be of interest to study whether the observed phenotypes from **Chapter 3** can be recapitulated *ex vivo* using cells and/or serum from DM patients. For example, metabolic activation of macrophages by combined exposure to high glucose levels, insulin and palmitate resulted in a distinct pro-inflammatory phenotype which resembled adipose tissue macrophages isolated from obese humans and mice (16, 17). Finally, only the direct effects of hyperglycemia on macrophage function and *Mtb* infection were assessed. Potential indirect effects of high circulating glucose levels include the formation of advanced glycation end-products (AGEs), which can modulate macrophage inflammatory pathways (18, 19) and have been implicated in TB-associated hyperglycemia and disease severity (20). In conclusion, while our results clearly showed that hyperglycemia did not directly promote macrophage *Mtb* infection *in vitro*, other effects of hyperglycemia during TB-DM pathogenesis *in vivo* cannot be excluded.

Lipids in TB-DM: parallels between TB and atherosclerosis

As we did not find evidence for direct modulation of macrophage *Mtb* infection by elevated glucose levels, we next investigated other relevant metabolic characteristics of DM. Both T1DM and T2DM are often accompanied by dyslipidemia, characterized by aberrant circulating lipid levels. Diabetic dyslipidemia is accompanied by elevated triglycerides, increased low-density lipoprotein (LDL) levels (in case of T1DM), decreased high-density lipoprotein (HDL) levels and small dense LDL particles (21). Together, these changes in blood lipid profile put DM patients at increased risk of developing cardiovascular disorders (CVD) such as atherosclerosis, a disease which exhibits some striking pathophysiological similarities with TB. Likewise, TB is also associated with elevated risk of CVD and peripheral arterial disease, although the underlying mechanisms remain unclear (22, 23). A key event during both TB and atherosclerosis is the formation of lipid-loaded macrophages so-called foam cells, which form an integral part of both TB granulomas and atherosclerotic plaques (24, 25). *Mtb* has been demonstrated to reprogram macrophage metabolism to accumulate intracellular lipid droplets (26-28), as *Mtb* requires host-derived lipids and

cholesterol as a source of carbon (29-32). Moreover, hypercholesterolemia has been shown to negatively impact the immune response to TB (33). Therefore, we hypothesized that DM-associated changes in lipid metabolism could be involved during TB-DM.

Atherosclerotic plaque formation is initiated by extravasation of blood monocytes through the endothelium in response to local inflammatory signals, an event which is thought to be driven by oxidized low-density lipoprotein (oxLDL) particles deposited in the sub-endothelial space (34). OxLDL is a pathologically modified lipoprotein which is formed as result of oxidative stress, and circulating oxLDL levels are elevated in DM patients (35, 36). In the artery wall, oxLDL is taken up by macrophages through scavenger receptor-mediated phagocytosis, culminating in foam cell formation (37). Interestingly, oxLDL was found to accumulate in granulomas of *Mtb*-infected guinea pigs (38), and thus represented a potential connection between TB and DM. We found that treatment with increasing concentrations of oxLDL induced a dose-dependent lipid accumulation in human macrophages, which strongly supported intracellular *Mtb* survival after infection (**Chapter 4**). Mechanistically, oxLDL induced lysosomal cholesterol accumulation, which was accompanied by reduced colocalization of *Mtb* with functional lysosomes. Treatment with acetylated LDL (acLDL), a modified lipoprotein which is taken up by similar pathways but does not accumulate in lysosomes (39), did not result in increased *Mtb* outgrowth unless combined with a lysosomal cholesterol transport inhibitor, highlighting that the subcellular localization of cholesterol was pivotal for the effect of oxLDL. These results were in line with earlier observations that cholesterol accumulation, for instance in the lysosomal storage disorder Niemann-Pick Disease Type C (NPC), can inhibit phagosome maturation and autophagy in macrophages, both involved in controlling intracellular infections (40-43). A study by Fineran *et al.* showed that mycobacterial infection itself triggered a NPC-like phenotype in macrophages which supported mycobacterial intracellular persistence (44), indicating that modulation of this pathway could be part of the pathogen's defense machinery. In agreement with these results, cholesterol depletion restored phagosome maturation in *Mycobacterium avium* infected macrophages (45).

While these results demonstrated that DM-associated lipids can promote *Mtb* infection *in vitro*, it was unknown whether lipid metabolism would be similarly altered in patients with concurrent TB-DM. In contrast to DM, TB is often accompanied by malnutrition and wasting syndrome (46). In **Chapter 5**, we analyzed plasma ¹H-nuclear magnetic resonance (NMR) spectroscopy biomarker profiles of TB, DM and TB-DM TB patients from South-Africa to examine the respective correlations of these markers with patients' lipid metabolism. As expected, DM patients presented with dyslipidemia, characterized by hypertriglyceridemia and decreased HDL-cholesterol, while TB patients showed clear signs of wasting disease in the form of low blood levels of amino acids. Interestingly, TB-DM presented with hallmarks of both wasting and dyslipidemia, seemingly reflecting a metabolic 'tug-of-war' between TB and DM and resulting in relatively high interindividual variation. Another explanation for this heterogeneity could be variations in DM duration,

as the TB-DM group consisted of both newly diagnosed and chronic diabetics. Besides high levels of triglycerides and low levels of HDL-C, TB-DM patients showed disease interaction-specific increases in remnant-like lipoprotein particles and sphingomyelin levels, both of which are associated with increased atherogenesis (47-49). Finally, we were able to confirm that circulating oxLDL levels are elevated in DM patients from this cohort (**Chapter 4**). This is an important observation as DM patients are the specific population at increased risk for developing active TB, indicating a possible relationship between increased circulating lipid, in particular oxLDL levels and TB. Although this increase was not observed in the TB-DM patient group, oxLDL levels showed a strong positive correlation with plasma triglyceride levels in these patients, implying that oxLDL levels were associated with severity of dyslipidemia.

Together, **Chapter 4** and **Chapter 5** support a role for atherogenic changes as risk factors during TB-DM development, both *in vitro* and *in vivo*. A major contributor to atherosclerosis is oxidative stress (50). Both TB and DM are associated with increased generation of free radicals and a reduction in anti-oxidative capacity (50-53), which can lead to formation of modified proteins and lipids such as oxLDL and AGEs. Moreover, DM and hyperglycemia increase expression of oxLDL scavenger receptors such as CD36 in macrophages (54-56), which has also been shown to promote *Mtb* growth by mediating uptake of surfactant lipids (57). Combined with the observed changes in circulating lipids, these changes could drive monocytes and macrophages towards foam cell formation during TB-DM, potentially contributing to granuloma caseation, a pathognomonic feature of TB (58). In support of this, histological analysis of TB patient lung biopsies showed that DM and dyslipidemia correlated with enlarged areas of caseous necrosis (59). Previous studies already established that *Mtb* can utilize host lipids for intracellular growth (57, 60). In **Chapter 4**, we demonstrated that lipid accumulation can also directly interfere with macrophage mycobacterial growth inhibition, depending on their intracellular localization. Accelerated foam cell biogenesis during TB-DM could therefore support both primary *Mtb* infection by interfering with mycobacterial growth inhibition and promoting (future) reactivation by providing a nutritionally rich niche for replication. These results support further investigation into the beneficial effects of lipid lowering drugs for treatment of TB-DM. Various studies have demonstrated the efficacy of statins for adjunctive therapy for TB (61-64), although some of these did not observe a protective effect of statin-usage against TB in patients with DM (65, 66). Another paper showed a reduced incidence of latent TB infection in DM patients receiving the cholesterol-lowering drug ezetimibe (67). Recently, antagonists of PCSK9 (68), a protein which regulates LDL-receptor expression, have shown promise for treatment of atherosclerosis, and it would therefore be of interest to investigate whether PCSK9 inhibitors could also benefit patients with TB-DM.

Despite the apparent similarities between atherosclerosis and TB, multiple questions remain to be answered. A recent study reported that triglycerides and not cholesteryl esters were the dominant storage lipids in granulomas of *Mtb*-infected

marmosets and rabbits, a process which was regulated by TNF- α signaling through activation of the caspase cascade and mammalian target of rapamycin complex 1 (mTORC1) (69). These results suggest that TB-associated foam cell biogenesis may be reliant on activation of specific intracellular signaling pathways and not on uptake of cholesterol-rich lipoproteins, as is the case during atherosclerosis. In addition, another recent paper found protective role for lipid droplet formation during *Mtb* control by supporting eicosanoid production in murine macrophages (70). However, neither paper assessed the impact of DM on lipid metabolism and foam cell formation during TB. It would be of interest to study granuloma lipid composition in an *in vivo* DM model and/or TB-DM patients. Simultaneously, the presence of oxidized lipid species in granuloma macrophages could be determined to substantiate potential involvement of oxLDL. Furthermore, while our results provide evidence for defective phagolysosomal killing in oxLDL-treated macrophages, the participating molecular players remain to be identified. Lysosomal lipid storage disorders can interfere with phagolysosomal function through dysregulated Ca²⁺-signaling (43, 71) and autophagy (41, 42), however, pharmacological modulation of these pathways could not rescue the oxLDL-induced phenotype (**Chapter 4**). Finally, due to the cross-sectional design of the study described in **Chapter 5**, the observed atherogenic changes cannot be causally linked to TB-DM pathophysiology as of yet. Some studies have reported a DM-independent protective effect of obesity on active TB development (72-74), further illustrating the complexity of the TB-DM conundrum. Longitudinal studies which assess and manipulate TB-DM patient lipid profiles in large prospective cohorts will be necessary to conclusively validate a possible link between atherogenic changes and TB-DM development.

Metabolomics of TB-DM: what have we learned?

The first usage of a primitive form of metabolomics can be traced back thousands of years to ancient physicians from China, Babylon and Egypt, who evaluated characteristics of urine to diagnose and predict onset of disease, including detection of diabetes by its sweet smell and taste (75). Since its first modern application in 1971 by Pauling *et al.* (76), metabolomics has developed into a powerful tool to study pathophysiological processes of human disease. Over the past decade researchers have successfully employed metabolomics to identify biomarkers for various human diseases, including Alzheimer's (77), cancer (78), and diabetes (79). In concert with the rise of immunometabolism as a field of research, metabolomics has also attracted growing attention as a method to study the impact of infectious diseases on host metabolism (80), for instance leading to the development of diagnostic signatures for sepsis (81). A recent study by Weiner *et al.* highlighted the potential of metabolomics for TB research (82), as they reported a prognostic metabolite signature for active TB with 69% sensitivity at 75% specificity within 5 months prior to TB diagnosis. Importantly, some of the observed metabolic changes

were already present 12 months before active disease was diagnosed, and can therefore potentially be used for timely identification of TB progressors (83).

We used targeted metabolomics to analyze the overall effects of TB-DM on plasma metabolic profiles in two different patient cohorts, respectively from South-Africa (**Chapter 5**) and Indonesia (**Chapter 6**), while employing different measurement platforms. In both studies, TB and TB-DM patients had signs of wasting as represented by strongly decreased levels of many amino acids. Specifically, low levels of circulating histidine showed very high predictive power for TB and TB-DM in both studies, which is in agreement with previous plasma metabolic profiling of TB patients (84). Weiner *et al.* showed that histidine levels started to deviate from 9 months prior to manifestation of clinical TB (82), substantiating its promise for early detection of TB. In contrast to histidine, plasma phenylalanine concentrations were increased in both TB patient cohorts. The ratio of phenylalanine over histidine (Phe / His) was a more potent signature for TB classification, as expected. In line with this, both amino acids were part of the 10 metabolite prognostic signature described by Weiner *et al.* (82). Other early changes in amino acid levels reported in this paper included low concentrations of citrulline and tryptophan with increasing kynurenine levels over time proximal to disease onset, all of which were in agreement with our own results from **Chapter 6**. Previous studies demonstrated similarly low levels of tryptophan and/or elevated concentrations of kynurenine in serum (84-86) or pleural fluid (87) from TB patients. This increased ratio of kynurenine over tryptophan (Kyn / Trp) is indicative of a higher activity of the immunoregulatory enzyme indoleamine 2,3-dioxygenase (IDO) which catalyzes the rate-limiting step of tryptophan catabolism and has been implicated in attenuated control of *Mtb* infection (73). Citrulline is an urea cycle intermediate which can be used to synthesize arginine, a process which has been demonstrated to contribute to the anti-mycobacterial response in macrophages (88, 89) and T-cells (90). Importantly, antibiotic treatment resulted in normalization to levels observed in healthy controls for the majority of the TB-associated amines investigated. In conclusion, we find that both TB and TB-DM are associated with major changes in amino acid levels; these results are validated by other metabolomics studies using different technical platforms as well cohorts from different geographical regions, thus enhancing the plausibility of our results.

Importantly, the results from **Chapter 5** and **Chapter 6** are suggestive of alterations in liver function during TB-DM. Our measurements reported in **Chapter 5** showed that TB-DM resulted in disease interaction-specific increases in remnant-like lipoprotein particles, sphingomyelins and LDL-triglyceride content, suggesting that concurrent TB-DM affects the function of hepatic enzymes involved in lipoprotein and lipid biosynthesis. Successive lipolysis by lipoprotein lipase (LPL) and hepatic triglyceride (HTGL) mediates conversion of triglyceride-rich chylomicrons and very low-density lipoprotein particles to intermediate density lipoprotein and LDL particles (91). The observed changes in lipoprotein size and content could therefore reflect a disruption of the relative activities of LPL and HTGL.

Sphingomyelin synthesis is mediated by serine palmitoyltransferase (SPT). Hepatic SPT activity was found to be elevated by inflammatory signaling, leading to alterations in lipoprotein composition (92). In line with these results, in **Chapter 6** we reported lower levels of glycine, serine, threonine and homoserine in TB-DM compared to TB patients. Low levels of these amino acids are associated with non-alcoholic fatty liver disease (NAFLD) development, potentially through their role in glutathione (GSH) synthesis (93, 94), although we did not observe significant alterations in GSH concentrations during TB-DM. Additionally, plasma concentrations of free choline were extremely low in TB-DM patients, and choline deficiency has been similarly connected to NAFLD (95, 96). Finally, we find that anti-TB therapy resulted in increased levels of metabolic markers of drug-induced liver injury, and it was previously demonstrated that streptozotocin-induced diabetes exacerbated liver injury and steatosis resulting from anti-tubercular treatment in rats (97). While NAFLD development as a common comorbidity of DM is widely recognized, much less is known about the occurrence of non-alcoholic hepatic steatosis during TB. Autopsy studies spanning multiple decades have demonstrated that TB is often associated with fatty liver infiltration (98-100), however, it is unclear whether this is directly related to disease or to comorbidities such as alcohol abuse or malnutrition. In conclusion, observed changes in plasma metabolic profiles from **Chapter 5** and **Chapter 6** could be related to increased liver dysfunction and/or damage as a result of concurrent TB-DM, calling for increased liver function monitoring in patients, especially during antibiotic treatment.

A major question which remains to be answered is whether the metabolic changes reported in **Chapter 5** and **Chapter 6** are truly specific for TB or TB-DM, or simply a reflection of ongoing oxidative stress and/or inflammation. For example, low levels of histidine, one of the strongest individual biomarkers for TB, have also been reported in patients with rheumatoid arthritis (101), sepsis (102) and obesity (103). It would therefore be of great interest to directly compare the metabolic effects of TB to other respiratory diseases in patients with or without concurrent DM, such as sarcoidosis or lung cancer, as this could both establish their association with disease and provide additional information on the involved pathological mechanisms. Additionally, future metabolomics studies on TB-DM will need to advance from cross-sectional to prospective patient cohorts akin to Weiner *et al.* (82) to substantiate a possible causal role of specific metabolites for TB-DM development, preferentially including a treatment arm to investigate the effect of modulating the circulating levels of a metabolite of choice such as statins. Finally, to effectively utilize potential diagnostic or predictive metabolic biomarker signatures for TB or TB-DM in clinical or field settings, current methodologies for quantification of these metabolites will have to be translated to user-friendly tests. An example of this could be the development of paper-based metabolic assays using metabolite-specific bioluminescent sensor proteins, a technique which has been successfully demonstrated for analysis of phenylalanine concentrations in finger-prick samples of phenylketonuria patients (104).

Finally, we performed cellular metabolomics using *Mtb*-infected macrophages

to increase our insights into the fundamental effects of *Mtb* infection on macrophage metabolism (**Chapter 7**). ¹H-NMR revealed that macrophage *Mtb* infection induced elevated levels in nicotinamide-adenine-dinucleotide (NAD⁺), creatine and creatine phosphate, glutamine catabolism and glycolysis. These results were corroborated by analysis of in-house and previously published (105) RNA-sequencing datasets of *Mtb*-infected macrophages revealed alterations in gene expression of key enzymes regulating these metabolic pathways. The role of NAD⁺ metabolism during macrophage *Mtb* infection is of particular interest, as multiple recent papers have demonstrated the importance of maintaining adequate NAD⁺ pools for macrophage activation (106-108). NAD⁺-boosting therapy has shown potential for treatment of various conditions (108), and these results prompt further investigation into the importance of NAD⁺ metabolism during macrophage *Mtb* infection. Another recent paper revealed that SLC6A8-mediated creatine uptake supported anti-inflammatory interleukin-4 (IL-4) polarization in macrophages, while simultaneously suppressing pro-inflammatory IFN- γ -mediated macrophage activation (109). As the results from **Chapter 2** illustrate the importance of polarization state for macrophage anti-mycobacterial functions, it would be of interest to study whether increased intracellular creatine levels differentially influence the capacity of macrophage subsets to control *Mtb* infection.

Concluding comments

In this thesis we present evidence derived from *in vitro* experiments and from *ex vivo* observational data which collectively suggest a pathogenic role of atherogenic lipid species during TB development. Mechanistically, increased intracellular levels of lipids and cholesterol could support *Mtb* survival by interfering with macrophage antimicrobial functions, while also providing increased access to nutrients and carbons sources during chronic disease. Although the results from our observational data by definition can only highlight correlations between dyslipidemia and TB-DM and not demonstrate causality, several interventional studies have demonstrated that lipid-lowering drugs such as statins have potential as adjunctive TB therapy (61-64). Besides their effect on blood cholesterol levels, statins have also been shown to modulate bacterial intracellular growth and virulence *in vitro*, making them an interesting candidate for drug repurposing (63, 110, 111). Future prospective studies should elucidate whether pharmacological normalization of blood lipid levels can reduce the risk of DM patients to develop active TB, or lead to improved TB and TB-DM treatment outcomes when given in conjunction with standard antibiotic regimens. To further dissect and determine the contribution of individual metabolic changes on DM-associated *Mtb* infection, future studies will be needed, including animal models of TB-DM, prospective interventional human cohort studies, as well as novel holistic and mechanistic models such as organs-on-chips, to determine mechanisms of action. These studies are important given the rapidly increasing TB-DM co-epidemic, which will have great impact on future global health if not controlled in time.

References

1. Amit I, Winter DR, & Jung S (2015) The role of the local environment and epigenetics in shaping macrophage identity and their effect on tissue homeostasis. *Nat.Immunol.* 17(1):18-25.
2. Lavin Y, Mortha A, Rahman A, & Merad M (2015) Regulation of macrophage development and function in peripheral tissues. *Nat.Rev.Immunol.* 15(12):731-744.
3. Sica A & Mantovani A (2012) Macrophage plasticity and polarization: in vivo veritas. *J.Clin.Invest* 122(3):787-795.
4. Harding JS, *et al.* (2019) VEGF-A from Granuloma Macrophages Regulates Granulomatous Inflammation by a Non-angiogenic Pathway during Mycobacterial Infection. *Cell reports* 27(7):2119-2131.e2116.
5. Walton EM, *et al.* (2018) Cyclopropane Modification of Trehalose Dimycolate Drives Granuloma Angiogenesis and Mycobacterial Growth through Vegf Signaling. *Cell host & microbe* 24(4):514-525.e516.
6. Marcovecchio ML, Lucantoni M, & Chiarelli F (2011) Role of chronic and acute hyperglycemia in the development of diabetes complications. *Diabetes Technol Ther* 13(3):389-394.
7. Grosick R, Alvarado-Vazquez PA, Messersmith AR, & Romero-Sandoval EA (2018) High glucose induces a priming effect in macrophages and exacerbates the production of pro-inflammatory cytokines after a challenge. *J Pain Res* 11:1769-1778.
8. Moganti K, *et al.* (2017) Hyperglycemia induces mixed M1/M2 cytokine profile in primary human monocyte-derived macrophages. *Immunobiology* 222(10):952-959.
9. Restrepo BI, Twahirwa M, Rahbar MH, & Schlesinger LS (2014) Phagocytosis via complement or Fc-gamma receptors is compromised in monocytes from type 2 diabetes patients with chronic hyperglycemia. *PLoS.One.* 9(3):e92977.
10. Montoya-Rosales A, Castro-Garcia P, Torres-Juarez F, Enciso-Moreno JA, & Rivas-Santiago B (2016) Glucose levels affect LL-37 expression in monocyte-derived macrophages altering the Mycobacterium tuberculosis intracellular growth control. *Microbial pathogenesis* 97:148-153.
11. Fainsod-Levi T, *et al.* (2017) Hyperglycemia Impairs Neutrophil Mobilization Leading to Enhanced Metastatic Seeding. *Cell reports* 21(9):2384-2392.
12. Javid A, *et al.* (2016) Hyperglycemia Impairs Neutrophil-Mediated Bacterial Clearance in Mice Infected with the Lyme Disease Pathogen. *PloS one* 11(6):e0158019.
13. Sakowicz-Burkiewicz M, *et al.* (2013) High glucose concentration impairs ATP outflow and immunoglobulin production by human peripheral B lymphocytes: involvement of P2X7 receptor. *Immunobiology* 218(4):591-601.
14. Martinez N, *et al.* (2014) Chromatin decondensation and T cell hyperresponsiveness in diabetes-associated hyperglycemia. *Journal of immunology* 193(9):4457-4468.
15. Ahmed M, de Winther MPJ, & Van den Bossche J (2017) Epigenetic mechanisms of macrophage activation in type 2 diabetes. *Immunobiology* 222(10):937-943.
16. Kratz M, *et al.* (2014) Metabolic dysfunction drives a mechanistically distinct proinflammatory phenotype in adipose tissue macrophages. *Cell Metab* 20(4):614-625.

17. Coats BR, *et al.* (2017) Metabolically Activated Adipose Tissue Macrophages Perform Detrimental and Beneficial Functions during Diet-Induced Obesity. *Cell reports* 20(13):3149-3161.
18. Son S, *et al.* (2017) Advanced glycation end products impair NLRP3 inflammasome-mediated innate immune responses in macrophages. *The Journal of biological chemistry* 292(50):20437-20448.
19. Pertynska-Marczewska M, *et al.* (2004) Advanced glycation end products upregulate angiogenic and pro-inflammatory cytokine production in human monocyte/macrophages. *Cytokine* 28(1):35-47.
20. Podell BK, *et al.* (2012) Non-diabetic hyperglycemia exacerbates disease severity in Mycobacterium tuberculosis infected guinea pigs. *PLoS one* 7(10):e46824.
21. Dake AW & Sora ND (2016) Diabetic Dyslipidemia Review: An Update on Current Concepts and Management Guidelines of Diabetic Dyslipidemia. *Am J Med Sci* 351(4):361-365.
22. Huaman MA, Henson D, Ticona E, Sterling TR, & Garvy BA (2015) Tuberculosis and Cardiovascular Disease: Linking the Epidemics. *Trop Dis Travel Med Vaccines* 1.
23. Wang SH, *et al.* (2017) Tuberculosis increases the risk of peripheral arterial disease: A nationwide population-based study. *Respirology* 22(8):1670-1676.
24. Russell DG, Cardona PJ, Kim MJ, Allain S, & Altare F (2009) Foamy macrophages and the progression of the human tuberculosis granuloma. *Nature immunology* 10(9):943-948.
25. Moore KJ & Freeman MW (2006) Scavenger receptors in atherosclerosis: beyond lipid uptake. *Arteriosclerosis, thrombosis, and vascular biology* 26(8):1702-1711.
26. Ouimet M, *et al.* (2016) Mycobacterium tuberculosis induces the miR-33 locus to reprogram autophagy and host lipid metabolism. *Nature immunology* 17(6):677-686.
27. Mahajan S, *et al.* (2012) Mycobacterium tuberculosis modulates macrophage lipid-sensing nuclear receptors PPARgamma and TR4 for survival. *J.Immunol.* 188(11):5593-5603.
28. Singh V, *et al.* (2012) Mycobacterium tuberculosis-driven targeted recalibration of macrophage lipid homeostasis promotes the foamy phenotype. *Cell host & microbe* 12(5):669-681.
29. Santucci P, *et al.* (2016) Experimental Models of Foamy Macrophages and Approaches for Dissecting the Mechanisms of Lipid Accumulation and Consumption during Dormancy and Reactivation of Tuberculosis. *Frontiers in cellular and infection microbiology* 6:122.
30. Maurya RK, Bharti S, & Krishnan MY (2018) Triacylglycerols: Fuelling the Hibernating Mycobacterium tuberculosis. *Frontiers in cellular and infection microbiology* 8:450.
31. Pandey AK & Sasseti CM (2008) Mycobacterial persistence requires the utilization of host cholesterol. *Proceedings of the National Academy of Sciences of the United States of America* 105(11):4376-4380.
32. Peyron P, *et al.* (2008) Foamy macrophages from tuberculous patients' granulomas constitute a nutrient-rich reservoir for M. tuberculosis persistence. *PLoS pathogens* 4(11):e1000204.
33. Martens GW, *et al.* (2008) Hypercholesterolemia impairs immunity to tuberculosis. *Infection and immunity* 76(8):3464-3472.

34. Miller YI, *et al.* (2011) Oxidation-specific epitopes are danger-associated molecular patterns recognized by pattern recognition receptors of innate immunity. *Circulation research* 108(2):235-248.
35. Toshima S, *et al.* (2000) Circulating oxidized low density lipoprotein levels. A biochemical risk marker for coronary heart disease. *Arteriosclerosis, thrombosis, and vascular biology* 20(10):2243-2247.
36. Njajou OT, *et al.* (2009) Association between oxidized LDL, obesity and type 2 diabetes in a population-based cohort, the Health, Aging and Body Composition Study. *Diabetes/ metabolism research and reviews* 25(8):733-739.
37. Park YM (2014) CD36, a scavenger receptor implicated in atherosclerosis. *Exp Mol Med* 46:e99.
38. Palanisamy GS, *et al.* (2012) Uptake and accumulation of oxidized low-density lipoprotein during Mycobacterium tuberculosis infection in guinea pigs. *PLoS.One.* 7(3):e34148.
39. Yancey PG & Jerome WG (1998) Lysosomal sequestration of free and esterified cholesterol from oxidized low density lipoprotein in macrophages of different species. *Journal of lipid research* 39(7):1349-1361.
40. Huynh KK, Gershenson E, & Grinstein S (2008) Cholesterol accumulation by macrophages impairs phagosome maturation. *The Journal of biological chemistry* 283(51):35745-35755.
41. Sarkar S, *et al.* (2013) Impaired autophagy in the lipid-storage disorder Niemann-Pick type C1 disease. *Cell reports* 5(5):1302-1315.
42. Schwerd T, *et al.* (2016) Impaired antibacterial autophagy links granulomatous intestinal inflammation in Niemann-Pick disease type C1 and XIAP deficiency with NOD2 variants in Crohn's disease. *Gut.*
43. Shen D, *et al.* (2012) Lipid storage disorders block lysosomal trafficking by inhibiting a TRP channel and lysosomal calcium release. *Nature communications* 3:731.
44. Fineran P, *et al.* (2016) Pathogenic mycobacteria achieve cellular persistence by inhibiting the Niemann-Pick Type C disease cellular pathway. *Wellcome open research* 1:18.
45. de Chastellier C & Thilo L (2006) Cholesterol depletion in Mycobacterium avium-infected macrophages overcomes the block in phagosome maturation and leads to the reversible sequestration of viable mycobacteria in phagolysosome-derived autophagic vacuoles. *Cellular microbiology* 8(2):242-256.
46. Schwenk A & Macallan DC (2000) Tuberculosis, malnutrition and wasting. *Curr Opin Clin Nutr Metab Care* 3(4):285-291.
47. Dong J, *et al.* (2006) Adenovirus-mediated overexpression of sphingomyelin synthases 1 and 2 increases the atherogenic potential in mice. *Journal of lipid research* 47(6):1307-1314.
48. Ruuth M, *et al.* (2018) Susceptibility of low-density lipoprotein particles to aggregate depends on particle lipidome, is modifiable, and associates with future cardiovascular deaths. *Eur Heart J* 39(27):2562-2573.
49. Varbo A, Benn M, & Nordestgaard BG (2014) Remnant cholesterol as a cause of ischemic heart disease: evidence, definition, measurement, atherogenicity, high risk patients, and present and future treatment. *Pharmacol Ther* 141(3):358-367.

50. Giacco F & Brownlee M (2010) Oxidative stress and diabetic complications. *Circulation research* 107(9):1058-1070.
51. Ceriello A, et al. (2002) Evidence for an independent and cumulative effect of postprandial hypertriglyceridemia and hyperglycemia on endothelial dysfunction and oxidative stress generation: effects of short- and long-term simvastatin treatment. *Circulation* 106(10):1211-1218.
52. Palanisamy GS, et al. (2011) Evidence for oxidative stress and defective antioxidant response in guinea pigs with tuberculosis. *PloS one* 6(10):e26254.
53. Venketaraman V, et al. (2008) Glutathione levels and immune responses in tuberculosis patients. *Microbial pathogenesis* 44(3):255-261.
54. Lu H, et al. (2013) High glucose induces upregulation of scavenger receptors and promotes maturation of dendritic cells. *Cardiovascular diabetology* 12:80.
55. Fukuhara-Takaki K, Sakai M, Sakamoto Y, Takeya M, & Horiuchi S (2005) Expression of class A scavenger receptor is enhanced by high glucose in vitro and under diabetic conditions in vivo: one mechanism for an increased rate of atherosclerosis in diabetes. *The Journal of biological chemistry* 280(5):3355-3364.
56. Chen M, et al. (2001) Diabetes enhances lectin-like oxidized LDL receptor-1 (LOX-1) expression in the vascular endothelium: possible role of LOX-1 ligand and AGE. *Biochem Biophys Res Commun* 287(4):962-968.
57. Dodd CE, Pyle CJ, Glowinski R, Rajaram MV, & Schlesinger LS (2016) CD36-Mediated Uptake of Surfactant Lipids by Human Macrophages Promotes Intracellular Growth of Mycobacterium tuberculosis. *Journal of immunology* 197(12):4727-4735.
58. Kim MJ, et al. (2010) Caseation of human tuberculosis granulomas correlates with elevated host lipid metabolism. *EMBO molecular medicine* 2(7):258-274.
59. Dong Z, et al. (2017) Hemostasis and lipoprotein indices signify exacerbated lung injury in tuberculosis with diabetes comorbidity. *Chest*.
60. Genoula M, et al. (2018) Formation of Foamy Macrophages by Tuberculous Pleural Effusions Is Triggered by the Interleukin-10/Signal Transducer and Activator of Transcription 3 Axis through ACAT Upregulation. *Frontiers in immunology* 9:459.
61. Su VY, et al. (2017) Statin Use Is Associated With a Lower Risk of TB. *Chest* 152(3):598-606.
62. Lai CC, et al. (2016) Statin treatment is associated with a decreased risk of active tuberculosis: an analysis of a nationally representative cohort. *Thorax* 71(7):646-651.
63. Parihar SP, et al. (2014) Statin therapy reduces the mycobacterium tuberculosis burden in human macrophages and in mice by enhancing autophagy and phagosome maturation. *J Infect Dis* 209(5):754-763.
64. Dutta NK, et al. (2016) Statin adjunctive therapy shortens the duration of TB treatment in mice. *J Antimicrob Chemother* 71(6):1570-1577.
65. Kim MC, et al. (2019) Association between Tuberculosis, Statin Use, and Diabetes: A Propensity Score-Matched Analysis. *Am J Trop Med Hyg* 101(2):350-356.

66. Kang YA, *et al.* (2014) The effects of statin use on the development of tuberculosis among patients with diabetes mellitus. *Int J Tuberc Lung Dis* 18(6):717-724.
67. Tsai IF, *et al.* (2017) Potential effect of ezetimibe against Mycobacterium tuberculosis infection in type II diabetes. *Respirology* 22(3):559-566.
68. Shapiro MD & Fazio S (2017) PCSK9 and Atherosclerosis - Lipids and Beyond. *Journal of atherosclerosis and thrombosis* 24(5):462-472.
69. Guerrini V, *et al.* (2018) Storage lipid studies in tuberculosis reveal that foam cell biogenesis is disease-specific. *PLoS pathogens* 14(8):e1007223.
70. Knight M, Braverman J, Asfaha K, Gronert K, & Stanley S (2018) Lipid droplet formation in Mycobacterium tuberculosis infected macrophages requires IFN-gamma/HIF-1alpha signaling and supports host defense. *PLoS pathogens* 14(1):e1006874.
71. Lloyd-Evans E, *et al.* (2008) Niemann-Pick disease type C1 is a sphingosine storage disease that causes deregulation of lysosomal calcium. *Nature medicine* 14(11):1247-1255.
72. Yen YF, *et al.* (2017) Obesity/overweight reduces the risk of active tuberculosis: a nationwide population-based cohort study in Taiwan. *Int J Obes (Lond)* 41(6):971-975.
73. Lin HH, *et al.* (2017) Association of obesity, diabetes, and risk of tuberculosis: two population-based cohorts. *Clin Infect Dis*.
74. Lonnoth K, Williams BG, Cegielski P, & Dye C (2010) A consistent log-linear relationship between tuberculosis incidence and body mass index. *Int J Epidemiol* 39(1):149-155.
75. Echeverry G, Hortin GL, & Rai AJ (2010) Introduction to urinalysis: historical perspectives and clinical application. *Methods Mol Biol* 641:1-12.
76. Pauling L, Robinson AB, Teranishi R, & Cary P (1971) Quantitative analysis of urine vapor and breath by gas-liquid partition chromatography. *Proceedings of the National Academy of Sciences of the United States of America* 68(10):2374-2376.
77. Varma VR, *et al.* (2018) Brain and blood metabolite signatures of pathology and progression in Alzheimer disease: A targeted metabolomics study. *PLoS Med* 15(1):e1002482.
78. Armitage EG & Ciborowski M (2017) Applications of Metabolomics in Cancer Studies. *Adv Exp Med Biol* 965:209-234.
79. Pallares-Mendez R, Aguilar-Salinas CA, Cruz-Bautista I, & Del Bosque-Plata L (2016) Metabolomics in diabetes, a review. *Ann Med* 48(1-2):89-102.
80. Zurfluh S, *et al.* (2018) The role of metabolomic markers for patients with infectious diseases: implications for risk stratification and therapeutic modulation. *Expert Rev Anti Infect Ther* 16(2):133-142.
81. To KK, *et al.* (2015) Lipid mediators of inflammation as novel plasma biomarkers to identify patients with bacteremia. *J Infect* 70(5):433-444.
82. Weiner J, *et al.* (2018) Metabolite changes in blood predict the onset of tuberculosis. *Nature communications* 9(1):5208.
83. Duffy FJ, *et al.* (2019) Immunometabolic Signatures Predict Risk of Progression to Active Tuberculosis and Disease Outcome. *Frontiers in immunology* 10:527.

84. Weiner J, 3rd, *et al.* (2012) Biomarkers of inflammation, immunosuppression and stress with active disease are revealed by metabolomic profiling of tuberculosis patients. *PLoS one* 7(7):e40221.
85. Suzuki Y, *et al.* (2012) Serum indoleamine 2,3-dioxygenase activity predicts prognosis of pulmonary tuberculosis. *Clin Vaccine Immunol* 19(3):436-442.
86. Feng S, *et al.* (2015) Analysis of serum metabolic profile by ultra-performance liquid chromatography-mass spectrometry for biomarkers discovery: application in a pilot study to discriminate patients with tuberculosis. *Chin Med J (Engl)* 128(2):159-168.
87. Suzuki Y, *et al.* (2013) Indoleamine 2,3-dioxygenase in the pathogenesis of tuberculous pleurisy. *Int J Tuberc Lung Dis* 17(11):1501-1506.
88. Lange SM, *et al.* (2019) L-Arginine Synthesis from L-Citrulline in Myeloid Cells Drives Host Defense against Mycobacteria In Vivo. *Journal of immunology*.
89. Rapovy SM, *et al.* (2015) Differential Requirements for L-Citrulline and L-Arginine during Antimycobacterial Macrophage Activity. *Journal of immunology* 195(7):3293-3300.
90. Lange SM, *et al.* (2017) L-Citrulline Metabolism in Mice Augments CD4(+) T Cell Proliferation and Cytokine Production In Vitro, and Accumulation in the Mycobacteria-Infected Lung. *Frontiers in immunology* 8:1561.
91. Goldberg IJ, *et al.* (1982) Lipoprotein metabolism during acute inhibition of hepatic triglyceride lipase in the cynomolgus monkey. *The Journal of clinical investigation* 70(6):1184-1192.
92. Memon RA, *et al.* (1998) Endotoxin and cytokines increase hepatic sphingolipid biosynthesis and produce lipoproteins enriched in ceramides and sphingomyelin. *Arteriosclerosis, thrombosis, and vascular biology* 18(8):1257-1265.
93. Mardinoglu A, *et al.* (2017) Personal model-assisted identification of NAD(+) and glutathione metabolism as intervention target in NAFLD. *Mol Syst Biol* 13(3):916.
94. Gaggini M, *et al.* (2018) Altered amino acid concentrations in NAFLD: Impact of obesity and insulin resistance. *Hepatology* 67(1):145-158.
95. Sharpton SR, Ajmera V, & Loomba R (2019) Emerging Role of the Gut Microbiome in Nonalcoholic Fatty Liver Disease: From Composition to Function. *Clin Gastroenterol Hepatol* 17(2):296-306.
96. Leermakers ET, *et al.* (2015) Effects of choline on health across the life course: a systematic review. *Nutr Rev* 73(8):500-522.
97. Srivastava RK, Sharma S, Verma S, Arora B, & Lal H (2008) Influence of diabetes on liver injury induced by antitubercular drugs and on silymarin hepatoprotection in rats. *Methods Find Exp Clin Pharmacol* 30(10):731-737.
98. JONES JM & PECK WM (1944) INCIDENCE OF FATTY LIVER IN TUBERCULOSIS WITH SPECIAL REFERENCE TO TUBERCULOUS ENTERITIS. *JAMA Internal Medicine* 74(5):371-374.
99. Amarapurkar A & Agrawal V (2006) Liver involvement in tuberculosis—an autopsy study. *Trop Gastroenterol* 27(2):69-74.
100. Amarapurkar A & Ghansar T (2007) Fatty liver: experience from western India. *Ann Hepatol* 6(1):37-40.

101. Gerber DA (1975) Low free serum histidine concentration in rheumatoid arthritis. A measure of disease activity. *The Journal of clinical investigation* 55(6):1164-1173.
102. Su L, *et al.* (2015) Dynamic changes in amino acid concentration profiles in patients with sepsis. *PloS one* 10(4):e0121933.
103. Niu YC, *et al.* (2012) Histidine and arginine are associated with inflammation and oxidative stress in obese women. *Br J Nutr* 108(1):57-61.
104. Yu Q, *et al.* (2018) Semisynthetic sensor proteins enable metabolic assays at the point of care. *Science* 361(6407):1122-1126.
105. Blischak JD, Tailleux L, Mitrano A, Barreiro LB, & Gilad Y (2015) Mycobacterial infection induces a specific human innate immune response. *Sci Rep* 5:16882.
106. Cameron AM, *et al.* (2019) Inflammatory macrophage dependence on NAD(+) salvage is a consequence of reactive oxygen species-mediated DNA damage. *Nature immunology* 20(4):420-432.
107. Minhas PS, *et al.* (2019) Macrophage de novo NAD(+) synthesis specifies immune function in aging and inflammation. *Nature immunology* 20(1):50-63.
108. Rajman L, Chwalek K, & Sinclair DA (2018) Therapeutic Potential of NAD-Boosting Molecules: The In Vivo Evidence. *Cell Metab* 27(3):529-547.
109. Ji L, *et al.* (2019) Slc6a8-Mediated Creatine Uptake and Accumulation Reprogram Macrophage Polarization via Regulating Cytokine Responses. *Immunity*.
110. Hennessy E, Adams C, Reen FJ, & O'Gara F (2016) Is There Potential for Repurposing Statins as Novel Antimicrobials? *Antimicrob Agents Chemother* 60(9):5111-5121.
111. Dutta NK, *et al.* (2019) Adjunctive host-directed therapy with statins improves tuberculosis-related outcomes in mice. *J Infect Dis*.

Nederlandse Samenvatting
Dankwoord
Curriculum Vitae
List of Publications



Nederlandse Samenvatting

Introductie

Tuberculose (TBC) is een longziekte die wordt veroorzaakt door een infectie met *Mycobacterium tuberculosis* (*Mtb*). De eerste aanwijzingen voor TBC in mensen kunnen worden herleid tot het neolithische tijdperk (~9.000 jaar geleden) en vormt tot op heden een belangrijke bedreiging voor de menselijke gezondheid. In 2017 kregen naar schatting 10 miljoen mensen TBC en stierven 1,6 miljoen mensen als gevolg van de ziekte, wat TBC de belangrijkste doodsoorzaak maakt door een enkel infectieus agens en één van top 10 doodsoorzaken wereldwijd. Het overgrote deel van TBC infecties (87%) vindt plaats in slechts 30 landen, waarvan India (27%), China (9%) en Indonesië (8%) de grootste TBC last dragen. De behandeling voor TBC bestaat uit een intensieve antibioticakuur van 6 maanden. Echter, de opkomst van antibioticumresistente stammen vormt een groot gevaar voor de behandeling van de ziekte in de toekomst. Hoewel vaccinatie met Bacille Calmette-Guérin (BCG), een levend verzwakt *Mycobacterium bovis*-vaccin dat sinds 1921 aan mensen wordt toegediend, gedeeltelijke werkzaamheid vertoont bij kinderen, ontbreekt een vaccin dat voldoende bescherming geeft in jongeren en volwassenen momenteel.

TBC wordt verspreid door inademing van *Mtb*-bevattende luchtdeeltjes, geproduceerd tijdens niezen of hoesten. De ingeademde bacteriën infecteren vervolgens macrofagen in de longen. Dit belangrijke cellen die deel uitmaken van het aangeboren immuunsysteem, met als primaire taak het direct doden van pathogenen door ingestie (fagocytose) om vervolgens het adaptieve immuunsysteem te activeren door het presenteren van antigenen aan T cellen. De immuunrespons tegen *Mtb* wordt gekenmerkt door de vorming van granulomen. Dit zijn complexe opeenhopingen van immuuncellen die enerzijds de gastheer beschermen door fysieke insluiting van geïnfecteerde cellen, maar tegelijkertijd een gunstig milieu vormen voor overleving van de bacterie (6). Na infectie volgt een klinisch asymptomatische periode van latente TBC (LTBI). Een recente schatting stelt dat ongeveer een kwart van de wereldbevolking latent besmet is met *Mtb* (7), waarvan 5 tot 10% tijdens het leven zal reactiveren en dus actieve TBC zal ontwikkelen. De precieze factoren die dit proces van TB reactivering bepalen zijn nog niet compleet duidelijk.

De associatie tussen tuberculose en diabetes

De incidentie van TBC wordt sterk beïnvloed door verschillende comorbiditeiten die het risico op het ontwikkelen van actieve ziekte vergroten. Hiervan was co-infectie met het humaan immunodeficiëntievirus (HIV) de afgelopen decennia het meest invloedrijk. Infectie met HIV leidt tot een 20-voudig verhoogd risico op TBC (77). In 2017 ontwikkelden 920.000 HIV-patiënten TBC en 300.000 mensen stierven als gevolg van de ziekte (2). Andere bekende risicofactoren voor TBC zijn roken, alcoholgebruik en ondervoeding

(78). Een TBC-geassocieerde comorbiditeit die pas sinds kort in de belangstelling staat is diabetes mellitus (DM), ondanks dat deze associatie al eeuwen geleden voor het eerst werd beschreven (79). Epidemiologisch onderzoek laat zien dat DM het risico op het ontwikkelen van TBC verdrievoudigt (81). Naar schatting kan 15% van de wereldwijde TBC gevallen worden toegeschreven aan gelijktijdige DM. Waar het aantal sterfgevallen door TBC onder HIV-patiënten met 44% is gedaald sinds het jaar 2000, wordt juist voorspeld dat het aantal patiënten met gelijktijdige TBC-DM de komende jaren sterk zal gaan toenemen. De reden hiervoor is de het aantal mensen met DM wereldwijd naar schatting met bijna 50% zal toenemen de komende 25 jaar; van 425 miljoen mensen in 2017 tot 629 miljoen mensen in 2045 (82). Deze stijging zal naar verwachting voor het overgrote deel plaatsvinden in ontwikkelingslanden als gevolg van toenemende welvaart en verstedelijking; dezelfde gebieden waar TBC nog veelvoorkomend is. Verder is DM geassocieerd met een verhoogde kans op falen van TBC-behandeling, terwijl actief TBC het effectief controleren van de glucosespiegel tijdens DM bemoeilijkt (83).

DM is een stofwisselingsstoornis die kan worden veroorzaakt door een gebrek aan productie van het glucose-regulerende hormoon insuline (type 1 / T1DM) of door de ontwikkeling van insulineresistentie (type 2 / T2DM), waarvan de laatste ongeveer 90% van diabetes patiënten betreft (82). Beide ziekte types worden gekenmerkt door een hoge bloedsuikerspiegel (hyperglykemie) die wordt veroorzaakt door het onvermogen van cellen om voldoende glucose op te nemen. Klinische symptomen van DM zijn o.a. terugkerende infecties, gewichtstoename, polyurie gepaard met overmatige dorst en een verslechterde wondgenezing. T1DM wordt veroorzaakt door destructie van insuline producerende β -cellen in de alvleesklier, meestal als gevolg van een auto-immuun reactie. De precieze oorzaken die ten grondslag liggen aan T2DM vallen echter minder duidelijk te definiëren. Obesitas en overgewicht zijn belangrijke risicofactoren voor de ontwikkeling van T2DM, wat de ziekte linkt aan voeding van lage kwaliteit en een gebrek aan fysieke inspanning. Verder heeft T2DM ook een hoge erfelijke belasting (85). Door de associatie met obesitas hebben veel T2DM-patiënten ook een verhoogd risico op cardiovasculaire complicaties zoals atherosclerose door afwijkingen in bloedlipideniveaus (dyslipidemie). Dit klinische beeld staat in schril contrast met het klinisch beeld van TBC-patiënten dat juist gepaard gaat met ondervoeding en gewichtsverlies (86).

Hoewel er dus veel bewijs is dat DM de ontwikkeling van TBC sterk kan beïnvloeden, is de precieze oorzaak hiervan nog niet duidelijk. Het doel van dit proefschrift was dan ook om de pathofysiologische mechanismen die ten grondslag liggen aan TBC-DM comorbiditeit te ontrafelen.

Humane macrofagen als model voor TBC (en DM)

Macrofagen spelen een belangrijke rol in de infectiecyclus van *Mtb* omdat ze de voorkeursomgeving van de bacterie vormen voor overleving. Om deze reden worden primaire humane macrofagen vaak gebruikt als *in vitro* model om *Mtb* infectie te bestuderen. Een belangrijk kenmerk van macrofagen is dat zij erg gevoelig zijn voor lokale veranderingen in het micromilieu en op basis hiervan kunnen wisselen van functie (plasticiteit). Dit kan dus ook gevolgen hebben voor hun vermogen om intracellulaire pathogenen zoals *Mtb* te bestrijden. Waar macrofagen in het verleden werden geclassificeerd als pro-inflammatoir (M ϕ 1) of anti-inflammatoir (M ϕ 2) is het inmiddels duidelijk dat zij nog veel meer vormen aan kunnen nemen als reactie op verschillende stimulaties (1, 2). Veranderingen in de balans tussen deze verschillende macrofaagtypen kan leiden tot verergering van meerdere ziektes, waaronder TBC (3). Om deze reden zou het gericht sturen van macrofaag-differentiatie een interessante optie zijn bij TBC therapie.

Het belang van macrofaagfuncties voor de reactie op *Mtb* wordt geïllustreerd in **hoofdstuk 2** waarin we verschillende M ϕ 2-subtypes hebben gekarakteriseerd. We identificeerden M ϕ 2b-macrofagen (geïnduceerd door gecombineerde blootstelling aan lipopolysaccharide (LPS) en immuuncomplexen) als een subtype met een krachtige antimicrobiële activiteit tegen zowel *Mtb* als *Salmonella* Typhimurium, maar met een matige capaciteit om Th1- en Treg-cellen te induceren in vergelijking met M ϕ 2a/c/d macrofagen. Deze vermindering in bacteriële belasting was niet het gevolg van verminderde opname van *Mtb*. Analyse van gen- en eiwitexpressie data liet zien dat M ϕ 2b-macrofagen werden gekenmerkt door een type I interferon profiel. Verder produceerden ze relatief hoge niveaus van vasculaire endotheliale groeifactor (VEGF), een belangrijke mediator van granulomateuze ontsteking en angiogenese in zowel muizen (4) als zebrafissen (5). Alle M ϕ 2-subtypes konden succesvol worden gepolariseerd naar M ϕ 2b na initiële differentiatie, wat aangeeft dat inductie van M ϕ 2b-polarisatie een mogelijke optie zou kunnen zijn voor gastheergerichte behandeling van infectieziekten.

Aangezien macrofaag-polarisatie sterk verweven is met veranderingen in cellulaire stofwisseling bieden zijn ook een interessant model voor het bestuderen van mogelijke interacties tussen TBC en DM. Allereerst hebben we onderzocht of hyperglykemie het infectieproces van macrofagen met *Mtb* negatief kon beïnvloeden (**hoofdstuk 3**). We vonden dat *in vitro* differentiatie van humane M ϕ 2 macrofagen in aanwezigheid van hoge glucose concentraties (25 mM) leidde tot een verhoogde uitscheiding van verschillende cytokines (TNF- α , IL-6, IL-10, IL-1RA) als reactie op stimulatie met LPS of *Mtb* lysaat in vergelijking met laag glucose (5 mM). Deze resultaten zijn vergelijkbaar met andere studies over het effect van hoog glucose op primaire macrofagen (7) en THP-1-cellen (8). Hyperglykemie had echter geen invloed op de productie van cytokines of mycobacteriële uitgroei na infectie met *Mtb*. In tegenstelling tot andere studies (9, 10) vonden wij geen

significante verschillen in fagocytose functie tussen macrofagen gekweekt in hoog of laag glucose. Wij concludeerden dat hyperglykemie op zichzelf niet de associatie tussen TBC en DM kon verklaren (althans vanuit het oogpunt van de macrofaag).

Lipiden in TBC-DM: een mogelijke parallel met atherosclerose?

Naast hyperglykemie waren wij ook geïnteresseerd in een mogelijke verband tussen DM-geassocieerde lipiden en TBC. Om deze reden hebben wij het effect van geoxideerde lage-dichtheid lipoproteïne deeltjes (oxLDL) op *Mtb* infectie bestudeerd in macrofagen. Meerdere studies hebben aangetoond dat oxLDL niveaus verhoogd zijn in het bloed van DM patiënten (35, 36). OxLDL deeltjes worden gevormd als gevolg van oxidatieve stress en spelen een belangrijke rol bij de ontwikkeling van atherosclerose (34): macrofagen in de vaatwand kunnen oxLDL deeltjes opnemen door middel van specifieke receptoren, wat leidt tot de vorming van vetdruppels in deze cellen (schuimcellen) (37). Een interessante observatie is dat oxLDL deeltjes zich ook ophoopten in granulomen van *Mtb* geïnfecteerde cavia's (38). Dit betekent dat oxLDL potentieel een verbindende factor vormt tussen TBC en DM. Behandeling van macrofagen met oxLDL leidde tot een dosisafhankelijke ophoping van vetdruppels in humane macrofagen en verhoogde intracellulaire overleving van *Mtb* (**hoofdstuk 4**). Dit ging gepaard met de ophoping van cholesterol in lysosomen en een verminderde lysosomale lokalisatie van *Mtb* in oxLDL-behandelde macrofagen. Behandeling met geacetyleerd LDL (acLDL), een ander gemodificeerd lipoproteïne dat niet leidt tot cholesterol ophoping in lysosomen (39), resulteerde niet in verhoogde uitgroei van *Mtb*, tenzij het werd gecombineerd met een lysosomale cholesteroltransportremmer. Deze resultaten benadrukken dat de intracellulaire lokalisatie van cholesterol cruciaal is voor het effect van oxLDL op *Mtb* infectie in macrofagen.

Hoewel bovenstaande resultaten suggereren dat DM-geassocieerde lipiden zoals oxLDL *Mtb* infectie zouden kunnen bevorderen, was het tot dusver onbekend hoe gelijktijdige TBC-DM circulerende lipiden niveaus beïnvloedt. In **hoofdstuk 5** hebben we door middel van kernspinresonantie (NMR) spectroscopie een veelvoud aan stofwisselingsproducten gemeten in bloedplasma van TBC, DM en TBC-DM patiënten uit Zuid-Afrika, waaronder veel aan lipiden gerelateerde parameters. Zoals verwacht vertoonden DM-patiënten dyslipidemie, gekenmerkt door hoge triglyceride niveaus en een verlaagd HDL-cholesterol, terwijl TBC vooral geassocieerd was met lage concentraties van meerdere aminozuren. TBC-DM patiënten vertoonden kenmerken van zowel TBC als DM, wat een vorm van 'getouwtrek' lijkt te weerspiegelen op stofwisselingsniveau. Naast hoge triglyceriden concentraties en lage niveaus van HDL-cholesterol, vertoonden TBC-DM-patiënten specifieke verhogingen van restachtige lipoproteïnedeeftjes en sfigomyeline; beiden zijn geassocieerd met ontwikkeling van atherosclerose (47-49). Ten slotte konden we bevestigen dat de hoeveelheid oxLDL deeltjes verhoogd was in DM-patiënten uit dit cohort (**hoofdstuk 4**). Dit is een belangrijke observatie, aangezien dit de specifieke

populatie betreft met een verhoogd risico op het ontwikkelen van TBC. Ondanks dat er geen duidelijke toename in oxLDL deeltjes waarneembaar was in TBC-DM patiënten, vertoonden oxLDL niveaus wel een sterke positieve correlatie met plasma triglyceriden. Dit impliceert dat oxLDL niveaus voornamelijk verhoogd waren in patiënten met ernstigere manifestaties van dyslipidemie.

Metabolomics analyse van TBC-DM:

De hierboven besproken NMR-metingen uit **hoofdstuk 5** betreffen een vorm van metabolomics analyse. Deze term omvat bepalingen van het metabooloom, de totale hoeveelheid stofwisselingsproducten (metabolieten) in een cel of weefsel. Het eerste bekende gebruik van een primitieve vorm van metabolomics is duizenden jaren terug te voeren op artsen uit China, Babylon en Egypte. Zij bestudeerden de kenmerken van urine om de aanvang van verschillende ziektes te diagnosticeren en te voorspellen. Diabetes kon bijvoorbeeld worden geïdentificeerd door een zoete geur en smaak van urine (75). Inmiddels is het gebruik van metabolomics een manier om de onderliggende pathofysiologische processen van menselijke ziektes te bestuderen. Een goed voorbeeld van de toepassing van metabolomics in TBC-onderzoek is een recente studie door Weiner *et al.* (82): zij beschrijven een prognostisch metabolietenprofiel voor actieve TBC met een gevoeligheid van 69% en specificiteit van 75% binnen 5 maanden voorafgaand aan diagnose. Sommige van de beschreven veranderingen konden al 12 maanden vóór de diagnose van actieve ziekte worden waargenomen, waardoor zij mogelijk zouden kunnen worden gebruikt voor de tijdige voorspelling van TBC ontwikkeling (83).

We gebruikten verschillende vormen van metabolomics om de effecten van TBC-DM op plasma metaboliet profielen te analyseren in twee verschillende patiëntcohorten uit Zuid-Afrika (**hoofdstuk 5**) en Indonesië (**hoofdstuk 6**). In beide studies vertoonden TBC en TBC-DM-patiënten zeer lage concentraties van meerdere aminozuren. In het bijzonder vertoonden lage niveaus van plasma histidine in beide onderzoeken een zeer hoog voorspellend vermogen voor TBC als TBC-DM, wat in overeenstemming is met een eerder uitgevoerde metabolomics analyse van TBC patiënten (84). Bovenal toonde de studie van Weiner *et al.* aan dat histidine concentraties al beginnen af te wijken vanaf 9 maanden voorafgaand aan de manifestatie van klinische TBC (82). In tegenstelling tot histidine was de plasmaconcentratie van fenylalanine juist verhoogd in beide TBC-cohorten. De verhouding van fenylalanine ten opzichte van histidine (Fe / His) had hierdoor een nog sterkere voorspellende waarde voor TBC dan de metabolieten op zichzelf. Beide aminozuren behoorden dan ook tot de 10 metabolieten die deel uit maken van het door Weiner *et al.* beschreven prognostische TBC profiel (82). Andere vroegtijdige veranderingen beschreven in dit artikel waren o.a. lagere concentraties van citrulline en tryptofaan gecombineerd met hogere kynurenine niveaus. Deze observaties zijn in overeenstemming met onze eigen resultaten uit **hoofdstuk 6**. Een verhoogde

verhouding van kynurenine ten opzichte van tryptofaan (Kyn / Trp) is een aanwijzing voor een verhoogde activiteit van het enzym indoleamine 2,3-dioxygenase (IDO), wat geassocieerd is met een verslechterende beheersing van *Mtb* infectie (73). Citrulline is een tussenproduct van de ureumcyclus dat kan worden gebruikt voor de synthese van arginine, een proces dat kan bijdragen aan de antibacteriële respons in macrofagen (88, 89) en T-cellen (90). Behandeling van TBC met antibiotica resulteerde in normalisatie van het overgrote deel van de aangedane plasmametabolieten tot concentraties die vergelijkbaar waren met gezonde controles. Deze resultaten laten zien dat TB en TBC-DM beide geassocieerd zijn met sterk veranderde aminozuurniveaus in de circulatie.

Ten slotte hebben we ook metabolomics uitgevoerd op *Mtb*-geïnfekteerde macrofagen, met als doel om meer inzicht te krijgen over de fundamentele effecten van *Mtb* infectie op de cellulaire stofwisseling (**hoofdstuk 7**). Infectie met *Mtb* leidde tot hogere concentraties van nicotinamide-adenine-dinucleotide (NAD⁺), creatine en creatinefosfaat in macrofagen. Daarnaast vonden wij aanwijzingen voor een verhoogde afbraak van glutamine en glucose door glycolyse. Dit correspondeerde met de analyse van genexpressieprofielen van *Mtb*-geïnfekteerde macrofagen (105). Hieruit bleek dat *Mtb* infectie meerdere enzymen uit deze specifieke stofwisselingscascades reguleerde. NAD⁺ is een belangrijke cofactor voor veel stofwisselingsreacties; medicijnen die NAD⁺ concentraties kunnen verhogen staan dan ook in de belangstelling voor de behandeling van verschillende ziektes (108). Meerdere studies hebben aangetoond dat NAD⁺ niveaus een groot effect hebben op macrofaagfunctie (106-108), wat het belang aangeeft om de rol die NAD⁺ speelt tijdens *Mtb* infectie in macrofagen verder te onderzoeken. Een ander recent artikel onthulde dat verhoogde creatine opname de anti-inflammatoire capaciteit van macrofagen kon ondersteunen, terwijl pro-inflammatoire functies tegelijkertijd werd onderdrukt (109). De resultaten van **hoofdstuk 2** onderstrepen het belang van macrofaagactivatie voor de betrijding van *Mtb* infectie. Het zou daarom erg interessant zijn om te onderzoeken of verhoogde intracellulaire creatine niveaus dit proces zouden kunnen beïnvloeden.

Conclusie

Gezamenlijk wijzen de resultaten van dit proefschrift op een mogelijke rol voor DM-geassocieerde lipiden tijdens de ontwikkeling van TBC. Verhoogde intracellulaire niveaus van lipiden en cholesterol zouden de overleving van *Mtb* in macrofagen kunnen ondersteunen; enerzijds door het remmen van antimicrobiële functies, anderzijds door te fungeren als bacteriële voedingsbron. Hoewel onze observationele resultaten alleen een correlatie en geen causaal verband kunnen aantonen tussen dyslipidemie en TBC, hebben verschillende interventiestudies aangetoond dat lipide-verlagende geneesmiddelen zoals statines, een gunstige werking kunnen hebben als aanvullende behandeling voor TBC (61-64). Naast hun effect op het cholesterolgehalte in het bloed is ook aangetoond

dat statines de intracellulaire bacteriële groei van *Mtb* kunnen remmen, waardoor ze een interessante behandelingsmogelijkheid vormen voor TBC-DM patiënten (63, 110, 111). Prospectieve vervolgstudies zullen moeten uitwijzen of het verlagen van bloedlipide niveaus het risico van DM-patiënten om TBC te ontwikkelen kan verminderen, of kan leiden tot verbeterde TBC behandelingsresultaten in combinatie met de gebruikelijke antibioticakuur. Verder onderzoek naar TBC-DM is van groot belang, aangezien deze snel toenemende co-epidemie grote gevolgen kan hebben voor de wereldgezondheid wanneer deze niet tijdig wordt beheerst.

Dankwoord

Hoewel het iets langer heeft geduurd dan ik in eerste instantie had ingeschat, ben ik echt heel erg blij met het proefschrift dat uiteindelijk voor jullie ligt. Ik heb dit echter niet allemaal in mijn eentje volbracht. Vandaar dat ik de volgende personen even in het bijzonder wilde bedanken.

Allereest natuurlijk **Simone en Tom**. Ik was super trots toen jullie mij vlak voor het einde van mijn studie benaderden voor een mogelijk promotietraject bij INZI. Jullie gaven mij veel ruimte om mijn eigen ding te doen, maar floten mij ook terug wanneer ik dit misschien wat te ver door dreef. Voor mij sprak uit deze verantwoordelijkheid die jullie mij gaven een hoop vertrouwen en dit heb ik erg gewaardeerd. Wij functioneerden met zijn drieën als een goed team en ik heb ontzettend veel van jullie geleerd de afgelopen jaren. Bedankt voor alles!

Vervolgens mijn paranimfen, **Matthias en Mariateresa**. Matthias, een dag op het lab met jou was altijd genieten; van het opblazen van Argon Boy tot onze wekelijkse ML-III raves. Daarnaast was je met jouw gevoel voor efficiëntie en techniek een ideale sparringpartner als het ging om proeven doen. Mariateresa, een dag bij INZI was voor mij niet compleet zonder het horen één van jouw kenmerkende zuchten schuin achter me. We begonnen ongeveer tegelijk met onze projecten, en heb zoveel goede herinneringen over gehouden aan onze tijd samen bij INZI; van onze dagelijkse cappuccino's tot jouw wedergeboorte. M&M: bedankt voor alles!

Dan natuurlijk alle K5'ers. **Kimberley, Krista, Louis, Susan, Cassandra, Anouk, Anne, Edwin, Maria, Paula, Calinda, Suzanne, Eleonora, Arthur, Roel**; bedankt voor al jullie hulp en gezelligheid de afgelopen jaren. Verder wil ik **Mariëlle** en alle leden van de Haks-groep bedanken. Het was voor mij erg fijn dat elke woensdag bij jullie wekelijkse meeting aan mocht sluiten, hier heb ik veel aangehad. **Emile**, jij was altijd een groot aanjager van etentjes en borrels en ik heb erg genoten van jouw aanwezigheid bij onze weekendjes op de Veluwe en in Zeeland.

Annemieke, Peter, Leo, bedankt voor jullie kritische blik en vragen tijdens donderdagmeetings. **Liesbeth en Ingrid**, bedankt voor alle secretariële hulp gedurende mijn project.

Annelies, Bep, Adriëtte, Tannie, Els, Alwin, Michella, Miriam en alle andere collega's op E5: bedankt voor al jullie hulp met labwerk tijdens mijn project en natuurlijk ook voor de gezellige tijd.

Mijn Master studenten, **Sevgi en Mouraya**: bedankt voor jullie inzet en enthousiasme.

Verder wil ik nog enkele mensen bedanken binnen het LUMC en de Universiteit. **Patrick**, bedankt voor jouw input en enthousiasme tijdens mijn oxLDL project. **Oleg**, bedankt voor alle tijd en moeite die je hebt gestoken in het metabolomics paper. **Bruno en Herman**, bedankt voor al jullie input en hulp, zowel binnen de TB-DM meetings als daarbuiten.

Alle (inter)nationale collega's en coauteurs die hebben bijgedragen aan stukken van dit proefschrift: **Ekta, Reinout, Mihai, Sarantos, Bacti, Edhyana, Amy, Thomas, Léanie, Katharina, Erik, Gerhard, Peter, Jeroen** en andere deelnemers aan het TANDEM consortium; bedankt!

Naast mijn collega's kan ik ook mijn familie niet vergeten. **Harry en Annie**, bedankt voor jullie steun en tolerantie voor mijn verhalen over TB, cholesterol en lysosomen aan de keukentafel. **Manouk**, samen met **Lindert** kon jij als immunoloog goed met mij sparren over experimenten, dat waardeerde ik zeer.

Ten slotte blijft er nog één persoon over: **Maria**. Fijn dat je altijd geduldig kon luisteren naar al mijn gedachten en zorgen over proeven, manuscripten en meer. Het duurde allemaal wat langer dan gepland, maar we hebben het geklaard. Ik geniet heel erg van ons nieuwe hoofdstuk samen in Wageningen.

Curriculum Vitae

Born in Alphen aan den Rijn on October 9th, 1989, Frank Vrieling first gained interest in biomedical sciences by watching his father add brightly colored cell culture medium to petri dishes in the old biology faculty building of Leiden University as a child. His fascination for biology and science remained throughout his pre-university education (Gymnasium) at the Ashram College in Alphen aan den Rijn. After graduating high school in 2008, he was admitted to study Biomedical Sciences at the Leiden University Medical Center (LUMC). He remained there for the duration of five years, obtaining his Bachelor and Research Master Degrees. During his first Master internship, he took part in a research project on the topic of alternative macrophage polarization at the Department of Infectious Diseases of the LUMC under the supervision of Prof. dr. Tom Ottenhoff, Dr. Simone Joosten and Dr. Mariëlle Haks. After graduating in 2013, he started his PhD project at the same department, studying the association between tuberculosis and type 2 diabetes using primary human macrophage infection models and various kinds of metabolomics as part of the TANDEM consortium. The results of his studies are described in this thesis. In 2019, he continued his work at the interface of macrophage immunology and metabolism as a post-doctoral researcher at the Department of Human Nutrition and Health at Wageningen University.

List of publications

1. [Vrieling F](#), Kostidis S, Spaik HP, Haks MC, Mayboroda OA, Ottenhoff THM, et al. Analyzing the impact of Mycobacterium tuberculosis infection on primary human macrophages by combined exploratory and targeted metabolomics. *Sci Rep.* 2020;10(1):7085.
2. Moreira JD, Koch BEV, van Veen S, Walburg KV, [Vrieling F](#), Mara Pinto Dabes Guimaraes T, et al. Functional Inhibition of Host Histone Deacetylases (HDACs) Enhances in vitro and in vivo Antimycobacterial Activity in Human Macrophages and in Zebrafish. *Front Immunol.* 2020;11:36.
3. [Vrieling F](#), Alisjahbana B, Sahiratmadja E, van Crevel R, Harms AC, Hankemeier T, et al. Plasma metabolomics in tuberculosis patients with and without concurrent type 2 diabetes at diagnosis and during antibiotic treatment. *Sci Rep.* 2019;9(1):18669.
4. [Vrieling F](#), Wilson L, Rensen PCN, Walzl G, Ottenhoff THM, Joosten SA. Oxidized low-density lipoprotein (oxLDL) supports Mycobacterium tuberculosis survival in macrophages by inducing lysosomal dysfunction. *PLoS Pathog.* 2019;15(4):e1007724.
5. [Vrieling F](#), Ronacher K, Kleynhans L, van den Akker E, Walzl G, Ottenhoff THM, et al. Patients with Concurrent Tuberculosis and Diabetes Have a Pro-Atherogenic Plasma Lipid Profile. *EBioMedicine.* 2018;32:192-200.
6. van Dam AD, Bekkering S, Crasborn M, van Beek L, van den Berg SM, [Vrieling F](#), et al. BCG lowers plasma cholesterol levels and delays atherosclerotic lesion progression in mice. *Atherosclerosis.* 2016;251:6-14.
7. Lachmandas E*, [Vrieling F](#)*, Wilson LG, Joosten SA, Netea MG, Ottenhoff TH, et al. The effect of hyperglycaemia on in vitro cytokine production and macrophage infection with Mycobacterium tuberculosis. *PLoS One.* 2015;10(2):e0117941.

* equal contribution

